

# **Analysis of Translationally Active RNAs**

## **Quantification by Microscale Thermophoresis and Modification Analysis by LC-MS/MS**

Dissertation zur Erlangung des Grades  
“Doktor der Naturwissenschaften”  
im Promotionsfach Pharmazie

am Fachbereich Chemie, Pharmazie und Geowissenschaften  
der Johannes Gutenberg-Universität Mainz

**Kathrin Luise Thüring**  
geboren am 09.01.1988 in Wiesbaden

Mainz, Oktober 2016



JOHANNES GUTENBERG  
UNIVERSITÄT MAINZ

---

Dekan:

1. Berichterstatter:

2. Berichterstatter:

Tag der mündlichen Prüfung: 15.12.2016

*D77 (Dissertation Mainz)*

---

Die vorgelegte Dissertation wurde am Institut für Pharmazie und Biochemie der Johannes Gutenberg-Universität in Mainz zur Erlangung des Grades "Doktor der Naturwissenschaften", unter Betreuung von     angefertigt.

Erstgutachter:

Zweitgutachter:

Hiermit versichere ich eidesstattlich:

1. Ich habe die jetzt als Dissertation vorgelegte Arbeit selbst angefertigt und alle benutzten Hilfsmittel (Literatur, Apparaturen, Material) in der Arbeit angegeben.
2. Ich habe oder hatte die jetzt als Dissertation vorgelegte Arbeit nicht als Prüfungsarbeit für eine staatliche oder andere wissenschaftliche Prüfung eingereicht.
3. Ich hatte weder die jetzt als Dissertation vorgelegte Arbeit noch Teile davon bei einer anderen Fakultät bzw. einem anderen Fachbereich als Dissertation eingereicht.

---

Ort, Datum

Kathrin Thüring



**Danksagung**



## Abstract

RNAs, and tRNAs in particular, play important roles not only in basic cellular processes like the translation of the genetic information, but also fulfill a variety of regulatory functions for example in the cell's response to various environmental stress factors and challenges. Furthermore, the involvement of RNA species in the pathophysiology of a number of human diseases, including cancer and neurobiological disorders, highlights the importance of a tight regulation of cellular RNA dynamics. Especially in case of tRNAs, regulation includes both dynamic changes in abundance and in RNA modification pattern. Hence, detailed investigations of both variations in (t)RNA levels and in their content of modifications are necessary to further uncover RNA functions in the regulation of cellular processes and the impact of RNA species on human diseases.

In this work, various approaches were applied to address the need for a detailed analysis of specific RNA species, including their isolation, quantification and modification analysis. Making use of fluorescently labeled DNA probes, an RNA quantification method based on microscale thermophoresis was developed, which showed not only to be applicable to both single RNA species as well as the subgroup of polyadenylated RNA, but also to be highly reproducible and extremely fast to conduct. The successful application to the quantification of most *S. cerevisiae* tRNA species revealed small, but in part significant changes of tRNA isoacceptor levels under various environmental and genetic conditions (*e.g.* temperature stress and RNA modification deficiencies), underlining the method's excellent suitability for examination of changes in relative tRNA abundances. Furthermore, a considerable reduction of mRNA abundance in *S. cerevisiae*, which was shown to be depleted of tRNA<sup>Gln</sup> due to PaT killer toxin treatment, was observed.

Using the same DNA probes, additionally tagged with biotin, various single (t)RNA species were successfully isolated from RNA mixtures employing a hybridization- and affinity purification-based protocol. The potentially immunoregulatory small tRNA-like mascRNA, whose precursor long non-coding RNA MALAT1 is a key factor in cancer progression, was chosen in particular as an attractive target for an isolation with subsequent RNA modification analysis by LC-MS/MS. Although the isolation of mascRNA was ultimately unsuccessful, RNA-Seq results still revealed an enrichment of mascRNA, albeit marginally significant, and furthermore suggested the presence of an 1-methyladenosine modification.

Analysis of an RNA's modification pattern is likewise important to assess the full range of the RNA's characteristics and functions. Here, highly sensitive LC-MS/MS analysis was employed to quantify changes in wobble U34 modifications present in the anticodon loop of tRNAs in various mutants of *S. cerevisiae*. Making use of different scan modi and instrument settings, further investigations included the prove of an introduction of queuosine into *S. pombe* tRNA, the verification of the successful isolation of single tRNA species and the confirmation of <sup>13</sup>C-labeling patterns of nucleobases in *E. coli* RNA.





## Zusammenfassung

RNA, und tRNA im Besonderen, spielen nicht nur in grundlegenden zellulären Prozessen wie der Translation der genetischen Information eine wichtige Rolle, sondern erfüllen auch eine Vielzahl an regulatorischen Funktionen, zum Beispiel in der Reaktion auf verschiedenste Stressfaktoren. Weiterhin zeigt die Beteiligung von RNA an der Pathophysiologie verschiedener Krankheiten, wie zum Beispiel Tumor- sowie neurobiologischen Erkrankungen, die Wichtigkeit einer engen Kontrolle der zellulären Dynamik von RNAs. Diese Kontrolle beinhaltet, insbesondere im Fall der tRNAs, dynamische Veränderungen sowohl in der Menge einzelner RNAs als auch in deren Modifikationsmustern. Um weitere Funktionen einzelner RNA-Moleküle in der Regulation zellulärer Abläufe und ihren Einfluss auf Erkrankungen aufdecken zu können, sind daher detaillierte Untersuchungen sowohl von (t)RNA-Leveln als auch von ihren Modifikationen erforderlich.

In dieser Arbeit wurden unterschiedliche Ansätze gewählt, um der Herausforderung einer detaillierten Analyse von RNA-Molekülen entgegenzutreten. Hierzu gehörten die Isolation einzelner RNAs, ihre Quantifizierung und die Analyse von RNA Modifikationen. Mit Hilfe von fluoreszenzmarkierten DNA-Sonden wurde eine auf Thermophorese basierende Methode zur RNA-Quantifizierung entwickelt, die sowohl auf einzelne RNA-Moleküle als auch auf die Gruppe der polyadenylierten RNAs angewendet wurde. Weiterhin zeigte die sehr schnell durchführbare Methode eine sehr hohe Reproduzierbarkeit der Ergebnisse. Erfolgreiche Anwendung fand die Methode in der Quantifizierung von tRNAs aus *S. cerevisiae* unter verschiedenen äußeren und genetischen Bedingungen, wie Temperaturstress und Defekten in tRNA Modifikationen. Hierbei konnten geringfügige, aber dennoch zum Teil signifikante Unterschiede in tRNA-Leveln festgestellt werden, was die hohe Eignung der Methode für Untersuchungen von relativen Veränderungen in RNA-Häufigkeiten bestätigte. Zusätzlich konnte mithilfe der Methode eine ausgeprägte Verringerung der mRNA Menge unter PaT Killer Toxin-Behandlung beobachtet werden, die auch zu einer drastischen Reduktion von tRNA<sup>Gln</sup> führte.

Mittels Hybridisierung und Affinitätsaufreinigung wurden unter Verwendung derselben DNA-Sonden (zusätzlich mit Biotin markiert) verschiedene (t)RNAs erfolgreich aus RNA-Mischungen isoliert. Hierbei wurde die kleine, tRNA-ähnliche und möglicherweise immunregulatorische mascRNA als besondere Ziel-RNA ausgewählt, deren Präkursor-RNA, MALAT1, entscheidend an der Progression von Tumorerkrankungen beteiligt ist. Auch wenn die Isolation der mascRNA letztendlich nicht erfolgreich war, konnten die Ergebnisse des RNA-Seq eine Anreicherung der mascRNA, wenn auch von schwacher Signifikanz, belegen sowie eine mögliche 1-Methyladenosin-Modifikation zeigen.

Desweiteren ist die Analyse von RNA Modifikation für eine vollständige Charakterisierung eines RNA-Moleküls erforderlich. Mittels LC-MS/MS in verschiedenen Detektionsmodi wurden Veränderungen in tRNA-U34 Modifikationen in Hefe-Mutanten quantifiziert, die Einführung von Queuosin in *S. Pombe* tRNA gezeigt, die erfolgreiche Isolation von tRNAs bestätigt sowie die Position von <sup>13</sup>C-Markierungen in den Nukleobasen von *E. coli* untersucht.



# Contents

<b>Abstract</b>	<b>vii</b>
<b>Zusammenfassung</b>	<b>ix</b>
<b>List of Figures</b>	<b>xv</b>
<b>List of Tables</b>	<b>xvii</b>
<b>Abbreviations</b>	<b>xix</b>
<b>1 Introduction</b>	<b>1</b>
1.1 Transfer RNA: Dynamics of abundance and modifications . . . . .	1
1.1.1 Dynamics of tRNA Levels . . . . .	3
1.1.1.1 Regulation of tRNA Abundance . . . . .	3
1.1.1.2 Abundance of tRNAs and Human Disease . . . . .	4
1.1.2 Modified Nucleosides in tRNA . . . . .	6
1.1.2.1 Structure and function of <i>S. cerevisiae</i> wobble U34 modifications	7
1.1.2.2 Functions of tRNA Modifications in the Regulation of Translation	
and Stress Response . . . . .	10
1.1.2.3 Connections of tRNA modifications with human diseases . . . . .	11
1.2 Analysis of tRNA Levels and RNA Modifications . . . . .	12
1.2.1 Quantification of tRNA Abundances . . . . .	12
1.2.2 Analysis of (t)RNA Modifications . . . . .	15
1.2.2.1 LC-MS/MS Analysis of Modified Nucleosides . . . . .	16
1.3 A tRNA-like Small RNA: mascRNA . . . . .	19
1.4 Microscale Thermophoresis . . . . .	21
1.4.1 Theory . . . . .	21
1.4.2 Experimental Details of Microscale Thermophoresis . . . . .	22
1.4.3 Thermophoresis of Nucleic Acids . . . . .	24
<b>2 Motivation and Objectives</b>	<b>27</b>
<b>3 Results and Discussion</b>	<b>31</b>
3.1 Microscale Thermophoresis-based Quantification of Single RNA Species . . . . .	31
3.1.1 Workflow: Quantification of Single RNA Species . . . . .	31

3.1.2	MST-Based Determination of tRNA Abundances . . . . .	32
3.1.2.1	Monitoring of DNA/RNA Hybridization Ratios . . . . .	32
3.1.2.2	Transfer to tRNA <sub>MAU</sub> <sup>Met</sup> Quantification in tRNA Mixtures . . . . .	35
3.1.2.3	MST of Native <i>E. coli</i> tRNA <sub>MAU</sub> <sup>Met</sup> . . . . .	37
3.1.2.4	MST of Native and Unmodified tRNA <sub>1<sup>Arg</sup>CU</sub> ( <i>Saccharomyces cerevisiae</i> ) . . . . .	38
3.1.2.5	Evaluation of the Method's Quantification Performance . . . . .	40
3.1.2.6	Biological Applications . . . . .	43
3.1.3	Investigation of PolyA-Tailored RNA . . . . .	52
3.1.3.1	Influence of PolyT Probe and PolyA Tail Length . . . . .	52
3.1.3.2	Transfer to Total RNA . . . . .	55
3.1.3.3	Influence of Sample Purity . . . . .	57
3.1.4	Summary . . . . .	58
3.2	Sequence-Specific Isolation of Small Non-Coding RNAs . . . . .	60
3.2.1	Introduction and Workflow . . . . .	60
3.2.2	Isolation of Single tRNAs . . . . .	61
3.2.2.1	Isolation of <i>S. cerevisiae</i> tRNA <sub>1<sup>Arg</sup>CU</sub> . . . . .	61
3.2.2.2	Isolation of tRNAs for LC-MS/MS analysis . . . . .	63
3.2.3	Isolation of the tRNA-like Small mascRNA . . . . .	63
3.2.3.1	Challenges of mascRNA Isolation . . . . .	64
3.2.3.2	Control Experiments for mascRNA Isolation . . . . .	64
3.2.3.3	Isolation of Native mascRNA . . . . .	65
3.2.4	Summary . . . . .	68
3.3	RNA Modification Analysis by Liquid Chromatography-Tandem Mass Spectrometry . . . . .	69
3.3.1	DMRM Mode: Analysis of Wobble U34 Modifications . . . . .	69
3.3.2	Neutral Loss Scan: Analysis of Isolated tRNAs . . . . .	72
3.3.3	Product Ion Scan: Analysis of the Fragmentation Pattern of Queuosine . . . . .	74
3.3.4	Pseudo-MS <sup>3</sup> : Determination of <sup>13</sup> C-Labeling Patterns of Nucleobases . . . . .	78
3.3.5	Summary . . . . .	81
<b>4</b>	<b>Conclusions and Outlook</b>	<b>83</b>
<b>5</b>	<b>Materials and Methods</b>	<b>89</b>
5.1	Materials . . . . .	89
5.1.1	Chemicals, Reagents and Ready-to-use Buffers and Solutions . . . . .	89
5.1.2	Buffers, Solutions and Media . . . . .	91
5.1.3	Enzymes . . . . .	92
5.1.4	DNA and RNA Oligonucleotides . . . . .	92
5.1.5	RNA Samples Obtained from Collaborators . . . . .	95
5.1.5.1	RNA for MST measurements . . . . .	95
5.1.5.2	RNA for LC-MS/MS measurements . . . . .	96

---

5.1.6	Cell Lines . . . . .	96
5.1.7	Disposables and Glassware . . . . .	97
5.1.8	Instruments . . . . .	97
5.1.8.1	Basic Laboratory Equipment . . . . .	97
5.1.8.2	Instrumentation and Equipment for Special Techniques . . . . .	98
5.2	Methods . . . . .	99
5.2.1	RNA Preparation and Microscale Thermophoresis . . . . .	99
5.2.1.1	RNA Precipitation . . . . .	99
5.2.1.2	Denaturing Polyacrylamide Gel Electrophoresis (PAGE) . . . . .	99
5.2.1.3	Non-Denaturing Polyacrylamide Gel Electrophoresis (PAGE) . . . . .	99
5.2.1.4	PAGE Gel Elution . . . . .	100
5.2.1.5	RNA Preparation by <i>in vitro</i> Transcription . . . . .	100
5.2.1.6	RNA Preparation by Splint Ligation . . . . .	100
5.2.1.7	Total RNA Extraction from HeLa and HEK Cells . . . . .	101
5.2.1.8	Size Fractionation of HeLa and HEK total RNA . . . . .	101
5.2.1.9	Isolation of Specific RNA Molecules . . . . .	102
5.2.1.10	RNA Hybridization . . . . .	102
5.2.1.11	Microscale Thermophoresis-based RNA Quantification . . . . .	104
5.2.2	Liquid Chromatography-Tandem Mass Spectrometry (LC-MS/MS) . . . . .	105
5.2.2.1	RNA Sample Preparation . . . . .	105
5.2.2.2	High Performance-Liquid Chromatography . . . . .	106
5.2.2.3	Mass Spectrometry . . . . .	107
5.2.2.4	Data analysis . . . . .	108
	<b>List of Publications</b>	<b>111</b>
	<b>Bibliography</b>	<b>113</b>
	<b>A Appendix</b>	<b>135</b>
	<b>Curriculum Vitae</b>	<b>151</b>



# List of Figures

1.1	Secondary structure of tRNAs and codon-anticodon interactions . . . . .	2
1.2	Regulation of tRNA levels in stress response . . . . .	3
1.3	<i>S. cerevisiae</i> wobble U34 modifications . . . . .	8
1.4	Formation of mcm <sup>5</sup> s <sup>2</sup> U in <i>S. cerevisiae</i> . . . . .	8
1.5	Concept of Modification Tunable Transcripts (MoTT) . . . . .	11
1.6	Challenges in tRNA quantification . . . . .	13
1.7	LC-MS/MS analysis of nucleosides by DMRM and NLS . . . . .	17
1.8	LC-MS/MS analysis of nucleosides by product ion and pseudo-MS <sup>3</sup> scans . . . . .	18
1.9	The MALAT1-masRNA system . . . . .	20
1.10	Setup and readout of microscale thermophoresis experiments . . . . .	23
3.1	Overview: MST-based RNA quantification protocol . . . . .	33
3.2	MST of <i>in vitro</i> transcribed tRNA <sup>Met</sup> (MAU) . . . . .	34
3.3	Non-denaturing PAGE of <i>in vitro</i> transcribed tRNA <sup>Met</sup> (MAU) . . . . .	35
3.4	Influence of the annealing step on the MST measurement . . . . .	35
3.5	Quantification of tRNA <sup>Met</sup> (MAU) in total tRNA . . . . .	36
3.6	Comparison of native and unmodified tRNA <sup>Met</sup> (MAU) . . . . .	37
3.7	<i>S. cerevisiae</i> tRNA <sup>Arg</sup> (1CU) . . . . .	38
3.8	MST of native and unmodified tRNA <sup>Arg</sup> (1CU) . . . . .	39
3.9	Non-denaturing PAGE of tRNA <sup>Arg</sup> (1CU) . . . . .	40
3.10	Quantification of 23 <i>S. cerevisiae</i> tRNAs . . . . .	42
3.11	Technical and biological reproducibility . . . . .	43
3.12	Long-term and strain-overlapping reproducibility . . . . .	44
3.13	Overview of the biological applications . . . . .	45
3.14	Application 1: Growth temperature influence on tRNA levels . . . . .	46
3.15	Application 2: MST fluorescence time traces . . . . .	48
3.16	Application 2: Binding curves . . . . .	48
3.17	Application 2: Overview of the quantification results . . . . .	49
3.18	Application 2: Comparison of double mutants and wildtype . . . . .	49
3.19	Application 2: Heat shock induced changes in tRNA abundances . . . . .	51
3.20	Application 3: PaT killer toxin-mediated cleavage of tRNA <sup>Gln</sup> (3UG) . . . . .	51
3.21	Binding of the polyT-DNA probes to polyadenylated RNA . . . . .	53
3.22	Fluorescence time traces of the polyT DNA probes . . . . .	54
3.23	Influence of PolyT DNA probe length . . . . .	55

---

3.24	Binding in dependence of polyA tail and polyT probe length . . . . .	56
3.25	PolyA measurement in total RNA . . . . .	57
3.26	Effect of sample impurities . . . . .	58
3.27	Overview: Isolation of single (t)RNAs . . . . .	61
3.28	PAGE analysis of isolated, native tRNA <sup>Arg</sup> (1CU) . . . . .	62
3.29	MST-based monitoring of the success of tRNA <sup>Arg</sup> (1CU) isolation . . . . .	63
3.30	Control experiments employing mascRNA <i>in vitro</i> transcript . . . . .	65
3.31	Test isolation of <i>in vitro</i> -transcribed mascRNA . . . . .	66
3.32	PAGE analysis of isolated mascRNA . . . . .	67
3.33	LC-MS/MS analysis of wobble U34 modifications . . . . .	70
3.34	Wobble U34 modifications in $\Delta$ elp3 and $\Delta$ uba4 mutants . . . . .	71
3.35	Neutral loss scan of isolated tRNAs . . . . .	73
3.36	Extracted ion chromatograms of $\Psi$ , D and ncm <sup>5</sup> U . . . . .	74
3.37	Analysis of the fragmentation pattern of queuosine . . . . .	76
3.38	Queuosine incorporation in <i>S. pombe</i> RNA . . . . .	76
3.39	LC-MS/MS-based detection of Q derivatives . . . . .	78
3.40	Pseudo-MS <sup>3</sup> spectra of labeled uracil and guanine . . . . .	80
A.1	Fluorescence time traces of native tRNA <sup>Met</sup> (MAU) ( <i>E. coli</i> ) . . . . .	135
A.2	Detection of tRNA <sup>Met</sup> (MAU) in total tRNA by PAGE . . . . .	136
A.3	MST measurement of native tRNA <sup>Arg</sup> (1CU) at pH 6.5 . . . . .	137
A.4	Hybridization conditions for MST measurement of tRNA <sup>Arg</sup> (ICG) . . . . .	137
A.5	Fluorescence time traces and binding curves of <i>S.cerevisiae</i> tRNAs - 1 . . . . .	139
A.6	Fluorescence time traces and binding curves of <i>S.cerevisiae</i> tRNAs - 2 . . . . .	140
A.7	Fluorescence time traces and binding curves of <i>S.cerevisiae</i> tRNAs - 3 . . . . .	141
A.8	Consistency of tRNA abundances in <i>S. cerevisiae</i> strains . . . . .	142
A.9	Quantification of 5S rRNA in <i>E. coli</i> total tRNA . . . . .	145
A.10	Isolation of <i>E. coli</i> tRNA <sup>Met</sup> (MAU) and 5S rRNA . . . . .	146
A.11	MST measurement of <i>in vitro</i> transcribed mascRNA . . . . .	147
A.12	Enrichment of mascRNA confirmed by RNA-Seq . . . . .	148
A.13	Pseudo-MS <sup>3</sup> spectra of unlabeled uracil and guanine . . . . .	149
A.14	Pseudo-MS <sup>3</sup> spectra of unlabeled and labeled cytosine and adenine . . . . .	150



## List of Tables

3.1	Peak assignment: NLS of tRNA <sup>Lys</sup> (3UU) and tRNA <sup>Pro</sup> (NGG) . . . . .	75
5.1	Sequences of DNA probes used for quantification and isolation of <i>Saccharomyces cerevisiae</i> tRNAs . . . . .	93
5.2	Additional probes for MST measurements . . . . .	94
5.3	Oligonucleotides used for IVT and splint ligation . . . . .	95
5.4	Gradient 1 for LC-MS/MS analysis . . . . .	106
5.5	Gradient 2 for LC-MS/MS analysis . . . . .	106
5.6	General settings of the mass spectrometer . . . . .	107
5.7	MS/MS parameters: modified uridines and queuosine . . . . .	108
5.8	MS/MS parameters: Product ion scan of queuosine . . . . .	108
5.9	MS/MS parameters: pseudo-MS <sup>3</sup> scan of labeled nucleobases . . . . .	109
A.1	EC <sub>50</sub> values of <i>S. cerevisiae</i> tRNA species, application 1 . . . . .	138
A.2	EC <sub>50</sub> values determined for <i>S. cerevisiae</i> tRNA <sup>Lys</sup> (3UU), application 2 . . . . .	143
A.3	EC <sub>50</sub> values determined for <i>S. cerevisiae</i> tRNA <sup>Pro</sup> (NGG), application 2 . . . . .	143
A.4	EC <sub>50</sub> values determined for <i>S. cerevisiae</i> tRNA <sup>Gln</sup> (3UG), application 2 . . . . .	143
A.5	EC <sub>50</sub> values determined for <i>S. cerevisiae</i> tRNA <sup>His</sup> (GUG), application 2 . . . . .	144
A.6	EC <sub>50</sub> values and hybridization ratios determined for the polyT-DNA probes to the <i>in vitro</i> -transcribed mRNAs . . . . .	144



## Abbreviations

A	Adenosine
ac <sup>4</sup> C	4-Acetylcytidine
ATP	Adenosine triphosphate
BSA	Bovine serum albumine
C	Cytidine
cDNA	Complementary DNA
CTP	Cytidine triphosphate
CVB3	Coxsackievirus B3
D	Dihydrouridine
Deg1 (Pus3)	DEpressed Growth rate (tRNA:Pseudouridine Synthase 3)
DMRM	Dynamic Multiple Reaction Monitoring
DNA	Deoxyribonucleic Acid
dNTP	Deoxynucleotide triphosphate
EC <sub>50</sub>	Half maximal effective concentration
<i>E. coli</i>	<i>Escherichia Coli</i>
EIC	Extracted Ion Chromatogram
Elp	Elongator (complex)
ESI	Electrospray Ionization
FBS	Fetal bovine serum
FL-PCR	Four-Leaf Clover qRT-PCR
G	Guanosine
GTP	Guanosine triphosphate
HPLC	High Performance-Liquid Chromatography
I	Inosine
i <sup>6</sup> A	N <sup>6</sup> -Isopentenyladenosine
IVT	In Vitro Transcript
K <sub>D</sub>	Dissociation Constant
Kti	Killer toxin insensitivity (proteins)
LC-MS/MS	Liquid Chromatography-Tandem Mass Spectrometry
lncRNA	long non-coding RNA
m <sup>1</sup> A	1-Methyladenosine
m <sup>6</sup> A	6-Methyladenosine
MALAT1 RNA (NEAT2)	Metastasis-Associated Lung Adenocarcinoma Transcript 1 (Nuclear-enriched abundant transcript 2)
masRNA	MALAT1-associated small cytoplasmatic RNA
Men $\beta$ RNA (NEAT1)	Multiple Endocrine Neoplasia $\beta$ RNA
m <sup>1</sup> G	1-Methylguanosine
m <sup>2</sup> G	N <sup>2</sup> -Methylguanosine
mcm <sup>5</sup> U	5-Methoxycarbonylmethyluridine
mcm <sup>5</sup> s <sup>2</sup> U	5-Methoxycarbonylmethyl-2-thiouridine
MELAS	Mitochondrial Encephalopathy, Lactic Acidosis and Stroke-like episodes
MERRF	Myoclonus Epilepsy associated with Ragged-Red Fibers
MoTT	Modification tunable transcript

## Abbreviations

---

mRNA	Messenger RNA
ms <sup>2</sup> t <sup>6</sup> A	2-Methylthio-N <sup>6</sup> -threonylcarbamoyladenosine
MS(/MS)	(Tandem) Mass Spectrometry
MST	MicroScale Thermophoresis
mt-tRNA	Mitochondrial tRNA
N	RNAMod abbreviation for an unknown modified uridine
NAT	Natural Antisense Transcript
ncm <sup>5</sup> U	5-Carbamoylmethyluridine
Ncs2/6	Need Cla4 to survive 2/6
NLS	Neutral Loss Scan
nt	Nucleotides
PAGE	Polyacrylamide Gel Electrophoresis
PaT	<i>Pichia Acaciae</i> killer toxin
PBS	Phosphate buffered saline
PCR	Polymerase Chain Reaction
PEG	Polyethylene Glycol
qRT-PCR/RT-qPCR	Quantitative Reverse Transcription-Polymerase Chain Reaction
QQQ	Triple Quadrupole Mass Spectrometer
RNA	Ribonucleic Acid
RNA-Seq	High throughput (deep) sequencing of RNA, <i>e.g.</i> Illumina Sequencing
rRNA	Ribosomal RNA
RTD	Rapid tRNA decay pathway
<i>S. cer.</i>	<i>Saccharomyces cerevisiae</i>
<i>S. pombe</i>	<i>Schizosaccharomyces pombe</i>
SSC	Saline-sodium citrate
S <sub>T</sub>	Soret coefficient
s <sup>2</sup> U	2-Thiouridine
T	Thymidine
t <sup>6</sup> A	N <sup>6</sup> -Threonylcarbamoyladenosine
TALAM1	Natural antisense transcript of MALAT1
Tcd1	tRNA Threonylcarbamoyladenosine Dehydratase
TIC	Total Ion Current
T-Jump	Temperature Jump
Tris	Tris(hydroxymethyl)-aminomethan
Trm	tRNA-Methyltransferase
tRNA	Transfer RNA
Tum1	Thiouridine modification protein 1
U	Uridine
Uba4	E1-like activator protein of Urm1
Um	2'-O-Methyluridine
Urm1	Ubiquitin-like modifier-1
UTP	Uridine triphosphate
Ψ	Pseudouridine
3	RNAMods abbreviation for mcm <sup>5</sup> s <sup>2</sup> U

# 1 Introduction

## 1.1 Transfer RNA: Dynamics of abundance and modifications

Transfer RNAs (tRNA) were first discovered as amino-acid delivering molecules in 1958 ([1], reviewed in [2]). They function as adaptor molecules during protein translation by base-pairing to the respective codon on the messenger RNA (mRNA) *via* their anticodon sequence and providing their cognate amino acid for protein synthesis. RNA polymerase III is responsible for transcription of tRNAs in form of tRNA precursor molecules, from which the final mature tRNAs are generated by 5'- and 3'-end processing, intron splicing, 3'-CCA-addition and nucleoside modification (reviewed in [3, 4]). Typically, tRNAs form a cloverleaf-like secondary structure consisting of the acceptor stem, the anticodon loop as well as the D- and T-loops, resulting in a L-shaped 3D-structure [5] (see figure 1.1). Remarkably, tRNAs usually contain a high proportion of modified nucleosides performing various functions in tRNA biology (reviewed in [6–8]). The correct amino acids corresponding to the tRNAs anticodon sequences are attached to the acceptor stem at the 3'-CCA end of tRNAs *via* an ester bond between the 2'- or 3'-OH of the terminal adenosine and the carboxy-group of the amino acid, yielding the charged aminoacyl-tRNA. This nongeneric charging of tRNA molecules is accomplished by specific aminoacyl-tRNA synthetases, which thus ensure the adequate translation of the genetic code (reviewed in [9, 10]). Altogether 61 different codons (plus 3 stop codons) present in mRNAs decode the 20 different amino acids required for protein synthesis, however, as certain tRNAs can decode more than one codon by wobble base pairing between position 34 of their anticodon and the third base of the codon (wobble hypothesis [11], see figure 1.1, inlet), in total less than 61 tRNA isoacceptors are required. Isoaccepting tRNAs are charged with the same amino acid, but have different anticodon sequences and thus bind to synonymous (identical amino acid decoding) mRNA codons. The pool of different tRNAs is further enlarged by the presence of isodecoders, which bear both the same amino acid and anticodon sequence, but differ in the remaining tRNA sequence and thus might not be functionally redundant [12]. The levels of tRNA isoacceptors were shown to vary considerably in various unicellular organisms [14–16], across different human tissues [17] and in different cellular states [18]. On the mRNA side, synonymous codons (encoding the same amino acid but pairing to different isoacceptor tRNAs) are not randomly used in transcripts, a phenomenon described as codon usage bias, and the choice of preferentially used codons within a transcript influences the efficiency of its expression [19, 20]. Remarkably, tRNA modifications, especially those present at the wobble position 34 and which thus influence the codon-anticodon interaction directly, were shown to be connected to the codon usage bias particularly of stress response genes and to potentially participate considerably in regulation of

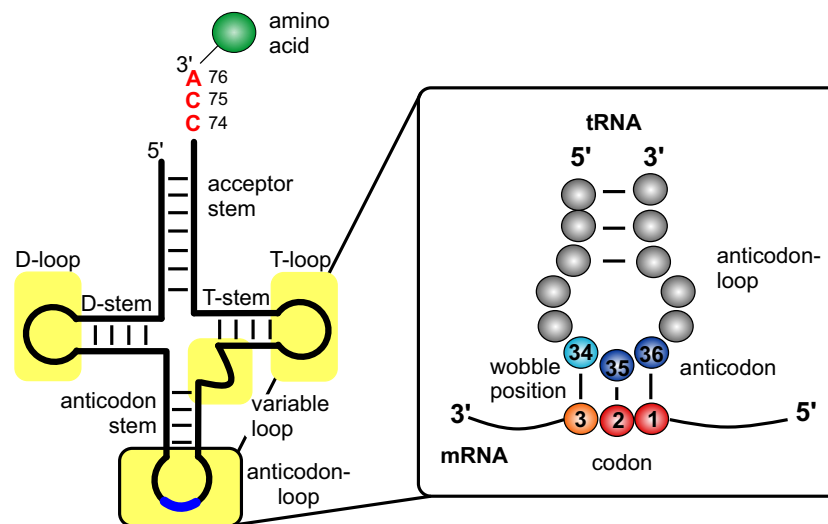


**Figure 1.1: Secondary structure of tRNAs and codon-anticodon interaction** Schematic depiction of the typical cloverleaf secondary structure of a tRNA, the different structural elements are indicated (adapted from [13]). The inset displays the codon-anticodon interaction between mRNA and tRNA, wobble base pairing is possible between the third base of the codon and position 34 in the anticodon loop. Anticodon and codon nucleotides are marked in blue and red, respectively, position 34 of the tRNA in bright blue and the third codon of the mRNA in orange.

translation [21–25]. Hereby, all three aspects, codon usage bias, tRNA abundance and tRNA modification, influence efficiency and speed of translation along with other crucial factors like tRNA charging ([19–23, 26–29], reviewed in [13, 24, 25, 30, 31]). For example, clusters of codons which are decoded by low abundant tRNA isoacceptors were shown to temporarily slow down translation and hereby to enable correct co-translational protein folding and to prevent protein aggregation [32, 33]. For unicellular organisms like *E. coli* and *S. cerevisiae*, preferred codon usage was shown to correlate well with the abundances of the respective isoacceptors, especially when taking nucleoside modifications at the wobble position 34 (modification of U34 and A34) into account [14, 15, 34]. Remarkably, considering A-to-I editing at position 34 enabled an improvement of the otherwise rather poor tRNA abundance-codon usage correlation in eukaryotes [35]. A codon usage-tRNA abundance correlation, however less distinct and only for highly expressed, tissue-specific genes, was also detected in several human tissues [17]. A study addressing codon usage and tRNA gene expression at different developmental stages of mouse liver and brain furthermore revealed that the tRNA pool is tightly adjusted throughout development to accord with the codon usage of expressed genes [36]. In addition, diverse but specific signatures of codon usage, tRNA abundance pattern and expressed proteins were described for proliferating and differentiated cells, demonstrating a close connectivity of concerted changes on both tRNA and mRNA levels for different cellular states [18]. Those studies indicate that there is indeed a connection of the by codon usage determined transcriptional “demand” and the tRNA “supply” [18, 20].

### 1.1.1 Dynamics of tRNA Levels

#### 1.1.1.1 Regulation of tRNA Abundance

In line with the above mentioned, recent research indicates that tRNA isoacceptor levels are strictly regulated and affect both expression of specific groups of mRNAs and global translation efficiency, which is, for example, highly relevant in stress response as well as various human diseases (reviewed in [13, 31, 37]). The levels of single tRNAs are regulated both transcriptionally and post-transcriptionally by multiple mechanisms (figure 1.2, reviewed in [3, 13, 31, 37]), which is especially important under stress conditions, when a fast adaptation of gene expression in order to deal with the stress-induced changes is required [38]. Transcription of tRNAs by RNA polymerase III [39, 40] is tightly regulated in response to variable stress conditions (reviewed in [41]), for example by the conserved protein Maf1, which represses polymerase III function under nutrient stress and other treatments [42] and thus decreases tRNA transcription. Posttranscriptionally, regulation of tRNA abundances is accomplished *via* several mechanisms [13, 31], however, not all of the ways leading to a functional inactivation of tRNA are accompanied by an actual decrease of the tRNA abundance. For example, withdrawal of amino acids causes an accumulation of tRNAs in the nucleus, which leads to a repression of translation [43, 44], nevertheless, the actual tRNA abundances inside the cell are not changed. Similarly, under oxidative stress, the ribonuclease angiogenin reversibly removes the 3'-CCA ends from mature tRNAs

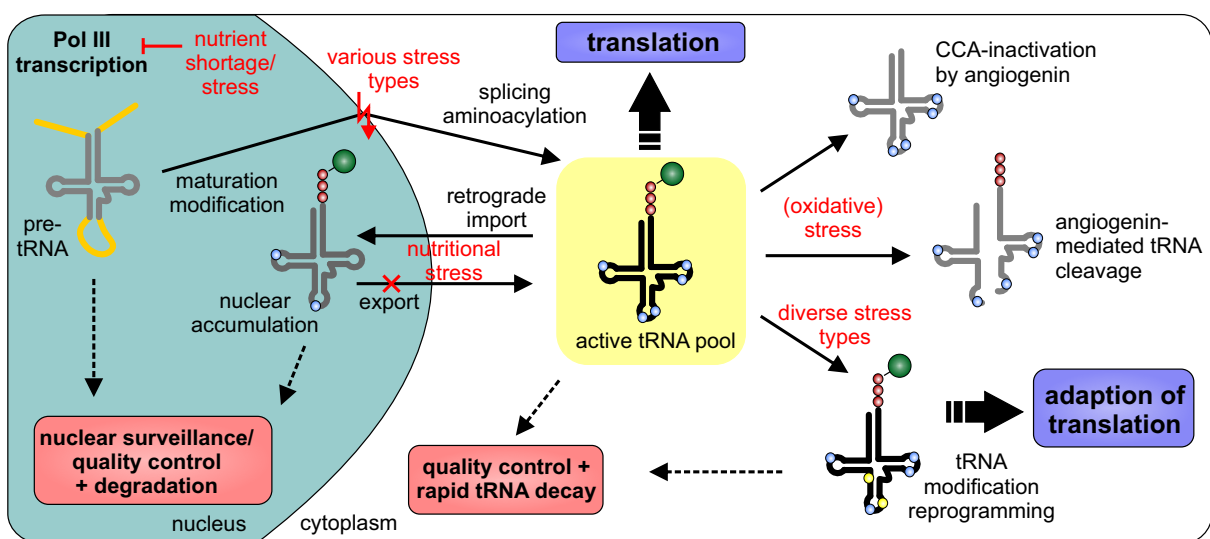


**Figure 1.2: Regulation of tRNA levels in stress response** Simplified depiction of mechanisms influencing tRNA abundance and their manipulation by various stress conditions (adapted from [13, 37]). Only stress-response mechanisms with potential impact on translationally active tRNAs are shown. Transcription and maturation of tRNAs in the nucleus can be hindered under, for example, nutrient stress, which also causes an accumulation of mature tRNAs in the nucleus, thus depleting translationally active tRNAs from the cytoplasm. Under oxidative stress, angiogenin cleaves the CCA-end of tRNAs, as well as certain tRNAs in their anticodon loop resulting in tRNA halves. In response to variable stresses, tRNA modifications dynamically change, which results in an adaptation of translation and may possibly lead to degradation of certain tRNAs by the rapid tRNA decay pathway, which acts in tRNA quality control of mature tRNAs. In the nucleus, the nuclear surveillance pathway recognizes and degrades improperly processed pre-tRNAs.

and thus leads to their transcriptional deactivation [45]. Furthermore, angiogenin is capable of cleaving certain tRNAs in their anticodon loop to form tRNA halves (tiRNA) [46] as response to different stresses, of which the 5'-tiRNAs (tRNA-derived stress-induced RNAs) were shown to inhibit protein translation [46]. Oxidative stress, amongst other stress influences, additionally increases the rate of methionine-misacylation of non-Met tRNAs, which is proposed to elevate Met-incorporation into proteins to protect them from reactive oxygen species [47]. Actual tRNA degradation is accomplished by different mechanisms including the rapid tRNA decay pathway (RTD)[48–51] for mature tRNAs, the nuclear RNA surveillance and polyadenylation pathway for precursor tRNAs [52, 53] as well as 3'-CCACCA addition [54] (reviewed in [3, 31, 55]) and might be triggered by (stress-induced [56–58]) changes of tRNA modifications and thus tRNA stability [48–50, 52, 53, 55]. Both RTD and nuclear surveillance pathway mediate the degradation of hypomodified (pre-)tRNA molecules missing certain modified nucleosides [48, 49, 51–53] or of tRNAs carrying mutations that destabilize the tRNA's structure [50]. 3'-CCACCA addition by the CCA-adding enzyme additionally tags tRNAs and tRNA-like small RNAs for degradation if they contain unstable acceptor stems including a 5'-G1G2 sequence pattern [31, 54]. Furthermore, the CCA-adding enzyme distinguishes stable and unstable tRNAs by adding either a single CCA or a CCACCA, respectively, and thus fullfills an important function in tRNA quality control [54, 59]. However, the various degradation pathways cannot be seen as entirely separated mechanisms, as substrates of the RTD pathway were shown to be tagged with either 3'-CCACCA or a short polyA-sequence at the 3'-end [54], indicating that the different pathways complement each other to effectively remove unstable or defective tRNAs. Altogether, numerous mechanisms act together to tightly regulate tRNA levels (and the tRNA's translational activity) under normal and stress conditions to ensure adequate gene expression.

### 1.1.1.2 Abundance of tRNAs and Human Disease

Considering the important influence of tRNA availability on gene expression, deregulation of the abundance of either single or the complete pool of tRNA isoacceptors/decoders can have drastic consequences [60]. Contribution of tRNA-related changes to the development of variable diseases have been discovered (reviewed in [13]) with different underlying mechanisms, including for example mutations in the tRNA sequence or defects in tRNA-maturing or -modifying enzymes [13], some of which directly or indirectly change the abundances of tRNA isoacceptors and are exemplified here. In tumor cells, transcription by RNA polymerase III is often deregulated resulting in elevated levels of its RNA products [61–64]. In line with that, using a tRNA microarray assay, up to 10-fold elevated levels of tRNAs were discovered in breast cancer cell lines as well as in tumor samples. The increase in abundance was more pronounced for particular isoacceptors, showing that the tRNA overexpression in cancer is selective [65]. Interestingly, when grouping the tRNAs for their amino acid type (small, polar, hydrophobic or charged), the extend of overexpression additionally correlated with the chemical properties of the amino acid attached, *e.g.* levels of tRNAs carrying polar or charged amino acids were more strongly elevated in breast cancer cells and tumor samples than those carrying hydrophobic or



small amino acids. Furthermore, in light of the selectivity of the detected tRNA overexpression, the authors suggested a correlation to the codon usage of cancer- and proliferation-related genes to enhance their expression [65]. Such a correlation was also found by Gingold and coworkers by comparing tRNA abundances determined by microassay, codon usage and gene expression in differentiated and proliferating (tumor) cells [18]. Remarkably, most of the in the study investigated cancer cell lines displayed elevated levels of initiator tRNA<sup>Met</sup> [18], and overexpression of initiator tRNA<sup>Met</sup> alone in breast epithelial cell lines led to an increase of cell proliferation and changed the expression of other tRNAs, although the tRNA expression pattern induced did not correlate to the one found in breast cancer cell lines [65, 66]. Recently, elevated levels of initiator tRNA<sup>Met</sup> (measured by qRT-PCR) in carcinoma-associated stromal fibroblasts were shown to promote tumor growth and angiogenesis by modulating the extracellular matrix (ECM) composition to a cell migration-supporting, collagen II-rich form rather than influencing cell growth, proliferation and global protein synthesis directly [67]. Additionally, an increase of the initiator tRNA<sup>Met</sup> in tumor cells, again examined by qRT-PCR, resulted in enhanced cell migration and invasion and thus promotion of metastasis, again without direct effect on cell proliferation and growth, indicating that overexpression of initiator tRNA<sup>Met</sup> promotes cancer progression by specific mechanisms rather than by globally upregulating translation and cell growth [68]. Only recently, both a change in tRNA abundance pattern as well as the direct metastasis-promoting function two specific tRNAs (tRNA<sup>Glu</sup><sub>UUC</sub> and tRNA<sup>Arg</sup><sub>CCG</sub>) were observed in highly metastatic breast cancer cells compared to their non-metastatic parent cells [60]. The increase of these two tRNAs, assessed by a newly developed method combining hybridization and qPCR/high throughput sequencing (compare section 1.2.1), correlated well with the enhanced expression of genes carrying the respective codons and enabled the detection of the EXOSC2 and GRIPAP1 as direct targets of tRNA<sup>Glu</sup><sub>UUC</sub> [60]. Thus, the adaption and modulation of tRNA isoacceptor availability in cancer was proposed to belong to “inducible pathways” in which particular tRNA isoacceptors are specifically upregulated to increase the expression of their direct target transcripts [60]. Additionally to breast cancer, elevated tRNA levels were also observed, using a tRNA-specific microarray, in multiple myeloma plasma cells [69], in which the charging of especially hydrophobic amino acids was reduced by treatment with a proteasome inhibitor [69]. Remarkably, an increasing number of mutations in mitochondrial tRNA genes have been shown to contribute to the outbreak of mitochondrial diseases *via* various mechanisms, which include those that result in changes in charging, processing, stability and steady-state levels of the affected tRNAs (reviewed for example in [13, 70–73]). In the following, several examples for mutations in mitochondrial tRNA genes that lead to changes in tRNA levels are described. In two patients suffering from combined oxidative phosphorylation (OXPHOS) system deficiencies, mutations in mitochondrial (mt)-tRNA<sup>Arg</sup> or mt-tRNA<sup>Trp</sup> genes, respectively, resulted in a drastic reduction of the stability and steady state levels of the tRNAs affected [74]. Furthermore, in patients with isolated hypertrophic cardiomyopathy, a mutation in the gene of mt-tRNA<sup>Ile</sup> was shown to result in reduced mt-tRNA<sup>Ile</sup> levels, deficiencies in cytochrome c oxidase and respiratory chain defects [75]. Another example for a mitochondria-related disease is a form of maternally inherited hypertension characterized by mutations in mitochondrial

tRNA genes [76, 77]. Depending on the mutation present, levels of mitochondrial mt-tRNA<sup>Ile</sup> or mt-tRNA<sup>Met</sup> were reduced by approximately 40-50 % which resulted in a pronounced reduction of mitochondrial translation, decreased respiratory activity and consequently increased levels of reactive oxygen species. While in case of mt-tRNA<sup>Ile</sup> a A to G mutation in the precursor-tRNA led to an impairment of the RNase P-mediated 5'-processing [76], in mt-tRNA<sup>Met</sup> the responsible mutation was localized directly in the tRNA sequence and exchanged the conserved A37 to G37 [77]. A highly detrimental outcome in form of neonatal death was observed for a mutation that affected the interactions in the D-loop of mt-tRNA<sup>Val</sup> and thus led to the degradation of the tRNA [78]. Those examples exemplify the possibly lethal pathophysiological outcomes of deregulated tRNA abundances and thus the importance of further investigations of tRNA levels. Additionally, for some disease like breast cancer, levels of specific tRNAs or the tRNA expression pattern itself might be suitable as biomarkers [65].

### 1.1.2 Modified Nucleosides in tRNA

As foreshadowed in the above sections, regulation of gene expression under both physiological and stress conditions is influenced by the presence of modified nucleosides in tRNA molecules [21–25] which thus need to be considered along with tRNA abundance and codon usage bias when, for example, analyzing translational adaptation to stress. To date, more than 150 different RNA modifications are known and listed in the MODOMICS database (<http://modomics.genesilico.pl/>) [79]. Typically, tRNAs are subject to extensive posttranscriptional modification and thus carry a considerable number of modified nucleosides at various positions [79, 80]. Depending on their chemical structure and position within a tRNA molecule, tRNA modifications can serve various functions, which mainly affect either the decoding process itself, the correct charging of the tRNA or the tRNA's stability, examples for each case are described below (details are reviewed for example in [3, 6–8, 55, 81]). However, defects regarding single modifications are often tolerated well and only become obvious in combination or under particular stress conditions. Modified nucleosides in the tRNA body rather than the anticodon loop are likely to have an influence on the stability, the correct folding and the susceptibility of the tRNA to degradation [55, 82]. For example, 1-methyladenosine (m<sup>1</sup>A) at position 9 of mt-tRNA<sup>Lys</sup> in human mitochondria was shown to enable the canonical cloverleaf folding [83]. Loss of modified nucleosides can also provoke a tRNA's degradation (compare section 1.1.1.1), as in the case of a combined loss of 4-acetylcytidine (ac<sup>4</sup>C) at position 12 and 2'-O-methyluridine (Um) at position 44, which results in RTD-mediated degradation of two tRNA<sup>Ser</sup> isoacceptors [49]. Another possible function of tRNA modifications is to ensure the correct aminoacylation by functioning as identity determinants or antideterminants for the cognate aminoacyl-tRNA synthetase [6]. For example, modification of C34 in bacterial tRNA<sup>Ile</sup><sub>CAU</sub> to lysidine enables recognition by the isoleucine aminoacyl-tRNA synthetase as well as decoding of AUA codons and simultaneously acts as negative identity determinant for methionine aminoacyl-tRNA synthetase [84]. In *yeast*, inosine at position 34 of tRNA<sup>Ile</sup><sub>AAU</sub> function as positive identity determinant for the isoleucine aminoacyl-tRNA synthetase [85]. Importantly, anticodon-loop modifications at the positions

34 (first nucleotide of the anticodon sequence, compare figure 1.1) and 37 (3'-adjacent to the anticodon) directly influence the tRNA's function in decoding by ensuring translation efficiency and fidelity as well as by preventing misreading and frameshifting (reviewed in [6–8, 86, 87]). Typically, position 37 in the anticodon loop harbors a modified purine, which is often m<sup>1</sup>G in case of an encoded G or a (derivative of) i<sup>6</sup>A or t<sup>6</sup>A in case of an originally encoded A. The m<sup>1</sup>G37 modification, which is considered to be a “primordial” modification due to its presence in all three kingdoms of life, was shown to prevent frameshifting and thus increases translation accuracy [88]. In contrast, the presence of i<sup>6</sup>A affects the decoding process by enhancing translation efficiency and fidelity [89]. At position 34, variable modified nucleosides can be introduced, which directly influence decoding efficiency by base pairing with the third nucleotide of the codon, but also participate in anticodon-loop conformational organization together with those modifications at position 37 [6, 7, 86, 87]. Modifications at U34 are considerably well-investigated, and, due to their importance for the present work, described in more detail below (section 1.1.2.1). The presence of modifications at both positions, 34 and 37, in the anticodon-loop helps, for example, to keep the anticodon loop in an open loop conformation, to promote its stability by base-stacking interactions and to enhance codon-anticodon interactions, as it was shown for ms<sup>2</sup>t<sup>6</sup>A37, Ψ39 and mcm<sup>5</sup>s<sup>2</sup>U34 in the anticodon-loop of human tRNA<sub>UUU</sub><sup>Lys</sup>, which decodes both the cognate codon AAA and the codon AAG by G3•mcm<sup>5</sup>s<sup>2</sup>U34 wobbling [90]. Furthermore, the mcm<sup>5</sup>s<sup>2</sup>U34 modification was proposed to enhance the decoding efficiency of the cognate codon (and the G-ending wobble codon) rather than reducing misreading of the U- and C-ending codons of the split codon box harboring tRNA<sup>Lys</sup> and tRNA<sup>Asn</sup> [91, 92].

### 1.1.2.1 Structure and function of *S. cerevisiae* wobble U34 modifications

In *S. cerevisiae* and other eukaryotic tRNAs, uridines at position 34 of the anticodon loop (U34), are usually modified at C5 and eventually additional positions. Of the 13 tRNAs containing an encoded U34 in *S. cerevisiae*, only tRNA<sub>UAG</sub><sup>Leu</sup> was reported to contain a completely unmodified U34, and Ψ34 is present in tRNA<sub>ΨAΨ</sub><sup>Ile</sup>. In the other U34-carrying tRNAs, U34 is further modified to ncm<sup>5</sup>U (tRNA<sub>UAC</sub><sup>Val</sup>, tRNA<sub>UGA</sub><sup>Ser</sup>, tRNA<sub>UGG</sub><sup>Pro</sup>, tRNA<sub>UGU</sub><sup>Thr</sup>, tRNA<sub>UGC</sub><sup>Ala</sup>), mcm<sup>5</sup>U (tRNA<sub>UCU</sub><sup>Arg</sup>, tRNA<sub>UCC</sub><sup>Gly</sup>), mcm<sup>5</sup>s<sup>2</sup>U (tRNA<sub>UUU</sub><sup>Lys</sup>, tRNA<sub>UUG</sub><sup>Gln</sup>, tRNA<sub>UUC</sub><sup>Glu</sup>) or ncm<sup>5</sup>Um (tRNA<sub>UAA</sub><sup>Leu</sup>) (see figure 1.3, [92]). The formation of the C5-side chains (mcm<sup>5</sup> and ncm<sup>5</sup>) requires all 6 subunits of the elongator complex (Elp1-6), the killer toxin insensitivity (Kti11-14) proteins as well as Sit4, Sap185 and Sap190 [93–95], and the final esterification step in the biosynthesis of mcm<sup>5</sup>U is catalyzed by the tRNA methyltransferase 9 (Trm9) in complex with the zinc finger protein Trm112 [96–98]. Introduction of the sulfur group into mcm<sup>5</sup>s<sup>2</sup>U requires the Urm1 pathway including the sulfur carrier Urm1 (Ubiquitin-like modifier 1), its E1-like activator protein Uba4, Tum1 (Thiouridine modification protein 1) as well as Ncs2/Ncs6 (Need Cla4 to survive 2/6) which finally thiolate uridine in position 2 [99, 100]. C5-modification and 2-thiolation might occur at least partly independent of each other, as *elp3* mutants accumulate s<sup>2</sup>U34 and *uba4* mutants are able to generate the n/mcm<sup>5</sup> side chain [93, 101, 102] (compare section 3.3.1). However, in some studies a dependency of an efficient 2-thiolation on the presence of a previously introduced C5-side

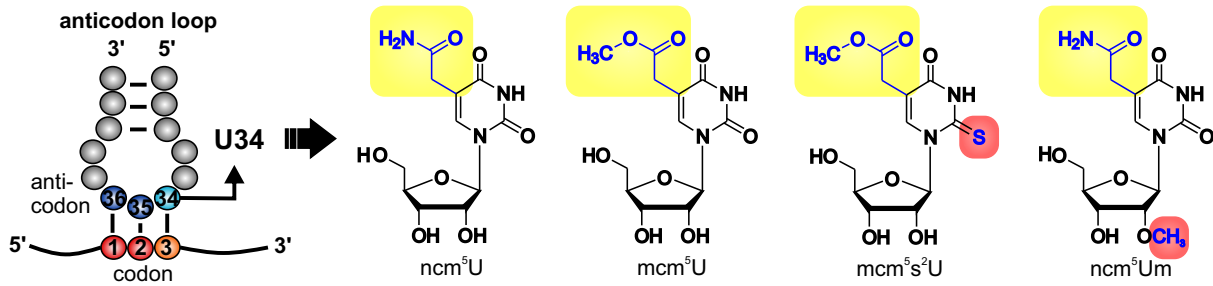


**Figure 1.3: *S. cerevisiae* wobble U34 modifications** Structures of the four wobble U34 modifications  $ncm^5U$ ,  $mcm^5U$ ,  $mcm^5s^2U$  and  $ncm^5Um$  occurring in *S. cerevisiae* cytosolic tRNA, which interact with the third codon nucleotide. Adapted from [79].

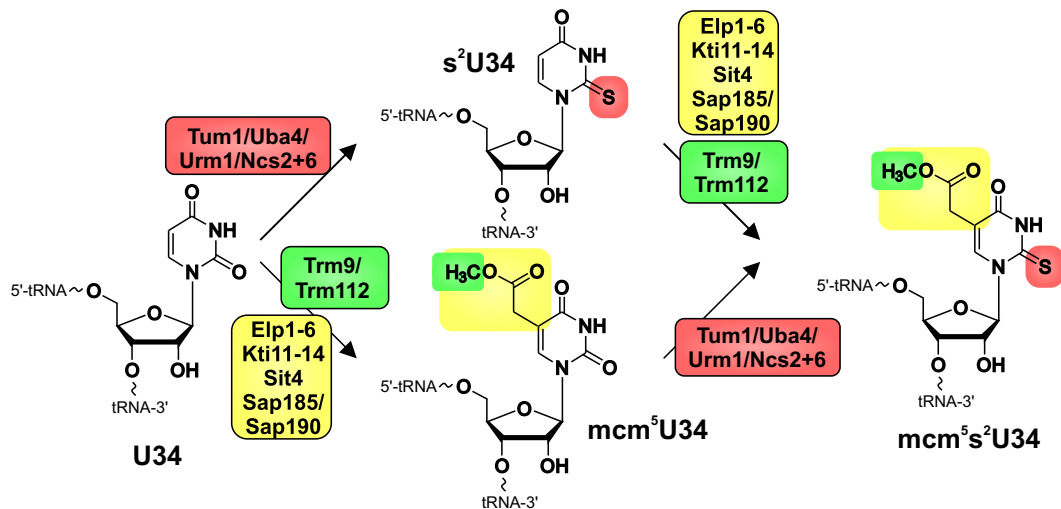


**Figure 1.4: Formation of  $mcm^5s^2U$  in *S. cerevisiae*** Possible pathways for  $mcm^5s^2U34$  formation, the introduction of the C5-side chain and 2-thiolation can occur at least partly independent of each other [93, 102]. The  $mcm^5$  side chain is generated by the elongator complex (Elp1-6), Kti11-14 and Sit4, Sap185 and Sap190 as well as the complex of Trm9 and Trm112, the later catalyzes the final esterification step. 2-Thiolation is accomplished by the Urm1 pathway (Tum1/Uba4/Urm1/Ncs2/Nsc6). Adapted from [21, 102].

chain modification has been reported [100, 103]. The schematic mechanism of  $mcm^5s^2U34$  formation is exemplarily depicted in figure 1.4. Notably, the  $mcm^5s^2U34$  containing tRNAs as well as  $mcm^5U34$ -carrying  $tRNA_{UCU}^{Arg}$  and  $ncm^5Um$ -bearing  $tRNA_{UAA}^{Leu}$  all occur in split codon boxes [92], where the two pyrimidine-ending codons decode another amino acid, indicating that the wobble U34 modifications are required for binding and thus decoding of the cognate purine-(A- and G-)ending codons by at the same time preventing decoding of the non-cognate pyrimidine-ending codons [104, 105]. In contrast, the  $ncm^5U34$  modifications occur in family codon boxes, in which all 4 (or 3) codons decode the same amino acid. Johansson *et al.* [92] determined the *in vivo* decoding properties of *S. cerevisiae* wobble U34 modifications, demonstrating that the  $mcm^5$ ,  $mcm^5s^2$  and  $ncm^5$  moieties at U34 improve decoding of the G-ending codons, and that the main function of the  $mcm^5s^2U34$  modification is to improve decoding of the A-ending codons, for which both modification sites ( $s^2$  and  $mcm^5$ ) are required. Remarkably, the  $ncm^5U34$  modification was reported to be incapable of preventing the interaction with

pyrimidine-ending codons, possibly indicating an important difference between the decoding properties of  $mcm^5U34$  and  $ncm^5U34$  [92]. In line with the requirement for efficient decoding of their cognate codons, the U34 modifications can also play important roles in the formation of a canonical, translationally active anticodon-loop structure together with additional anticodon-loop modifications [90, 106]. Furthermore, both the  $mcm^5$  and  $s^2$  groups of  $tRNA_{UUU}^{Lys}$ ,  $tRNA_{UUG}^{Gln}$  and  $tRNA_{UUC}^{Glu}$  are required for efficient binding of the tRNAs to the ribosomal A-site and for proper decoding of AAA, CAA and GAA codons and thus translation of mRNAs enriched in those codons [107]. Loss of the  $mcm^5s^2U34$  modification by deletion of Ncs2 and/or Elp6 has been shown to result in ribosomal pausing and hereby delayed translation of AAA and CAA codons as well as in accumulation of protein aggregates and proteotoxic stress, which was proposed to be the responsible factor causing the overall stress sensitivity of the mutants [28]. Translation errors in form of amino acid misincorporations and frameshifting as well as an activation of protein stress pathways have also been linked to the translational infidelity observed in Trm9 mutant cells [108]. However, using the Trm9 mutant model, in which the  $mcm^5$  side chain formation is impaired, a decrease of translation efficiency specifically at AGA and GAA codons (decoded by  $tRNA_{UCU}^{Arg}$  and  $tRNA_{UUC}^{Glu}$ ) was described, resulting in a drop of translation of specific transcripts enriched in those codons and finally in an alteration of the translational machinery and certain stress phenotypes (see section 1.1.2.2, [21, 108]). Thus, phenotypes caused by defects in the wobble U34 modifications might be due to both specific alterations of the translation of codon-biased transcripts and a more global defect in protein homeostasis. The phenotypes detectable in *S. cerevisiae* mutants deficient in either one of the Elp subunits or of components of the Urm1 pathway include slow growth, zymocin resistance, cell cycle delay and hypersensitivity to various stresses like temperature and drugs like caffeine and rapamycin [91, 102, 109, 110]. Depending on the background *S. cerevisiae* strain, simultaneous loss of both elongator and thiolation pathway components add up to inviability [91] or a synthetic growth defect combined with synergistic effects on stress sensitivity, reduction of protein levels and protein aggregation [28, 102]. Remarkably, the phenotypes as well as the translational delay and protein stress observed in  $mcm^5s^2U34$  deletion strains are (mostly) reversible by overexpression of unmodified  $tRNA_{UUU}^{Lys}$ , eventually aided by  $tRNA_{UUG}^{Gln}$  and  $tRNA_{UUC}^{Glu}$  overexpression, suggesting that  $tRNA_{UUU}^{Lys}$  is the most affected tRNA and that the modification defect reduces the tRNA's ability to decode its cognate codons efficiently [28, 91, 101, 102]. Physiologically, the wobble U34 modifications has been proposed to play a role in cell cycle control, DNA damage and stress response as well as the elongator-associated roles in transcription and exocytosis [101, 103, 111–113]. Remarkably, due to the pleiotropic phenotypes observed in mutants defective in elongator components, diverse functions had originally been allocated to the elongator complex, including roles in transcription elongation, histone acetylation, exocytosis and DNA repair (reviewed in [95]). However, in *S. cerevisiae*, all phenotypes observed could be suppressed by overexpression of  $mcm^5s^2U34$ -carrying tRNAs, indicating that the primary and potentially only relevant function of the elongator complex is the modification of U34 in tRNAs and that the respective phenotypes are caused by impaired translation due the tRNA modification defect [95, 101].

### 1.1.2.2 Functions of tRNA Modifications in the Regulation of Translation and Stress Response

In recent years, the results of several reports indicated a more complex regulatory potential of tRNA modifications in translation, especially during stress response [21, 108], which led to the postulation of a model connecting the dynamic changes of wobble tRNA modifications to codon-specific translation of stress response-related proteins [22, 24, 25]. Such a link between changes in wobble tRNA modifications and stress response at the translational level was observed for *S. cerevisiae* tRNA methyltransferase 9 (Trm9, [96, 98]), which catalyzes the final esterification step in the biosynthesis of the mcm<sup>5</sup> side chain at U34 of several tRNAs, for example tRNA<sub>UCU</sub><sup>Arg</sup> and tRNA<sub>UUC</sub><sup>Glu</sup>, hereby enhancing their interaction with AGA and GAA codons. Loss of Trm9 and thus mcm<sup>5</sup>U34 was shown to result in translation infidelity, amino acid misincorporation and protein stress [108]. The mcm<sup>5</sup>U34 and mcm<sup>5</sup>s<sup>2</sup>U34 modifications of tRNA<sub>UCU</sub><sup>Arg</sup> and tRNA<sub>UUC</sub><sup>Glu</sup>, respectively, were identified to globally regulate translation of transcripts enriched in their cognate codons, AGA and GAA [21]. Remarkably, Trm9-mediated tRNA modification was shown to fulfill important functions in cell cycle regulation and DNA damage response by positively regulating, for example, the translation of ribonucleotide reductase subunits (RNR) in a codon-specific manner, as the respective transcript displays a codon bias concerning the AGA codon recognized by mcm<sup>5</sup>U34-modified tRNA<sup>Arg</sup> [111, 112]. Increased levels of RNR are required during S-Phase as well as after DNA damage for DNA synthesis, and this requirement was observed to be accompanied by upregulation of mcm<sup>5</sup>U34 in both situations [111, 112]. Matching those results, loss of Trm9 resulted in a DNA damage-like phenotype with reduced RNR levels [111], allowing the assumption of a model in which Trm9 can codon-dependently promote the expression of transcripts enriched for the respective codon at the level of translation and actively participates in DNA damage response [111, 112]. Of note, the wobble U34 modification mcm<sup>5</sup>s<sup>2</sup>U of tRNA<sub>UUU</sub><sup>Lys</sup>, tRNA<sub>UUG</sub><sup>Gln</sup> and tRNA<sub>UUC</sub><sup>Glu</sup> was shown to become hypomodified (in form of mcm<sup>5</sup>U) at elevated temperature due to a decrease of the 2-thiolation activity of the Urm1 pathway resulting in an impaired decoding of the respective AAA, CAA and GAA codons [57, 58]. Additionally, in *Saccharomyces pombe*, the same wobble U34 modification was required for the effective translation of the AAA-codon-enriched transcript of a stress-related transcription factor under oxidative stress [113]. A similar connection between a tRNA modification at the wobble position and the codon-selective translation of stress-response proteins was found for the Trm4-mediated m<sup>5</sup>C34 modification of tRNA<sub>CAA</sub><sup>Leu</sup>, which was shown to be increased under oxidative treatment allowing enhanced translation of UUG codon-enriched transcripts, for example ribosomal proteins [23, 56]. Notably, analysis of changes of most *S. cerevisiae* tRNA modifications under a variety of stress conditions demonstrated the existence of signature patterns of modification changes for each toxicant group applied, and even indicated a predictive power of the respective pattern concerning the stress type [56, 114]. The above mentioned results, amongst others, demonstrated a link between tRNA modification reprogramming and codon-specific translation of stress-response factors and thus a potentially distinct role of modifications in regulation of stress-induced translation and hereby gave rise

to the concept of MoTTs, “Modification Tunable Transcripts” (see figure 1.5 and [22, 24, 25]). By definition, MoTTs are transcripts that encode proteins critically involved in stress response, display a biased codon usage by an above average use of specific degenerate codons and whose translation is regulated by changes of tRNA modifications at the wobble position 34 [22, 24, 25]. Notably, the MoTT concept can also be linked to the phenomenon of stop-codon recoding occurring during translation of selenocysteine-containing proteins [22, 25].

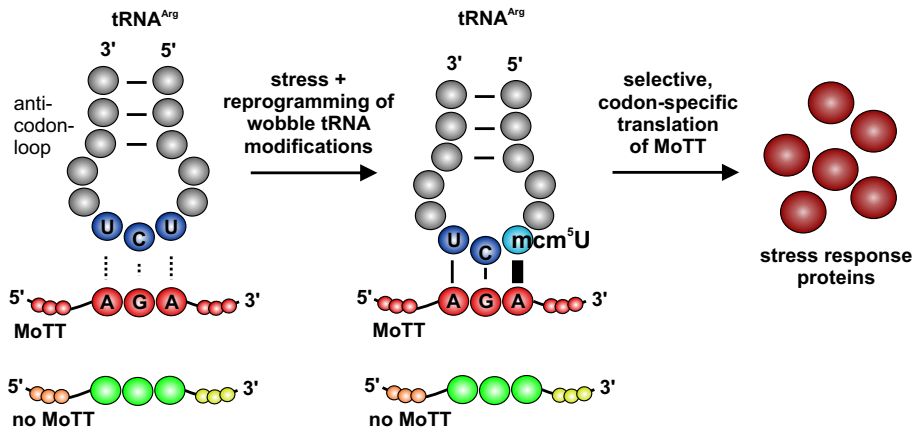


**Figure 1.5: Concept of Modification Tunable Transcripts (MoTT)** Translational regulation of MoTTs using tRNA<sup>Arg</sup>(UCU) as example. Under stress such as DNA damage, modification of U34 of tRNA<sup>Arg</sup> with the mcm<sup>5</sup> side chain by Trm9 is increased and promotes the interaction with AGA codons, for which the respective MoTTs are enriched compared to normal transcripts. Subsequently, the MoTTs are selectively transcribed, resulting in the expression of critical stress-related proteins (adapted from [22, 24, 25]).

### 1.1.2.3 Connections of tRNA modifications with human diseases

Like other characteristic features of tRNA biology, tRNA modification defects have been linked to various human diseases (reviewed in [13, 25, 73, 115]). Perhaps the most prominent examples of an involvement of tRNA modifications in human pathophysiology are the two mitochondrial encephalomyopathies MELAS (Mitochondrial Encephalopathy, Lactic Acidosis and Stroke-like episodes) and MERRF (Myoclonus Epilepsy associated with Ragged-Red Fibers), which are partly caused by mutations in the mt-tRNA genes for mt-tRNA<sup>Leu</sup> and mt-tRNA<sup>Lys</sup> resulting in impaired wobble U34 modification [116–118]. In several MELAS-associated mutations, mt-tRNA<sup>Leu</sup><sub>UUR</sub> lacks 5-taurinomethyluridine ( $\tau\text{m}^5\text{U}$ ) at the wobble position 34 resulting in a drastic reduction of the decoding efficiency of UUG codons by mt-tRNA<sup>Leu</sup><sub>UUR</sub>. Remarkably, the transcript encoding ND6, a protein of the respiratory complex I, displays a high enrichment of UUG codons and thus is translationally repressed, matching the complex I deficiency observed in MELAS patients [119]. Similarly, in MERRF, mt-tRNA<sup>Lys</sup> lacks the wobble U34 modification 5-taurinomethyl-2-thio-uridine ( $\tau\text{m}^5\text{s}^2\text{U}$ ), and the unmodified tRNA was shown to fail to decode its cognate AAA and AAG codons due to complete loss of codon-anticodon binding [120]. Hereby, mitochondrial translation is drastically impaired [120]. Only recently, the NSun3 protein was identified as novel m<sup>5</sup>C RNA methyltransferase, which targets C34 of mt-tRNA<sup>Met</sup> and is required for the subsequent oxidation of m<sup>5</sup>C34 to formylcytidine (fC) [121, 122]. Loss of

NSun3 and hereby of both m<sup>5</sup>C and fC at position 34 of mt-tRNA<sup>Met</sup> was shown to result in an impaired mitochondrial protein synthesis and respiratory chain activity and thus in severe symptoms of mitochondrial disorder in a patient carrying a mutation in the NSun3 gene [121]. Notably, tRNA modifications and their respective tRNA-modifying enzymes were observed to be involved in various human diseases, including neurological disorders, type 2 diabetes and cancer [25, 115], underlining their pathophysiological importance. For example, loss of the tRNA methyltransferase NSun2, required for m<sup>5</sup>C introduction at specific positions, is involved in the onset of several neuro-developmental diseases [123, 124]. In contrast to the neurobiological effects of NSun2 deficiency, overexpression of NSun2 has been connected with cancer [125–127]. Notably, the human homolog of *S. cerevisiae* Trm9 ([128], see section 1.1.2.2), ALKBH8, has been shown to be required for bladder cancer cells to survive, and knockdown of ALKBH8 resulted in cell apoptosis [129]. However, a second potential human Trm9 homolog, human tRNA methyltransferase 9-like protein (hTRM9L), is downregulated in several tumor types, and its re-expression displayed tumor-suppressive effects [130]. Those examples underline the importance to investigate the regulatory mechanism in which tRNA modifications are involved in detail in order better understand their pathophysiological impact.

## 1.2 Analysis of tRNA Levels and RNA Modifications

Considering the obvious impact of both the abundance of single tRNA isoacceptors and their degree of modification especially in the anticodon loop on the regulation of (stress-adapted) translation described in the previous sections, methods for accurate quantification of both tRNA and modification levels are mandatory for the investigation of translational regulation under various stress and pathophysiological conditions. While for tRNA quantification, several methods ranging from traditional northern blotting to more recently developed microarray- and RNA sequencing-based approaches are applicable [131, 132], for exact quantification of tRNA modification levels, especially if changes in levels of a set of modifications are of interest, liquid chromatography-tandem mass spectrometry (LC-MS/MS) is the method of choice. Thus, in the following sections, methods suitable for analyzing tRNA abundances as well as RNA modifications are described, the latter one with emphasis on the LC-MS/MS analysis of modified nucleosides.

### 1.2.1 Quantification of tRNA Abundances

Given the high importance of detailed investigations of tRNA expression patterns, methods that are capable of adequately quantifying tRNA isoacceptors are highly desirable. Several methods have been developed for the quantification of single tRNA species, with some new methods emerging only recently (reviewed in [131, 132]). Difficulties in the quantification of single tRNAs arise from the presence of isoacceptors (tRNAs carrying the same amino acid but differ in their anticodon sequence) and especially isodecoders (tRNAs sharing both loaded amino acid and anticodon sequence), whose sequences often differ only in a few nucleotides and



which are problematic to distinguish. Furthermore, the high portion of modified nucleosides inside a tRNA molecule as well as the complex secondary structure might interfere with tRNA quantification, particularly if the methods rely on reverse transcription or hybridization [17]. These properties, in contrast, have been exploited in both cases for detection of modified nucleosides [133–136]. In addition, next to the mature, translationally active tRNAs, precursor tRNA molecules as well as tRNA-derived fragments might be present in a sample and are possibly detected along with the mature forms. For some applications, the degree of tRNA charging with the cognate amino acid might be of interest as well, thus in such cases methods that allow a distinction of aminoacylated and non-aminoacylated tRNAs are advantageous. The various challenges encountered in tRNA quantification are summarized in figure 1.6. The

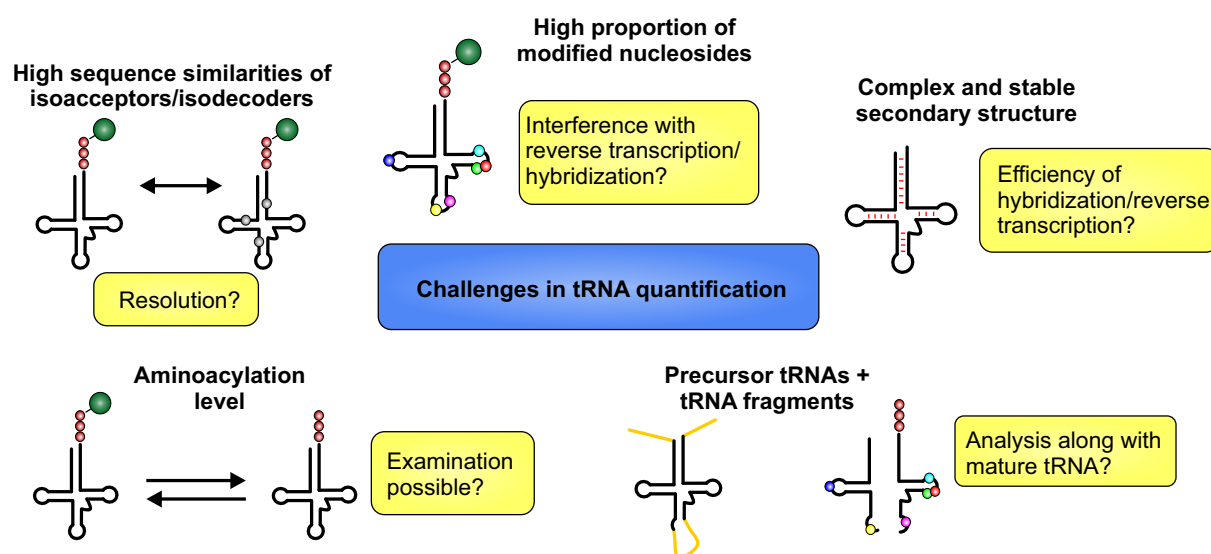


**Figure 1.6: Challenges in tRNA quantification** Quantification of mature tRNAs is hampered by various, tRNA-related features: Both the complex secondary structure and the high prevalence of modified nucleosides might interfere with hybridization- and reverse transcription-based methods. The high sequence similarities along isoacceptors and isodecoders possibly limits the resolution of the detection methods. Furthermore, both precursor tRNA molecules and tRNA fragments might be detected along with their mature counterparts. For some applications, the additional investigation of the degree of aminoacylation might be of interest.

various methods applied for tRNA quantification differ in their ability to distinguish very similar sequences, their sensibility to modified nucleosides and their applicability for high-throughput investigations. In general, the methods rely either on the hybridization of complementary, labeled probes (with or without the combination with electrophoresis) or on reverse transcription into DNA followed by quantification of the cDNA [132]. One of the probably most common ways of quantifying tRNAs are northern blots [137], which rely on electrophoretic separation of RNA with subsequent transfer to a functionalized paper or membrane and hybridization to a labeled DNA probe complementary to the target tRNA. One advantage of northern blot-based quantification is the possibility to distinguish aminoacylated and non-aminoacylated tRNAs [138, 139]. Anyhow, altogether the method is quite laborious and hardly suitable for higher throughput investigations, since only one tRNA at a time can be detected per membrane, and the

reconditioning of the membrane is time-consuming. Another possibility for tRNA quantification making use of gel-based separation is the two-dimensional gel electrophoresis [15, 16, 140], in which tRNAs are separated from each other by two subsequently performed electrophoretic runs varying in their urea content and thus in their denaturing effect on the tRNA's secondary structure. Resulting spots of single tRNA species can afterwards be identified by hybridization with labeled, complementary oligonucleotides. This approach, while working well for *E. coli* tRNAs [15], is less suitable for organisms employing a more diverse set of tRNAs. A further method relying on hybridization to complementary probes is the microarray-based detection of tRNAs [16, 17, 65, 69, 140, 141] applied for relative quantification of tRNA abundances. Here, tRNAs are first ligated to a fluorescently labeled, stem-loop shaped oligonucleotide at the 3'-CCA end, and then hybridized to complementary probes immobilized on a microarray. Using this approach, relative quantification of changes in tRNA abundances between two samples is achieved by using two different fluorescent dyes for labeling. Interestingly, the microarray method was also applied to examine tRNA packaging into human HIV-1, demonstrating that not only tRNA<sup>Lys</sup> isoacceptors [142] but additionally tRNA<sup>Asn</sup> and tRNA<sup>Ile</sup> are selectively incorporated by the virus [140]. A variation of the microarray method allowed the investigation of the degree of the charging of tRNAs by the cognate amino acid [69, 143]. The microarray method is principally well-suitable for high-throughput analysis, however, the discrimination of isoacceptors or isodecoders with very similar sequences (sequence differences of less than 8 nucleotides) is not possible due to cross-hybridization effects [17, 141]. However, a variation of the tRNA microarray allowed the detection of isoacceptors at single nucleotide resolution by adding an ligation step, in which two DNA probes are ligated in a non-enzymatic way by a phosphorothioate linker, templated by the target tRNA [65]. The ligation product, which is only generated for matching nucleotides at the ligation junction, is subsequently purified and finally submitted to hybridization to the microarray. By including the specific ligation step, a discrimination between isoacceptors differing only in few nucleotides is achieved [65]. Next to the tRNA quantification methods relying on specific hybridization, there are a number of methods which depend on a reverse transcription step followed by either quantitative PCR (qRT-PCR) or RNA sequencing (RNA-Seq). However, the high occurrence of modified nucleosides in tRNAs has to be considered, as they may interfere with the reverse transcription step, e.g. by leading to an abortion [132, 144]. Recently, a variation of the traditional qRT-PCR, called four-leaf clover qRT-PCR (FL-PCR), was developed to circumvent this disadvantage [144]. This approach makes use of the ligation of a stem-loop adaptor to the 5'- and 3'-end of mature tRNAs forming the four-leaf clover structure, which is then followed by TaqMan qRT-PCR. The design of the TaqMan probe (complementary to the stem-loop) and primers (corresponding to D- and T-loops) achieves an exclusive amplification of the putatively unmodified acceptor stem of the tRNA and thus limits the influence of modifications on the quantification [144]. In contrast to the use of qRT-PCR, several RNA-Seq-based methods have been developed attempting to address and limit the influence of RNA modifications [132]. Making use of the relatively unmodified 3'-end (covering 30 nt) of tRNAs and adapter ligation in two separate steps (instead of concurrent ligation of both 5' and 3'-adapter), relative changes of *S. cerevisiae* tRNA levels

under cytotoxic stress induced by hydrogen peroxide and methyl methanesulfonate could be investigated without the disturbance by modification-induced transcriptase fall-offs [145]. Another approach, called DM-tRNA-Seq, includes the use of a reverse transcriptase that displays a higher processivity and fidelity (thermostable group II intron reverse transcriptase [146]) and the enzymatic removal of the methylated bases  $m^1A$ ,  $m^3C$  and  $m^1G$ , which are highly abundant in tRNAs and are prone to cause RT stops [147]. Remarkably, the same method was recently shown to be applicable to the identification and quantification of base methylations [148]. A similar approach, called ARM-Seq (AlkB-facilitated RNA methylation sequencing), made use of *E. coli* AlkB to demethylate the above mentioned nucleosides and enabled the detection of methylated small tRNA fragments [149]. However, sequencing-based methods are more suitable for relative quantification of changes in tRNA abundances than for absolute quantification, as both ligation and PCR amplification steps can introduce a bias due to unequal efficiencies for different tRNAs [16, 145]. Recently, a method combining both hybridization and sequencing/PCR was developed, which makes the error prone reverse transcription step dispensable [60]. Using a pair of specific DNA probes for each tRNA that is hybridized to the target tRNA, forms a nick in the anticodon region and is subsequently ligated in a splint ligation reaction, the cDNA of the tRNA is generated. Following purification of the ligation product, quantification can be performed by either sequencing for high throughput, or qPCR for a smaller set of tRNAs (low throughput analysis)[60].

### 1.2.2 Analysis of (t)RNA Modifications

As well, various methods have been developed for identification, detection and in part quantification of modified nucleosides (reviewed in [150, 151]), reaching from rather basic techniques like thin-layer chromatography (TLC, [152, 153]) over high pressure liquid chromatography (HPLC) with or without coupling to mass spectrometry (LC-MS(/MS), [154, 155]) to microarray-based assays [135, 136, 156] and, more recently, approaches relying on RNA sequencing (RNA-Seq) [151]. The comparably new RNA-Seq methods, which are often combined with an (antibody-based) enrichment by immunoprecipitation, offer the advantage of a transcriptome-wide positional mapping of in most cases specific nucleosides, for example, a variety of approaches have been developed for  $m^5C$  (RNA bisulfite sequencing, [157],  $m^5C$ -RIP ( $m^5C$ -RNA immunoprecipitation, [158]), miCLIP (methylation-individual nucleoside resolution crosslinking immunoprecipitation, [159]) and Aza-IP (5-azacytidine-mediated RNA immunoprecipitation, [160]), reviewed in [161]) and  $m^6A$  ( $m^6A$ -/MeRIP-Seq, [162, 163] and PA- $m^6A$ -seq (photo-crosslinking-assisted  $m^6A$  sequencing, [164])) detection and localization. However, all of these approaches display limitations, such as relying on the indirect detection of modified nucleosides, showing restricted resolution and being confined to specific modifications [151, 161]. In contrast, modification analysis by LC-MS/MS offers not only an unambiguous identification of modified nucleosides within an RNA sample, but also allows simultaneous analysis of complete sets of modifications as well as highly precise quantification of modification levels [56, 150, 154, 165–168]. Furthermore, if performed at the level of short oligonucleotides produced by endoribonuclease (RNase)

cleavage, mass spectrometry can be applied for both detection and positional mapping of modifications, albeit not at a transcriptome-wide level ([155], reviewed in [168–170]). For analysis and especially quantification of modified nucleosides in total (t)RNA samples without the need for positional information, as for example required to analyse stress-induced changes of modifications in tRNAs (see section 1.1.2.2), electrospray-ionization based LC-MS/MS using a triple quadrupole mass spectrometer (QQQ) is the method of choice [56, 165–167]. However, the applications of a triple quadrupole mass spectrometer in nucleoside analysis are versatile, depending on the instrument settings and scan modes applied, and due to their importance for the present work, described in more detail below.

### 1.2.2.1 LC-MS/MS Analysis of Modified Nucleosides

LC-MS/MS analysis of RNA modifications at the nucleoside level requires the digestion of the RNA sample to single nucleosides [171], which are usually separated using a polar embedded C18 reverse phase HPLC column [165, 167], yielding a characteristic retention time for each modified nucleoside. The column eluate enters the mass spectrometer, is ionized in the electrospray ionization source using the positive ionization mode and the hereby protonated nucleoside (precursor ion) is detected in the first quadrupole. The precursor ion is subsequently fragmented in the collision cell (also called quadrupole 2), yielding the product ion, which resembles the protonated nucleobase in most cases and is recorded by the second quadrupole (labeled quadrupole 3). The combination of the thus detected, characteristic mass transition between precursor and product ion and the retention time finally allows the exact determination of identity and quantity of the sample's modifications. In most cases, one of two main scan modes is suitable for the analysis of RNA modifications, namely the (dynamic) multiple reaction monitoring (DMRM) and the neutral loss scan (NLS), each of which covers a distinct application range. While the DMRM mode detects predefined modified nucleosides by combining the characteristic retention time and the respective fragmentation pattern of the nucleoside in a highly sensitive manner (figure 1.7, top) and is the method of choice for quantitative analysis [165, 167, 172], its applicability in the search of new modifications is limited. Furthermore, the DMRM mode is not capable of investigating the whole modification landscape of an RNA sample as it only analyzes predefined nucleosides and thus fails to detect any other nucleosides eventually present in the sample. However, that is the predominant application of a neutral loss scan [173], which detects all precursor ions losing predefined neutral moieties during fragmentation (figure 1.7, bottom). As for most nucleosides the fragmentation takes place at the glycosidic bond, cleaving off a neutral ribose moiety, searching for neutral losses of 132 (ribose) and 146 (2'-O-methylribose) Da allows the detection of almost all nucleosides present in a sample, including unknown ones [173]. However, a neutral loss scan is less sensitive compared to the DMRM mode and thus less suitable for quantitative analysis. Furthermore, nucleosides with unusual fragmentation pattern (*e.g.* queuosine, see section 3.3.3) are not detected using the neutral loss scan, as they do not or not only lose a ribose moiety. Achieving highly exact quantification results for modified nucleosides requires, due to variability of the MS signal

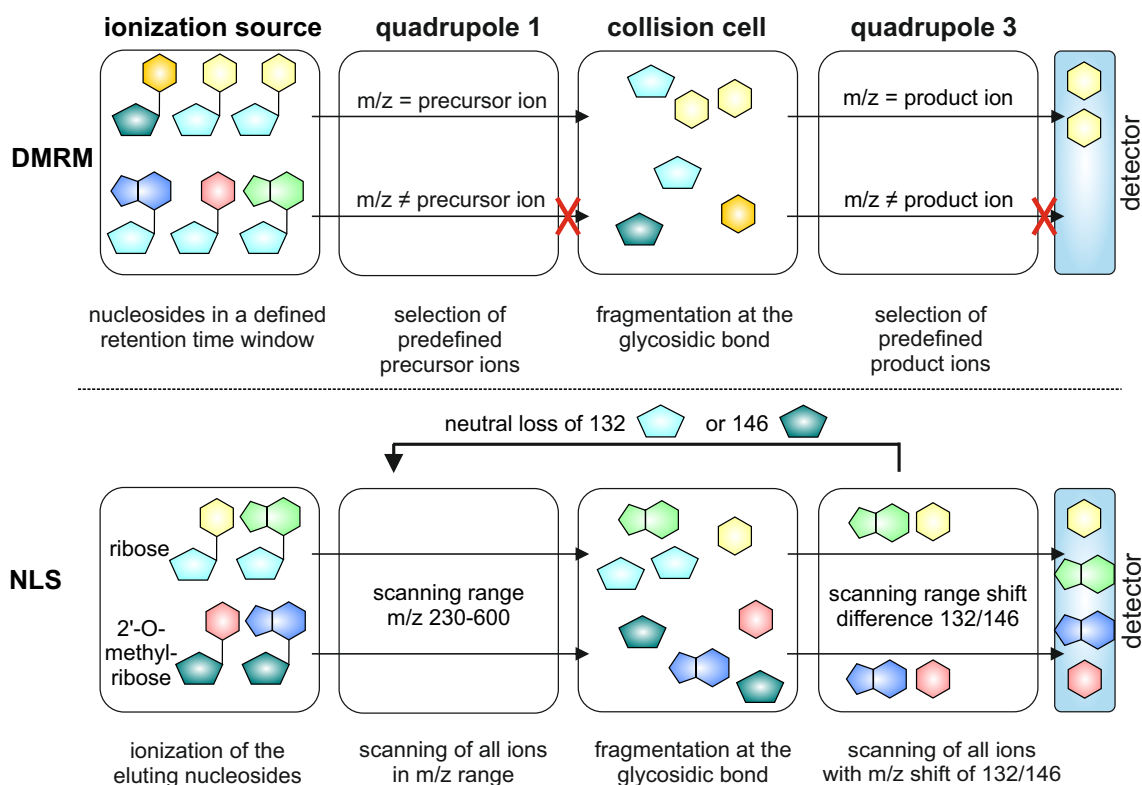


**Figure 1.7: LC-MS/MS analysis of nucleosides by DMRM and NLS** Description of the DMRM mode (top) and NLS (bottom). Nucleosides are ionized in the ionization source and enter the first quadrupole. In the DMRM mode, only defined nucleosides with a specific  $m/z$  value pass the quadrupole (in a configured retention time window) and are fragmented at the glycosidic bond in the collision cell. Quadrupole 2 again filters for a defined product ion, which is collected at the detector. Nucleosides sharing a precursor mass but differing in their product ions can thus be distinguished. The neutral loss scan detects all compounds that lose a defined neutral moiety in the collision cell, which is either a ribose (-132) or a 2'-O-methylribose (-146) in case of nucleosides. Thus, all nucleosides that fragment at the glycosidic bond are detected.

intensities depending on various parameters [167], spiking of an internal standard into the sample. As internal standards, isotope-labeled nucleosides are well suited, either in form of a heavy-atom labeled main nucleoside (e.g.  $^{15}\text{N}$ -deoxyadenosine, [165]) or, even more accurate, by using a labeled counterpart of each modified nucleoside of interest [174–176]. The requirement of the latter option to synthesize a large number of different labeled internal standard can be elegantly bypassed by using total RNA from *Escherischia coli* or *Saccharomyces cerevisiae* grown under  $^{13}\text{C}$ -carbon supply [167]. Although the DMRM mode and the neutral loss scan are powerful tools in the LC-MS/MS analysis of RNA modifications, they require supplementation by other scan types for certain analytic tasks. Nucleosides that do not show the usual cleavage at the glycosidic bond and for which the exact fragmentation pattern is unknown, cannot be analyzed by either NLS or DMRM. In this case, a product ion scan can be performed, which detects the fragmentation products of a predefined precursor ion, which is the protonated nucleoside. Analysis of the product ions then allows the determination of the fragmentation pattern, and thus enables the establishment of a suitable DMRM method for the respective nucleoside. Prerequisite for a product ion scan is the knowledge of the nucleoside's molecular mass, as the

precursor ion has to be defined. Although not a typical application of a triple quadrupole mass spectrometer, it can additionally be used for structural investigations of modified nucleosides in form of pseudo-MS/MS (pseudo-MS<sup>3</sup>) scans [177], which in principle represent a variation of the product ion scan. The fragmentation of the glycosidic bond is here already achieved in the ionization source by applying high fragmentor voltages, and the resulting protonated base is detected in quadrupole 1 in form of the (predefined) precursor ion. In the collision cell, the nucleobase is further fragmented and the ions produced are collected in the second quadrupole. By the additional fragmentation of the base, the structure of the nucleoside of interest can be investigated in more detail. Figure 1.8 describes the set-up of the triple quadrupole and the differences of product ion and pseudo-MS<sup>3</sup> scans.

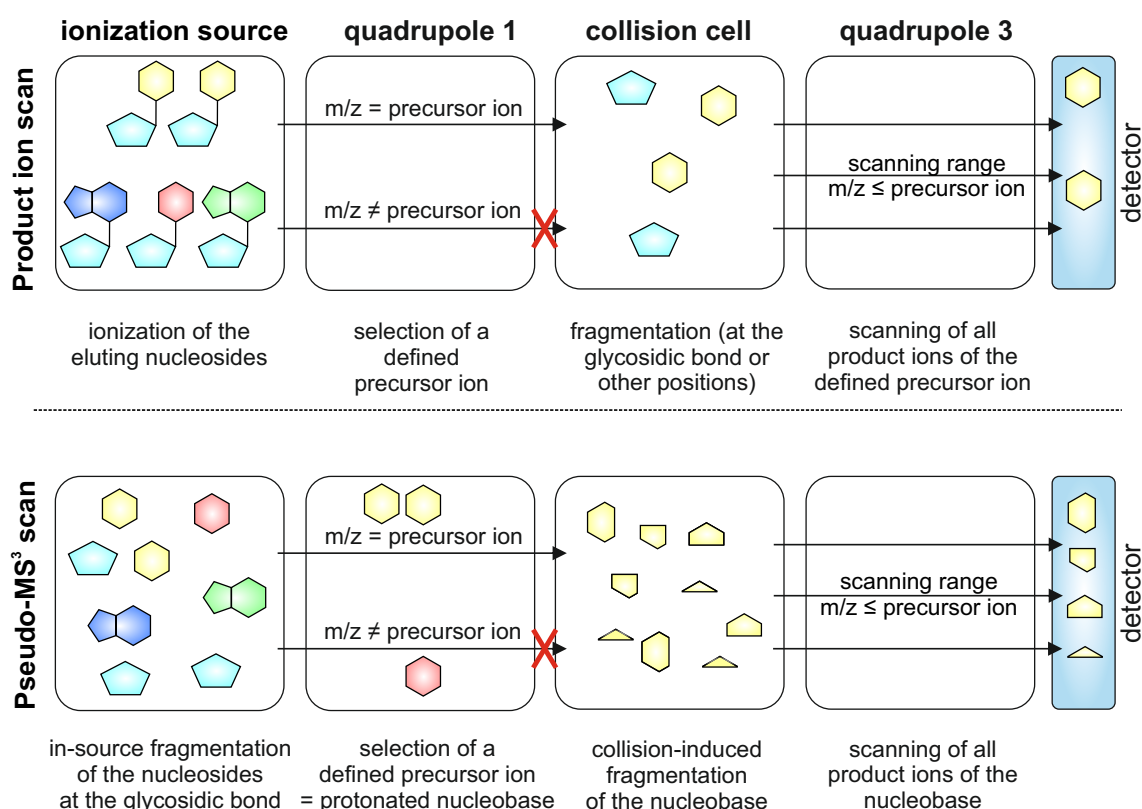


**Figure 1.8: LC-MS/MS analysis of nucleosides by product ion and pseudo-MS<sup>3</sup> scans** Description of the product ion (top) and the pseudo-MS<sup>3</sup> scan (bottom). In product ion scans, all nucleosides are ionized, of which only those displaying a defined precursor nucleoside  $m/z$  value pass quadrupole 1. After fragmentation (at the glycosidic bond or other positions) in the collision cell, all generated product ions are collected by the detector. Pseudo-MS<sup>3</sup> scans are principally product ion scans of the protonated nucleobases (instead of the protonated nucleosides) as precursor ions, which are produced by in-source fragmentation at the glycosidic bond.

### 1.3 A tRNA-like Small RNA: mascRNA

A unusual 3'-end processing of the long non-coding RNA (lncRNA) MALAT1 (Metastasis-Associated Lung Adenocarcinoma Transcript 1, also named Nuclear-Enriched Abundant Transcript 2 (NEAT2)) does not only generate the mature MALAT1 RNA, but also a small, tRNA-like RNA named mascRNA (MALAT1-associated small cytoplasmic RNA) of 61 nucleotides length [178]. Interestingly, the same 3'-end maturation mechanism can be observed for MEN $\beta$  lncRNA (Multiple Endocrine Neoplasia  $\beta$ , or NEAT1), yielding a similar tRNA-like small RNA, menRNA, which, however, is in contrast to mascRNA rapidly degraded mediated by 3'-CCACCA addition and was only detectable in liver [54, 179]. The MALAT1-mascRNA system (as well as the MEN $\beta$ -menRNA system) displays several remarkable features: the cleavage of small tRNA-like RNA and thus 3'-end generation of the respective lncRNA is accomplished by RNaseP and the 3'-end of the small RNA moiety is produced by RNaseZ cleavage, both of which are tRNA-maturing enzymes [178, 179]. While mascRNA undergoes 3'-CCA addition through the CCA-adding enzyme [54, 178], menRNA is, due to its unstable acceptor stem, subject to 3'-CCACCA addition and rapid degradation [54]. In case of the MALAT1-mascRNA pair, the cleavage reaction was shown to be directly promoted in a kind of positive feed forward mechanism by a natural anti-sense transcript (NAT) of MALAT1, termed TALAM1 [180]. Remarkably, the 3'-end of mature MALAT1 contains a conserved short A-rich stretch together with two upstream U-rich motifs [178], which form a highly stable triple helical structure in which the 3'-end is protected from degradation [181–183]. The formation of the stable triple helix requires the efficient cleavage of mascRNA and is thus facilitated by TALAM1, furthermore enabling the accumulation of MALAT1 to high levels [180]. The MALAT1-mascRNA system is in detail depicted in figure 1.9. The mature MALAT1 transcript is a ubiquitously expressed, highly abundant and highly conserved lncRNA [184], which is localized in the nucleus in nuclear speckles [178, 185] and was first discovered in connection with metastasis in non-small cell lung cancer (NSCLC), indicating its potential as prognostic marker in cancer [186]. Remarkably, despite its high degree of conservation and its high expression rates, MALAT1 lncRNA appears to be non-essential for life and development, at least under physiological conditions [184, 187]. MALAT1 lncRNA is upregulated in various tumor types showing a, amongst others, metastasis promoting effect and while several mechanisms underlying its regulation and oncogenic potential have been proposed, the exact modes of action still require further examinations, especially as results from studies of different cell types and knockout models displayed discrepancies ([184, 187], reviewed in [188, 189]). One possible function of MALAT1 is the regulation of gene expression, *e.g.* it was shown to interact with unmethylated polycomb 2 resulting in a relocalization of growth-related genes to nuclear speckles and activation of their transcription [190]. Proposed oncogenic modes of action of MALAT1 include, for example, the regulation of the expression of metastasis- and migration-related genes [191], MALAT1 upregulation under hypoxia and promotion of hypoxia-induced angiogenesis [192, 193], and function as miRNA sponge or endogenous competing RNA (ceRNA, [194, 195]) [196, 197]. In contrast to the nuclear retention of its precursor MALAT1, the small, tRNA-shaped mascRNA is exported to the cytoplasm where it might fulfill

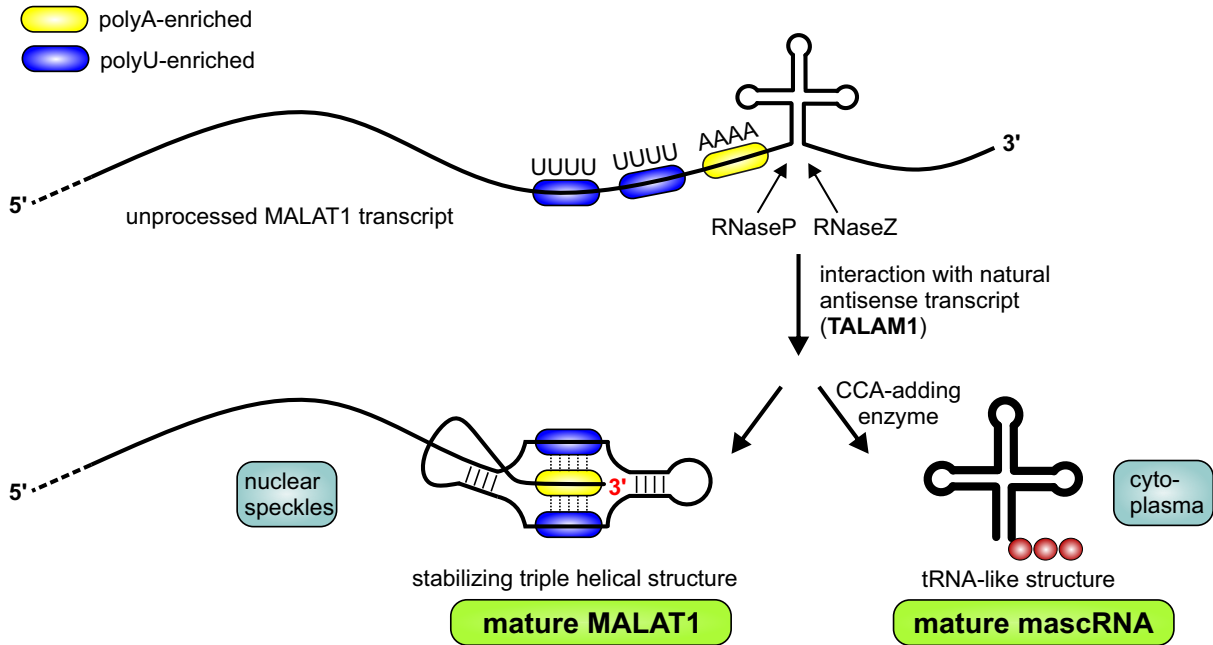


**Figure 1.9: The MALAT1-mascRNA system** The 3'-end of mature MALAT1 is generated by RNaseP cleavage (enhanced by the presence of a natural antisense transcript (TALAM1)) and highly stable due to formation of a triple helical structure protecting the 3'-end. The short 3'-cleavage product is further processed by RNaseZ and CCA-adding enzyme yielding mature, tRNA-like mascRNA, which is exported to the cytoplasm. Adapted from [178, 180].

MALAT1-independent functions [178]. Furthermore, mascRNA has been shown to be highly conserved, widely expressed among human cell types tissues, to have a rather short half life and, despite carrying a 3'-CCA added by the CCA-adding enzyme, not to be aminoacylated like canonical tRNAs [178]. Interestingly, in a MALAT1 knockout mouse model, a small amount of residual mascRNA was detectable in the brain in spite of the complete deletion of MALAT1 [187]. Remarkably, a recent study discovered a non-according regulation of MALAT1 and mascRNA in line with a function of the MALAT1-mascRNA system in cardiovascular innate immunity, hereby uncovering an immunoregulatory function of mascRNA in monocytes and macrophages which is no mediated by MALAT1 [198]. While MALAT1 showed high expression in tissues, including heart, and peripheral blood mononuclear cells (PBMC) and was induced by infection with Coxsackievirus B3 (CVB3) as well as under hypoxia, mascRNA in contrast displayed only high levels in PBMCs and no induction under infection and hypoxia. However, mascRNA was induced during the differentiation of monocytes to macrophages, and selective depletion of mascRNA (but not MALAT1) in monocytes resulted in a deregulation of genes associated with monocyte and macrophage function (*e.g.* TNF- $\alpha$  and IL-6), indicating a function of mascRNA in immunoregulation [198]. Furthermore, mascRNA expression in cardiomyocytes induced several antiviral factors and provoked resistance to an infection with CVB3 [198]. Knockout of MALAT1 (accompanied by mascRNA depletion) in CVB3-infected mice moreover resulted in a profound deregulation of immune-related genes going along with a higher CVB3-burden in heart, indicating an important role of the MALAT1-mascRNA pair, and in particular of



masRNA, in the innate immune system [198]. Nevertheless, further studies are required to unravel the exact mechanisms mediating the immunoregulating function of masRNA and to examine if masRNA might be suitable as a therapeutical target [198]. Noteworthy, a MALAT1 fragment containing the 3'-end of MALAT1 including masRNA was found to be importantly involved in the promotion of cell migration, invasion and proliferation by MALAT1 in colorectal cancer, implying that masRNA could have a function in cancer metastasis as well [199]. The results of the two studies indicate that masRNA, instead of just being a cleavage product of MALAT1, fulfill innate, MALAT1-independent functions that require further investigations of the small, tRNA-like RNA. These should include the examination of modified nucleosides potentially present in masRNA, not only because of its tRNA-like structure and recognition by tRNA-maturing enzymes, but also because clues pointing to the presence of at least one modification have already been detected [178].

## 1.4 Microscale Thermophoresis

### 1.4.1 Theory

Microscale thermophoresis is a recently developed, all-optical technique applied to the examination of a wide range of biomolecular interactions [200–202]. It relies on the directed movement of molecules in a temperature gradient, an effect termed thermophoresis or thermodiffusion that was first discovered by Carl Ludwig in 1865 [203]. However, its transfer to microscopic systems was first implemented almost 150 years later in 2002 [204]. The analytic method nowadays referred to as microscale thermophoresis (MST) and the corresponding instrumental setup were developed by Dieter Braun, Stefan Duhr, Philipp Baaske and coworkers ([205–208], reviewed in [200]). Although the exact theoretical basis and mechanisms underlying thermophoresis are not completely understood, thermophoresis can be described as a linear drift response [205], and the resulting velocity  $v$  of the molecule is proportional to the temperature gradient applied. The thermal diffusion coefficient (or thermophoretic mobility)  $D_T$  represents the proportionality constant in equation 1.1 describing the thermophoretic flow ( $j_T$ ) of molecules (initial concentration  $c_0$ ) in a temperature gradient ( $grad T$ ) [200, 201]:

$$j = -c_0 D_T grad T \quad (1.1)$$

The thermophoretic movement is counterbalanced by mass diffusion ( $j_D$ , with the diffusion coefficient  $D$ ) caused by the concentration changes due to the thermophoretic effect, resulting in a steady-state situation for which no net molecular flow is present (equation 1.2):

$$0 = j_T + j_D = -c D_T grad T - c D grad c \quad (1.2)$$

$S_T$  represents the Soret coefficient which correlates  $D_T$  and  $D$  by  $S_T = \frac{D_T}{D}$ . A positive  $S_T$  values describes a molecule movement from hot to cold and thus leads to a depletion of the respective molecule in the heated area (positive thermophoresis), which is typically the case

[200]. Inversely, negative thermophoresis characterized by a negative Soret coefficient provokes an accumulation of the molecule. The resulting concentration change  $\frac{c}{c_0}$  in the area heated by  $\Delta T$  is finally defined by equation 1.3 [204, 206]:

$$\frac{c}{c_0} = \exp(S_T \Delta T) \approx 1 + S_T \Delta T \quad (1.3)$$

By labeling the molecule under investigation fluorescently, the movement and thus the concentration change can be easily monitored optically by recording the fluorescence signal [205, 209], enabling the determination of the extend of thermodiffusion defined by the Soret coefficient and hereby, for example, effective charge and solvation entropy [205]. The Soret coefficient  $S_T$  of a molecule depends on molecule properties like size, conformation and charge, but also on its interplay with the surrounding solvent [205, 206, 208–210]. Thereby, the thermophoretic response of a molecule is highly sensitive to any variations of those parameters, and even small changes might have an unexpectedly high influence on the molecule's thermodiffusion. Since interaction with a binding partner presumably influences at least one of these properties and hereby the thermophoretic movement of the molecule, microscale thermophoresis is applicable to the investigation of a broad range of molecular interactions [200]. The dependence of the thermophoretic response on a variety of properties of the molecule is one of the major advantages of microscale thermophoresis compared to traditional methods used for biomolecular interaction studies, which often rely on profound changes in a single property, *e.g.* size, and thus display a much narrower application range. For example, fluorescence correlation spectroscopy (FCS) depends on quite pronounced changes in size induced by a binding event, a prerequisite that is often not fulfilled [200]. Other advantages of microscale thermophoresis lie in the very low sample consumption, the fast implementation, the possibility to perform label-free studies and the flexibility regarding solvents and buffers. Altogether, microscale thermophoresis is thus highly suitable for application to a wide range of interaction studies and other biomolecular investigations [202].

### 1.4.2 Experimental Details of Microscale Thermophoresis

The detailed setup of the instrumentation applied for microscale thermophoresis analysis (MST) is described in [200, 201, 206]. Briefly, an infrared (IR)-laser (wavelength 1480 nm) is used to induce the temperature gradient in a locally tightly limited area of the capillary, which contains the sample solution. The IR laser-induced temperature increase achieved lies between 1-10 °C (usually 2-6 °C) and is dependent on the capillary type and controlled by the applied IR-laser power [200, 201]. Using exactly the same optic path, a second laser system is set up for fluorescence excitation and subsequent emission detection. By labeling one of the interaction partners to be examined fluorescently, this setup allows the monitoring of the thermophoretic movement of the labeled molecule yielding a fluorescence time trace which displays the fluorescence intensities detected in the heated spot throughout the experiment. Typically, MST experiments are executed in form of titration series, in which the concentration of the labeled compound is kept constant and the concentration of the second, unlabeled binding

partner is varied in up to 16 samples. For each of the prepared samples, a MST fluorescence time trace is recorded and analyzed. A typical example for fluorescence time traces received in this work is depicted in figure 1.10 a (adapted from [202]). After starting with recording the initial

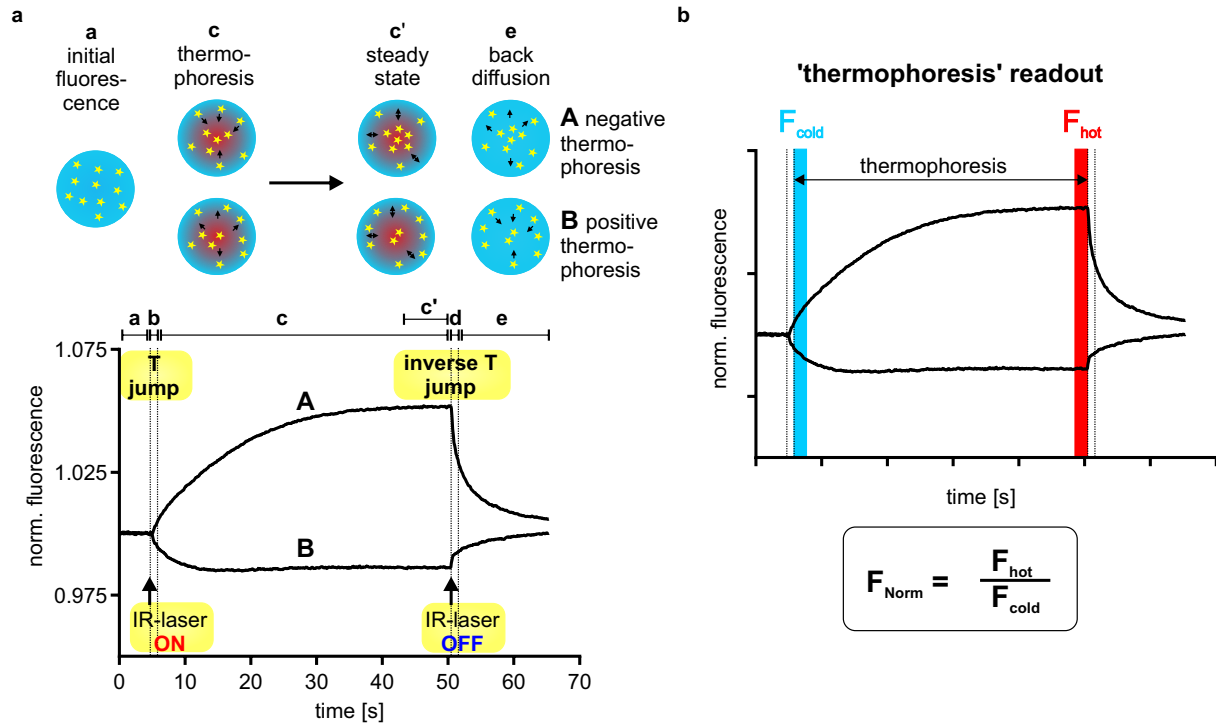


**Figure 1.10: Setup and readout of microscale thermophoresis experiments** Typical fluorescence time traces (a, bottom) for both positive and negative thermophoresis together with respective molecular movements observed by fluorescence monitoring (a, top) are depicted. The different regions and processes occurring are indicated (a initial fluorescence, b T jump, c thermophoresis, c' steady state, d inverse T jump, e back diffusion). The standard readout of the time traces is the “thermophoresis” setting, for which hot and cold areas for calculation of  $F_{\text{Norm}}$  are marked in (b) (adapted from [202]).

fluorescence for 5 s without heating, the IR-Laser is switched on for 45 s, which leads to two different effects. In a time range of  $< 1$  s after the beginning of the heating, the temperature jump (T jump) takes place, which is characterized by a change of the initial fluorescence exclusively caused by temperature-dependent changes of the properties of the fluorescent dye, *e.g.* the quantum yield [200] and which is not influenced by thermophoretic movement. Fluorescence changes resulting from the actual thermophoresis starts with a time delay of approximately 1 s and last until the IR-laser is turned off. During that time span, a steady state is reached, in which thermophoresis and mass diffusion balance each other out and which is indicated by constant fluorescence. Switching off the IR-laser induces an inverse T jump followed by backdiffusion, which is solely driven by mass diffusion. The divergent regions of the fluorescence time trace allow different conclusions about the properties of the labeled molecule as well as the characteristics of the interaction event [200]. In some cases, changes in the initial fluorescence result from the binding event itself and can in principle be used for evaluation of the interaction. The T jump displays changes that are solely caused by the properties of the fluorescent dye,

*e.g.* quantum yield changes due to the temperature increase. Potentially, if binding of the second compound is close to the position where the dye is attached, the binding event might influence the temperature sensitivity of the dye and thus the T jump. Thermophoresis itself is dependent on molecule properties like size, charge and hydration shell and thus is prone to be affected by the binding event, which likely changes at least one of those parameters. Finally, backdiffusion might be altered if aggregates are present. While all parts of the time traces may contain valuable information, the evaluation of the MST time trace most often applied is the analysis of the thermophoresis event alone, which holds true for the present work as well [200]. The T jump is excluded from analysis in order to investigate only changes in fluorescence that depend on the thermophoretic effect and thus on the binding event. Analysis of the fluorescence time traces in the “thermophoresis” setting is performed by defining a hot region in the steady state part of the time trace and a cold area beginning approximately 1 s after laser-induced heating has started (see figure 1.10 b). The ratio of the fluorescence detected in the hot and the cold area ( $\frac{f_{\text{hot}}}{f_{\text{cold}}}$ ) represents the normalized fluorescence change  $F_{\text{Norm}}$  (multiplied by 1000 to yield ‰ changes) and is plotted *vs.* the logarithmic concentration of the unlabeled binding partner to receive a binding curve. Changes in the binding state of a molecule are indicated by changes in the detected  $F_{\text{Norm}}$  values, which can be used to determine the fraction of the labeled molecule that is bound (equation 1.4,  $x$  denotes the bound fraction,  $F_{\text{Norm}}(\text{unbound})/(\text{bound})$  display normalized fluorescences in the completely free or fully complexed state [200, 206]).

$$F_{\text{Norm}} = (1 - x)F_{\text{Norm}}(\text{unbound}) + xF_{\text{Norm}}(\text{bound}) \quad (1.4)$$

### 1.4.3 Thermophoresis of Nucleic Acids

Given the well-characterized molecular structure and length of DNA (and RNA) molecules, especially DNA was employed as model polymer for studies addressing the theoretical background of thermophoresis [209]. First investigations of the thermophoretic behavior of double-stranded DNA were conducted in 2002 with the simultaneous aim to monitor thermophoresis under microfluidic conditions based on fluorescence detection [204]. In 2004, Braun and coworkers again used DNA as model to refine and evaluate their optical method to investigate thermophoresis in microscopic volumes [211]. In both studies, DNA displayed a positive thermodiffusion behavior and thus a concentration depletion in the heated area. This thermophoretic response, however, was later shown to reverse its direction at a surrounding temperature of approximately 4 °C, leading to an accumulation at temperatures below [205]. The same group applied double-stranded DNA (along with polystyrene beads) in a study that contributed profoundly to the theoretical comprehension of microscopic thermophoresis by demonstrating a theoretical model on the basis of the solvation entropy under the assumption of a local thermodynamic equilibrium [205]. Herein, the linear connection of the Soret coefficient with the Debye length  $\lambda_{\text{DH}}$ , the surface area and the temperature was shown as well as the quadratic correlation with the effective charge of the molecule. This theory was furthermore affirmed and extended by the results of the thermophoresis of single-stranded DNA of various length and under variable salt conditions [209,

210], which additionally uncovered the dependence of the Soret coefficient on the DNA length and the contribution of the thermoelectric Seebeck effect [210]. Amazingly, thermophoresis of a short 21mer DNA oligonucleotide was monitored even inside living cells by adapting the experimental setup, displaying both a reduced diffusion coefficient and thermophoretic mobility indicating that molecule movement is slowed down inside cells [212]. Further studies on the thermophoretic characteristics of DNA were conducted by using polyethylene glycol (PEG) as crowding agent [213]. PEG itself displays thermophoretic depletion, and in the resulting PEG concentration gradient, DNA (0.01 % volume fraction) showed depletion, ring-formation or accumulation in the heated area depending on the initial PEG concentration. While at low PEG concentrations (< 1 % volume fraction) the previously described depletion was observable, intermediate PEG concentrations (1.5-2.5 %) resulted in ring-like accumulation, with the ring radius being a function of the DNA size. Even higher PEG concentrations (> 3 %) caused accumulation in the heated spot and thus an inversion of thermophoretic response of the DNA [213]. By thermophoresis in PEG solutions, separation of DNA and RNA was achievable, as well as separation of RNA molecules of different length [213]. Notably, the crowding effect of a large volume fraction of PEG on DNA/RNA was observed not to be specific for PEG, as the PEG could be replaced by high concentrations (3-4 %) of a larger RNA that resulted in either accumulation or ring-like trapping of a shorter RNA applied in a small volume fraction [214]. Furthermore, depletion or accumulation of RNA and DNA during thermophoresis (equivalent to a sign change of thermophoresis) in PEG gradients was shown to be dependent on the presence of stem-loop structures, showing profound differences between single- and double-stranded DNA and RNA in thermophoresis [214]. This finding, however, was not confirmed by another study, which demonstrated quite similar thermophoretic responses for both single- and double-stranded nucleic acids [215].

Notably, the sensitivity of thermophoresis to nucleic acid hybridization events was confirmed in several studies [202, 208] and in this work (see section 3.1.2.1). Besides investigations regarding the thermodiffusion of nucleic acids, thermophoresis was applied to examine the melting behavior of nucleic acids by monitoring the thermophoretic response (characterized by the Soret coefficient) over a temperature range [208]. Herein, the difference in thermophoresis of single- and double-stranded nucleic acids as well as the temperature dependence of the Soret coefficient were exploited to receive thermophoretic melting curves, which resulted in melting temperatures according well with UV absorbance measurements and theoretical calculations. Additionally, intermediate transition states and conformational changes as well as the influence of modified nucleosides on the melting temperature were demonstrated [208]. The possibility of monitoring the hybridization of nucleic acids by microscale thermophoresis was utilized to determine the dissociation constant ( $K_D$ ) of two complementary, 16mer DNA strands, which also demonstrated the capability of MST to investigate binding affinities in the picomolar range [202]. The ease of measuring the  $K_D$  of the hybridization reaction *via* MST finally enabled the determination of the thermodynamic parameters of the DNA binding (enthalpy  $\Delta H^\circ$  and entropy  $\Delta S^\circ$ ) by measuring the  $K_D$  over a range of temperatures [202]. Again, the values determined by MST showed good consistency with theoretical calculations. Microscale thermophoresis was also employed to *in*

*vitro* confirm the binding of a newly detected small non-coding RNA in *Pseudomonas stutzeri* that enhances nitrogenase activity, NfiS, to its target *nifK* mRNA by using synthetic ssRNA oligonucleotides with or without mutations in the relevant sequences [216]. Interestingly, an approach combining thermophoresis, hybridization and functionalized gold nanoparticles was used to sequence-specifically detect DNA molecules [217]. Herein, target DNA oligonucleotides were hybridized to both DNA-functionalized gold nanoparticles and fluorescently-labeled DNA probes resulting in a connection of the nanoparticles with the labeled probe. The target DNA-dependent binding to the gold nanoparticles caused a thermophoretic accumulation of the labeled probes in the heated area, and the extend of accumulation correlated with the amount of target DNA present [217]. Interestingly, under the experimental conditions applied, the fluorescent DNA probes themselves did not show sufficient thermodiffusion to be analyzed, which was greatly enhanced by the combination with the gold nanoparticles in a PEG-containing solution [217].

Microscale thermophoresis, however, was not only applied to investigate properties and characteristics of nucleic acids, but also to reveal their interaction with other molecule species. One prominent application area is the investigation of nucleic acid aptamer-small molecule interactions [206, 218], taking advantage of the possibility of monitoring the binding of even small molecules like drugs and metabolites that do not result in a profound size change of the complex. Due to the MST-innate characteristics like free buffer choice (including biological fluids) and fast, highly sensitive, low material consuming analysis, microscale thermophoresis outperforms alternative methods like surface plasmon resonance and fluorescence anisotropy in the study of aptamer interactions [218]. Other applications that concern the binding of nucleic acids to other molecule species include the investigation of RNA- or DNA-protein interactions [202, 219–221]. For example, microscale thermophoresis was successfully applied in the investigation of the binding of the pseudouridine synthase TruB to fluorescently labeled tRNA constructs carrying a 5-fluorouridine instead of the substrate uridine at position 55, for which the formation of a covalent reaction intermediate could be ruled out [220, 222].

## 2 Motivation and Objectives

**RNA Quantification by Microscale Thermophoresis** Changes in abundance of single RNA species like, for example, specific tRNA isoacceptors can have drastic consequences for the regulation of gene expression and can even contribute to disease development and progression, like it was shown for specific tRNAs in breast cancer [60]. Currently, more and more non-canonical functions of tRNAs besides their traditional role as adaptor molecules during translation are discovered, highlighting their biological importance [13]. Considering that, the availability of a method that reliably quantifies single RNA species, particularly tRNAs, is a highly desirable feature. Although a variety of methods for (t)RNA quantification have been developed, many of them show limitations in regard to resolution, in their suitability for high throughput analysis, by being highly laborious or cost-intensive or by being only applicable for relative quantification of changes in abundance. In consideration of those limitations, the main objective of this work was the implementation of an RNA quantification method with focus on tRNAs and polyadenylated RNAs that offers reliable relative and absolute quantification of specific RNA molecules (*e.g.* tRNA isoacceptors) as well as subsets of RNA sharing a common sequence element (*e.g.* polyA-tailored RNAs) while being quickly and effortlessly executable. Many methods for (t)RNA quantification exploit the specific binding of the RNA of interest to a complementary DNA probe. However, monitoring of the hybridization event often requires a quite complex or laborious experimental setup, *e.g.* in case of microarrays or northern blots. In contrast, microscale thermophoresis is a recently emerging technique suitable for a wide range of biomolecular interaction studies which was shown to be applicable for tracking nucleic hybridization events [202]. Thus, the main goal was to ease and speed up the read-out of the hybridization event by implementing a microscale thermophoresis-based method, which was desired to enable a reliable, fast and low-material consuming, possibly absolute quantification of (t)RNAs. The successful establishment of the MST-based protocol was to be followed by a demonstration of its usefulness in biological applications of various settings. One of such an application could be the analysis of changes in *Saccharomyces cerevisiae* tRNA abundances under different environmental and genetic conditions. Considering the many advantages of the MST-based protocol observed, the initial goal to set up a tRNA quantification method was extended to the complete class of mRNAs. By taking advantage of the polyA tail, a common sequence feature of mRNAs, as target for the required DNA probe rather than using specific sequences, implementation of a mRNA quantification method allowing a fast and effortless evaluation of total mRNA levels was desired. Such a method would allow for a quick screen of relative changes in mRNA abundance under a variety of conditions without the need to concentrate on specific sequences and thus could be applicable to total RNA samples regardless

of the organism in investigation.

**Isolation of the Small tRNA-Like mascRNA** The small mascRNA is of tRNA-like structure and generated during the maturation process of its parent lncRNA, MALAT1, by the action of the tRNA-processing enzymes RNaseP, RNaseZ and the CCA-adding enzyme [178]. Considering the critical roles MALAT1 plays during cancer progression and metastasis, the requirement of mascRNA cleavage for MALAT1 accumulation and the only recently discovered immunoregulatory function of mascRNA in the cardiovascular system, a more detailed investigation of mascRNA might be promising, also in regard to therapeutical options [198]. Sequencing data of mascRNA cDNA clones suggested the presence of at least one modified nucleoside in mascRNA, and given its tRNA-like shape, mascRNA might be a target for tRNA modifying enzymes as well [178]. Thus, the investigation of the modification pattern of mascRNA was the main objective of the second part of this work. Ultimate prerequisite for a successful modification analysis by LC-MS/MS, however, was the isolation of mascRNA in both pure form (without contaminations by other RNAs) and sufficient amounts. Herefore, development of a suitable isolation protocol, based on hybridization and affinity purification, was an important stopover in the progress of this sub-project.

**LC-MS/MS Analysis of Modified Nucleosides** The use of a triple quadrupole mass spectrometer for LC-MS/MS analysis of modified nucleosides, both in the DMRM and the NLS mode, is well-established [165, 167, 173, 223]. Nevertheless, applications are not limited to quantification of known nucleosides or the determination of the complete modification pattern, including hitherto uncharacterized nucleosides, of an RNA sample, like they are typical for those two scan types. Thus, the main goals of the LC-MS/MS subproject in this work were on the one side the optimization and extension of the priorly established DMRM and NLS methods, for example with respect to a possible improvement of the sensitivity and an enhancement of other important features like the reproducibility and the quantification reliability by using an internal standard [173]. Furthermore, in regard to method establishment, an extension of the existing methods to both successful analysis and quantification of previously not included modifications was anticipated. On the other side, the development of methods addressing more complex scientific problems going beyond the “standard” nucleoside analysis was a major goal to be tackled. Once established, the usefulness of the various methods in biological applications was to be demonstrated, for example by analysis of RNA samples obtained from several collaboration partners. As wobble U34 tRNA modifications played an important role throughout this work, one objective regarding the LC-MS/MS analysis was the DMRM-based investigation of wobble U34 modifications in a variety of RNA samples obtained from the laboratories of Prof. Dr. R. Schaffrath and Prof. Dr. M. Stark, which derived from different *Saccharomyces cerevisiae* mutant strains deficient in one or more enzymes involved in the biosynthesis of wobble U34 modifications. The use of NLS was anticipated to serve as a mean to evaluate the isolation success of specific tRNA molecules, which was crucial for the progress and performance of the other two sub-projects (see above). Besides those applications of the standard scan types, two



---

additional analytical challenges were to be addressed. In cooperation with Dr. M. Müller and Prof. Dr. A. Ehrenhofer-Murray, the introduction of the hypermodified nucleoside queuosine (Q) into the tRNA of *Schizosaccharomyces pombe* was to be analyzed, however, Q is one of the modified nucleosides showing a fragmentation pattern that deviates from the usual cleavage at the glycosidic bond [224]. Hence, the aim was to confirm the additional cleavage positions *via* LC-MS/MS to be able to set up a DMRM method adequate for Q detection and relative quantification. Furthermore, the presence of the sugar-modified Q derivatives mannosyl-Q and galactosyl-Q was of interest, introducing additional challenges for method development. An even more sophisticated goal was addressed in collaboration with J. Schmidt and Prof. Dr. H. Schwalbe: the positions of  $^{13}\text{C}$ -introduction within the nucleobases in RNA of *E. coli* grown under  $^{13}\text{C}$ -2-glycerol as only carbon source were supposed to be analyzed, which included the necessity of developing a  $\text{MS}^3$  scan method using the triple quadrupole mass spectrometer, whose usual instrumental setup is designed for  $\text{MS}^1$ - and  $\text{MS}^2$ -scans.



## 3 Results and Discussion

### 3.1 Microscale Thermophoresis-based Quantification of Single RNA Species

#### 3.1.1 Workflow: Quantification of Single RNA Species

While there are several methods available for quantification of single RNA species, which were in many cases specifically designed to quantify tRNA molecules (see section 1.2.1), they all suffer from various disadvantages that limit their applicability for a fast, cost- as well as material-saving and precise quantification of (t)RNAs. Particularly, considering the recently emerging additional functions of tRNAs besides their traditional role as adaptor molecules during protein translation (reviewed in [13]), a method that is capable of quantifying tRNAs quickly and reproducibly without the requirement of high-end technologies (like a sequencing platform) is highly desirable. Nevertheless, a method that is not limited to tRNA quantification but is additionally applicable to measure levels of other RNA molecules, *e.g.* other small RNAs or ribosomal RNA (rRNA), or even complete subsets of RNAs, for example the pool of polyadenylated RNA, is advantageous due to its much broader application range. Envisaged was a microscale thermophoresis-based method monitoring the hybridization of a sequence-specific, fluorescently-labeled DNA probe to the target RNA in titration curves and hereby allowing a quantitative assessment of the RNA's abundance. Although sharing the same underlying principle of the sequence-specific hybridization of a probe with other (t)RNA quantification methods, the pursued MST-based method was anticipated to outperform the established methods in several points, *e.g.* by comprising a fast and effortless implementation without complex assay designs or readouts required, by consuming only low sample amounts, by being cost-efficient and to some extent applicable to higher throughput investigations and, particularly, by displaying broad applicability.

The thermophoretic behavior of a molecule is influenced, amongst others, by its size, charge and solvation shell (see section 1.4.1), and thus is sensitive to nucleic acid hybridization events. Although the possibility of monitoring hybridization events of nucleic acids by MST has been shown previously by the determination of the dissociation constant ( $K_D$ ) of an 16mer DNA duplex as well as of melting temperatures of nucleic acids [202, 208], it has to the authors knowledge not been exploited for RNA quantification purposes yet. Notably, Yu and coworkers developed a hybridization- and thermophoresis-based method for detection of DNA (see section 1.4.3, [217]). In order to address the need for a fast and reliable RNA quantification method, a protocol for quantification of single RNA species as well as the group of polyadenylated RNAs using microscale thermophoresis was developed with special emphasis on tRNAs and

polyA-tagged RNAs and tested for its suitability in biological applications. The workflow of the protocol established for the quantification of specific RNA species included the following steps (illustrated in figure 3.1, using tRNAs as model):

- 1. Preparation of a titration series:** The first step consisted of the annealing of increasing amounts of total (t)RNA to a constant amount of fluorescently labeled DNA probe complementary to the target RNA, or in case of the measurement of polyadenylated RNA, comprising a short polyT-DNA sequence (figure 3.1 a). The annealing of probe and target was achieved by performing a denaturation step at 90 °C followed by the actual hybridization at 65 or 37 °C, respectively (see section 5.2.1.10).
- 2. MST measurement:** Each of the up to 16 samples of the titration series was submitted to MST measurement as described in sections 1.4.2 and 5.2.1.11 (figure 3.1 b).
- 3. Extraction and analysis of the fluorescence time traces:** For each sample of the titration series, the fluorescence time trace recorded throughout the experiment was extracted. Herein, free and complexed DNA probe displayed different or even opposite thermophoretic behavior. The normalized fluorescence change ( $F_{\text{Norm}}$ ) was determined in the “thermophoresis” mode for each sample of the titration series using the indicated hot and cold regions of the time traces (figure 3.1 c).
- 4. Binding curve:** The normalized fluorescence change  $F_{\text{Norm}}$  was plotted *vs.* the logarithm of the respective RNA concentration in each sample yielding a sigmoidal binding curve. Using a sigmoidal dose-response fit, an  $EC_{50}$  value, representing the RNA concentration at which 50 % of the probe was bound, was received (figure 3.1 d).
- 5. Quantification:** The  $EC_{50}$  value was applied to calculate (1) DNA/RNA hybridization ratios, (2) tRNA abundances in % of total tRNA and (3) polyA-RNA levels in total RNA.

#### 3.1.2 MST-Based Determination of tRNA Abundances

##### 3.1.2.1 Monitoring of DNA/RNA Hybridization Ratios

To evaluate the general applicability of microscale thermophoresis for quantification of single tRNA species, *in vitro*-transcribed tRNA<sub>MAU</sub><sup>Met</sup> (*E. coli*) was investigated as model system together with its complementary, fluorescently labeled DNA probe. The DNA probe was designed to cover the full-length tRNA in order to maximize the specificity of the probe for its target tRNA and the stability of the formed RNA/DNA duplex (compare section 3.1.2.4). To investigate, if MST-analysis of a titration series of the model IVT and its DNA probe was applicable for determination of the hybridization ratio of the two compounds, increasing amounts of the IVT were hybridized to constant amounts of the DNA probe and submitted to MST analysis. The fluorescence time traces recorded for the 16 samples demonstrated clear changes in the thermophoretic behavior compared to the free DNA probe when increasing amounts of the

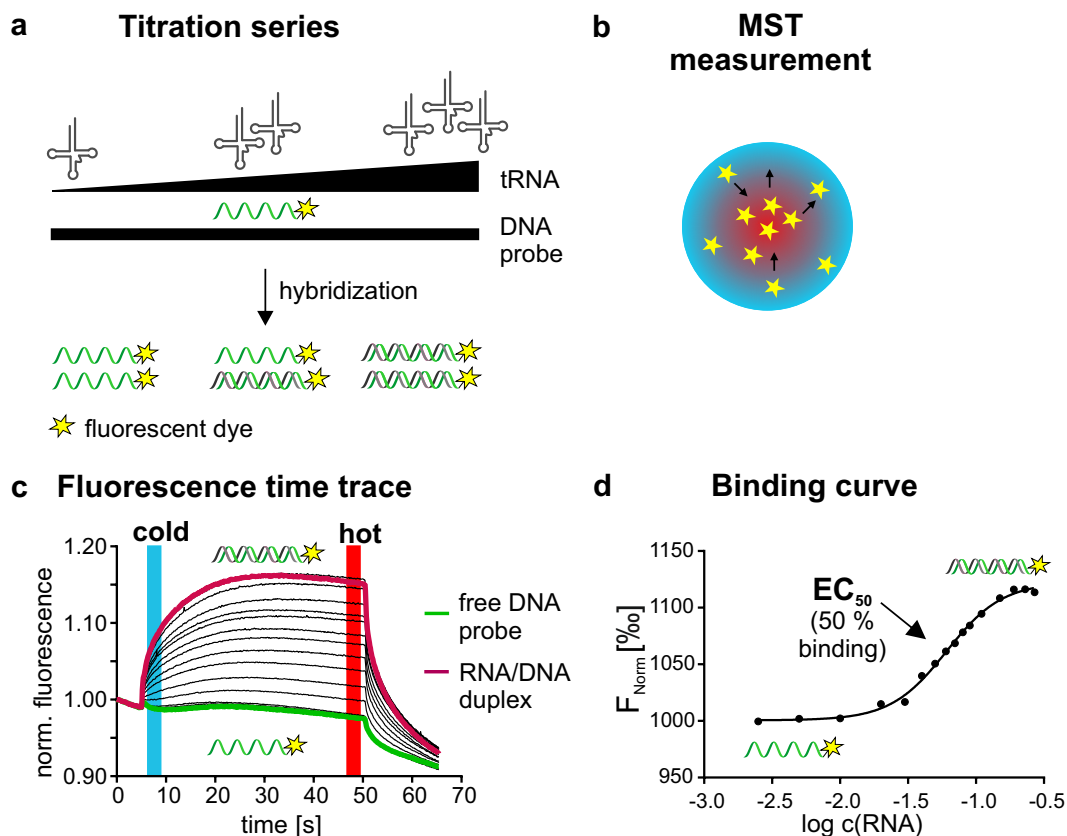


**Figure 3.1: Overview: MST-based RNA quantification protocol** The workflow of the MST-based RNA quantification exemplified using tRNAs as model is depicted. Titration series of the tRNA with its complementary DNA probe were prepared (a) and submitted to MST measurements (b). Resulting MST fluorescence time traces (c) were analyzed in the “thermophoresis” mode using the indicated hot (red) and cold (blue) areas, and the herefrom received normalized fluorescence changes ( $F_{\text{Norm}}$ ) were plotted vs. the logarithmic RNA concentration. The obtained sigmoidal binding curve (d) allowed the determination of an  $EC_{50}$  value, which was then applied to calculate hybridization ratios and (t)RNA abundances.

RNA/DNA-duplex were formed (figure 3.2 a). While the free DNA probe showed negative thermophoretic movement (from the cold to the hot region in the capillary), adding the IVT reversed this behavior to positive thermophoresis to an extent depending on the RNA concentration. For further analysis of the thermophoretic effect, the “thermophoresis” setting (compare section 1.4.2 and figure 1.10) was applied by normalizing the fluorescence in the steady-state, hot region to the one in the cold region excluding the T-jump (areas are indicated in figure 3.1). Plotting the normalized fluorescence change  $F_{\text{Norm}}$  against the logarithm of respective IVT concentration yielded a well-defined binding curve of sigmoidal shape, allowing a sigmoidal dose-response fit (section 5.2.1.11) and with that determination of an  $EC_{50}$  value (figure 3.2 b) presenting the IVT concentration at 50 % binding of the probe. To evaluate, if the double  $EC_{50}$  value (“ $EC_{100}$ ”) was applicable for calculating the concentration at which all probe molecules are bound (corresponding 100 % binding) and thus hybridization ratios, the dissociation constant ( $K_D$ ) determined for the 16mer DNA duplex (167 pM) in [202] was considered. Using the in the present work applied concentration of the labeled probe (100 nM), the law of mass action

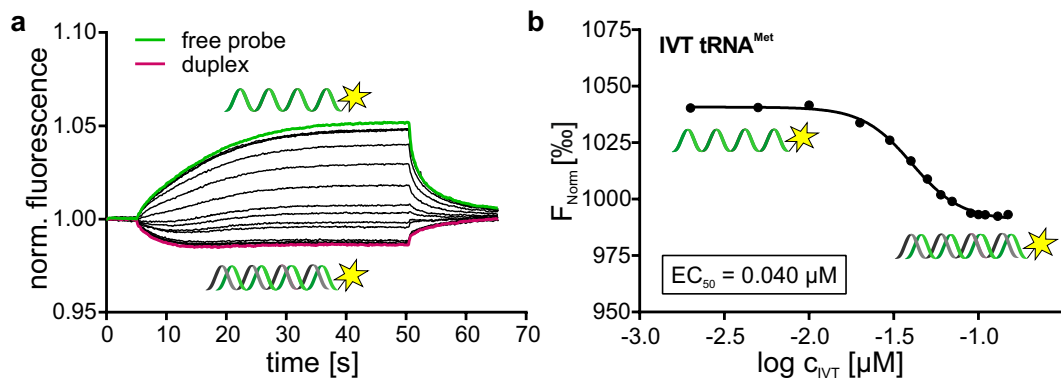


**Figure 3.2: MST of *in vitro* transcribed tRNA<sup>Met</sup>(MAU)** The IVT of tRNA<sup>Met</sup>(MAU) (*E. coli*) was titrated against its specific DNA probe. (a) displays the MST fluorescence time traces recorded, free and bound DNA probe are marked (green and magenta, respectively), for which the “thermophoresis” analysis resulted in the sigmoidal binding curve shown in (b). The determined EC<sub>50</sub> value is indicated, probe concentration was 0.1 μM.

was used for calculating the fraction bound at equimolar concentration of the tRNA. Using following equation (3.1) derived from the law of mass action as described in [201] and setting the concentration of probe and RNA ([A] and [B]) to 100 nM, the fraction bound ([FB]) was calculated to be > 95 % under the here applied experimental conditions. Considering the much higher length of the RNA/DNA duplexes generated here (75-80 nt), an even higher portion of the duplex can be expected to be formed, thus allowing the assumption of a 100 % binding at a concentration resembling the double EC<sub>50</sub>.

$$[FB] = \frac{[AB]}{[B]} = \frac{[A] + [B] + K_D - \sqrt{([A] + [B] + K_D)^2 - 4[AB]}}{2[B]} \quad (3.1)$$

Thus, using the determined EC<sub>50</sub> value of 0.04 μM for the IVT-DNA probe duplex formation, a hybridization ratio of 0.8:1 (IVT:probe) was calculated, which could additionally be confirmed by analyzing the binding ratio *via* an electrophoretic mobility shift assay (EMSA) on an 8 % non-denaturing PAGE gel (ratio 0.8-1:1, see figure 3.3). The deviation of the binding ratio from the expected 1:1 binding can at least partly be explained by uncertainties lying in the UV absorption-based determination of the RNA concentration. To ensure that the changes in thermophoretic behavior are actually caused by the formation of the duplex and not due to unspecific effects from the sole addition of RNA to the DNA probe, the same titration series was prepared again without performing the preceding annealing protocol. Although small changes in the time traces recorded were detectable with increasing IVT concentration (figure 3.4 a), their extent was not sufficient to result in profound changes in the  $F_{\text{Norm}}$  values (figure 3.4 b), indicating that an at the most small amount of hybrid was formed when the annealing step was omitted. These results confirmed the capability of the method to monitor hybridization events as well as the requirement of the annealing step for the MST-based quantification approach.

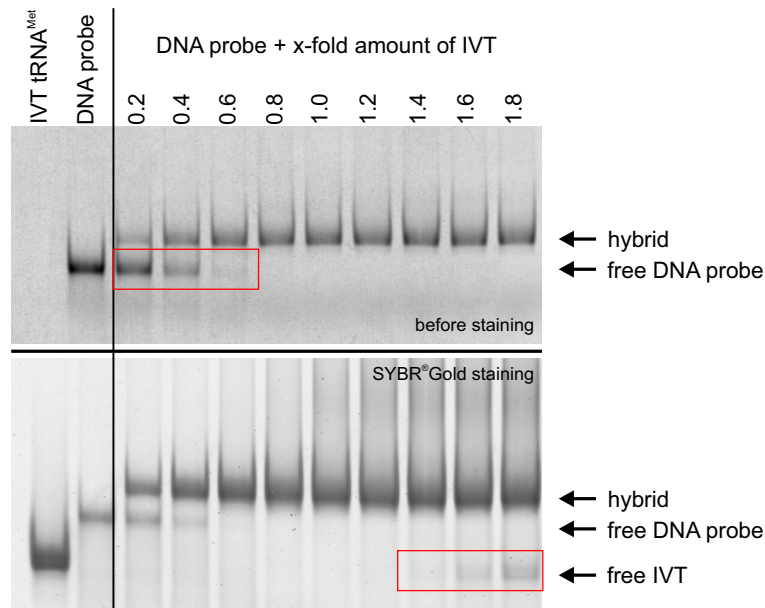


**Figure 3.3: Non-denaturing PAGE of *in vitro* transcribed tRNA<sup>Met</sup> (MAU)** A titration series of a constant amount of DNA probe (10 pmol) to increasing amounts of IVT (as indicated) was prepared and analyzed by non-denaturing PAGE. Hybridization ratios (IVT:probe) resulting in excess free DNA probe or free IVT are indicated (red boxes), as well as respective bands corresponding to hybrid and free forms (black arrows). The upper gel image represents the unstained gel showing only the fluorescently labeled DNA probe, the lower image depicts the same gel after staining for nucleic acids.

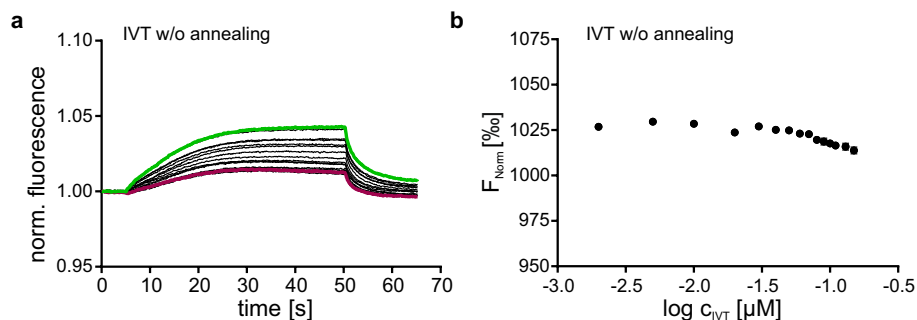


**Figure 3.4: Influence of the annealing step on the MST measurement** (a) displays the MST fluorescence time traces recorded for the titration series of the IVT which was prepared under omission of the annealing step. Time traces recorded for the free probe as well as the highest IVT concentration are marked (green and magenta, respectively). Plotting the  $F_{\text{Norm}}$  values against the IVT concentration did not yield a binding curve, indicating the formation of an at the most small amount of hybrid (b). Probe concentration was 0.1  $\mu\text{M}$ .

### 3.1.2.2 Transfer to tRNA<sub>MAU</sub><sup>Met</sup> Quantification in tRNA Mixtures

The same model tRNA, tRNA<sub>MAU</sub><sup>Met</sup>, was employed to test the transferability to total tRNA mixtures instead of the pure target tRNA in form of the IVT. For this purpose, a constant concentration of the DNA probe complementary to tRNA<sub>MAU</sub><sup>Met</sup> was used in a hybridization series with increasing amounts of a commercially available *E. coli* total tRNA mixture. The fluorescence time traces displayed similar changes along the titration samples as were observed for the IVT, resulting in a well-shaped binding curve and an  $\text{EC}_{50}$  of 1.92  $\mu\text{M}$  (figure 3.5, a and d (black)).

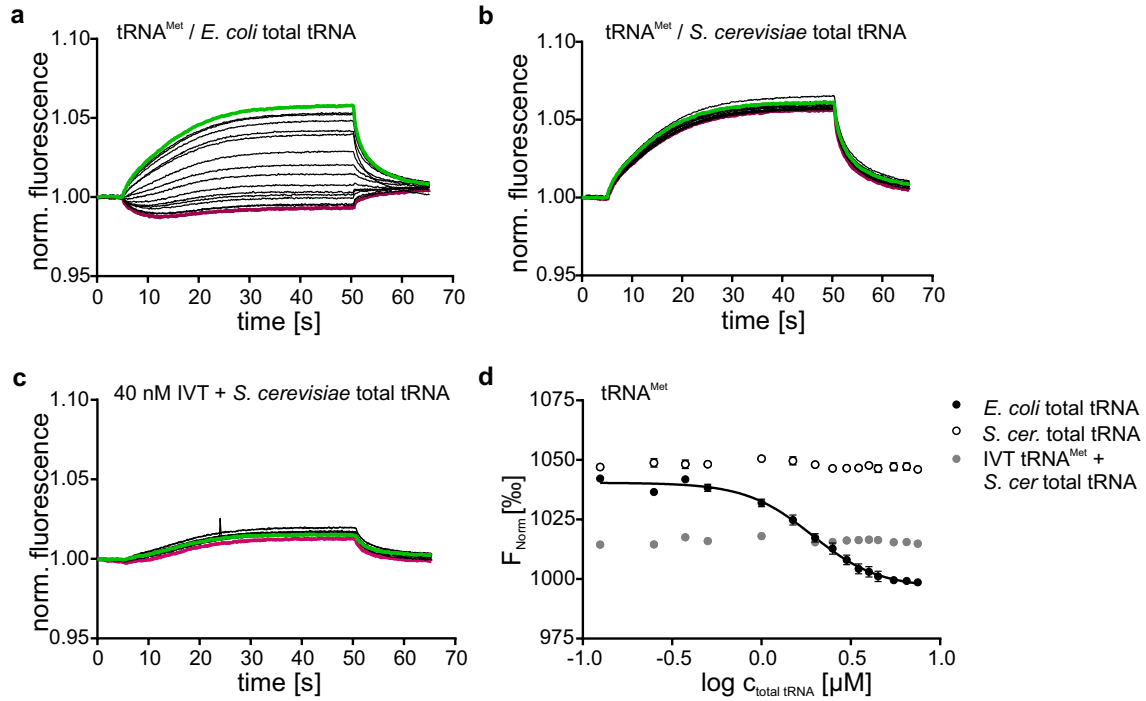


**Figure 3.5: Quantification of tRNA<sup>Met</sup>(MAU) in total tRNA** Fluorescence time traces of the titration series of the tRNA<sup>Met</sup>(MAU)-specific probe (MH630) with increasing concentrations of *E. coli* total tRNA (a), *S. cer.* total tRNA (b) and *S. cer.* total tRNA in presence of 40 nM IVT (tRNA<sup>Met</sup>(MAU), c) are displayed. The missing thermophoretic response in b and c indicated the presence of neither an unspecific binding to *S. cer.* tRNA nor an influence of increasing amounts of unspecific tRNA on the hybridization. (d) A binding curve was only received for total tRNA of *E. coli*, demonstrating the binding of the probe to the native tRNA<sup>Met</sup>(MAU) in tRNA mixtures. Probe concentration was 0.1 μM, fluorescence time traces of the lowest and highest total tRNA concentrations are marked (green and magenta, respectively.)

These results demonstrated the successful hybridization of the probe to its target tRNA in total tRNA mixtures, which was additionally confirmed by non-denaturing PAGE (see appendix, figure A.2). Considering the constant concentration of 100 nM DNA probe, which corresponds to the concentration of the target tRNA at 100 % binding, the EC<sub>50</sub> enabled the calculation of the portion of tRNA<sup>Met</sup><sub>MAU</sub> in total tRNA to be 2.6 % (molar ratio) using following equation 3.2 ( $c_{\text{probe}}$  probe concentration,  $vol$  sample volume,  $n_{\text{probe/total tRNA}}$  amount probe/total tRNA in sample):

$$\% \text{ target tRNA} = \frac{c_{\text{probe}} \times vol}{EC_{50} \times 2 \times vol} \times 100 = \frac{n_{\text{probe}}}{n_{\text{total tRNA}}} \times 100 = \frac{n_{\text{target}}}{n_{\text{total tRNA}}} \times 100 \quad (3.2)$$

To exclude any unspecific binding of non-target tRNAs that could potentially interfere with the quantification of the target tRNA, the same titrations series was repeated under substitution of the *E. coli* total tRNA by a tRNA mixture from *S. cerevisiae*. Fluorescence time traces did not reveal any changes in thermophoresis (figure 3.5 b and d (white)), thus ruling out unspecific binding events. Additionally, this experiment was repeated under addition of a constant concentration of 40 nM IVT to each titration solution, resulting in duplex formation with half of the probe molecules present in the sample. That concentration was chosen because it corresponded to the above determined EC<sub>50</sub> value and thus constituted the inflexion point of the binding curve,



at which little changes in the duplex formation were expected to have the most pronounced effect on the fluorescence time traces and the  $F_{\text{Norm}}$  values due to the high steepness of the curve in this area. Hence, if the presence of increasing amounts of non-target tRNAs interfered with the hybridization efficiency, a change in the time traces as well as in  $F_{\text{Norm}}$  values due to the change of the ratio of bound and unbound DNA probe should be easily detectable at the chosen IVT concentration. However, the MST time traces and thus  $F_{\text{Norm}}$  displayed no changes over the complete titration series, indicating that the applied concentrations of total RNA did not influence hybridization of the DNA probe to its target tRNA (figure 3.5 c and d (grey)).

### 3.1.2.3 MST of Native *E. coli* tRNA<sup>Met</sup><sub>MAU</sub>

In contrast to *in vitro* transcripts, native tRNAs contain a considerable share of modified nucleosides, which might potentially interfere with the hybridization of the probe similar to mismatches. This feature has been exploited for detection of certain RNA modifications by microarrays or northern blots [135, 136, 156]. However, only modifications at the Watson-Crick face of the nucleosides were expected to influence hybridization (e.g. m<sup>1</sup>A and m<sup>1</sup>G), as well as modifications that strongly disturb the nucleoside's conformation (e.g. dihydrouridine) [135]. In a first test to evaluate the influence of modified nucleosides on the binding to the DNA probe, native tRNA<sup>Met</sup><sub>MAU</sub>, which contains four dihydrouridine modifications in the D-loop [80], was isolated from *E. coli* total tRNA as described in section 5.2.1.9 and titrated against the same DNA probe previously used for the IVT. MST analysis revealed a slightly higher EC<sub>50</sub> value than received for the IVT (0.056 μM vs. 0.041 μM, resembling hybridization ratios (tRNA:probe) of 1.1:1 vs. 0.8:1), possibly indicating in fact a small decrease in binding efficiency (figure 3.6). However, as for the IVT, the binding ratio was still close to the expected 1:1 binding, and the small deviation might as well have been partly due to errors in the RNA concentration determination. The respective fluorescence time traces are shown in the appendix, figure A.1.

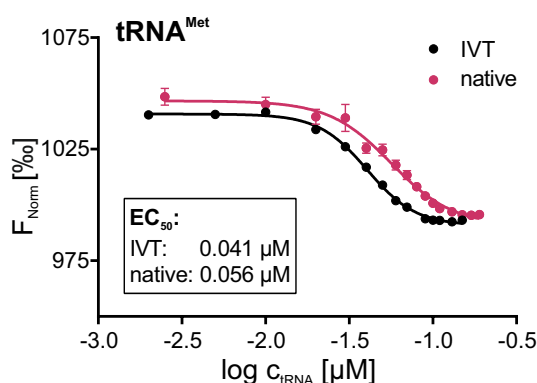


**Figure 3.6: Comparison of native and unmodified tRNA<sup>Met</sup>(MAU)** Binding curves of *in vitro* transcribed (IVT, black) and native (magenta) tRNA<sup>Met</sup>(MAU) (*E. coli*) received from MST measurements are displayed. The native tRNA displayed a marginally right-shifted curve, corresponding to a slightly increased EC<sub>50</sub> value. EC<sub>50</sub> values are indicated (probe concentration 0.1 μM), error bars represent the standard deviation of technical triplicates.

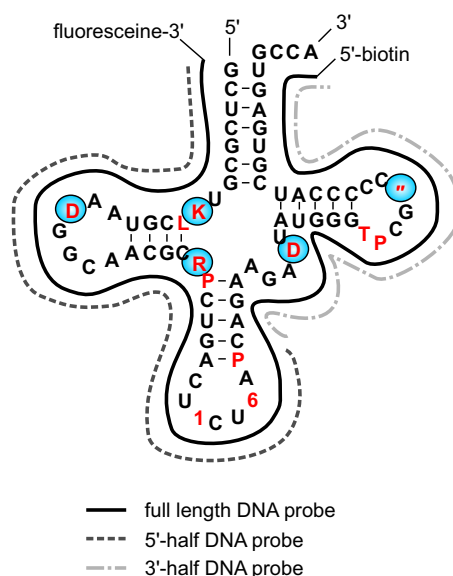


**Figure 3.7: *S. cerevisiae* tRNA<sup>Arg</sup>(1CU)** The secondary structure of tRNA<sup>Arg</sup>(1CU) including modified nucleosides is shown, adapted from the tRNAdb 2009 [80]. Complementary DNA probes covering the full length tRNAs or fragments are indicated (continuous black or dotted grey lines, respectively), as well as modified nucleosides (red). Modifications that have been shown to interfere with hybridization in [135] are circled in light blue. K - m<sup>1</sup>G, L - m<sup>2</sup>G, D - dihydrouridine, R - m<sup>2</sup>G, P - Ψ, 1 - mcm<sup>5</sup>U, 6 - t<sup>6</sup>A, T - m<sup>5</sup>U, '' - m<sup>1</sup>A.

#### 3.1.2.4 MST of Native and Unmodified tRNA<sub>1CU</sub><sup>Arg</sup> (*Saccharomyces cerevisiae*)

To further investigate the influence of modifications on the performance of the quantification method, tRNA<sub>1CU</sub><sup>Arg</sup> was chosen as model tRNA (see figure 3.7). This tRNA species contains four of the five modified nucleotides that had been shown to interfere with hybridization in [135] when using short probes of 15-25 nt length, resulting in five possible positions across the tRNA that might cause hybridization errors. Three of the putative positions are located in the 5'-half of the tRNA, a region for which the mentioned study [135] confirmed the presence of RNA modifications by differential hybridization. To assess the influence of modifications on the hybridization event in dependence of the probe length, native (modified) and unmodified tRNA<sub>1CU</sub><sup>Arg</sup> were prepared by either isolation from total tRNA (see 5.2.1.9) or splint ligation (see 5.2.1.6), respectively. For MST measurements, both tRNA forms were hybridized to either the full-length probe (MH778) or shorter probes targeting only the 5'- or 3'-half of the tRNA (MH808 and MH809). Analysis of the hybridization efficiencies by MST revealed a similar binding of the full-length probe to both the native and the unmodified tRNA, with, surprisingly, a slightly better binding of the modified tRNA indicated by the left-shift of the binding curve in respect to the one of the unmodified tRNA, corresponding to a marginally lower EC<sub>50</sub> value (EC<sub>50</sub>: 0.061 μM (native) and 0.069 μM (unmodified), see figure 3.8 a). However, the detected difference is well in the range of potential UV-based quantification errors in the RNA concentrations and hereby the results altogether confirm that using a full-length probe counterbalances negative effects caused by modified nucleosides. Contrariwise, the shorter probes displayed clear differences in thermophoretic response and binding: while the unmodified tRNA<sub>1CU</sub><sup>Arg</sup> was bound by both

of the short probes with only slight impairment compared to the full-length probe, which was more pronounced for the 5'-half probe ( $EC_{50}$ : 0.092  $\mu$ M (5'-half probe) and 0.072  $\mu$ M (3'-half probe)), the probes apparently failed to hybridize to the native, modification-containing tRNA as indicated by the absence of a change in thermophoresis and thus  $F_{Norm}$  (see figure 3.8 b, c). An improvement of the binding of the 3'-half probe could be achieved by changing the pH to 6.5,

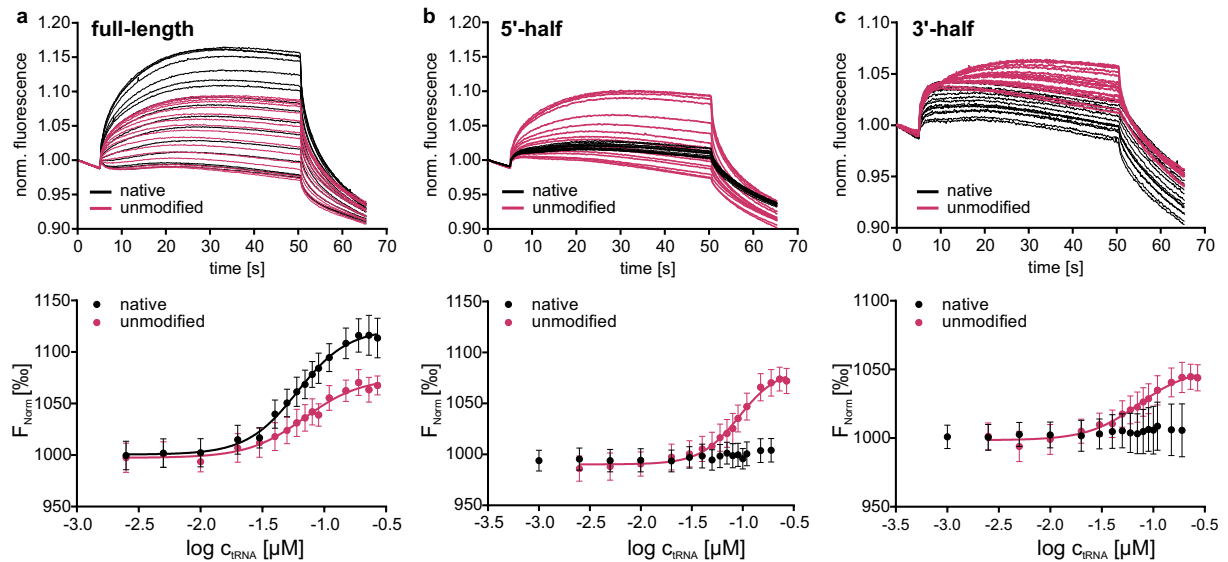


**Figure 3.8: MST of native and unmodified tRNA<sup>Arg</sup>(1CU)** Both MST time traces (top) and resulting binding curves (bottom) of the native (black) and unmodified (magenta) tRNA<sup>Arg</sup>(1CU) are depicted for the full-length probe (a), the 5'-half probe (b) and the 3'-half probe (c). Probe concentration was 0.1  $\mu$ M. Error bars represent the standard deviation of technical replication,  $n=3$ .

with an  $EC_{50}$  values only slightly higher than for the full-length probe at pH 7.4 (0.077 *vs.* 0.069  $\mu$ M), however, neither the full-length probe nor the 5'-half probe displayed a thermophoretic response under these conditions (see appendix, figure A.3). Considering that various factors like effective charge and solvation shell influence the thermophoretic response (see section 1.4.3), varying the hybridization conditions might help to improve the applicability of the shorter probes in MST-based hybridization monitoring. However, under the conditions applied throughout the present work, the full-length probe clearly outperformed the shorter probes in the MST-based tRNA quantification. Addressing that, the hybridization performances of the DNA probes under the standard conditions were additionally examined on a non-denaturing PAGE gel for comparison. While all three probes again displayed complete hybridization to the unmodified form of tRNA<sup>Arg</sup><sub>1CU</sub>, the binding efficiency of the probes was clearly reduced for the native tRNA as apparent from the presence of bands corresponding to unbound tRNA. This effect was especially pronounced for the 5'-half probe, while the 3'-half probe as well as the full-length probe showed a higher degree of binding (see figure 3.9). Altogether, results of MST measurement and native PAGE illustrated the same trend and demonstrated that tRNA binding of shorter DNA probes of up to 40 nt was indeed severely impeded by the presence of modified nucleosides and that using a full-length tDNA as probe was able to recover binding. Thus, a MST-based quantification assay making use of full-length, complementary DNA probes

should be able to adequately determine tRNA abundances in total RNA samples. This improved performance of full-length oligonucleotides in hybridization to native tRNAs was also exploited in microarray-based tRNA quantification approaches [17, 141].

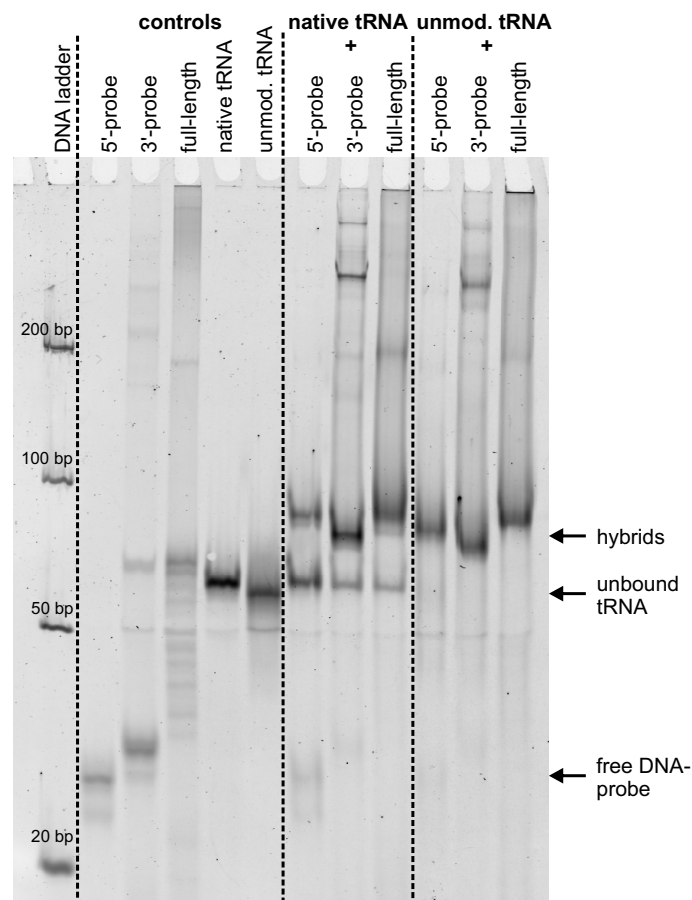


**Figure 3.9: Non-denaturing PAGE of tRNA<sup>Arg</sup>(1CU)** The non-denaturing PAGE gel (10 %) displays the hybridization of the three DNA probes to native and unmodified tRNA<sup>Arg</sup>(1CU). In all lanes containing native tRNA excess of free tRNA was observable after staining, indicating incomplete hybridization. Bands corresponding to free DNA probe, free tRNA and the RNA/DNA hybrids are indicated. For hybridizations and controls, 10 pmol of each binding partner were applied. Gel staining was performed using SYBR<sup>®</sup>Gold.

### 3.1.2.5 Evaluation of the Method's Quantification Performance

**Profiling of 23 tRNA Species in *S. cerevisiae*** Further investigation and evaluation of the MST-based tRNA quantification method was conducted by expanding the range of target tRNAs. For this purpose, 27 fluorescent dye-labeled DNA probes complementary to 27 out of the 34 *S. cerevisiae* tRNAs listed in the tRNAdb 2009 [80] were designed and tested using a total tRNA mixture of *S. cerevisiae*. All 27 DNA probes covered the full length of their respective target tRNA to ensure a high specificity and strength of the duplex formation (compare [17, 141] and section 3.1.2.4). However, differential analysis of isoacceptors or isodecoders differing only in a few nucleotides was presumed to be not feasible (for microarray-based detection, the difference required for sufficient differentiation was determined to be at least 8 nt [17, 141]), so in such cases

only one probe expected to capture both tRNA isoacceptors/isodecoders was designed (see section 5.1.4). For 22 of the 27 probes, MST experiments displayed sufficient differences in  $F_{\text{Norm}}$  values of free and bound probe to receive a well-defined binding curve with the respective  $EC_{50}$  value. Notably, most of the probes showed, in contrast to the probe for tRNA<sub>MAU</sub><sup>Met</sup> (*E. coli*), a more pronounced negative thermophoresis (accumulation in the hot area) in the duplex form compared to the free probe, or even a change from positive to negative thermophoresis upon binding (compare appendix, figures A.5-A.7). For the remaining 5 tRNA-probe pairs, using the standard annealing conditions (1x PBS buffer, pH 7.4) did not result in adequate changes in  $F_{\text{Norm}}$  values to obtain a binding curve, indicating either a missing thermophoretic response to the hybridization event or an only weak hybridization of the probe to the target tRNA. For those tRNAs, changing the hybridization conditions in respect to salt concentration and pH was tested, as those parameters might have an effect on the thermophoretic response due to their possible influence on the Soret coefficient, for example by causing changes in duplex size, effective charge or solvation shell (see section 1.4.3). In the case of tRNA<sub>ICG</sub><sup>Arg</sup>, lowering the pH to 6.5 and doubling the salt concentration (2x PBS) enabled a MST-based quantification due to an improved thermophoretic response (see appendix, figure A.4). However, the Soret coefficient of DNA was shown to be not influenced profoundly by the pH over a wide range [210], thus the exact reasons for the improvement of the thermophoretic response remain to be investigated as well as possible conditions which might enable the measurement of the remaining four tRNA-probe pairs (tRNA<sub>NGA</sub><sup>Ser</sup>, tRNA<sub>UAG</sub><sup>Leu</sup>, tRNA<sub>&AC</sub><sup>Val</sup>, tRNA<sub>CAC</sub><sup>Val</sup>). The 23 functionally DNA probes were then applied in the quantification of the respective tRNA species in a total tRNA mixture isolated from *S. cerevisiae* (strain S288C) grown at 30 °C (kindly provided by Dr. Sebastian Leidel in biological triplicates). MST fluorescence time traces recorded for each tRNA are displayed in the appendix (figures A.5, A.6 and A.7). Mean  $EC_{50}$  values (see appendix, table A.1) obtained from the MST data of triplicate experiments were used for calculation of the abundance of each tRNA species analyzed in the total tRNA mixture, the results are summarized in figure 3.10. Abundances of the single tRNAs varied from 0.8 (tRNA<sub>B<sub>CA</sub></sub><sup>Trp</sup>) to 5.7 % (tRNA<sub>IAC</sub><sup>Val</sup>), counting up to 55 % in total (95 % confidence interval: 51-61 %). Reasons for not adding up to 100 % probably include that not all tRNA species listed in the tRNAdb 2009 [80] are covered by the 23 oligonucleotides (*e.g.* the DNA probe for tRNA<sup>Phe</sup> could not be synthesized successfully by the oligonucleotide supplier) and that the total tRNA mixture eventually contained small impurities like, for example, 5S rRNA.

**Technical and Biological Replicates** The data set of the 23 tRNA species quantified in *S. cerevisiae* total tRNA was used for further investigations of the method's performance. For all 23 tRNAs examined in this work, MST analysis was performed using three biological replicates of total tRNA fractions isolated from *S. cerevisiae* (strain S288C, kindly provided by Dr. S. Leidel). Additionally, technical replicates in terms of triple MST measurements of the same capillaries were conducted for 19 out of the 23 tRNAs. The data collected in this way was then applied to evaluate the robustness of the method's results. Relative standard deviations (rel. SD) of the calculated abundances (% tRNA in total tRNA) showed very little variations for technical

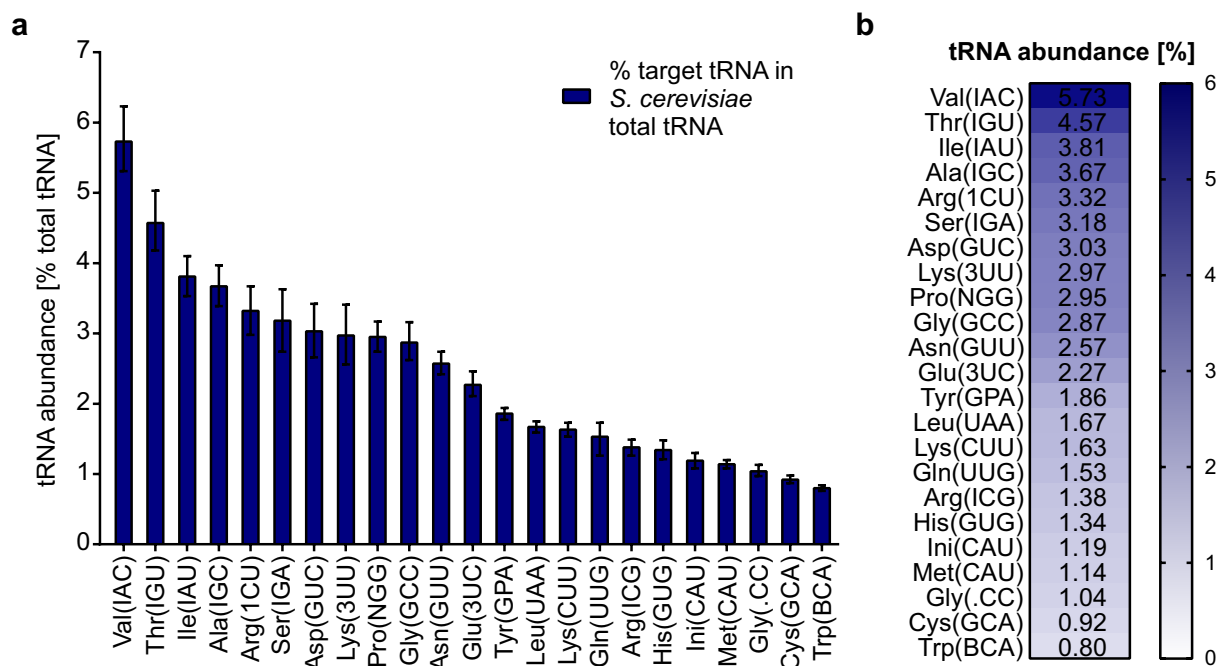


**Figure 3.10: Quantification of 23 *S. cerevisiae* tRNAs** The abundances of 23 *S. cerevisiae* tRNAs were assessed by MST measurement. (a) Bar chart summarizing the quantification results (error bars represent the 95 % confidence intervals of the % values calculated,  $n=3$ ). (b) Levels of the tRNAs illustrated in a heatmap, highly abundant tRNAs are colored in dark blue (compare legend at the right). Mean values of biological triplicates are indicated. The total tRNA samples employed in the experiments were obtained from Dr. S. Leidel.

replicates, ranging from as low as 0.2 to a maximum of 12.4 % (figure 3.11 a). Only one tRNA,  $\text{tRNA}_{\text{CAU}}^{\text{Ini}}$ , displayed a rel. SD above 10 %, and only 5 tRNAs a rel. SD larger than 5 %, indicating the high technical reproducibility of the method. Slightly larger deviations were observed for the biological replicates, with a mean rel. SD of 7.7 % (technical replicates: 3.5 % mean rel. SD). Six tRNAs exhibited a rel. SD of more than 10 % with a maximum of 17 %, among them  $\text{tRNA}_{\text{GUC}}^{\text{Asp}}$ , which performed best in technical replication (0.2 % rel. SD) (figure 3.11 b). Altogether, both technical and biological replication illustrated the robustness of the quantification method and the high reproducibility of the results.

**Long-Term Reproducibility** The long-term reproducibility of the MST measurements were tested using  $\text{tRNA}_{\text{UAA}}^{\text{Leu}}$ . The same titration series was prepared twice in a time span of two months, and analyzed by MST. Figure 3.12 a displays the two binding curves received, which displayed only minor deviations in shape and in the calculated  $\text{EC}_{50}$  values (6 % difference). Altogether, the results demonstrated that MST measurements of the hybridizations are well reproducible over a longer time span.

**Consistency in Different *S. cerevisiae* Strains** Furthermore,  $\text{tRNA}_{\text{3UU}}^{\text{Lys}}$  was quantified in total tRNA pools derived from two different *S. cerevisiae* strains (S288C and BY4741, kindly provided by Dr. S. Leidel and Prof. Dr. R. Schaffrath, respectively). Figure 3.12 b displays the binding

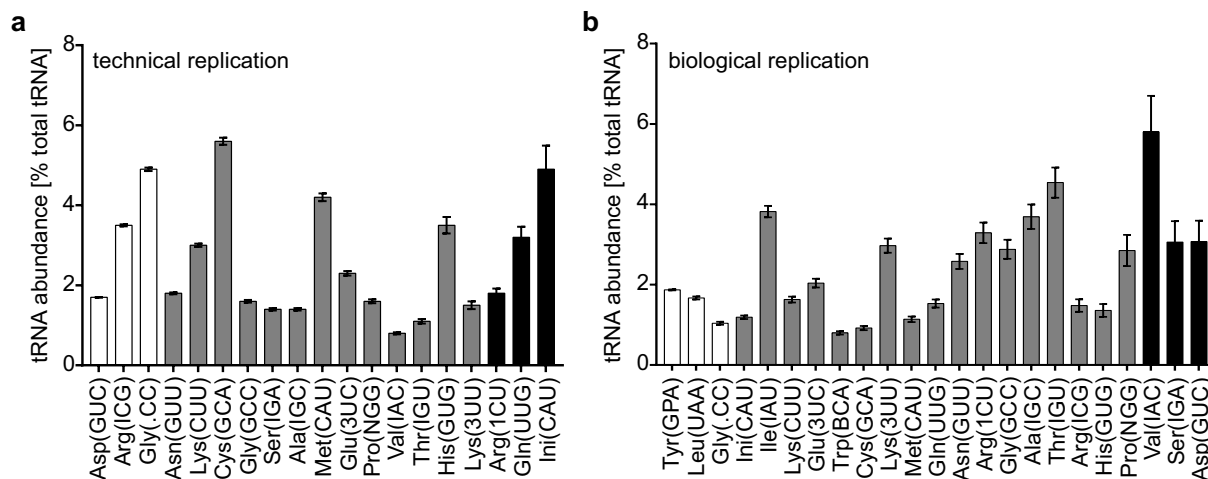


**Figure 3.11: Technical and biological reproducibility** For the set of 23 DNA probes targeting *S. cerevisiae* tRNAs, technical and biological replicates were measured and the variation between the replicates assessed. The tRNA levels determined as means of technical (a) and biological replicates (b) were sorted by increasing relative standard deviations, with the best (white) and worst (black) results indicated. Error bars present the standard deviation,  $n=3$ . The total tRNA mixtures used as basis for the quantification were kindly provided by Dr. S. Leidel.

curves received from the MST measurements, which again showed excellent agreement. These results further confirmed the robustness of the MST-based tRNA quantification, and additionally showed the consistency of the results for total tRNA mixtures prepared by different methods and laboratories (tRNA separation by anion exchange or denaturing PAGE, respectively). Similar consistency of the tRNA levels in the two strains were observed for  $\text{tRNA}_{3\text{UG}}^{\text{Gln}}$ , however, both  $\text{tRNA}_{\text{NGG}}^{\text{Pro}}$  and  $\text{tRNA}_{\text{GUG}}^{\text{His}}$  displayed elevated levels in the BY4741 strain, potentially indicating that quantities of those two tRNAs might be differentially regulated in the two strains due to some strain-specific requirements (see appendix, figure A.8).

### 3.1.2.6 Biological Applications

To demonstrate the suitability of the developed MST-based tRNA quantification protocol for biological investigations, it was applied to examine changes in *S. cerevisiae* tRNA abundances under different environmental and genetic conditions. First, changes in levels of all tRNAs covered by the 23 DNA probes under two different growth conditions, namely growth temperatures of 30 and 39 °C, were assessed. Respective total tRNA pools were obtained from the laboratory of Dr. S. Leidel in biological triplicates. Secondly, the frequencies of  $\text{tRNA}_{3\text{UU}}^{\text{Lys}}$ ,  $\text{tRNA}_{\text{NGG}}^{\text{Pro}}$  and  $\text{tRNA}_{3\text{UG}}^{\text{Gln}}$  were examined in wildtype *S. cerevisiae* cells as well as in five double mutant strains deficient in various tRNA modifying enzymes. Additionally, the six different strains were either grown constantly at 30 °C, or heat shock was applied by increasing the temperature to 37 °C for 2 h prior to RNA extraction. Those total RNA samples were prepared from the respective *S. cerevisiae* cultures by Akif Ciftci from the laboratory of Prof. Dr. R. Schaffrath, who also kindly provided the samples for the third biological investigation, which was the quantification of the cleavage of  $\text{tRNA}_{3\text{UG}}^{\text{Gln}}$  by the *Pichia acaciae* killer toxin PaT. As the samples received from the

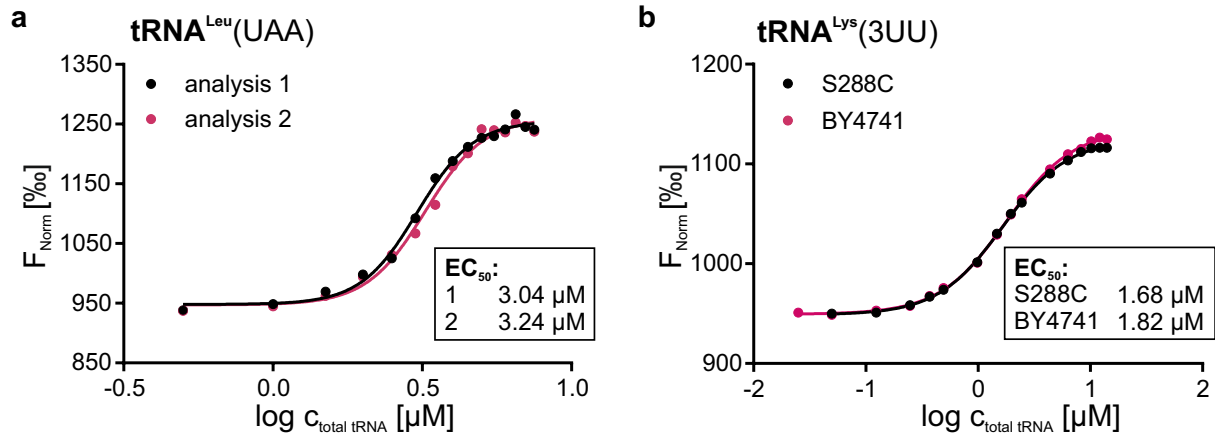


**Figure 3.12: Long-term and strain-overlapping reproducibility** To assess the long-term reproducibility, MST measurements of tRNA<sup>Leu</sup>(UAA) were repeated after a time span of two month (analysis 2). Respective binding curves (a) displayed only minor variation between the two preparations and measurements, affirming the good reproducibility of the method. In (b), tRNA<sup>Lys</sup>(3UU) was quantified in the two *S. cerevisiae* strains S288C and BY4741, with only a small deviation in the binding curves detectable. Obtained EC<sub>50</sub> values are indicated (probe concentration 0.1  $\mu\text{M}$ ). Total (t)RNA samples were supplied by Dr. S. Leidel and Prof. Dr. R. Schaffrath, respectively.

laboratory of Prof. Dr. R. Schaffrath consisted of total RNA, total tRNA pools were extracted by denaturing PAGE prior to the use in MST experiments. Figure 3.13 summarizes the three different applications including the differences in sample preparation, target tRNAs and scientific question to be examined.

**Application 1: Growth Temperature Influence on tRNA Levels in *S. cerevisiae*** To assess changes in tRNA levels under elevated growth temperature, total tRNA pools (provided by the laboratory of Dr. S. Leidel) from *S. cerevisiae* (strain S288C), grown at either 30 (control) or 39 °C, were examined by the MST quantification assay. Therefore, titration series for all 23 DNA probes were prepared for each biological replicate (three for each temperature) and analyzed by MST. For the analysis of the variations of technical as well as the biological replicates (30 °C growth temperature) see section 3.1.2.5. EC<sub>50</sub> values (appendix, table A.1) obtained from the biological triplicates were used to calculate the abundance of each analyzed tRNA in % of total tRNA, which ranged from 0.7 to 5.7 % (see figure 3.14 a). Obtained abundances were compared for the two growth temperatures by calculating the ratio of the abundances at 39 and 30 °C, which varied from a 0.85-fold reduction to an 1.15-fold increase of tRNA levels (see figure 3.14 b). Thus, growth temperature-induced changes of tRNA abundances appeared to be rather small, and by comparing the 95 % confidence intervals of the EC<sub>50</sub> values (compare table A.1), only five tRNAs revealed a significant reduction (indicated by non-overlapping confidence intervals, see figure 3.14 c). The corresponding right shift of the binding curve is depicted in figure 3.14 d using tRNA<sup>Leu</sup><sub>UAA</sub> as example, binding curves of all other tRNAs are shown in the appendix (figures A.5, A.6 and A.7). However, even for those five tRNAs the reduction was quite small with up to 15 %, indicating that elevated growth temperature did not lead to a



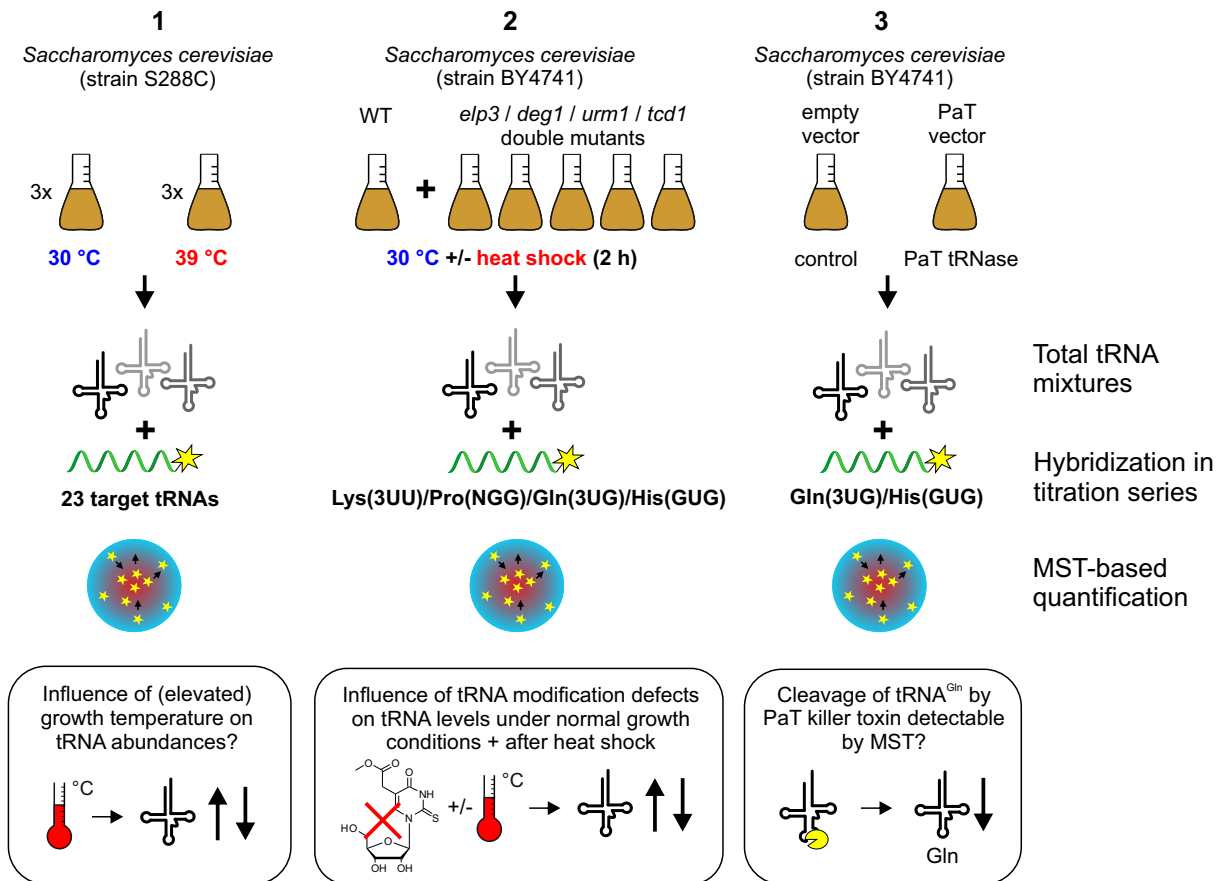


**Figure 3.13: Overview of the biological applications** described in 3.1.2.6: Three sets of *S. cerevisiae* tRNA mixtures grown under various conditions were kindly provided by the laboratories of Dr. S. Leidel (strain S288C) or Prof. Dr. R. Schaffrath (strain BY4741), respectively. tRNAs were quantified in each set as indicated, and their abundance analyzed under the scientific questions stated.

drastic change of the abundance of one or more tRNAs and challenging the biological relevance of the small changes detected. See appendix for binding curves of the other tRNAs as well as for the respective fluorescence time traces (figures A.5-A.7).

### Application 2: Influence of tRNA Modification Deficiencies and Heat Shock on tRNA Levels

In collaboration with the laboratory of Prof. Dr. R. Schaffrath, a second set of *S. cerevisiae* total tRNA samples was examined for changes in tRNA abundances. Next to a wildtype sample, total RNA from double mutant cells deficient in following combinations of the tRNA-modifying enzymes Elp3, Urm1, Deg1 and Tcd1 were obtained (growth temperature 30 °C, prepared by A. Ciftci, detailed description in [225]):  $\Delta elp3 \Delta deg1$ ,  $\Delta elp3 \Delta urm1$ ,  $\Delta urm1 \Delta deg1$ ,  $\Delta tcd1 \Delta elp3$  and  $\Delta tcd1 \Delta urm1$ . Those enzymes are required for introduction of the  $mcm^5$  side chain at the wobble U nucleoside at position 34 (Elp3, [93]), the formation of the  $s^2$  moiety at the same nucleoside (Urm1, [99]), the deployment of the pseudouridine modification at position 38/39 (Deg1, [226]) or the dehydration of  $t^6A37$  to its cyclic form  $ct^6A$  (Tcd1, [227]). While 11 *S. cerevisiae* tRNAs carry a  $n/mcm^5(s^2)U34$  modification [92], only  $tRNA_{3UU}^{Lys}$  and

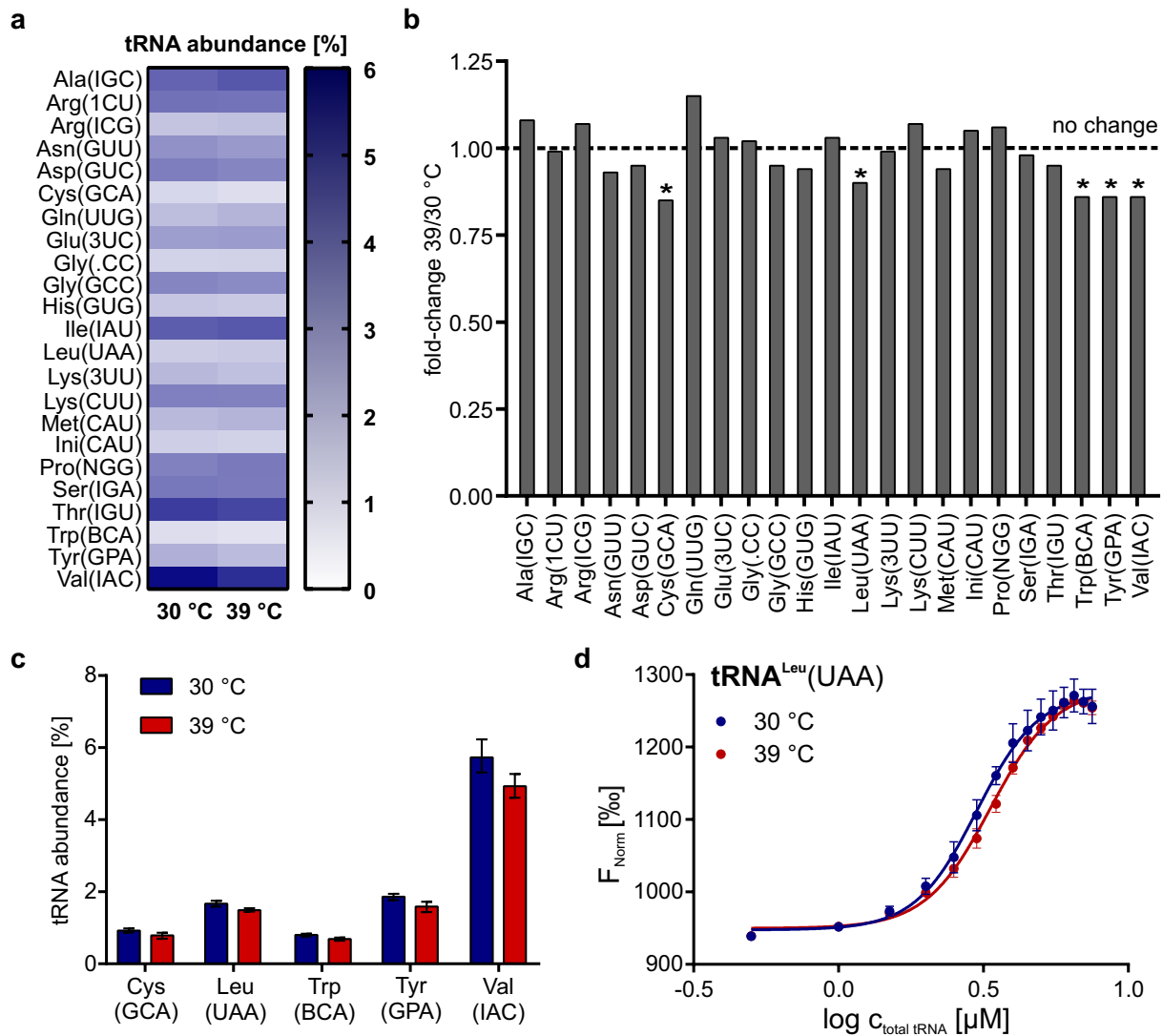


**Figure 3.14: Application 1: Growth temperature influence on tRNA levels** The abundances of 23 *S. cerevisiae* tRNAs in dependence of the growth temperature (30 or 39 °C, respectively) are summarized in (a). (b) displays the fold-changes between elevated and normal growth temperature for each tRNA analyzed, significant changes are marked with an asterisk. Only five tRNAs showed a significant reduction at 39 °C growth temperature (c), indicated by non-overlapping 95 % confidence intervals (error bars in c). The shift of the binding curve demonstrating the increase of the EC<sub>50</sub> at 39 °C growth temperature is exemplified for tRNA<sup>Leu</sup>(UAA) in (d). Binding curves obtained for the other tRNAs are shown in the appendix, figures A.5-A.7. The total tRNA samples investigated were kindly provided by Dr. S. Leidel.

tRNA<sup>Gln</sup><sub>3UG</sub> carry both a mcm<sup>5</sup>s<sup>2</sup>U34 and either ct<sup>6</sup>A37 or Ψ38, and are thus probably the most affected tRNAs in the described mutants [225]. Single mutants deficient in Elp3 (or other elongator subunits), in components of the thiolation pathway (*e.g.* Urm1, Ncs2, Uba4) or in the pseudouridylase Deg1 have previously been shown to, amongst others, confer a growth and temperature sensitivity phenotype [91, 93, 101, 102, 228] which was drastically enhanced in the here investigated double mutants [225]. Furthermore, the double mutants displayed morphological abnormalities due to protein aggregation and severe translational defects due to the reduced decoding capacity of the affected tRNAs [225]. Since all those phenotypes

could at least partly be suppressed by overexpression of either tRNA<sup>Lys</sup><sub>3UU</sub> (in  $\Delta tcd1\Delta elp3$  and  $\Delta tcd1\Delta urm1$ ) or tRNA<sup>Gln</sup><sub>3UG</sub> (in  $\Delta urm1\Delta deg1$  and partially in  $\Delta elp3\Delta deg1$ ), the malfunction of those two tRNAs, caused by the combined lack of anticodon modifications (see above), was determined to be responsible for the severe growth phenotypes [225]. To further investigate the influence of the different double mutant combinations on those two tRNAs, their abundances in wildtype and mutant cell were analyzed using the MST-based quantification assay including additionally the examination of tRNA<sup>Pro</sup><sub>NGG</sub> and tRNA<sup>His</sup><sub>GUG</sub> levels. Analysis of tRNA<sup>Pro</sup><sub>NGG</sub> was incorporated in the assay as it was observed to aid the function of tRNA<sup>Gln</sup><sub>3UG</sub> in a  $\Delta deg1\Delta kti12$  background, which also leads to a defect in both wobble U34 modification and  $\Psi38/39$  [228] and thus is similar to the  $\Delta elp3\Delta deg1$  mutant, in which tRNA<sup>Gln</sup><sub>3UG</sub> overexpression achieved only a partial rescue [225]. Additionally, tRNA<sup>His</sup><sub>GUG</sub> was analyzed as putatively unaffected control to exclude unspecific effects that concern non-target tRNAs. In addition to the total RNA samples extracted from cultures grown at 30 °C, samples from the same *S. cerevisiae* strains treated with a 2 h heat shock (37 °C) prior to RNA isolation (prepared by A. Ciftci) were examined, as the temperature sensitivity phenotype observed [225] might possibly amplify a potential effect on tRNA abundances. Representative examples for MST fluorescence time traces received for the four tRNAs of interest (WT samples, 30 °C) are displayed in figure 3.15, respective binding curves obtained by analysis in the “thermophoresis” setting are shown in figure 3.16. All EC<sub>50</sub> values obtained from the MST measurements are listed in the appendix (tables A.2, A.3, A.4 and A.5). Quantification results for all four tRNAs are summarized in figure 3.17 a (30 °C growth temperature) and figure 3.17 b (heat shock), giving the mean values received from technical triplicates. To investigate changes in tRNA levels more profoundly, the data was examined addressing the two following scientific questions:

**Changes in Double Mutant Strains Compared to Wildtype** The results of the MST-based quantification of the four tRNAs were first examined in respect to changes of tRNA levels in mutant strains compared to the wildtype separately for normal growth temperature and heat shock application. Fold-changes of the single tRNA abundances were rather small, ranging from 0.8 to 1.6, and are summarized in figure 3.18. Only in five cases the decrease or increase was significant (significance criterium: non-overlapping 95 % confidence intervals, marked with an asterisk in figure 3.17 and with red boxes in figure 3.18). Of those, the 20 %-reduction of tRNA<sup>Lys</sup><sub>UUU</sub>, carrying a mcm<sup>5</sup>s<sup>2</sup>U34 but no pseudouridine-38/39 modification in wildtype [80, 102], was detectable under both growth conditions in the  $\Delta elp3\Delta deg1$  double mutant, but interestingly not in the other  $\Delta elp3$  double mutant combinations in which the mcm<sup>5</sup> side chain was abolished. Additionally, tRNA<sup>Pro</sup><sub>NGG</sub> (containing a wobble U34 modification as well as pseudouridine-38) showed significant increases up to 1.6-fold in the  $\Delta elp3\Delta deg1$  mutant (heat shock) and the  $\Delta elp3\Delta urm1$  mutant (30 °C) compared to wildtype. tRNA<sup>Gln</sup><sub>UUG</sub>, likewise containing a mcm<sup>5</sup>s<sup>2</sup>U modification at U34 and pseudouridine-38, showed only a non-significant, small increase in the respective  $\Delta elp3$  double mutants. Loss of the ct<sup>6</sup>A modification in the  $\Delta tcd1$  mutants displayed no significant changes of any of the four tRNAs. Altogether, the results indicated that in strains lacking various tRNA modification enzymes, the abundance of the

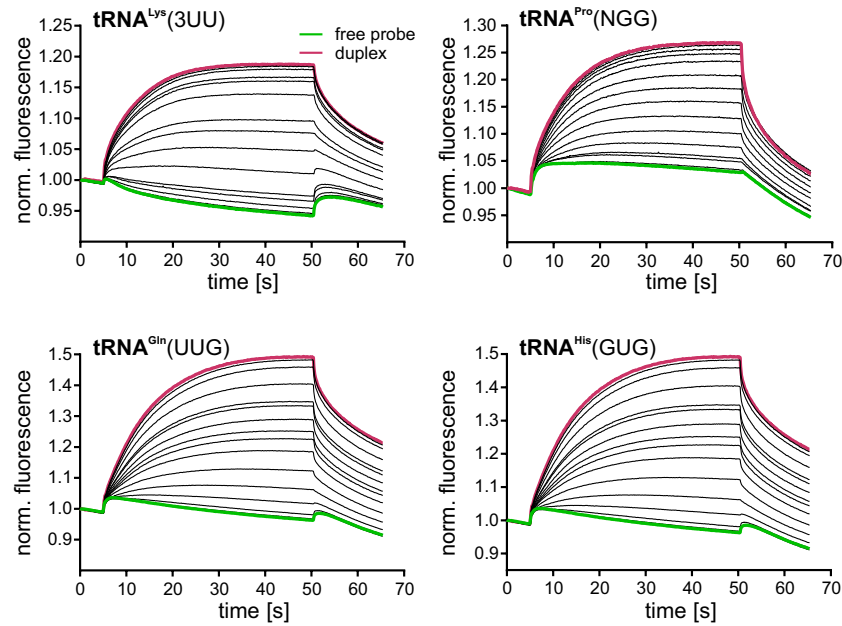


**Figure 3.15: Application 2: MST fluorescence time traces** obtained for the four tRNAs indicated in wildtype *S. cerevisiae* total tRNA (30 °C growth temperature, prepared by A. Ciftci). Time traces of the lowest and highest tRNA concentration, resembling free and bound DNA probe, are indicated in green and magenta, respectively.

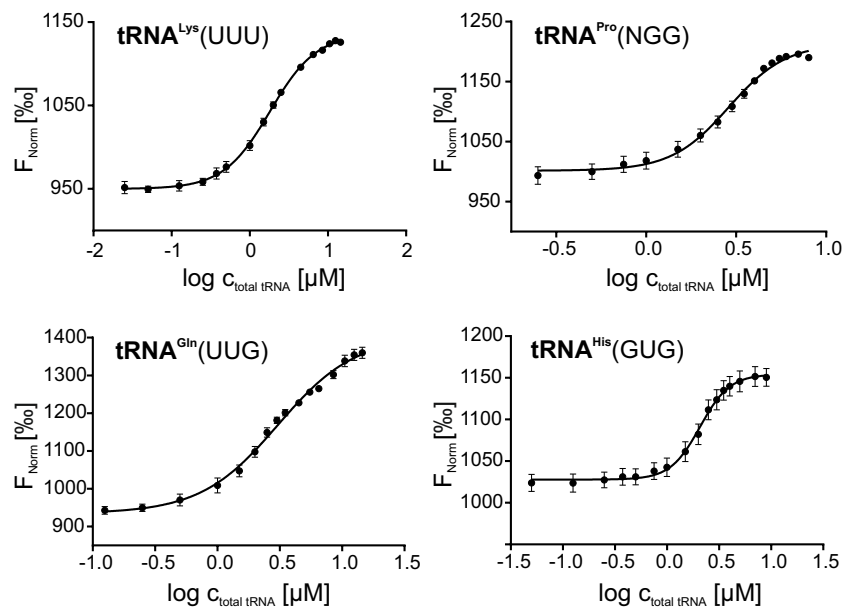


**Figure 3.16: Application 2: Binding curves** obtained for the four tRNAs by analyzing the time traces shown in figure 3.15 in the “thermophoresis” mode. Mean values of technical triplicates are shown, error bars represent the standard deviation,  $n=3$ .

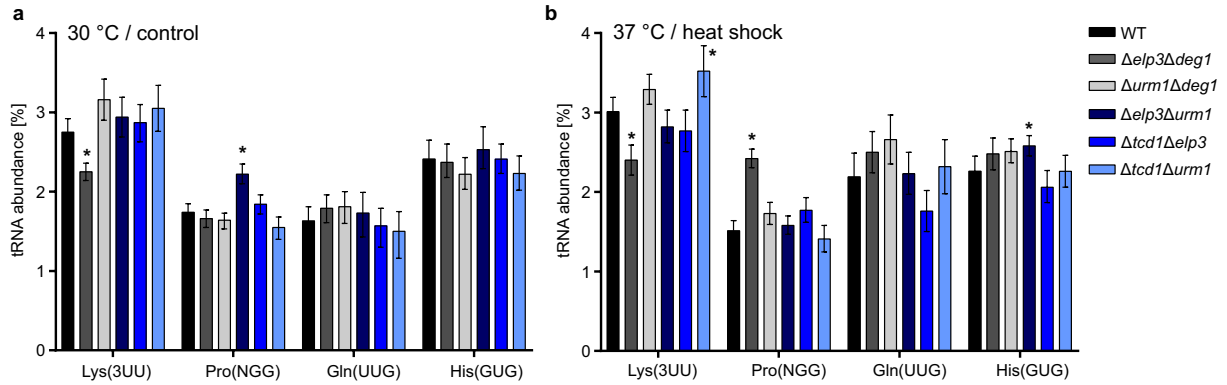


**Figure 3.17: Application 2: Overview of the quantification results** of the four target tRNAs indicated in wildtype and five double mutant *S. cerevisiae* strains grown under normal (30 °C, a) conditions and under application of heat shock (37 °C, b). Significant differences compared to wildtype are marked with an asterisk. Error bars represent the 95 % confidence intervals calculated for the % tRNA values. Total RNA samples used for the analysis were kindly provided by A. Ciftci.

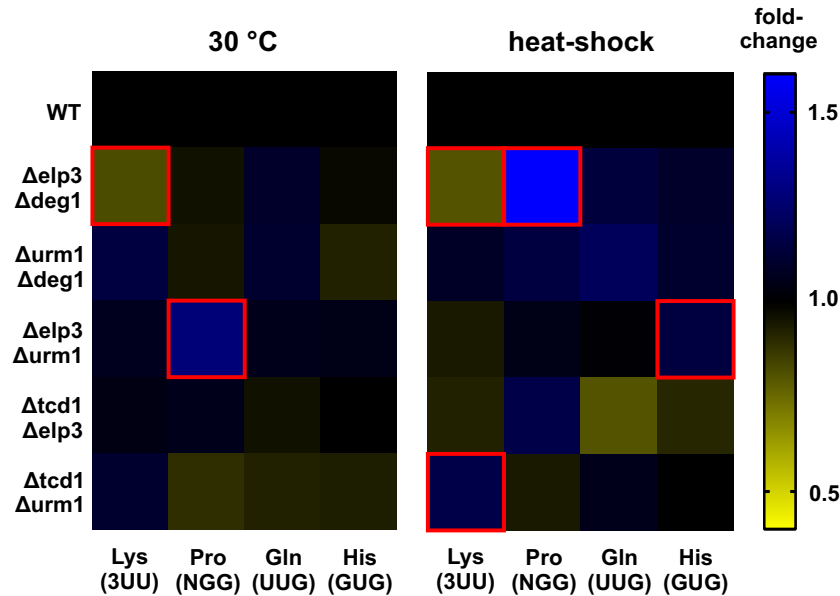


**Figure 3.18: Application 2: Comparison of double mutants and wildtype** The heatmaps display the fold-changes of the abundances of the four tRNAs in the double mutant strains compared to wildtype, separately for 30 °C growth temperature (left) and heat shock application (right). Significant changes are marked with red boxes. Total RNA samples forming the basis of the experiments were received from A. Ciftci.

tRNAs targeted by the respective modification enzyme was not drastically changed, and that tRNAs containing a  $\text{mcm}^5(\text{s}^2)$  side chain at U34 with or without the presence of a pseudouridine-38/39 modification were more susceptible for changes. These results are in line with studies on the various single knockdowns, with did not shown any alterations in steady state levels of the respective target tRNAs [91, 92, 228]. However, additional studies are required to further examine the interaction of  $\text{mcm}^5$  and  $\Psi_{38/39}$  in regard to changes of tRNA abundances in the respective double knockouts.

**Heat Shock-Induced Changes** Secondly, changes in tRNA abundances induced by the heat shock treatment were determined by comparing the tRNA levels under heat shock to the ones under normal growth conditions for each mutant and the wildtype separately. Here, tRNA<sub>3UG</sub><sup>Gln</sup> displayed the most distinct changes (see figure 3.19 b), with significantly increased levels under heat shock in four out of the six strains analyzed (fold-changes 1.34 to 1.55), including the WT and  $\Delta tcd1\Delta urm1$  strains in which the formation of the anticodon loop modifications of tRNA<sub>3UG</sub><sup>Gln</sup> was not comprised. The other two strains,  $\Delta elp3\Delta urm1$  and  $\Delta tcd1\Delta elp3$ , likewise showed increases of tRNA<sub>3UG</sub><sup>Gln</sup> abundance of 29 and 12 %, which however were not significant. Considering that the increase of tRNA<sub>3UG</sub><sup>Gln</sup> was detectable in all strains, it might rather represent a general consequence of the temperature increase than be caused by the lack of the respective tRNA modifications. However, a temperature increase was shown to result in a loss of the s<sup>2</sup>-moiety of mcm<sup>5</sup>s<sup>2</sup>U in both wildtype and  $\Delta deg1$  strains [57, 228] and thus the elevation of tRNA<sub>3UG</sub><sup>Gln</sup> might comprise a response to the loss of s<sup>2</sup>U induced by heat shock. Furthermore, a compensatory increase in response to the lack of the s<sup>2</sup>-moiety (or any other of the anticodon loop modifications) seemed plausible considering the suppression of the growth defects of the double mutants by overexpression of (hypomodified) tRNA<sub>3UG</sub><sup>Gln</sup> [225]. Interestingly, tRNA<sub>3UU</sub><sup>Lys</sup> which likewise contains a mcm<sup>5</sup>s<sup>2</sup>U34 and thus is affected by the temperature-induced loss of the s<sup>2</sup>-moiety, did not display any significant changes in the analyzed strains. Thus, tRNA<sub>3UG</sub><sup>Gln</sup> might be more susceptible to temperature-induced changes of the U34 modification. Of the other tRNAs investigated, only tRNA<sub>NGG</sub><sup>Pro</sup> showed significant changes under heat shock in two strains:  $\Delta elp3\Delta deg1$  (1.46-fold) and  $\Delta elp3\Delta urm1$  (0.71). Altogether, fold-changes under heat shock treatment ranged from 0.71 to 1.55 and are summarized in figure 3.19.

**Application 3: Cleavage of tRNA<sub>3UG</sub><sup>Gln</sup> by the *Pichia acaciae* Killer Toxin PaT** Again in collaboration with the laboratory of Prof. Dr. R. Schaffrath, the effects of PaT killer toxin on tRNA<sub>3UG</sub><sup>Gln</sup> levels were analyzed by MST (for effects on the polyA levels, see section 3.1.3.2, application). The PaT killer toxin of *Pichia acaciae* is a tRNase targeting predominantly tRNA<sub>3UG</sub><sup>Gln</sup>, and the reduction of the tRNA<sub>3UG</sub><sup>Gln</sup> abundance after PaT application has previously been shown by comparative RT-PCR and northern blots [229]. This effect was intended to be confirmed using the newly-established MST-based quantification method in order to further underline the applicability of the method as well as its advantages, e.g. the low analysis time and sample consumption. Therefore, total RNA samples from wildtype BY4741 *S. cerevisiae* cells containing an empty vector as well as from cells containing a galactose-inducible PaT vector were prepared by A. Ciftci. In order to remove all possible shorter fragments of tRNA<sub>3UG</sub><sup>Gln</sup> which might hybridize to the probe as well and interfere with the quantification of the intact tRNA, total tRNA pools were extracted by denaturing PAGE. MST measurements were performed using the DNA-probe specific for tRNA<sub>3UG</sub><sup>Gln</sup> as well as for tRNA<sub>GUG</sub><sup>His</sup>, which served as control tRNA expected to be unaffected by PaT. While levels of tRNA<sub>GUG</sub><sup>His</sup> remained mainly unchanged (EC<sub>50</sub> 2.1 and 2.2  $\mu$ M, figure 3.20 b), the abundance of tRNA<sub>3UG</sub><sup>Gln</sup> was drastically decreased in the PaT-vector sample, as indicated by the pronounced right-shift of the binding curve (figure 3.20 a). Analysis of the MST data revealed a 6.7-fold increase in the EC<sub>50</sub> value under PaT induction (23.3 vs. 3.5  $\mu$ M in

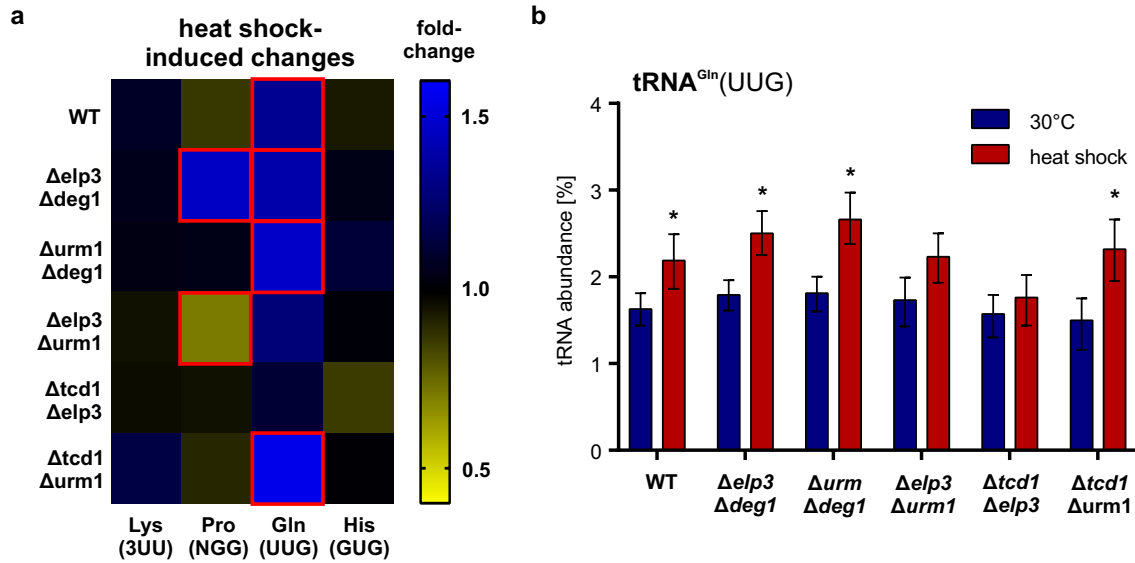


**Figure 3.19: Application 2: Heat shock induced changes in tRNA abundances** The fold-changes (heat shock vs. 30 °C) of the abundances of the four tRNAs induced by heat shock are summarized in (a), significant fold-changes are highlighted by red boxes. The most affected tRNA under heat shock was tRNA<sup>Gln</sup>(3UG), displaying significant increases in four of six strains compared to normal growth temperature (b). Error bars present the 95 % confidence intervals, n=3. Asterixes mark significant differences. The basis total RNA mixtures for analysis were provided by A. Ciftci.

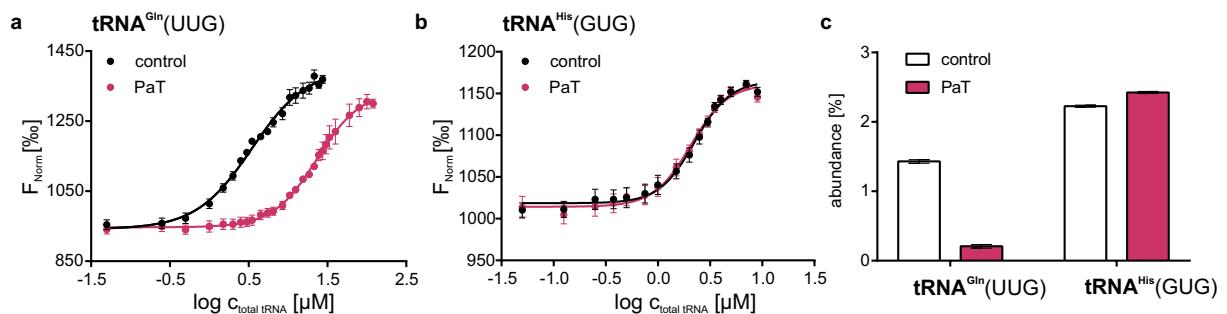


**Figure 3.20: Application 3: PaT killer toxin-mediated cleavage of tRNA<sup>Gln</sup>(3UG)** The cleavage of tRNA<sup>Gln</sup>(3UG) was monitored by MST: Binding curves received from the MST measurements of tRNA<sup>Gln</sup>(3UG) (a) and tRNA<sup>His</sup>(GUG) (b) in both control and PaT-treated total tRNA samples. The abundance of tRNA<sup>Gln</sup>(3UG) was severely reduced under PaT induction, while tRNA<sup>His</sup>(GUG) remained mainly unaffected (c). Error bars represent the standard deviation of technical replicates, n=3. Total RNA samples applied in the analysis were obtained from A. Ciftci.

the control sample), equivalent to a 85 % reduction of intact tRNA<sup>Gln</sup><sub>3UG</sub> (figure 3.20 c). Thus, the MST-based quantification method proved to be well suitable for reproducing and confirming the results from other methods of tRNA quantification, furthermore allowing to quantify the extend of PaT-induced tRNA<sup>Gln</sup><sub>3UG</sub> cleavage.

#### 3.1.3 Investigation of PolyA-Tailored RNA

Having established a MST-based protocol for the quantification of single tRNA species in total tRNA, the next goal was to test the transferability of the method to other RNA classes to increase the application possibilities. In contrast to quantifying other single small RNA molecules by MST, for which the method should be easily adaptable by designing the respective DNA probes (e.g. for 5S rRNA of *E. coli*, see appendix, figure A.9), the more sophisticated attempt to quantify the pool of polyA-tagged RNA *via* MST was addressed, making use of polyT-DNA probes. A method for a fast and effortless determination of changes in the subset of polyadenylated RNA, mostly composed of mRNA, is highly desirable, because it would offer a quick insight into changes of the mRNA pool in response to variable conditions. Considering the variable length of polyA tails [230, 231] across the transcriptome, a set of DNA probes of different length was tested, ranging from 10 to 80 nt (polyT). Various *in vitro* transcribed mRNAs (kindly provided by Isabell Hellmuth and Prof. Dr. Katalin Karikó) carrying polyA tails of 64, 51 and 101 nt length were included in the experimental test set for evaluation of the probes' binding. Finally, total RNA from HeLa cells as well as from *S. cerevisiae* (see 3.1.2.6, application 3) was examined for its polyA content.

##### 3.1.3.1 Influence of PolyT Probe and PolyA Tail Length

Starting with an *in vitro* transcribed mRNA carrying a 64 nt polyA tail (MelanA/GFP mRNA, kindly provided by I. Hellmuth), a set of six different DNA/RNA probes was tested for their performances in quantifying the *in vitro* transcript. These probes included five polyT-DNA probes of 10, 20, 30, 50 and 80 nt (MH824, 820, 825, 821, 822), as well as a specific 40 nt RNA probe (MH819) complementary to the 3'-untranslated region (UTR) of the mRNA. To evaluate the performance of the single probes in measuring the polyA content in an RNA sample, examined for the IVT of MelanA/GFP mRNA as model, following considerations were made (illustrated in detail in figure 3.21):

Given both the length of the polyA tail and the polyT-DNA probes, the possibility of a binding of two or more probes per polyA tail had to be taken into account, especially for the shorter probes. To assess that possibility, for each probe-mRNA pair, the hybridization ratio (probe:mRNA) at 100 % binding of the probe (corresponding to a full saturation of the DNA probe at an mRNA concentration of  $2 \times \text{EC}_{50}$ ) was calculated from the MST data as described in section 3.1.2.1. As depicted in figure 3.21 (middle), a "perfect" hybridization ratio of 1:1 (probe:mRNA) resembled the case in which each mRNA molecule was statistically bound by one oligonucleotide molecule and thus efficient capture of all mRNA molecules in a sample by the probe was considered to be possible. That was, for example, expected to be the case for the specific RNA probe targeting the mRNA transcript specifically outside the polyA tail. In contrast, a measured hybridization ratio  $<1:1$  (probe:mRNA), e.g. 0.5:1, implied that for complete binding of all probe molecules, an excess of mRNA molecules over the DNA-probe was required and thus not every mRNA molecule present in the sample was bound at a concentration of  $2 \times \text{EC}_{50}$  (e.g. for a ratio of 0.5:1, only every second mRNA was bound on average, figure 3.21, right). That,



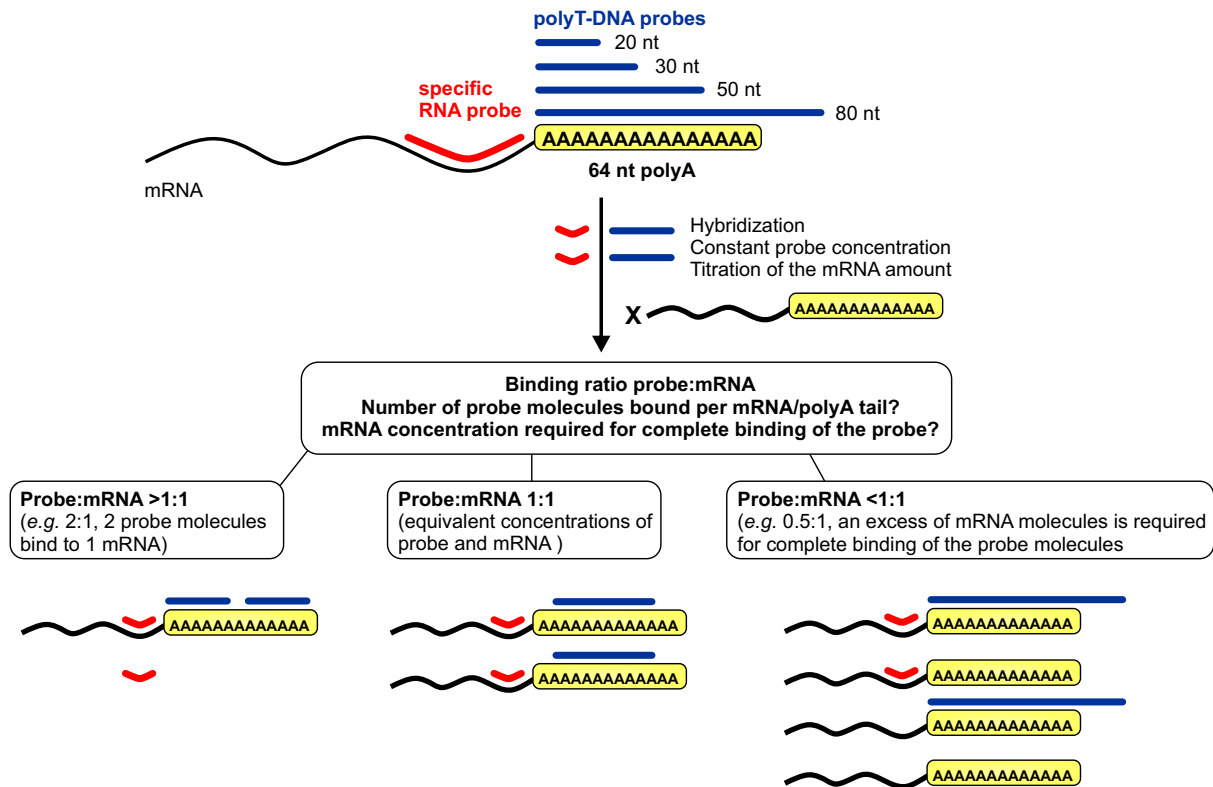


**Figure 3.21: Binding of the polyT-DNA probes to polyadenylated RNA** Possible binding behaviors of the different polyT probes are depicted. Binding ratios (probe:mRNA) refer to an mRNA concentration of  $2x EC_{50}$ , which is required for a 100 % binding of the probe molecules. An specific probe (red) as well as probes with a similar length compared to the polyA tail were expected to bind in equimolar concentrations to the mRNA transcript and thus in a 1:1 ratio. In case of the shorter probes (left), the polyA tail of the transcript might be bound by more than one oligonucleotide, hence the hybridization ratio is  $>1:1$  (probe:mRNA). Notably, in case of the longer polyT-DNA probes, a binding ratio of  $<1:1$  was observed (right), indicating that an excess of mRNA molecules was required to ensure complete binding of all probe molecules.

in turn, indicated that a certain portion of mRNA molecules present in a sample would not be captured by the probe and thus would escape detection. On the other side, a hybridization ratio of  $>1:1$  (probe:mRNA), e.g. 2:1, suggested that more than one oligonucleotide was bound to each mRNA molecule (e.g. 2 oligonucleotides per mRNA, figure 3.21, left). This case, as well as the “perfect 1:1” binding, was expected to ensure that all mRNA molecules in a total RNA sample were included in analysis. Taking those considerations into account, the theoretical hybridization ratio of the respective probe:IVT pair obtained from the MST measurements was used as parameter to evaluate the probes performance in quantifying the polyA content in total RNA samples. Of note, the calculated hybridization ratios represented a conceptual parameter illustrating the average number of oligonucleotides bound to the mRNA’s polyA tail, and did not reflect the actual hybridization status of each mRNA molecule. For example, a binding ratio of  $<1:1$  suggested that there was a mixture of mRNAs bound by one oligonucleotide and unbound mRNAs at 100 % binding of the probe, and that on average each mRNA was hybridized to  $0.x$  oligonucleotides. These considerations were subsequently tested for their relevance in the MST-based quantification using the 64 nt polyA-mRNA transcript. The MST

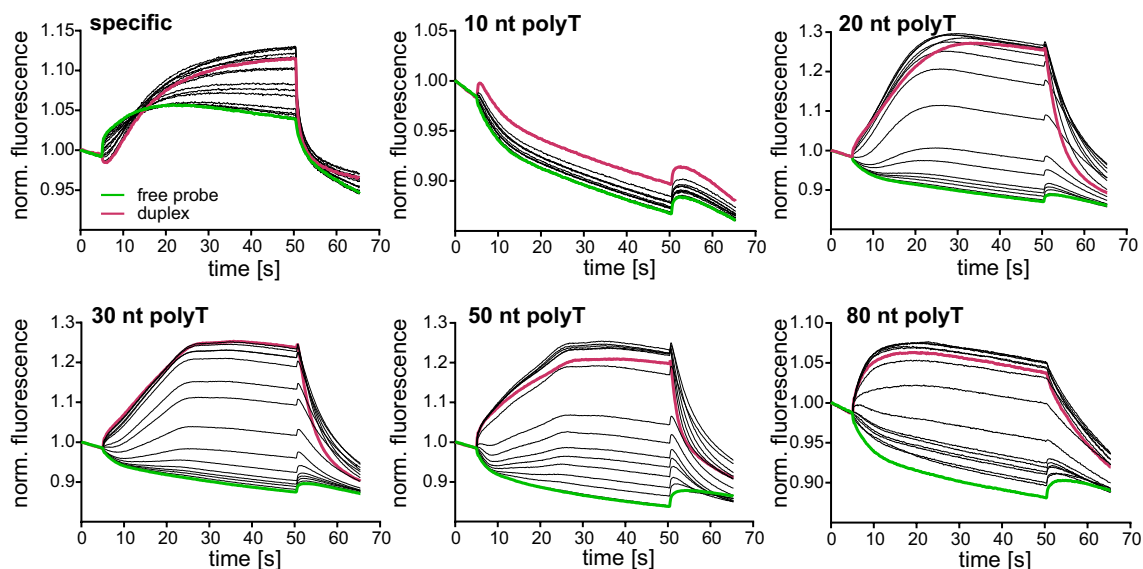


**Figure 3.22: Fluorescence time traces of the polyT DNA probes** For all polyT DNA probes as well as a specific RNA probe, titration series were prepared using the MelanA/GFP mRNA IVT and analyzed by MST. The fluorescence time traces showed clear differences between unbound and bound probe for all probes tested except for the 10 nt polyT probe. For each titration series, the time traces of the lowest and highest IVT concentration are marked (green and magenta, respectively), representing the free and fully bound probe. The mRNA was kindly provided by I. Hellmuth.

time traces received for the titration series of the MelanA/GFP mRNA with each of the five polyT-DNA probes are depicted in figure 3.22, demonstrating binding of all probes to the mRNA by clear changes in the thermophoretic response upon hybridization, with the exception of the 10 nt polyT-DNA (MH824), for which no considerable changes were observed. Of note, hybridization of the shorter probes (10-30 nt) was performed at 37 °C instead of the standard 65 °C, and receiving a MST response for the specific RNA probe (MH819) required the change of the hybridization conditions to pH 6.5.  $EC_{50}$  values obtained from the respective binding curves (figure 3.23 a) were used for calculation of the hybridization ratios (probe:mRNA, figure 3.23 b), with only the specific RNA probe displaying a almost perfect 1:1 binding (1.09:1).  $EC_{50}$  values and hybridization ratios are listed in the appendix, table A.6. As expected, the shorter probes MH820 and MH825 (20 and 30 nt, respectively) displayed a statistical hybridization ratio of >1:1, indicating that indeed the IVT's polyA tail can be bound by more than one oligonucleotide simultaneously. In case of the 20 nt polyT-DNA probe, the hybridization ratio indicated a binding of 2 oligonucleotides per mRNA on average. The hybridization ratio of the 30 nt probe of 1.5:1 probably resulted from the fact that the binding of two probes to one mRNA molecule did not occur exactly simultaneous, hence the first probe might have bound in a position that disabled the binding of a second probe. That effect was more pronounced for the 30 nt than for the 20 nt probe, explaining the higher binding ratio of the 20 nt probe. That possibility was further supported by the results of an 1:1 mix of the two probes (20 and 30 nt), which displayed an  $EC_{50}$  almost identical to the 30 nt probe (0.0166 vs. 0.0170  $\mu$ M). Furthermore, the mix clearly performed better than the 50 nt probe (figure 3.23 c). However, none of the

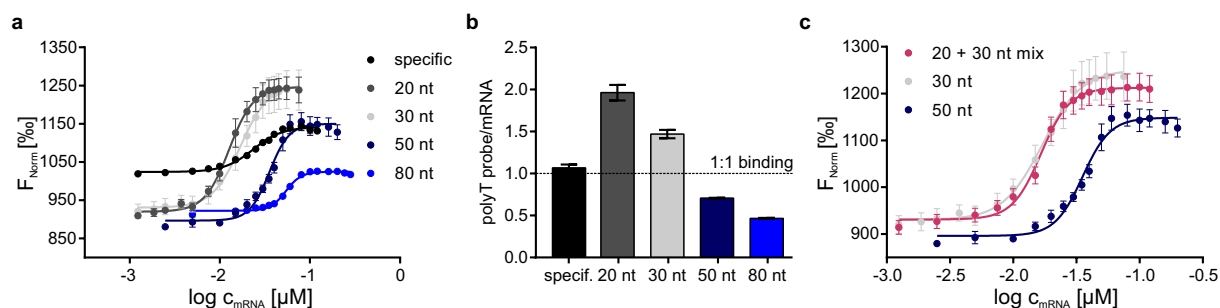


**Figure 3.23: Influence of PolyT DNA probe length** Binding curves (a) of the four polyT DNA probes and the specific RNA probe to MelanA/GFP mRNA (IVT) and the respective hybridization ratios calculated for each polyT-mRNA pair (b) are displayed. A 1:1 mix of the 20 and 30 nt probes performed almost identical to the 30 nt probe, and clearly outmatches the 50 nt probe, as indicated by the binding curves displayed in (c). Error bars present the standard deviation of technical triplicates, probe concentration was 50 nM in each experiment. The mRNA was kindly provided by I. Hellmuth.

two probes compassed the theoretically possible hybridization ratio (3:1 or 2:1, respectively). Interestingly, to achieve complete saturation of the longer probes of 50 and 80 nt (MH821 and MH822), an excess of the mRNA transcript was necessary (hybridization ratios  $<1:1$ ), indicating that they did not bind to every mRNA molecule present. The influence of the variable lengths of probes and tails were further investigated by including two more *in vitro* transcribed mRNAs (kind gifts of Prof. Dr. K. Karikó), containing polyA tails of 51 and 101 nt, respectively. The obtained hybridization ratios are depicted in figure 3.24, again, only the shorter probes were capable of binding to all mRNAs in a ratio of  $\geq 1:1$  (probe:mRNA). The 50 nt probe (MH821) showed indeed a  $>1:1$  binding to the 101 A-mRNA, but failed to bind every mRNA molecule for the IVTs with shorter polyA tails. All  $EC_{50}$  values and hybridization ratios are listed in table A.6 (appendix). Altogether, the results indicated that overhangs of the probe over the poly A tail were not well tolerated, and that shorter probes yielded better results, especially the 20 nt probe. Of note, the two mRNAs provided by Prof. Dr. K. Karikó contained five additional nucleotides at the 3'-end of the polyA tail, which might have interfered with the binding of probes longer than the respective polyA tail. However, as the 50 and 80 nt probes displayed incomplete binding to the 64 nt polyA of the MelanA/GFP mRNA as well, that effect, if present, could not explain the results sufficiently. In summary, for quantifying polyA contents in total RNA samples, which contain mRNAs with shorter and longer PolyA tails [230, 231], the 20 nt probe was considered to be the probe of choice to ensure the capture of (almost) all mRNA molecules.

### 3.1.3.2 Transfer to Total RNA

Since the results from the *in vitro*-transcribed mRNAs were quite promising, the transfer to total RNA samples was intended. One major problem of applying the method to mRNA was its low abundance in total RNA and hereby the necessity to use high amounts of total RNA in the titration series. Thus, the standard conditions (100 nM labeled probe, 20  $\mu\text{L}$  sample volume) used for the tRNA quantification would comprise the requirement of high sample

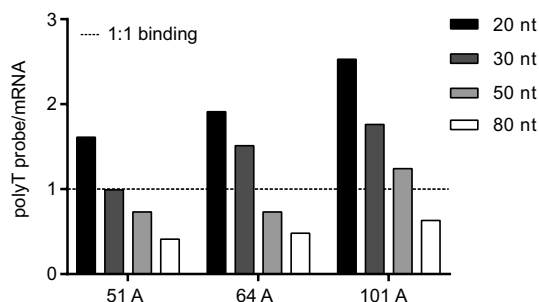


**Figure 3.24: Binding in dependence of polyA tail and polyT probe length** Binding ratios of the four polyT probes to three *in vitro*-transcribed mRNAs carrying polyA tails of 51, 64 and 101 nt length (kindly provided by Prof. Dr. K. Karikó and I. Hellmuth). A 1:1 binding is indicated by the dotted line. Probe concentration was 50 nM in each experiment. Exact ratios and corresponding  $EC_{50}$  values are tabled in the appendix (table A.6).

amounts of up to 400  $\mu\text{g}$  total RNA per titration series, which might not be practicable when investigating biological samples. However, due to the quite high fluorescence signal of the 100 nM probe solutions, a reduction of the probe concentration to 50 and even 25 nM was technically possible without problems, and polyA quantification results in HeLa cell RNA were excellently comparable displaying less than 1 % deviation for the 25 nM pipetting scheme compared to the 100 nM one (figure 3.25 a). Further downscaling was achieved by reducing the final sample volume to 10  $\mu\text{L}$  and resulted in a sample requirement of approximately 55  $\mu\text{g}$  per titration, which should be a feasible amount for many applications. Here, the method was applied to determine polyA contents in *S. cerevisiae* cells lacking  $tRNA_{3'UTR}^{Gln}$  due to PaT-mediated cleavage (see section 3.1.2.6, application 3). Obtained  $EC_{50}$  values were applied to calculate the number of polyT probes binding to one  $\mu\text{g}$  of total RNA (polyT/ $\mu\text{g}$ ), which is proportional to the amount of polyA-tagged RNAs and hence could be used to compare levels of polyadenylated RNA in differently treated samples of the same cell type or organism (under assumption that the polyA tail length distribution does not change).

**Application: PolyA Abundance in PaT Killer Toxin Exposed *S. cerevisiae* Cells** Total RNA samples of *S. cerevisiae* cells containing either an empty or a PaT killer toxin encoding vector (described in 3.1.2.6, application 3) were investigated for their polyA content using the 20 nt polyT-DNA probe. Binding curves received from the MST measurement are displayed in figure 3.25 b, showing a slight right-shift of the curve and with that a small but significant increase of the  $EC_{50}$  value of the PaT-exposed sample. This increase resembled a quite pronounced reduction of 28 % of the polyA levels compared to the untreated control, which might be a result of the toxin's functions which include DNA damage induction and cell cycle arrest in S-Phase [232, 233]. This example highlights the suitability of the MST-based protocol for relative quantification of changes in the global mRNA content under threatening conditions. Nevertheless, the results from the experiments employing mRNA with different polyA tail lengths and various polyT-DNA oligonucleotides indicated that the method developed is not only sensitive to changes in polyA-RNA abundance, but also to some extent to changes in

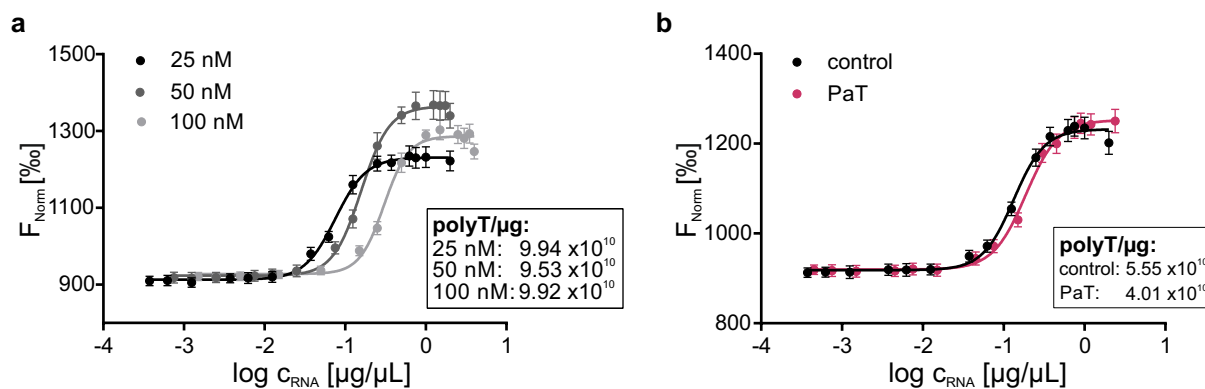


**Figure 3.25: PolyA measurement in total RNA** The reduction of the required RNA amount was possible by reducing the DNA probe concentration to 25 nM in the MST experiments, as shown by the binding curves of HeLa total RNA received at 25, 50 and 100 nM DNA probe concentration (a). Application to total RNA of PaT-induced and control *S. cerevisiae* cells, revealed an approximately 28 % reduction of the polyA content in the treated cells (b). The number of polyT probes bound per  $\mu\text{g}$  total RNA ( $\text{polyT}/\mu\text{g}$ ) is indicated for each sample. Samples of *S. cerevisiae* total RNA used in (b) were prepared by A. Ciftci.

the lengths of polyA tails. Thus, detected changes in polyA abundance might be caused by changes in total mRNA abundance or by changes in the polyA tail length, or both. For example, various stress types were shown to lead to an inhibition of mRNA deadenylation and thus mRNA decay, hereby influencing both mRNA levels and polyA tail length [234]. Therefore, the presented method is especially powerful in allowing an fast overview over global changes in the transcriptome, however, depending on its results, further investigations might be required for in-detailed analysis of the biological background of the changes. Due to its easiness, low cost and broad applicability, the developed method, however, might outperform the more specific, standard mRNA quantification methods such as RNA-Seq [235, 236] and RT-qPCR [237] if the aim is to quickly check possible global changes in the transcriptome.

### 3.1.3.3 Influence of Sample Purity

Although the required RNA amount for the measurement of polyA abundance in total RNA samples was reduced successfully to an amount feasible for many applications, analysis of the *S. cerevisiae* samples described above highlighted an additional prerequisite for the quantification by MST, which was sample purity. As high RNA concentrations were applied in the titration series (up to  $2 \mu\text{g}/\mu\text{L}$  RNA), purity of the RNA stock was essential, and any potential impurities like salts or other compounds that might interfere with the hybridization had to be removed carefully. Figure 3.26 shows the effect of an additional purification step on the MST time trace and binding curve for the *S. cerevisiae* samples described above. The non-purified samples revealed severe changes in the thermophoretic behavior at higher concentrations leading to an abrupt decline in the binding curve, which was not caused by the high RNA concentration, since this effect was not observed for the HeLa total RNA employed in the same amounts. Additional purification of the samples reestablished a well-shaped and evaluable binding curve. Of note, for tRNA measurements in total tRNA pools isolated by PAGE, sample purity after gel elution

and precipitation was high enough for immediate use without the need of further purification steps.

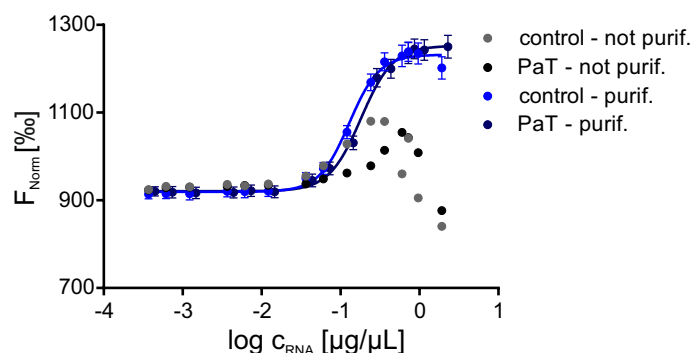


**Figure 3.26: Effect of sample impurities** Sample contamination with, for example, high amounts of salts or other compounds led to an abrupt change of the thermophoretic response as displayed by the pronounced drop in the binding curves at higher concentrations of non-purified samples (black, grey). This effect was completely reversed by an additional purification and desalting step prior to MST measurements (blue). Non-purified *S. cerevisiae* total RNA samples were obtained from A. Ciftci.

### 3.1.4 Summary

Here, microscale thermophoresis was applied to develop a method for the quantification of single tRNAs and other RNA species including the subgroup of polyadenylated RNAs. The hybridization-based quantification approach appeared to be a very fast, low sample-consuming and easy to accomplish alternative to traditional, more laborious methods like northern blots, making (t)RNA quantification possible in only a couple of hours. The method successfully determined hybridization ratios between a DNA probe and a complementary tRNA (IVT) with results in good agreement with gel shift-based assays. Furthermore, the implemented conditions allowed the quantification of native tRNAs in total tRNA mixtures, unperturbed by the presence of modifications and were successfully applied to the determination of tRNA abundances in various biological samples. While an absolute quantification of tRNAs in form of their content in a total tRNA mixture was feasible using the described approach, the method proved to be even more powerful in relative quantification of changes in (t)RNA abundances, *e.g.* in mutant strains compared to a wildtype sample. Such changes were easily detectable by shifts of the respective binding curves and thus the determined  $EC_{50}$  value, without the need for an absolute quantification. Moreover, the method was effectively transferred to the investigation of polyA-marked RNA present in total RNA samples by using short polyT DNA probes. Herein, the method proved to be suitable to detect relative changes in global polyA abundance in an extremely short time and thus to gain a general insight into overall changes in the transcriptome under, for example, stress conditions. However, the method was observed to be sensitive to not only mRNA abundance, but also to the length of the polyA tail, which should be considered when evaluating the results. In general, the MST-based method should be easily adaptable to other single RNA species as well, provided the sequence is known, however,

the abundance of the target RNA determines the RNA amount required for analysis. Although there were no negative effects of high amounts of non-target RNAs on the MST result in the applied concentrations, influences of even higher concentration on the MST experiment cannot be excluded due to the increasing viscosity of the solutions.

## 3.2 Sequence-Specific Isolation of Small Non-Coding RNAs

### 3.2.1 Introduction and Workflow

The isolation of single tRNA or other small RNA species from total (t)RNA is required for various scientific applications. Here, the isolation of single tRNAs, *e.g.* tRNA<sup>Arg</sup><sub>1CU</sub>, was mandatory to assess the influence of modified nucleosides on the MST-based tRNA quantification method (see section 3.1.2.4). Furthermore, LC-MS/MS analysis of single RNA species requires, due to the loss of sequence information during nuclease digestion, the previous isolation of the RNA of interest. However, while in case of tRNAs the modification pattern is well investigated [79, 80], that does not apply as thoroughly to other classes of small non-coding RNAs. For a specific small non-coding RNA (ncRNA), named mascRNA (see section 1.3), the presence of a modified nucleoside was suspected due to a high mismatch rate in sequencing data [178] but not confirmed yet. The small mascRNA resembles a short tRNA (61 nt), carries a 3'-CCA and is cleaved off the long non-coding RNA MALAT1 by tRNA-processing enzymes [54, 178]. Given that features, mascRNA might well be a target for tRNA-modifying enzymes as well. In order to be able to investigate the possibility of modified nucleosides in mascRNA more deeply by LC-MS/MS, an isolation of this small ncRNA was a prerequisite. Isolation of tRNAs has been successfully accomplished by using hybridization-based approaches [238–242], in which the target tRNA is bound to a complementary, immobilized DNA capture probe and subsequently separated from non-target RNA. The here applied, likewise hybridization-based protocol was loosely adapted from [128], with certain adaptations to increase yield and specificity. The workflow developed is depicted in figure 3.27 using tRNA as model and consisted on the following steps (for experimental details, see section 5.2.1.9):

- 1. Hybridization of target (t)RNA and complementary DNA probe:** Complementary probes were essentially the same probes as used for the MST measurements, covering the full-length (t)RNA and carrying both a fluorescent and a biotin label at opposite ends. If applicable (especially in case of tRNAs), the required hybridization ratios of total tRNA and DNA probe were determined by MST to maximize tRNA yields (figure 3.27 a).
- 2. Immobilization of the duplex of target RNA and DNA probe:** The RNA/DNA duplex was bound to streptavidin-coated magnetic beads *via* the biotin label of the probe and separated from non-target RNA by application of a magnet. Several washing steps ensured the thorough removal of all remaining RNA (figure 3.27 b).
- 3. Elution of the target RNA and DNase1 digestion:** Release of the target RNA from the duplex was achieved by incubation at elevated temperature in pure water. A small portion of the biotinylated probe was found to be cleaved off the beads as well, making an additional DNase1 digestion step necessary to remove the DNA probe (figure 3.27 c).
- 4. PAGE purification:** The eluted (t)RNA was purified by denaturing PAGE to remove any residual impurities like the DNase1 digestion products, unspecifically bound RNA or fragments of the target tRNA, *e.g.* tRNA halves (figure 3.27 d).



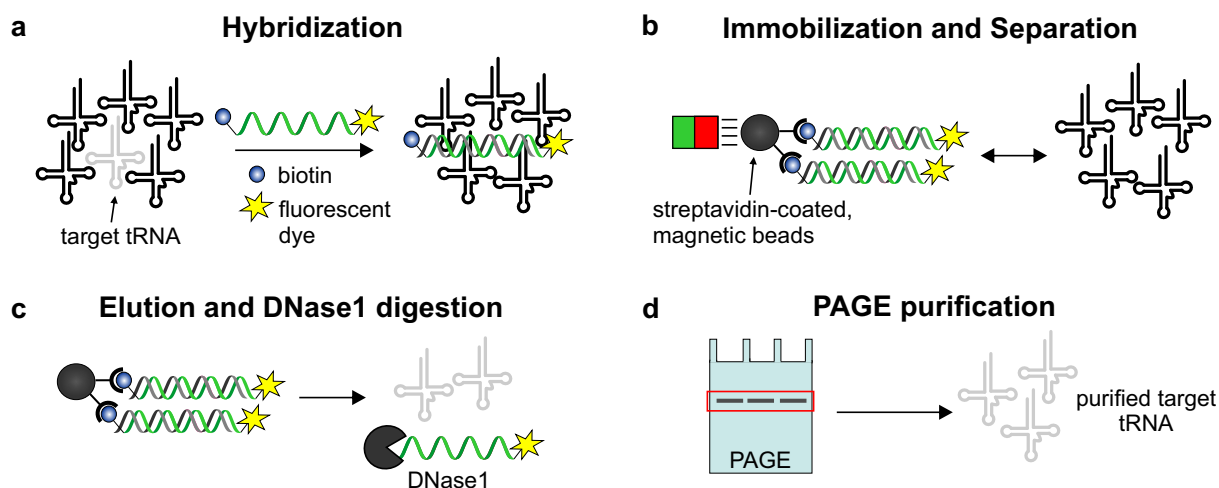


**Figure 3.27: Overview: Isolation of single (t)RNAs** The workflow of the hybridization-based isolation of single (t)RNA species using tRNA molecules as model is described. In total tRNA, only the target tRNA (grey) was able to hybridize to the complementary DNA probe (biotin-labeled, green) forming an RNA/DNA duplex (a), which was immobilized on streptavidin-coated, magnetic beads to remove non-target RNA (b). The target tRNA (plus a part of the DNA probe) was eluted from the beads, and a subsequent DNase1 digestion step ensured the removal of residual DNA probe (c). PAGE purification finally yielded the pure target tRNA (d).

### 3.2.2 Isolation of Single tRNAs

The isolation protocol presented in section 3.2.1 was applied to several tRNAs including *E. coli* tRNA<sub>MAU</sub><sup>Met</sup>, which served as model tRNA for optimization of the protocol, as well as several *S. cerevisiae* tRNAs. Here, tRNA<sub>1CU</sub><sup>Arg</sup> isolation results are described representatively, as results for the other isolated tRNAs were comparable. The native tRNA<sub>1CU</sub><sup>Arg</sup> was required in purified form for microscale thermophoresis experiments and is more thoroughly described in section 3.1.2.4. Further tRNAs that were successfully isolated included: tRNA<sub>3UU</sub><sup>Lys</sup>, tRNA<sub>NGG</sub><sup>Pro</sup>, tRNA<sub>3UG</sub><sup>Gln</sup>, tRNA<sub>1GU</sub><sup>Thr</sup>, and tRNA<sub>1AU</sub><sup>Ile</sup> (all *S. cerevisiae*). Furthermore, the protocol was effectively applied to *E. coli* 5S rRNA. Example PAGE gels of the two isolated *E. coli* RNAs are shown in the appendix (figure A.10).

#### 3.2.2.1 Isolation of *S. cerevisiae* tRNA<sub>1CU</sub><sup>Arg</sup>

For the MST experiments detailed in section 3.1.2.4, the isolation of native tRNA<sub>1CU</sub><sup>Arg</sup> in amounts sufficient for several MST titration series was necessary. MST quantification of tRNA<sub>1CU</sub><sup>Arg</sup> in total tRNA revealed an EC<sub>50</sub> value of 1.5 μM (see section 3.1.2.5), which was applied to calculate the required total tRNA amount (75 μg per 100 pmol DNA probe) employed for the isolation. In a first, small batch test isolation, the final PAGE gel was stained to verify the success of the isolation (figure 3.28). The lane of the isolation sample revealed a single band corresponding to the isolated tRNA, and no further bands which would indicate degradation products, tRNA<sub>1CU</sub><sup>Arg</sup> fragments or unspecifically bound RNA. Thus, in the following larger batch isolations, the tRNA band was excised making use of UV shadowing without prior staining. Furthermore, the success of the

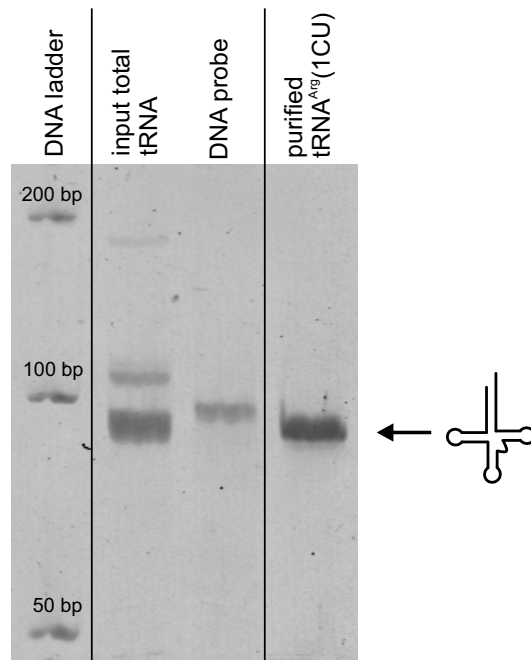


**Figure 3.28: PAGE analysis of isolated, native tRNA<sup>Arg</sup>(1CU)** The isolation success of tRNA<sup>Arg</sup>(1CU) was monitored by denaturing PAGE (10 %): The lane of isolated tRNA showed a single band in the region of the total tRNA control, indicating successful tRNA<sup>Arg</sup>(1CU) isolation and the absence of degradation products or unspecific RNAs of other sizes. Furthermore, no residual DNA probe was detectable in the sample, demonstrating successful DNase1 digestion. Gel Staining was performed using GelRed.

isolation was monitored by measuring the depletion of tRNA<sup>Arg</sup><sub>1CU</sub> in the supernatant containing the non-target RNA (obtained in the separation step in figure 3.27 b) *via* MST. Herefore, the supernatant was first concentrated by precipitation and subsequently DNase1 digested to remove leftover DNA probe which had not been immobilized on the beads. Removal of residual DNA probe was obligatory to prevent any interference with the MST measurement. Finally, the RNA was purified and concentrated by an additional precipitation step. Purified supernatant was then used for preparation of a titration series with the tRNA<sup>Arg</sup><sub>1CU</sub> specific probe as described for total tRNA (see section 5.2.1.10). As control to evaluate the success of the isolation, the input total tRNA batch was analyzed as well. Figure 3.29 shows the resulting binding curves from MST measurements, which was clearly right shifted but did not reach saturation levels for the supernatant compared to the input total tRNA, thus not allowing the calculation of an EC<sub>50</sub> value and the exact amount of residual tRNA<sup>Arg</sup><sub>1CU</sub> in the supernatant. Nevertheless, these results indicated that tRNA<sup>Arg</sup><sub>1CU</sub> was drastically reduced in the supernatant and demonstrated the successful isolation. The residual tRNA<sup>Arg</sup><sub>1CU</sub> present in the supernatant might presumably be explainable by an incomplete binding of the RNA/probe-duplex to the beads. This explanation seemed quite plausible, considering that the probe amount applied was calculated using the maximum binding capacity of the beads stated by the manufacturer, which might not have been practically achievable under the chosen conditions. Altogether, by performing a large batch isolation approach for MST experiments, approximately 5.65 µg tRNA<sup>Arg</sup><sub>1CU</sub> were obtained from 750 µg total tRNA, which corresponds to 0.75 %. Considering that the abundance of

tRNA<sub>1CU</sub><sup>Arg</sup> in total tRNA was determined to be approximately 3.3 % by MST measurement (see section 3.1.2.5), the isolation yield was about 25 % of the total tRNA<sub>1CU</sub><sup>Arg</sup> content. Taking the high RNA losses during the final PAGE elution and precipitation step and the above described incomplete depletion of tRNA<sub>1CU</sub><sup>Arg</sup> in the supernatant into account, that result was considered to be realistic and thus quite satisfactory.

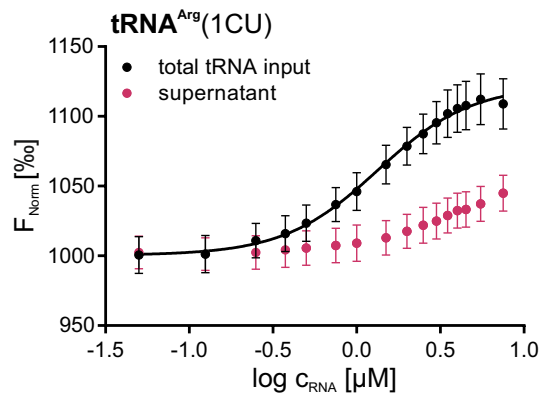


**Figure 3.29: MST-based monitoring of the success of tRNA<sup>Arg</sup>(1CU) isolation** Both input total tRNA and the supernatant containing non-target tRNAs were analyzed by MST for tRNA<sup>Arg</sup>(1CU) abundance. The right shift of the binding curve indicated a profound depletion of tRNA<sup>Arg</sup>(1CU) in the supernatant (magenta data points), but also revealed that some residual tRNA<sup>Arg</sup>(1CU) was still present and bypassed the isolation process. Error bars represent the standard deviation of technical triplicates, n=3.

### 3.2.2.2 Isolation of tRNAs for LC-MS/MS analysis

The *S. cerevisiae* tRNAs tRNA<sub>3UU</sub><sup>Lys</sup> and tRNA<sub>NGG</sub><sup>Pro</sup> were isolated from commercially available total tRNA in the same manner as described for tRNA<sub>1CU</sub><sup>Arg</sup> with the aim of a subsequent LC-MS/MS analysis. Altogether, about 2-6 μg of each single tRNA were obtained, depending on the target tRNA and batch size. Aliquots of each tRNA were digested to nucleosides and analyzed by LC-MS/MS using a neutral loss scan (NLS). Altogether, the results of the NLS were in good agreement with the tRNA modification patterns described in the tRNAdb 2009 [80] and underlined the successful isolation of the single tRNAs in pure forms. Two unexpected peaks detectable in both tRNAs were likely resulting from degradation products of adenosine and m<sup>1</sup>A and did not illustrate contaminations by other tRNAs. For a more detailed analysis of the neutral loss scans, see section 3.3.2.

### 3.2.3 Isolation of the tRNA-like Small mascRNA

Since the developed isolation protocol performed well in case of tRNA isolations, it was intended to employ it for other small non-coding RNAs as well. As new target, mascRNA (see section 1.3) was chosen, which is a small, tRNA-like RNA generated during MALAT1 lncRNA maturation (section 1.3, [178]). Interestingly, mismatches observed during sequencing of mascRNA cDNA clones gave rise to the presumption that mascRNA carries at least one modified nucleoside [178]. The modified adenosine in question (highlighted in figure 3.30 a) was presumed to be localized

at a position resembling position 58 in tRNAs, which is often modified to m<sup>1</sup>A [243]. Thus, it seemed well possible that the enzyme responsible for m<sup>1</sup>A58 introduction in tRNAs is also capable of modifying mascRNA, and considering its overall tRNA-like structure, that might apply to other tRNA modification enzymes as well. Hence, mascRNA constituted an appealing target for isolation and LC-MS/MS analysis. Employing the isolation protocol described for mascRNA isolation, however, required considering certain special circumstances.

#### 3.2.3.1 Challenges of mascRNA Isolation

Although the parent long non-coding RNA, MALAT1 (Metastasis-Associated Lung Adenocarcinoma Transcript 1), is broadly expressed and of relatively high abundance [186], that is not the case for mascRNA and considering that the half life of the small RNA was shown to be rather short, its abundance in total RNA was expected to be quite low [178]. Thus, high amounts of total RNA were assumed to be required for a successful isolation attempt. Since it was intended to isolate the human mascRNA, HeLa cells as well as HEK cells were chosen for cell culture and total RNA isolation was performed on a large scale aiming at a minimum of 5 mg total RNA. Given the low abundance of mascRNA, a MST-based quantification prior to the isolation itself seemed unfeasible, thus the hybridization ratio of RNA to probe had to be estimated roughly and was limited by the available RNA amount. Using high amounts of total RNA during the isolation process, however, comprised a higher probability of unspecific RNA binding to the beads, possibly leading to contaminations of the isolated small RNA. To address these challenges, following control experiments were performed.

#### 3.2.3.2 Control Experiments for mascRNA Isolation

In order to ensure that the DNA probe designed to capture mascRNA would effectively hybridize to the RNA, which was the prerequisite for its successful isolation, an *in vitro* transcript of mascRNA was prepared. The binding of the IVT to the probe was tested in hybridization titration series both on non-denaturing PAGE (figure 3.30 b) and by MST measurement (figure 3.30 c). Both methods displayed binding ratios slightly larger than 1:1 (IVT:DNA probe), however the results clearly demonstrated the hybridization success and hereby the applicability of the designed probe. Fluorescence time traces corresponding to the MST binding curve are displayed in the appendix, figure A.11. To evaluate the extend of unspecific binding of excess non-target RNA to the beads, a test isolation of mascRNA was performed using the *in vitro* transcript (100 pmol) with or without increasing amounts of *S. cerevisiae* total tRNA (up to 500 µg, equivalent to 5 µg/µL). After isolation and DNase1 digestion, the samples were analyzed by denaturing PAGE (figure 3.31). In each sample, a band of comparable intensity which corresponded to the mascRNA IVT was detectable, indicating that the isolation was successful and obviously not hindered by the presence of larger amounts of unspecific RNA. However, the gel results clearly illustrated unspecific binding (of tRNA) starting at an RNA concentration of 2 µg/µL. Thus, when applying large total RNA amounts for mascRNA isolation, a contamination with non-target RNAs had to be taken into account.

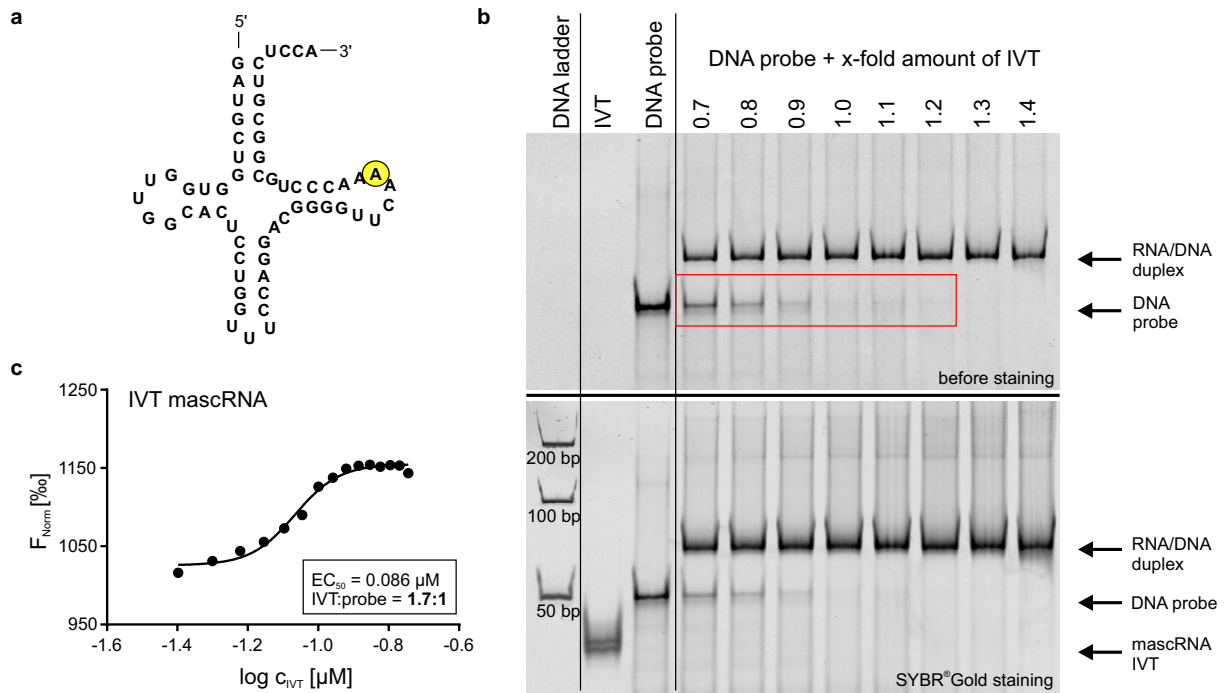


**Figure 3.30: Control experiments employing mascRNA *in vitro* transcript** To evaluate the probe's capability to bind mascRNA, an *in vitro* transcript (a, adapted from [178]) of human mascRNA was tested in hybridization series both on non-denaturing PAGE (b) and by MST (c). The nucleoside circled in yellow represents the putatively modified adenosine. Bands corresponding to free probe, free IVT and the formed duplex are indicated in (b), the red box marks hybridization ratios at which excess probe was detectable. Both (b) and (c) display a hybridization ratio of  $>1:1$  (IVT:probe) (approximately 1.2:1 in PAGE analysis and 1.7:1 in MST experiments, respectively).

### 3.2.3.3 Isolation of Native mascRNA

In a first attempt to isolate mascRNA, total RNA isolated from HeLa cells was used as input RNA. Two samples, each containing approximately 1 mg (3.7  $\mu\text{g}/\mu\text{L}$ ) total RNA and 200 pmol (0.74  $\mu\text{M}$ ) DNA probe were hybridized and loaded onto the appropriate amount of beads for immobilization. Due to the high RNA concentration applied resulting in an increase of viscosity, removal of beads after the elution step was difficult and only possible by an additional precipitation step. Both samples were DNase1 digested and precipitated, followed by either high throughput RNA sequencing (RNA-Seq) or denaturing PAGE, respectively. Of note, the yields of approximately 2  $\mu\text{g}$  RNA per sample were unexpectedly high, especially in light of the yields achievable for single tRNAs (see section 3.2.2.1). In line with that, analysis on PAGE clearly demonstrated the high degree of unspecific RNA binding to the beads, especially of the larger RNAs (figure 3.32) and thus explained the high RNA amounts isolated. No distinct band resembling mascRNA was detectable on PAGE (red box in figure 3.32), possibly due to its very low abundance, which was in good agreement with the results of RNA-Seq (kindly performed by Lyudmil Tserovski) displaying only very few reads for mascRNA in the sample. Nevertheless, the RNA-Seq results pointed to the possibility of an enrichment of mascRNA using the isolation procedure (the isolated RNA contained a small number of reads mapping to

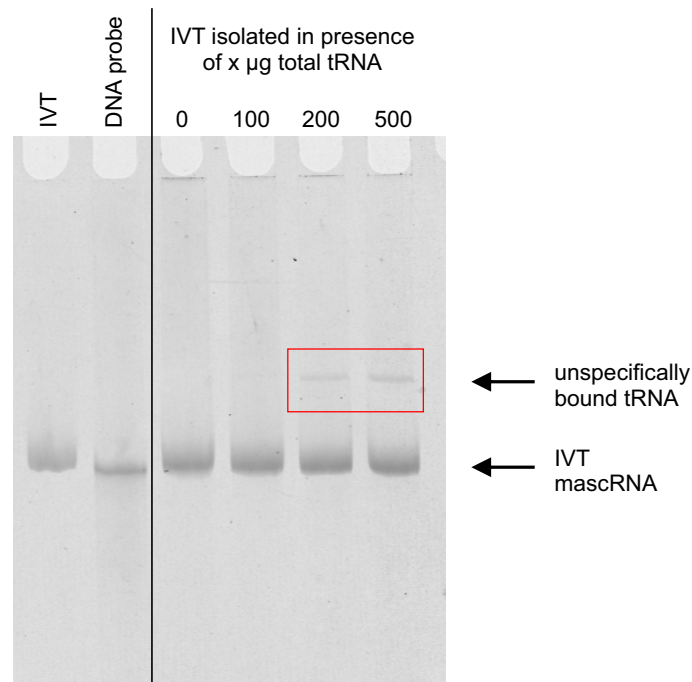


**Figure 3.31: Test isolation of *in vitro*-transcribed mascRNA** To evaluate the probability of unspecific RNA binding to the beads during the isolation process, a test isolation of mascRNA IVT was performed in the presence of increasing amounts of unspecific, *S. cer.* total tRNA (1-5 µg/µL), DNase1 digested and analyzed on 10 % denaturing PAGE. Starting at a concentration of 2 µg/µL, an additional band corresponding to tRNA was detectable, indicating unspecific binding (marked by the red box). Gel staining was performed using GelRed.

mascRNA, confirming its presence), hence it was intended to reduce the binding of non-target RNAs to the beads and to prove the enrichment compared to the input RNA. Therefore, the amount of input RNA used for the hybridization was reduced by size-fractionating the total RNA and using only the small RNA fraction (< 200 nt, see section 5.2.1.8) as input RNA. By removing all longer, non-target RNAs, which made up a large portion of the total RNA isolated, not only the total RNA amount used for hybridization was reduced, but also a higher concentration of the target mascRNA in the sample was achieved. For the subsequent isolation attempt, two samples were prepared, each containing 100 pmol DNA probe and 3.9 µg/µL small HeLa cell RNA (sample HeLa 2 in figure A.12) or 2.4 µg/µL small HEK cell RNA (amounts applied were limited by the yields obtained for the small RNA fractions). After DNase1 digestion, samples were directly precipitated and due to the low amount recovered, an analysis by PAGE was not feasible. Isolated RNA yields were approximately 390 ng for the HeLa RNA sample (sample HeLa 2 in figure A.12) and 280 ng in case of the HEK cell RNA. Both samples as well as the respective input small RNA fractions (as controls to evaluate the enrichment) were analyzed by RNA-Seq (library preparation and data analysis were kindly performed by L. Tserovski, S. Werner and D. Jacob; Illumina sequencing of the prepared samples was kindly conducted by Prof. Dr. Yuri Motorin). Analysis of the RNA-Seq data revealed a clear enrichment of reads mapping to mascRNA in the HeLa RNA samples compared to its input control, although the total read number was still low (137 in 220,000 mapped reads (623 reads per million) in sample 2 *vs.* 1 read in 510,000 mapped

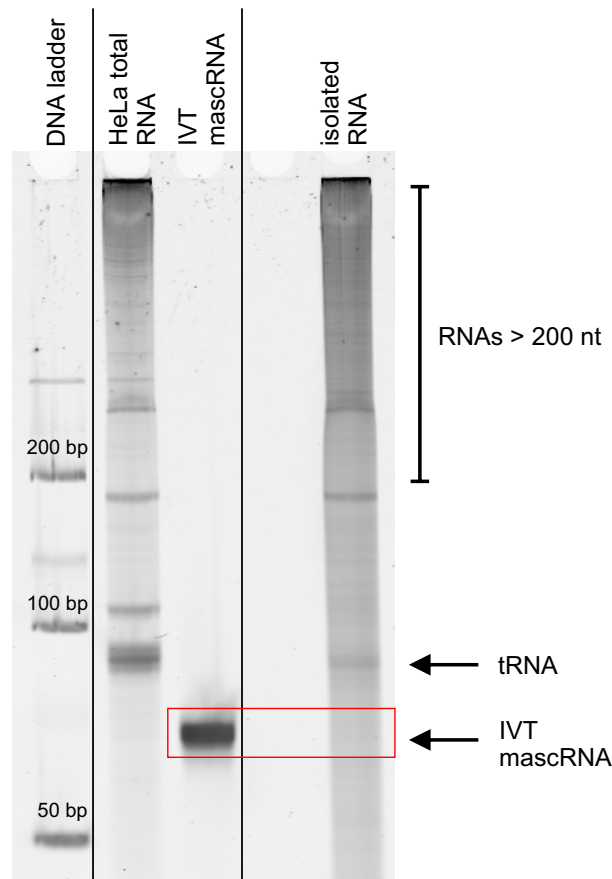


**Figure 3.32: PAGE analysis of isolated mascRNA** The isolated RNA eventually containing mascRNA was analyzed on denaturing PAGE (10 %). The sample contained mostly non-target RNA of all sizes (roughly resembling the total RNA control), and no distinct band in the size range of mascRNA (red box) was detectable. Bands and regions of mascRNA IVT, tRNA and larger RNA are indicated. Gel staining was performed using GelRed.

reads (2 per million) in the input control), indicating once again the low abundance of mascRNA (see appendix, figure A.12). In the HEK RNA sample, only a small number of reads mapping to short stretches of mascRNA could be aligned, and no reads were detected in the control samples. As the reads in the isolated RNA were too short to clearly identify mascRNA in the sample, it was not possible to evaluate a possible enrichment compared to the input control in case of the HEK cell samples. While the sequencing results of the HeLa RNA samples clearly demonstrated an enrichment of mascRNA by the isolation procedure, the applied concentration of input small RNA was in a range that likely resulted in a contamination with non-target RNAs, *e.g.* tRNAs, as it was shown in figure 3.31. This assumption was additionally confirmed by the sequencing data, as only a small portion of the total reads mapped in the HeLa RNA sample actually were assigned to mascRNA. Thus, the isolated RNA likely contained non-target RNAs and thereby an isolation of pure, non-contaminated mascRNA was unfortunately not accomplishable due to its low abundance.

**Putative 1-Methyladenosine Modification in mascRNA?** The above mentioned hypothesis of mascRNA carrying an m<sup>1</sup>A modification at the position corresponding to m<sup>1</sup>A58 in tRNAs [243] was supported by the finding that the reads mapping to mascRNA displayed m<sup>1</sup>A-characteristic mismatch pattern (described in [133, 244]) at the position of interest (marked in figure A.12). However, since an isolation of pure mascRNA free of contaminants of other RNA species was not feasible, a LC-MS/MS analysis was not appropriate (even small contaminations with tRNAs carrying m<sup>1</sup>A58 would have led to false positive results). Considering that, the m<sup>1</sup>A modification suggested by sequencing could not be confirmed properly. One possibility to circumvent the requirement of isolating pure mascRNA could be to repeat isolation and sequencing using a knockout of the respective enzyme responsible for m<sup>1</sup>A58 introduction in tRNAs, and to compare the results with the wildtype. This, however, is presumably not easy or even impossible to accomplish, since the enzyme complex responsible for the m<sup>1</sup>A58 introduction might potentially be indispensable for viability (as it is the case for the *S. cerevisiae* enzyme complex, [245]).

#### 3.2.4 Summary

The isolation of single RNA species using a hybridization-based approach was successfully performed for several *E. coli* and *S. cerevisiae* tRNAs. Isolation efficiency and purity of the separated tRNAs was monitored by PAGE, MST and LC-MS/MS analysis, confirming that the protocol applied is well capable of isolating pure tRNAs in appropriate yields. However, the transfer of the approach to small RNAs with abundances drastically lower than those of tRNAs was quite challenging. The attempt to isolate the small tRNA-like mascRNA in pure form actually failed due to its low abundance and the accompanying high RNA amounts required. Nevertheless, an enrichment of even such a low abundant RNAs was well possible, indicated by the RNA-Seq results. Here, special care had to be taken to limit unspecific binding of non-target RNAs by using only the RNA fraction < 200 nt instead of total RNA for the isolation. Although mascRNA isolation was not possible in pure-enough form to allow an LC-MS/MS analysis for confirmation, sequencing data suggested the presence of an m<sup>1</sup>A modification at the position resembling A58 in tRNAs.



### 3.3 RNA Modification Analysis by Liquid Chromatography-Tandem Mass Spectrometry

In the following sections, exemplary results of each an application of the four scan modes DMRM, NLS, product ion scan and pseudo-MS<sup>3</sup> scan (see section 1.2.2.1) are presented. The instrumental and experimental details of the LC-MS/MS methods described were mainly adapted from [223] and are specified in more detail in [172].

#### 3.3.1 DMRM Mode: Analysis of Wobble U34 Modifications

For quantitative analysis of modified nucleosides with known fragmentation pattern, the dynamic multiple reaction monitoring (DMRM) mode was the method of choice [165], as it offered the highest sensitivity among the available scan types. The combination of characteristic mass transition between precursor and product ion and the retention time allowed the exact and precise identification and detection of the nucleoside of interest. Fragmentation of nucleosides typically takes place at the glycosidic bond, making the fragmentation pattern predictable for most modified nucleosides, which however cannot be said for the retention time, especially if new or uncharacterized modifications are of interest. Thus, identification of the retention time of a nucleoside required either a synthetic standard of the nucleoside, or, if that was not feasible, at least an RNA sample known to contain the modified nucleoside of interest. Care had to be taken to identify the correct retention time if several nucleosides shared the same precursor and product ions because they differ only in the position at which they are modified, as it is the case for isomers, *e.g.* m<sup>1</sup>G and m<sup>2</sup>G. The DMRM mode can be applied for both relative and absolute quantification of modification levels in RNA samples. Absolute quantification of modification contents requires the use of either external calibration or of an internal standard [165, 167] and thus the availability of the nucleoside of interest in pure form. Quantification methods practicable using the DMRM mode are described in [167, 172] in detail giving exact guidelines for the execution and data analysis. Relative quantification of modification levels is a straightforward alternative if the aim is to solely examine changes of modification abundances between different biological samples, *e.g.* wildtype and knockout samples for RNA-modifying enzymes. Such an analysis was performed in the following application example.

**Application** Varius sets of *S. cerevisiae* wildtype and knockout samples were analyzed for changes in the wobble U modifications ncm<sup>5</sup>U, mcm<sup>5</sup>U and mcm<sup>5</sup>s<sup>2</sup>U (see figure 3.33 a and section 1.1.2.1) in collaboration with Prof. Dr. Raffael Schaffrath, Prof. Dr. Mike Stark, Dr. Roland Klassen and André Jüdes. The identification of the three nucleosides and the determination of their retention times and fragmentation patterns is described in [173] and was in case of mcm<sup>5</sup>U and mcm<sup>5</sup>s<sup>2</sup>U additionally confirmed using synthetic standards kindly provided by Prof. Dr. Andrzej Malkiewicz. Figure 3.33 b shows the mass chromatogram of the analysis of total tRNA (*S. cerevisiae*) with clear peaks for the modified uridines detectable for the mass transitions indicated in figure 3.33 a. The modified nucleoside s<sup>2</sup>U, which was additionally

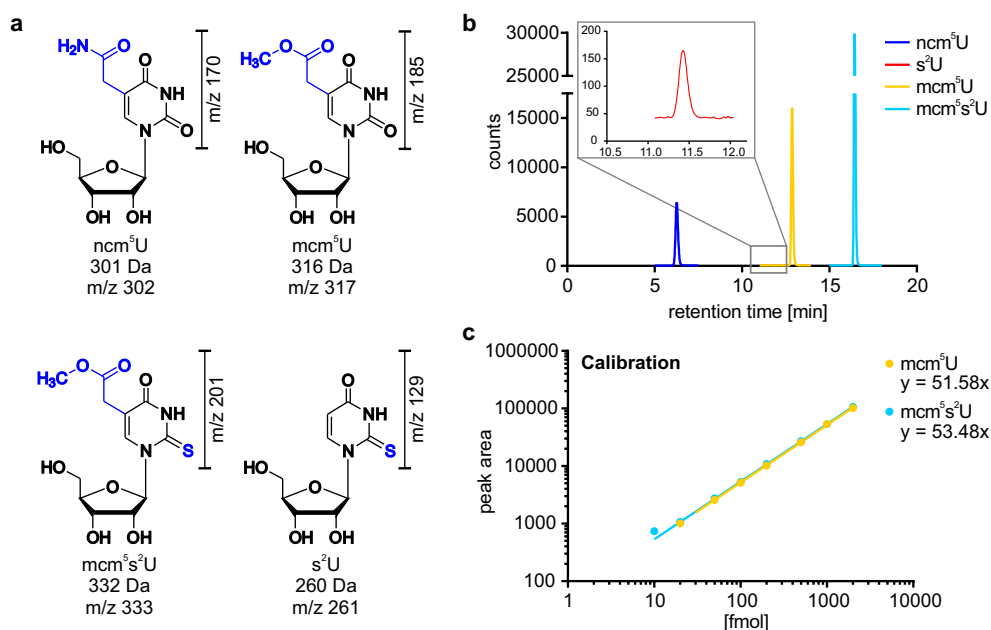


**Figure 3.33: LC-MS/MS analysis of wobble U34 modifications** The neutral structures of  $\text{ncm}^5\text{U}$ ,  $\text{mcm}^5\text{U}$ ,  $\text{mcm}^5\text{s}^2\text{U}$  and  $\text{s}^2\text{U}$ , labeled with the respective  $m/z$  values of protonated precursor (nucleoside) and product (nucleobase) ions, are depicted in (a) (adapted from [79]). The chromatogram (b) shows the detection of all three modified uridines in *S. cerevisiae* total tRNA, whereas  $\text{s}^2\text{U}$  was observed only in traces (inlet in b). Synthetic standards of  $\text{mcm}^5\text{U}$  and  $\text{mcm}^5\text{s}^2\text{U}$  were applied in a calibration series (c) and enabled the determination of limits of detection  $\leq 20$  fmol. The synthetic standards were kind gifts of Prof. Dr. A. Malkiewicz.

analyzed for the reasons stated below, was detectable in traces as well (inlet in figure 3.33 b). In order to evaluate the sensitivity of the mass detection of the wobble U modifications, the synthetic standards of  $\text{mcm}^5\text{U}$  and  $\text{mcm}^5\text{s}^2\text{U}$  were used to run a calibration series (figure 3.33 c). Limits of quantification (assigned by a signal-to-noise ratio of  $>10$ ) were in the low double-digit femtomol range and signals displayed a linear increase over the complete concentration range analyzed (linear range  $\geq 2$  orders of magnitude), confirming the high sensitivity of the DMRM method. The described DMRM method was applied to several sets of wildtype and knockout RNA samples prepared by the laboratories of Prof. Dr. R. Schaffrath and Prof. Dr. M. Stark, the detailed results are presented in [102, 246, 247]. Here, the LC-MS/MS results of the samples examined for [102] (prepared by Dr. R. Klassen) are shown exemplarily, for which the analysis was performed to verify the loss of the wobble modifications in the constructed mutants of *S. cerevisiae*. Next to a wildtype total tRNA sample, which served as control, single knockouts of Elp3 and Uba4 as well as a  $\Delta\text{elp3}\Delta\text{uba4}$  double mutant were analyzed for  $\text{ncm}^5\text{U}$ ,  $\text{mcm}^5\text{U}$ ,  $\text{mcm}^5\text{s}^2\text{U}$  and  $\text{s}^2\text{U}$  abundance. While Elp3 is a component of the elongator complex responsible for the  $\text{mcm}^5$ -/ $\text{ncm}^5$ -side chain introduction, Uba4 belongs to the independently acting thiolation pathway which forms the  $\text{s}^2$ -moiety (see figure 3.34 a) [93],[99]. Figures 3.34 b-e display the chromatograms (normalized to identical RNA content using the UV peak area of uridine) of  $\text{ncm}^5\text{U}$ ,  $\text{s}^2\text{U}$ ,  $\text{mcm}^5\text{U}$  and  $\text{mcm}^5\text{s}^2\text{U}$  recorded for each of the four samples. While in the wildtype sample all three modifications carrying the C5-moiety were present, they were

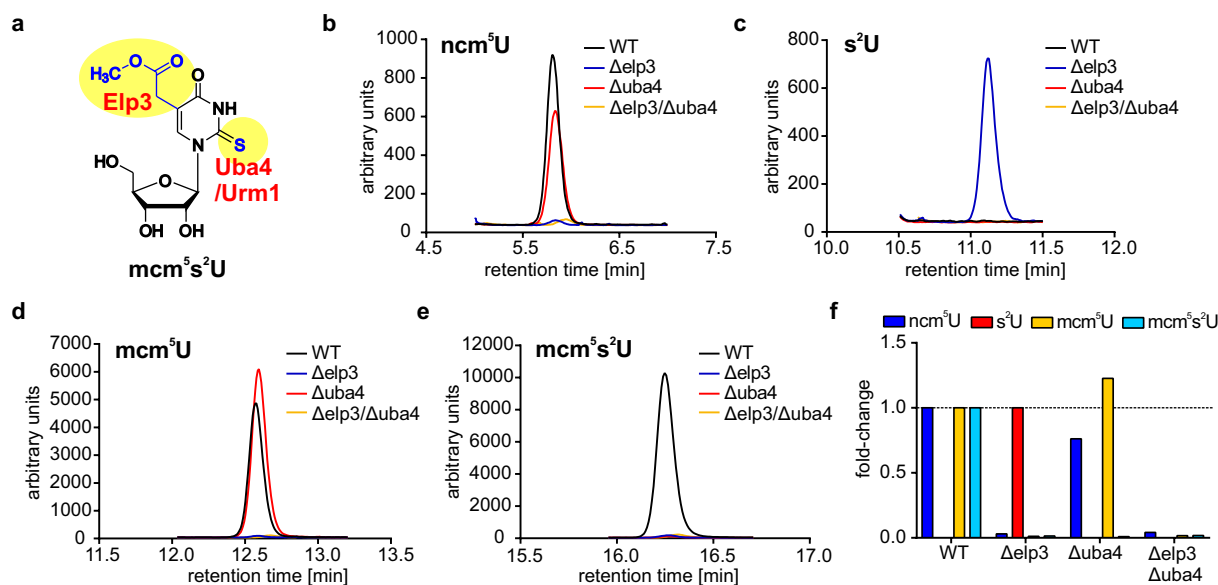


**Figure 3.34: Wobble U34 modifications in  $\Delta elp3$  and  $\Delta uba4$  mutants** Elp3 and Uba4 are responsible for introduction of the ncm<sup>5</sup>-/mcm<sup>5</sup>- and the s<sup>2</sup>-side chain, respectively (a, adapted from [102]). (b)-(e) depict the chromatograms of the four analyzed modified nucleosides measured in total tRNA of each of the indicated *S. cer.* strains (WT (BY4741),  $\Delta elp3$ ,  $\Delta uba4$ ,  $\Delta elp3\Delta uba4$ ). Fold-changes of the modification levels in the knockout samples compared to wildtype are shown in (e). In case of s<sup>2</sup>U, the level in the  $\Delta elp3$  is set to 1 as no other sample contained s<sup>2</sup>U. The dotted line indicates no change of modification levels compared to wildtype. Total tRNA samples were prepared by Dr. Roland Klassen, and results presented are published in [102].

severely reduced in the  $\Delta elp3$  and  $\Delta elp3\Delta uba4$  samples. The  $\Delta uba4$  mutant was still capable of generating the ncm<sup>5</sup>-/mcm<sup>5</sup>-side chain, but could not synthesize the mcm<sup>5</sup>s<sup>2</sup>U modification due to the inactive thiolation pathway. In the  $\Delta elp3$  mutant, s<sup>2</sup>U accumulated due to the defective elongator function but still active and independent thiolation pathway, which was in agreement with previous studies [91, 93]. In contrast, the other three strains analyzed showed only traces of s<sup>2</sup>, if any. The fold-changes of the modification abundances (determined by normalizing the peak area of the respective modification to the UV peak of uridine) between mutant strains and wildtype are depicted in figure 3.34 f, in case of s<sup>2</sup>U the abundance in the  $\Delta elp3$  strain was set to 1, as the modification was only present in traces or completely absent in all other strains. Altogether, the LC-MS/MS results confirmed the anticipated parallel loss of the n/mcm<sup>2</sup>-side chain and the s<sup>2</sup>-moiety in the  $\Delta elp3\Delta uba4$  mutant strain and the independence of the two pathways leading to the introduction of the respective modifications. Next to the analysis of wobble U34 modifications under various biological aspects which are described in [102, 246, 247], another application of the multiple reaction monitoring mode was the quantification of m<sup>1</sup>A in synthetic oligonucleotides as well as in wildtype and mutant *S. cerevisiae* rRNA. Details of the results can be found in [133], and the performed quantification steps are in-depth explained in [172].

### 3.3.2 Neutral Loss Scan: Analysis of Isolated tRNAs

For applications which require the analysis of the overall modification pattern of an RNA sample instead of only the analysis of a defined subset of one or more modifications, the NLS was the method of choice, as it does not rely on the exact informations about precursor and product ions and retention time like it is the case for the DMRM mode. Furthermore, if no information about possible modified nucleosides within a sample is available, or the intention is to find previously uncharacterized nucleosides, the neutral loss scan outperforms the DMRM mode. Here, the main prerequisite to detect a modified nucleoside *via* NLS was that it showed the typical fragmentation at the glycosidic bond, otherwise it was expected to escape analysis. Furthermore, very low abundant modified nucleosides might be hard to detect next to more abundant ones, so care had to be taken not to miss peaks in the mass chromatogram (compare figure 3.36).

**Application** In order to investigate the modification pattern of two isolated *S. cerevisiae* tRNAs, tRNA<sub>3UU</sub><sup>Lys</sup> and tRNA<sub>NGG</sub><sup>Pro</sup> (see section 3.2.2.2), NLS was the method of choice because of its capability not only to detect the expected modifications (as it would be the case for the DMRM mode) but also unexpected ones, which might result from contaminations with non-target tRNAs. Thus, by comparison with the respective modifications listed for the respective tRNA in the tRNAdb 2009 [80] or in MODOMICS [79], NLS results allowed an evaluation of the purity as well as, to a certain extent, the identity of the isolated tRNA. To analyze the obtained neutral loss scans, total ion currents (TIC) were extracted and examined for the presence of peaks corresponding to nucleosides (see figure 3.35, NLS chromatograms). The mass-to-charge ratio of the precursor ion of each detected peak (numbered in figure 3.35) was extracted and the identity of the respective modified nucleoside assigned by comparison with the modifications listed in the tRNAdb 2009 [80] for the tRNA of interest. The  $m/z$  values and thus the identities of peaks that were hardly detectable in the TIC due to the much higher abundance of other peaks were confirmed by extracting the respective EICs (extracted ion chromatograms) of the supposed precursor  $m/z$ . An example of the usefulness of EICs in the detection of low abundant peaks is displayed in figure 3.36, showing the EICs of pseudouridine, dihydrouridine and  $ncm^5U$  in comparison to the TIC (respective part of the TIC is marked in figure 3.35 b by a black box). In contrast to the TIC, in which the three peaks were barely visible next to the  $m^1A$ -peak, the extracted ion chromatograms showed clear, distinct peaks for the three modified nucleosides, thereby verifying their presence. Of note, certain modifications show peaks in the UV chromatogram (see figure 3.35, bottom) as well, for some modifications even considerably better detectable than in the mass chromatogram, *e.g.* pseudouridine (peak 1) and  $ncm^5U$  (peak 11). In those cases, the UV peaks helped to identify the respective mass peaks in the TIC. Table 3.1 summarizes the assignment of the peaks to the respective modified nucleoside. For each of the two tRNAs, all modifications listed in the database could be allocated to a peak in the respective chromatogram, thereby confirming the isolation success of the tRNAs. In case of tRNA<sub>NGG</sub><sup>Pro</sup>, the modified U (not further characterized in [80]) at position 34 (N) was determined

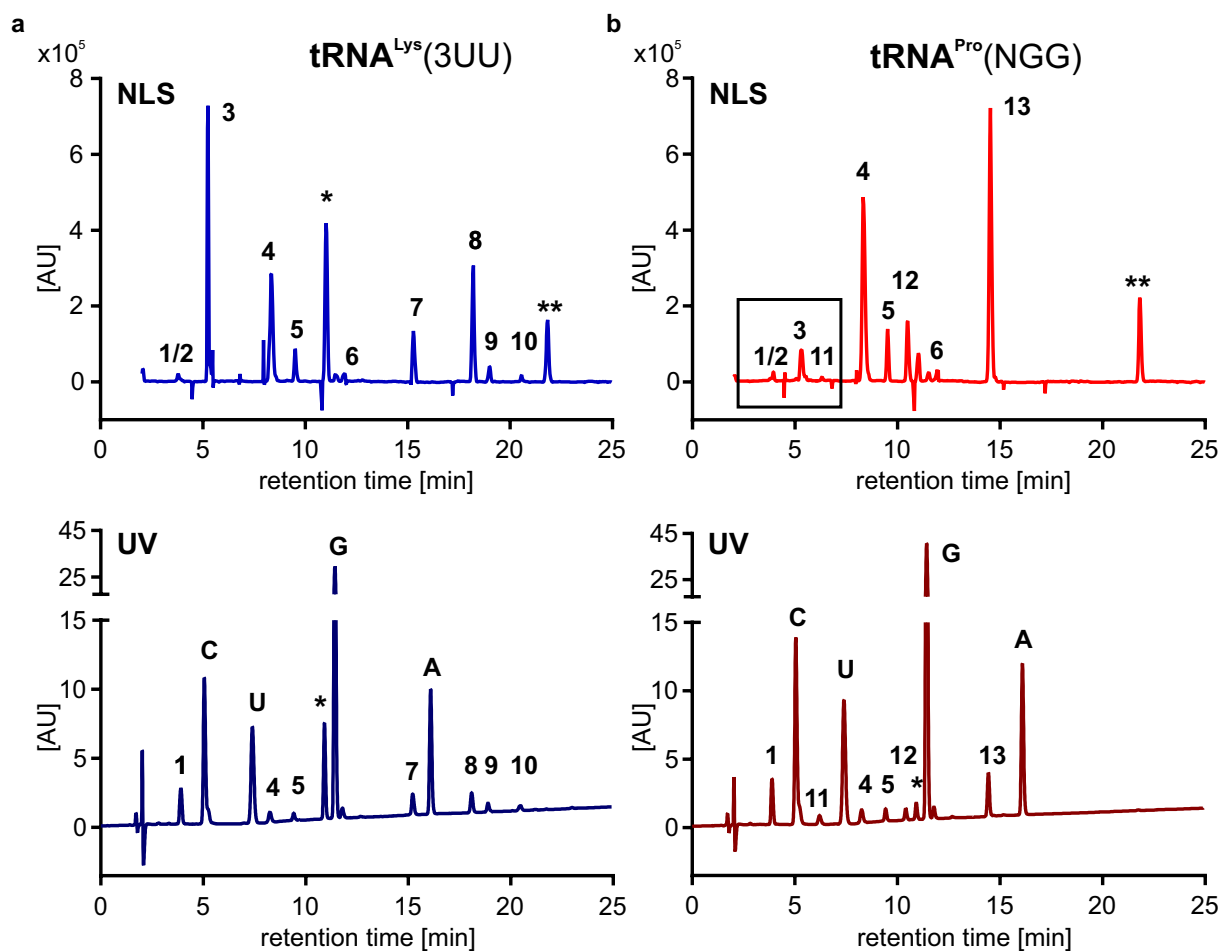


**Figure 3.35: Neutral loss scan of isolated tRNAs** *S. cerevisiae* tRNA<sup>Lys</sup>(3UU) (a) and tRNA<sup>Pro</sup>(NGG) (b) were isolated as described, digested to nucleosides and analyzed by LC-MS/MS using a neutral loss scan. Both mass (top) and UV (bottom) chromatograms are shown, with the main nucleosides directly labeled in the chromatograms. Mass peak numbering corresponds to the numbering in table 3.1. If a modified nucleoside displayed both mass and UV peaks, both are numbered. Asterisks mark inosine and a methylated adenosine moiety that both probably derived from degradation processes. AU - arbitrary units.

to likely be a  $\text{ncm}^5\text{U}$ , which was in agreement with [92, 228]. In both chromatograms, two additional, non-expected peaks were detected: one with a mass-to-charge ratio of 269, which presumably derives from inosine produced by adenosine deamination and thus represents a degradation product, and one with a mass-to-charge ratio of 282, which due to its high retention time probably resembled a contamination by  $\text{m}^6\text{A}$ , which might have occurred through Dimroth rearrangement of  $\text{m}^1\text{A}$  during RNA preparation procedures [248, 249]. Altogether, the neutral loss scans of the two isolated tRNAs were in good agreement with the respective entries in the tRNA database 2009 [80], and underline the good suitability of the isolation protocol to yield highly pure, single tRNAs.

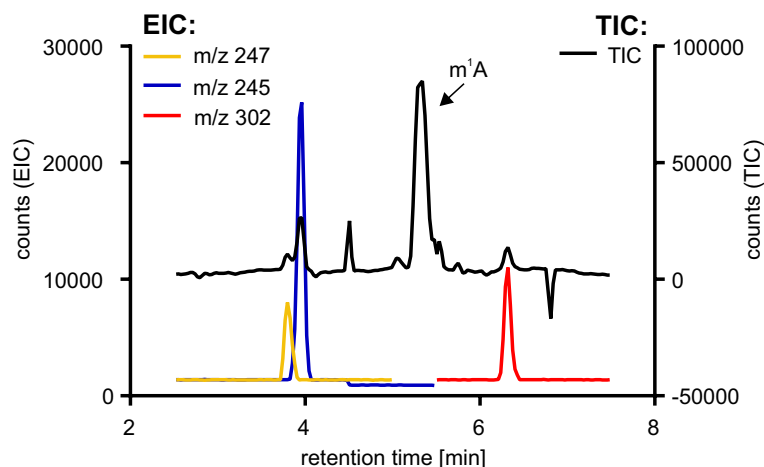


**Figure 3.36: Extracted ion chromatograms of  $\Psi$ , D and  $\text{ncm}^5\text{U}$**  Excerpt from the NLS scan of *S. cer.*  $\text{tRNA}^{\text{Pro}}(\text{NGG})$ . The EICs of  $\Psi$ , D and  $\text{ncm}^5\text{U}$  (precursor  $m/z$  245, 247 and 302) displayed clear peaks of the respective modified nucleosides, which were barely detectable in the TIC (black) due to the much higher intensity of the  $\text{m}^1\text{A}$  peak. Extraction of the EICs thus allowed a more precise detection of low intensity peaks. The excerpt shown relates to the TIC displayed in figure 3.35 b.

### 3.3.3 Product Ion Scan: Analysis of the Fragmentation Pattern of Queuosine

To investigate the fragmentation pattern of nucleosides of known molecular mass, which were expected to display deviations from the typical fragmentation pattern during collision-induced dissociation, performing a product ion scan was the method of choice. Although most nucleosides are cleaved at the glycosidic bond, especially modified nucleosides with complex side chains attached are susceptible to other or additional fragmentation reactions. The nucleoside queuosine (Q) is an example of such a hyper-modified nucleoside that contains a 7-deazaguanosine structure carrying a cyclopentenediol side chain attached by an amino-methyl linker [250, 251] (figure 3.37 a), which is prevalent in all kingdoms of life. However, eukaryotes are in contrast to eubacteria not capable of a *de novo* synthesis of Q and have to recycle it from its base queuine, which they acquire from the gut microflora and by food intake [251]. Subsequently, tRNA-guanine transglycosylases (TGT) replace the guanine at position 34 in certain tRNAs (Tyr, Asp, Asn and His, [252]) with the acquired queuine base yielding the respective Q nucleoside [253]. For LC-MS/MS analysis of Q, the hyper-modified structure of Q had to be considered (shown in figure 3.37 a), which accounts for the alterations from the usual fragmentation pattern. In figure 3.37 a, fragmentation positions are depicted, which were kindly provided by Prof. Dr. Patrick Limbach (Biological Mass Spectrometry, Department of Chemistry, University of Cincinnati, USA) [224, 254]. Next to the expected cleavage at the glycosidic bond, the cyclopentenediol moiety might be cleaved off at the amino-methyl linker, resulting in the three possible fragments indicated in figure 3.37 a. While exclusive cleavage of the glycosidic bond would yield a product ion with a  $m/z$  of 278, fragmentation only at the linker would result in a nucleoside with a  $m/z$  of 295. Cleavage at both positions would produce a nucleobase structure with a  $m/z$  value of 163. *E. coli*  $\text{tRNA}^{\text{Tyr}}$ , which is known to contain a Q34 modification [252], was used to establish the exact fragmentation pattern for

**Table 3.1: Peak assignment: NLS of tRNA<sup>Lys</sup>(3UU) and tRNA<sup>Pro</sup>(NGG)** Allocation of the peaks indicated in figure 3.35 to the modified nucleosides present in *S. cerevisiae* tRNA<sup>Lys</sup>(3UU) and tRNA<sup>Pro</sup>(NGG) according to the tRNAdb 2009 [80]. For each peak, the mass-to-charge ratio of the precursor nucleoside as well as the allocated modification is stated. In case of identical precursor m/z values, assignment was performed by including retention time information.

Peak	m/z	nucleoside
1	245	Ψ
2	247	D
3	282	m <sup>1</sup> A
4	298	m <sup>7</sup> G
5	258	m <sup>5</sup> C
6	259	m <sup>5</sup> U
7	298	m <sup>2</sup> G
8	312	m <sub>2</sub> <sup>2</sup> G
9	413	t <sup>6</sup> A
10	333	mcm <sup>5</sup> s <sup>2</sup> U
11	302	ncm <sup>5</sup> U
12	258	Cm
13	298	m <sup>1</sup> G
*	269	I
**	282	m <sup>6</sup> A

detection of Q with the final aim of setting up an appropriate DMRM method. Therefore, the retention time and fragmentation pattern of Q was first determined by performing a product ion scan with the precursor m/z of 410 comprising unfragmented, protonated Q. Using the standard gradient 1 (table 5.4), a clear peak was detected at a retention time of approximately 10.5 min, and analysis of the respective mass spectrum showed two product ions for Q (see figure 3.37 b) with mass-to-charge ratios of 295 and 163. Those correspond to the sole cleavage at the amino-methyl linker and fragmentation at both possible fragmentation positions. In contrast, a cleavage only at the glycosidic bond, which would result in a protonated queuine moiety, was not observed. This was additionally confirmed by the subsequently developed DMRM method, in which only the mass transitions of m/z 410 to 295 and m/z 410 to 163 yielded a peak at the retention time of 10.5 min (figure 3.37 c). As the peak resulting from monitoring the cleavage reaction only at the linker displayed higher intensity than the peak corresponding to a double cleavage reaction, the mass transition m/z 410 to m/z 295 was used for Q analysis in later applications.

**Application** The established DMRM method for the detection of Q was applied in collaboration with Dr. Martin Müller and Prof. Dr. Ann Ehrenhofer-Murray in order to investigate the incorporation of Q into *Schizosaccharomyces pombe* tRNA in dependence on the presence of queuine in the growth medium. Total tRNA samples (prepared by Dr. M. Müller) deriving from wildtype and  $\Delta pm1$  mutant cells grown with or without queuine supply were examined for the appearance of Q in the extracted tRNA, the results are depicted in figure 3.38. Both

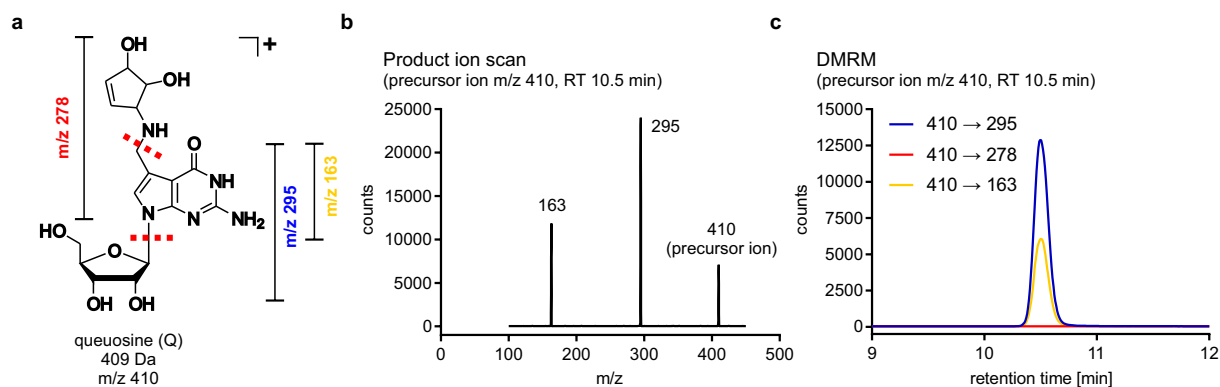


**Figure 3.37: Analysis of the fragmentation pattern of queuosine** The structure of queuosine is shown in (a) (adapted from [79]), fragmentation spots are indicated by dotted lines. Possible product ions are marked and labeled with the expected mass-to-charge ratio according to literature [224, 254]. Native tRNA<sup>Tyr</sup> (*E. coli*) was used to confirm the fragmentation pattern by a product ion scan (b) of the precursor ion ( $m/z$  410), which yielded two fragments ( $m/z$  295 and  $m/z$  163). The exclusive fragmentation at the glycosidic bond was not detectable in either the product ion scan or a DMRM analysis (c), and the cleavage of the side chain attached to the base was determined as the most pronounced fragmentation reaction (mass shift  $m/z$  410 to 295).

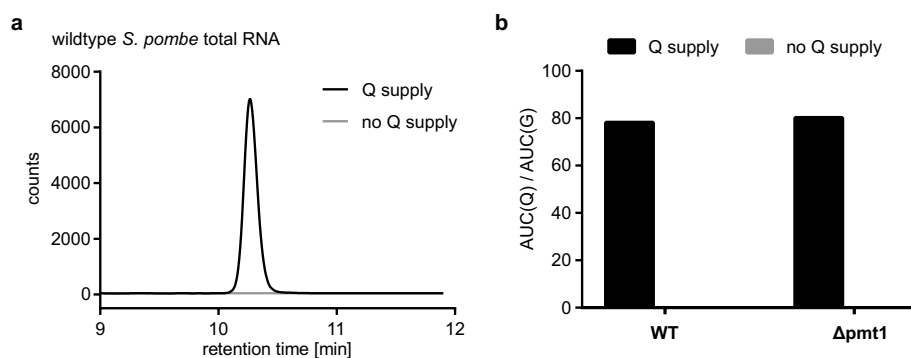


**Figure 3.38: Queuosine incorporation in *S. pombe* RNA** Wildtype and  $\Delta pmt1$  mutant *S. pombe* total tRNA samples from cells grown with or without a nutritional source of queuine were analyzed for their Q content. The mass chromatograms displayed clear peaks corresponding to Q in samples grown under queuine supply but not in those grown without (a). Relative quantification of Q levels in the samples by normalization of the peak areas to guanosine revealed similar Q levels in both wildtype and Pmt1 mutant cells grown under queuine supplementation (c). Samples analyzed were prepared by Dr. M. Müller, results shown are part of [255].

wildtype and mutant cells were able to introduce the supplied queuine into their tRNA in form of Q, which was clearly detectable in the Q-fed samples in comparable quantities. However, Q was completely missing in the samples grown under deprivation of Q. Both the presented results and the biological context of the presence of Q in tRNA and the activity of Pmt1 (*pombe* methyltransferase 1), which is a tRNA methyltransferase, are described in [255].

In mammals, the Q nucleoside can, dependent on the tRNA species, be further modified by attachment of a galactosyl(galQ)- or mannosyl(manQ)-moiety to the cyclopentenediol structure as shown in figure 3.39 a [256, 257]. In order to establish a DMRM method that included not only Q but also its glycosylated derivatives, total RNA extracted from HeLa cells was used to perform a product ion scan using the respective precursor ion ( $m/z$  572, identical



for both derivatives). To reduce the possibility of a cleavage of the sugar-moiety already during ionization and thus missing the detection of the precursor ion comprising the complete galQ or manQ, the fragmentor voltage was reduced from 80 to 40 V. A single peak for the precursor ion was detected eluting slightly earlier than Q, and the product ion spectrum indeed displayed an ion with a  $m/z$  value of 295 (figure 3.39 b), which resembles a fragmentation at the amino-methyl linker (see figure 3.37. Programming a DMRM method for both mass transitions ( $m/z$  572 to 295 and  $m/z$  572 to 163) revealed an additional, considerably smaller peak corresponding to the fragmentation at both possible positions (figure 3.39 c) in HeLa total RNA. The detected fragments were in good agreement to those identified previously for the glycosylated Q-derivatives [258], showing that the sugar-modified Q derivatives were well detectable by LC-MS/MS. However, a differentiation between the two stereoisomers was not feasible using the available equipment and methodology. The subsequently adapted DMRM method including the parameters for the detection of the the Q derivatives was then used for a second analysis of the *S. pombe* RNA samples described above (prepared by Dr. M. Müller). In those samples, however, a peak correlating to galQ/manQ was absent, possibly indicating that Q might no further modified in *S. pombe* in contrast to mammals. Notably, considering that the applied method specifically detected Q and its mannosyl- and galactosyl-derivatives, the possibility of the presence of an otherwise modified, hitherto unknown form of Q cannot be excluded. For example, in *E. coli*, queuosine at position 34 in tRNA<sup>ASP</sup> was shown to be modified to glutamyl-Q [259]. To search for new, potential Q modifications, the obviously common fragmentation of Q derivatives at the amino-methyl linker structure might be exploitable. When comparing the product ion spectra of Q, manQ and galQ, it was striking that they all displayed the same main product ion with a  $m/z$  value of 295, indicating that the amino-methyl linker cleavage was predominant during collision-induced fragmentation. Most likely, cleavage at that position is relevant in other, putative Q derivatives as well. If those carried an additional modification at the cyclopentenediol structure attached to the amino-methyl linker, a precursor ion scan, essentially the reversed form of a product ion scan, might be helpful for their identification. A precursor ion scan detects all precursor ions (in quadrupole 1) whose collision-induced fragmentation result in a pre-defined product ion in quadrupole 3. Thus, using the Q-specific product ion of  $m/z$  295 as defined product ion, precursor ion masses of potential Q-derivatives might be accessible, however, information about the modification's exact composition beyond its molecular mass cannot be obtained from such an analysis. Consequently, determination of the exact structure of such potential Q variants detected by a precursor ion scan would require additional investigations including the comparison to a synthetic standard. Of note, any Q derivatives carrying additional modifications at any other position of the 7-deazaguanosine structure would not be detected by the precursor ion scan, because the product ion generated would deviate from the described, Q-characteristic one. Another possibility imaginable, although likewise limited to putative Q derivatives with additional moieties at the amino-methyl linker structure, would be the setup of a modified NLS method that detects the loss of both ribose and 7-deazaguanosine ( $m/z$  295) instead of the ribose part alone ( $m/z$  132). The prerequisite for the applicability of such an adapted NLS method is the detectability of the

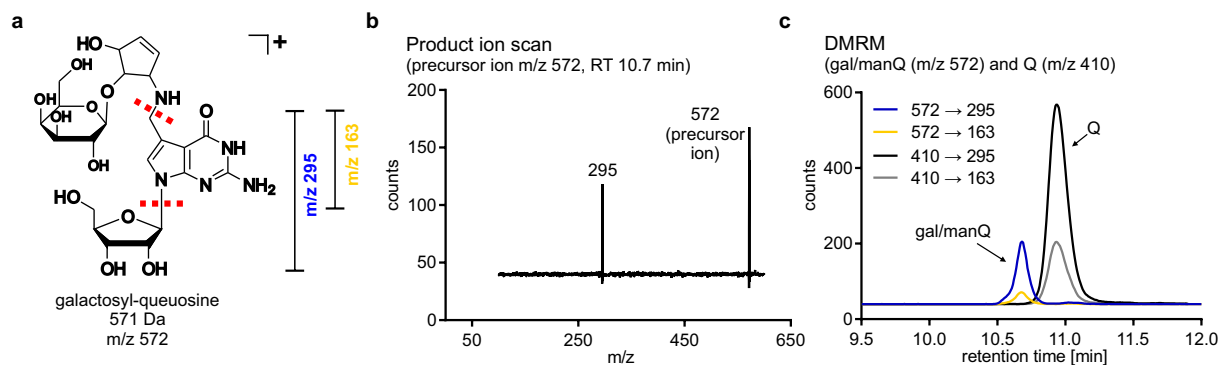


**Figure 3.39: LC-MS/MS-based detection of Q derivatives** Structure and fragmentation positions of galactosyl-queuosine are depicted in (a) (adapted from [79]), expected  $m/z$  values for protonated precursor and product ions are indicated. A product ion scan of HeLa total RNA confirmed the fragmentation at the amino-methyl linker (b), resulting in a product ion with a  $m/z$  of 295. Using a DMRM analysis, fragmentation at both possible positions was observable, however, the sole cleavage at the side chain dominates as it is the case for Q (c). For each peak, the mass transition monitored is indicated. Of note, the chromatograms shown in (c) displayed a slightly shifted retention time for Q compared to figure 3.37, which was probably caused by column aging.

cyclopentenediol moiety as product ion in quadrupole 3, which would comprise  $m/z$  values of 115 (Q) or 277 (galQ/manQ), respectively. Neither of those ions were detected in the product ion scans (figure 3.37 b and 3.39 b) of Q and its derivatives, indicating that an adapted NLS scan, however theoretically conceivable, might not be the method of choice for the search for to date uncharacterized Q variants. Nevertheless, the possibility of an adapted NLS scan might be exploited in future for analysis of other subsets of modified nucleosides that share the loss of a certain moiety other than the ribose part.

### 3.3.4 Pseudo-MS<sup>3</sup>: Determination of <sup>13</sup>C-Labeling Patterns of Nucleobases

Although the triple quadrupole mass spectrometer is designed for MS- and especially MS/MS analysis, the possibility to control the fragmentor voltage, which is responsible for the transport of the ions produced in the source through the ion transfer capillary, enables so-called pseudo-MS<sup>3</sup> scans (MS/MS/MS). Pseudo-MS<sup>3</sup> scans still use only the two quadrupoles for mass detection (in the product ion scan mode), however, altogether two consecutive fragmentation stages can be monitored [177]. In the present work, that was achieved by applying high fragmentor voltages (e.g. 150 V), which led to in-source fragmentation of the molecule of interest. In case of nucleosides, in-source cleavage of the glycosidic bond was hereby accomplished and the protonated nucleobase entered the first quadrupole. For MS<sup>3</sup>-analysis of a certain nucleoside, the protonated nucleobase was then the (defined) precursor ion for the subsequent product ion scan, which passed the first quadrupole and was further fragmented in the collision cell (collision energy 3-6 times higher than used for fragmentation of the glycosidic bond). Produced fragments were allowed to go through quadrupole 2 and finally detected in the detector. The resulting mass spectrum contained the respective ions produced by the fragmentation of the nucleobase and thus enabled a more detailed analysis of the nucleoside's structure. A pseudo-

MS<sup>3</sup> approach was recently employed for the detection of pseudouridine in RNase T1-digested RNA fragments, however, the analysis was performed at the level of small oligonucleotides instead of nucleosides and thus differed remarkably from the here applied method [260]. The possibility of performing pseudo-MS<sup>3</sup> scans was exploited in collaboration with Prof. Dr. Harald Schwalbe and Jochen Schmidt in order to investigate the introduction of labeled nucleosides into *E. coli* RNA. Total RNA from *E. coli* (strain DL323, displaying a defect tricarboxylic acid cycle [261]) grown using <sup>13</sup>C-2-glycerol as carbon source [261] (RNA preparation performed by J. Schmidt) was supposed to be analyzed for the exact positions of the incorporation of the <sup>13</sup>C-atom into the nucleosides, which previously had been assessed by NMR-analysis [261]. Additionally, the RNA was completely labeled with <sup>15</sup>N atoms. Test single MS scans (MS2 scan mode, detection of all ions present without fragmentation) of the RNA were used to determine the mass-to-charge ratios of the unfragmented nucleosides, and by comparing those to the ones of the unlabeled nucleosides, the number of heavy-labeled atoms in each of the main nucleosides was determined (each labeled atom led to a +1 shift of the m/z value). Subsequent product ion scans of the nucleosides revealed the incorporation of two <sup>13</sup>C-labeled atoms into the ribose moiety, which was in agreement with [261]. Furthermore, by considering the number of <sup>15</sup>N-atoms present, the nucleobases were determined to contain one <sup>13</sup>C-labeled atom each, which again matched the previous results [261]. However, the product ion scans did not allow an identification of the exact positions of the incorporated atoms. Therefore, the obtained m/z values of the nucleobases were used as precursor masses in pseudo-MS<sup>3</sup> scans, and the product ions resulting from base fragmentation were recorded in the respective mass spectra. The m/z values received for the fragments were compared to the fragmentation patterns of the bases described in literature [262–266] to evaluate which position was labeled. For uracil as an example of a pyrimidine base, the results strongly suggested a labeling of position 6 and the respective spectrum and assignments are displayed in figure 3.40 a. For the purine bases, the spectrum of guanine was analyzed and compared to the fragmentation pathways described in [263]. Figure 3.40 b shows the spectrum received with annotation of the peaks with the respective m/z values. One of the possible fragmentation reaction series is included in the figure, which indicated that the C5-atom was labeled by <sup>13</sup>C. For comparison and verification of the fragmentation patterns, MS<sup>3</sup> spectra of the unlabeled counterparts of the two nucleobases were recorded (see Appendix, figure A.13). Mass spectra of labeled and unlabeled cytosine and adenine are shown in the appendix, figure A.14. Altogether, the results suggested a labeling of position 6 in pyrimidines as well as of position 5 in purines, matching the previous NMR results [261].

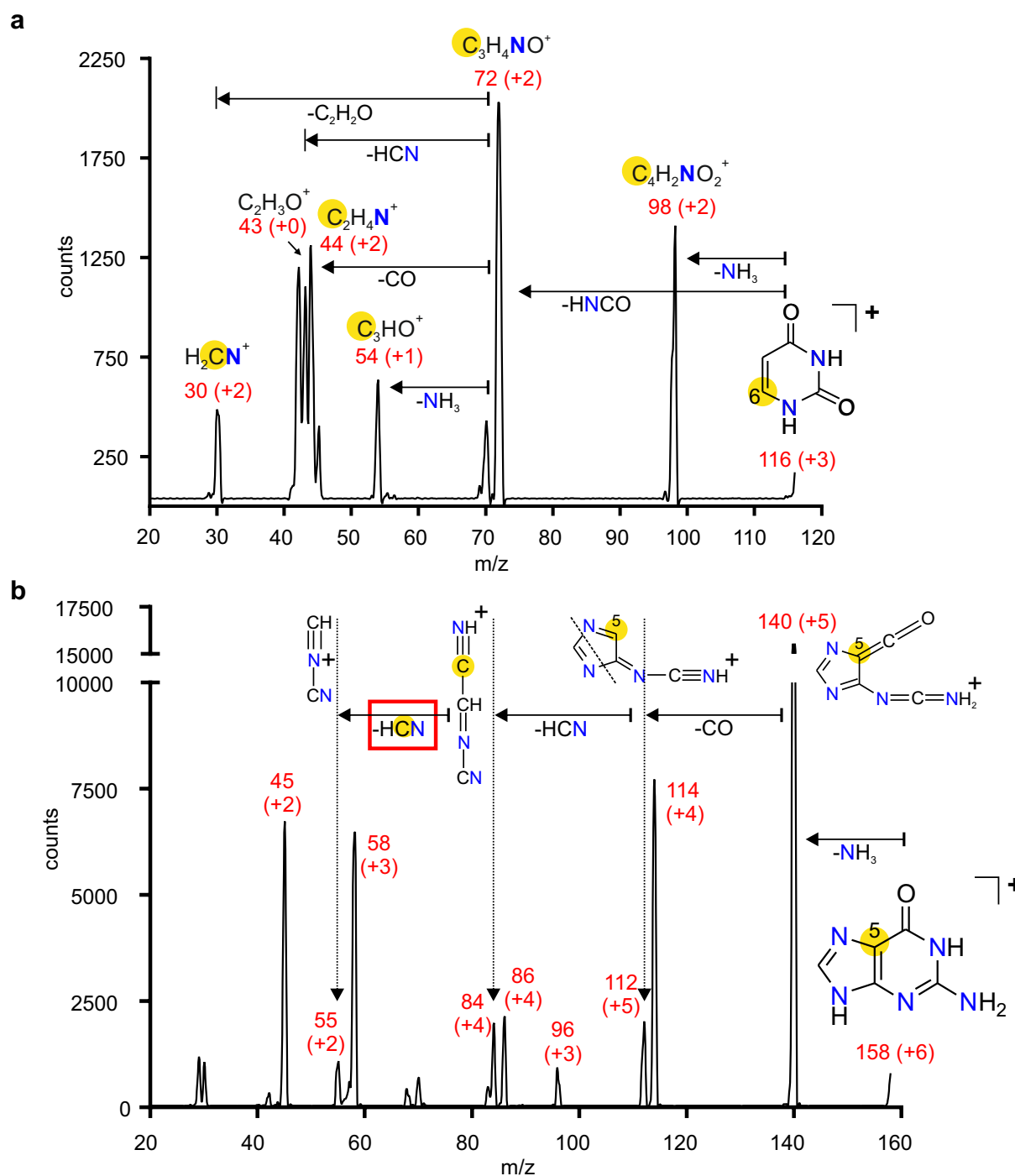


**Figure 3.40: Pseudo-MS<sup>3</sup> spectra of labeled uracil and guanine** Mass spectra displaying the fragmentation of labeled uracil (a) and guanine (b) detected using a pseudo-MS<sup>3</sup> scan. The C6-atom (uracil) and C5-atom (guanine) expected to be labeled with  $^{13}C$  are highlighted with a yellow circle,  $^{15}N$ -labeled nitrogen atoms are depicted in blue. Peaks are labeled with their  $m/z$  value (red) and the difference to unlabeled uracil is given in brackets. The assignment of the peaks with the respective elemental formulas of the fragments was performed using the fragmentation pathways described in [262, 263]. The labeling of position 6 of pyrimidines is best seen in the fragment with a  $m/z$  of 30 when comparing it to the unlabeled fragment ( $m/z$  28), as it only contains one C-atom (C6) and one N-atom, thus C6 had to be labeled by  $^{13}C$ . For guanine, only one possible fragmentation reaction pathway is displayed, including the final cleavage of a moiety containing the labeled C5-atom (red box). RNA samples were prepared and provided by J. Schmidt.

### 3.3.5 Summary

For the analysis of RNA modifications, highly sensitive LC-MS/MS was the method of choice. While the (dynamic) multiple reaction monitoring enabled the most sensitive detection of modified nucleosides and thus was the most suitable mode for the quantitative investigations accomplished [102, 133, 246, 247], the neutral loss scan outperformed the DMRM mode when information about the overall modification pattern of an RNA sample was required. Both scan modes are described in [172] including experimental details. However, both DMRM and NLS modes showed limits in the detection of previously uncharacterized modifications or modifications with unusual fragmentation pattern. While the DMRM mode is largely unsuitable for detection of new modifications due to the requirement of knowing mass transition and retention time, the NLS is applicable to detect such modifications, but, if conducted as described in 1.2.2.1, limited to modified nucleosides displaying the typical fragmentation pattern at the glycosidic bond. Of note, the NLS method can in principle be programmed to monitor any neutral loss of choice and thus is not restricted to the neutral loss of (2'-O-methyl)-ribose. Therefore, nucleosides that lose another neutral moiety are technically accessible as well, however, neutral moieties applicable in such an extended NLS method remain to be examined. Here, in order to establish a method for detection of the nucleoside queuosine, a product ion scan was performed to confirm the cleavage pattern of the nucleoside [224]. A product ion scan only required the knowledge of the precursor mass, which was extracted from the MODOMICs database for Q [79] and either a synthetic standard or an RNA sample that was known to contain the modification of interest (which in case of Q was tRNA<sup>Tyr</sup> of *E. coli*). The results from the product ion scan indicated cleavage at the amino-methyl linker and, less efficiently, at the glycosidic bond and enabled the programming of the respective DMRM method. The determined cleavage pattern furthermore agreed well with [224, 254]. An application of the established LC-MS/MS method in collaboration with Dr. M. Müller and Prof. Dr. A. Ehrenhofer-Murray is described in [255]. Furthermore, possible approaches that might enable the identification of potential Q derivatives other than the known galQ and manQ variants were outlined, including precursor ion scans and modified NLS methods. A rather unusual employment of the triple quadrupole mass spectrometer was the implementation of pseudo-MS<sup>3</sup> scans, which relied on in-source fragmentation of the glycosidic bond and allowed the investigation of the fragmentation patterns of the nucleobases. Here, pseudo-MS<sup>3</sup> scans were performed in collaboration with Prof. Dr. H. Schwalbe and J. Schmidt to investigate the positions at which <sup>13</sup>C-atoms were introduced into the nucleobases when feeding *E. coli* with 2-<sup>13</sup>C-glycerol as carbon source. Results indicated a labeling of position 6 in pyrimidines and position 5 in purines in accordance to [261]. Altogether, the described applications underline the broad applicability of LC-MS/MS in the investigation of RNA modifications. However, one major disadvantage had to be considered: the requirement to digest the RNA to the nucleoside level. This involves the loss of any sequence information, thus neither the RNA species carrying the modification nor the position of the modified nucleoside inside the RNA molecule is accessible. Accompanying that, analyzing a single RNA species, e.g. a specific tRNA, requires its previous isolation, like it was performed for the two

*S. cerevisiae* tRNAs, tRNA<sub>3UU</sub><sup>Lys</sup> and tRNA<sub>NGG</sub><sup>Pro</sup> to enable a NLS analysis. Thus, for a more global, transcriptome-wide detection of modifications in their sequence context, switching to alternative detection methods is necessary (reviewed in [151]).

## 4 Conclusions and Outlook

**RNA Quantification by Microscale Thermophoresis** The applicability of microscale thermophoresis for the quantification of (single) RNA species was investigated with particular emphasis on the analysis of single tRNA abundances as well as on the more general determination of polyA-RNA levels. In case of a specific target tRNA, monitoring the hybridization of a fluorescently labeled, complementary DNA probe by MST in form of a titration curve allowed for the determination of its abundance in total tRNA mixtures in an extraordinary short time. The developed quantification method proved to be highly sensitive and reproducible and, compared to alternative tRNA quantification methods, extremely fast (accomplishable in < 2 hours) and quite easy to implement, as additional to standard laboratory equipment, only the microscale thermophoresis device and the labeled DNA probe were required. The MST-based method not only enabled an absolute quantification of specific (t)RNAs, but also displayed substantial power in the relative quantification and intersample comparison of (t)RNA levels, as changes in the target RNA abundance could be easily obtained from the shift of the binding curve and thus from the  $EC_{50}$  value. By using DNA probes that covered the full-length tRNA sequence a potential negative effect of the presence of modified nucleosides, which was particularly expectable for the highly modified tRNAs, on the quantification could be compensated. Furthermore, the method should be readily transferable to the quantification of other RNA species, for example rRNA molecules, provided a sufficient abundance in the RNA sample is achievable. Admittedly, limitations of the method lie in the possibly inefficient distinguishment of very similar sequences, which is especially relevant in tRNA analysis due to the presence of highly similar isoacceptors and isodecoders. Testing more stringent hybridization conditions might help to improve the analysis of highly analogous sequences and thus enable the analysis of here excluded isoacceptors. Similarly, changing the hybridization conditions for example in respect to salt concentration and pH might help to improve the thermophoretic response for some RNA-probe pairs that could not be analyzed using the standard protocol described in this work. Although the original aim was to develop a quantification method for single RNA molecules, with the main focus on tRNAs, the possibility of a quantification of the mRNA pool within an RNA sample, sharing the polyA tail as common sequence element, was examined. Exploiting this characteristic feature, labeled polyT-DNA probes of varying length were employed instead of sequence-specific probes in order to quantify the complete group of polyadenylated RNAs rather than single transcripts. Using the polyT-DNA probes, relative quantification of polyA-tagged RNAs in total RNA by MST was demonstrated to be well possible with only a small amount of total RNA sample (< 60  $\mu$ g) required. Considering the variable length of polyA tails [230, 231] and the shown inability of longer probes to sufficiently bind shorter polyA stretches, the 20 nt polyT-DNA probe proved

to be the best choice for an overall polyA analysis. Together with the easy and fast operability, the MST-based method enables a quick evaluation of overall changes of mRNA abundances, for example in response to environmental changes, stress or other treatments. As the complete set of polyA-tagged RNAs is captured by the same DNA probe, various RNA samples from different organisms can be thus analyzed for their mRNA content without the need for sequence-specific DNA probes. However, as the polyA tails vary in their length, in this case the MST-based method does not allow an absolute quantification but rather is suitable for relatively comparing polyA contents of samples deriving from the same organism. Of note, as shown by using probes and polyA tails of different lengths, the method is additionally responsive to changes in polyA tail length, which for example occur in specific transcripts during cell cycle progression [267], thus changes in polyA abundance as determined by the presented MST-based method could in principle result from both changes in mRNA abundance and polyA tail length. However, due to its easiness and particular fast performance, the MST-based polyA-RNA quantification should be well suitable for gaining a first insight into changes of transcriptome-wide mRNA abundance in response to various conditions, which can afterwards be supplemented by more detailed investigations on the sequence-specific level. Remarkably, hybridization of a specific RNA probe complementary to *in vitro* transcribed MelanA/GFP mRNA was readily observable by MST, indicating that, in principle, the method might also be applicable for quantification of specific transcripts. However, considering the low abundance of mRNAs in total RNA, such an approach presumably requires an additional mRNA enrichment step, for example by rRNA depletion from the sample.

The performance of the newly established method was tested applying several biological samples, targeting both specific tRNAs and polyA-RNA. The cleavage of *Saccharomyces cerevisiae* tRNA<sub>3UG</sub><sup>Gln</sup> by PaT killer toxin was easily monitored and quantified using the MST-based method, displaying a reduction of tRNA<sub>3UG</sub><sup>Gln</sup> levels by approximately 85 %. Notably, in the PaT-induced sample, a considerable reduction of polyA-levels could be detected, indicating a substantial influence of tRNA<sub>3UG</sub><sup>Gln</sup> depletion on the cell's fitness. Furthermore, investigation of the abundances of 23 *S. cerevisiae* tRNAs using the MST-based method revealed quite pronounced differences in the amounts of the single tRNA species, ranging from less than 1 % to approximately 6 % in total tRNA. However, temperature stress-induced changes in tRNA levels were small, and only significant in a small subset of tRNAs. Analyzing *S. cerevisiae* double mutants lacking tRNA anticodon-loop modifications indicated, amongst others, an upregulation of tRNA<sub>3UG</sub><sup>Gln</sup> upon temperature stress, which might represent a mechanism to counterbalance the poor function of the hypomodified tRNA at elevated temperature [228].

Although the method proved to be suitable for both tRNA and mRNA quantification and transferability to other RNA species such as rRNA seems consequential, the actual confirmation of a much broader application range remains to be rendered, with a special emphasis of the limits of detection and quantification of the method. Although the labeled DNA probe was applied in concentrations as low as 25 nM (up to 100 nM), thereby in principle enabling the detection and quantification of lower abundant RNAs as altogether only a few pmol of the target RNA are required, the concentration of the target RNA in the total RNA pool has to be considered and



---

is potentially the limiting factor. Thus, size selection steps or enrichment by other means, for example rRNA depletion, prior to MST analysis might be necessary to enable the investigation of low abundant RNAs. Another interesting aspect in respect to tRNA quantification is the quantification of tRNA fragments, *e.g.* tRNA halves produced by angiogenin-mediated cleavage. In this work, tRNA fragments, *e.g.* those produced by the PaT killer toxin, were actively excluded from analysis by using PAGE-purified total tRNA pools which did not contain any RNA fragments smaller than tRNAs. By that, a simultaneous detection of fragments and full-length tRNA was prevented, allowing the quantification of merely the intact tRNA. Additional experiments are required to evaluate the possibility of detecting tRNA fragments together with or, even more desirable, separately from the full-length parent tRNA, for example by varying stringency of hybridization conditions or measurement at elevated temperatures.

**Isolation of Native mascRNA** A detailed investigation of mascRNA, a tRNA-like small RNA recently shown to be involved in the cardiovascular immune system [198], in respect to the presence of modified nucleosides, especially of m<sup>1</sup>A, was anticipated. For this, the isolation of mascRNA in pure form was the ultimate prerequisite to be able to perform an RNA modification analysis by LC-MS/MS. An isolation protocol based on hybridization and subsequent affinity purification using streptavidin-coated beads was optimized, successfully applied to a range of tRNAs and its general suitability for mascRNA isolation was verified. Total RNA isolated from HeLa cells was used in a first, due to extremely high unspecific binding of non-target RNAs unsuccessful attempt to purify mascRNA. Nevertheless, RNA-Seq results of the isolated RNA indicated, when compared to the total RNA input, a potential enrichment of mascRNA by the isolation protocol. In a second attempt, pre-purified small RNA fractions (< 200 nt) of HeLa and HEK cell RNA were used as input to limit unspecific binding, and although it was again unfeasible to obtain pure mascRNA, RNA-Seq results confirmed the enrichment of mascRNA for the HeLa RNA sample. Furthermore, RNA-Seq analysis revealed a potential m<sup>1</sup>A at a site equivalent to the often m<sup>1</sup>A-modified A58 in tRNAs, however, this could not be confirmed by LC-MS/MS due to the lack of pure mascRNA and thus requires additional examinations. Adaptions of the isolation protocol, *e.g.* by including a second round of bead-based affinity purification, and higher amounts of small input RNA might help to obtain mascRNA in purified form in future. Additionally, switching from HeLa/HEK cells to peripheral blood mononuclear cells (PBMC), which were recently shown to contain high levels of mascRNA [198], might permit a successful isolation. Another possibility to indirectly prove the presence of the m<sup>1</sup>A modification would be the use of a knockdown of the putative m<sup>1</sup>A-introducing enzyme and comparing the RNA-Seq results of mascRNA-enriched samples of wildtype and mutant, however, as the m<sup>1</sup>A58-generating enzyme is presumably indispensable for life [245], that approach is probably not feasible. Nevertheless, improving the isolation protocol for mascRNA might not only enable mascRNA isolation in uncontaminated form, but also the application to other small non-coding RNA, which could be targets for RNA modifications as well. Considering that the efficient cleavage of mascRNA from its precursor lncRNA MALAT1 is essential for MALAT1 accumulation to high levels [180] and thus its role in cancer progression, future attempts of a

detailed investigation of mascRNA and its potential modifications, also in regard to the time-point of their introduction, are required to fully understand the MALAT1-mascRNA system. This requirement is additionally highlighted by the recent detection of a distinct function of mascRNA in cardiovascular immunity [198].

**LC-MS/MS Analysis of Modified Nucleosides** LC-MS/MS analysis of modified nucleosides using a triple quadrupole mass spectrometer was conducted under a variety of scientific tasks, requiring different kinds of experimental setups and subsequent data analysis. The rather standard DMRM mode, applicable for highly sensitive quantitative analysis of known RNA modifications, was mainly used for analysis of wobble U34 modifications in collaboration with the laboratories of Prof. Dr. R. Schaffrath and Prof. Dr. M. Stark in order to both prove the knockout efficiency of mutants for the U34-modifying enzymes and to investigate their effects on the presence of the respective wobble U34 modifications [102, 246, 247]. In order to verify the successful isolation of several tRNAs from *Saccharomyces cerevisiae*, the second “standard” scan mode, namely the neutral loss scan, was used to evaluate the presence of both expected and unexpected modifications in the isolated tRNAs. The analyzed tRNAs contained, next to all of the expected modified nucleosides, only two more nucleosides, whose presence could be explained by either degradation or rearrangement of another modification. Hereby, LC-MS/MS analysis confirmed the suitability of the isolation protocol for the isolation of pure tRNAs. A more sophisticated analysis was required for the nucleoside modification queuosine (Q), which displays an unusual fragmentation pattern [224]. A product ion scan was performed to confirm the fragmentation at the aminomethyl-linker structure and to enable the programming of a suitable DMRM method, which was finally used to investigate the incorporation of Q into *S. pombe* tRNA under nutritional supply of queuine in collaboration with Dr. M. Müller and Prof. Dr. A. Ehrenhofer-Murray [255]. Remarkably, Q can occur in form of sugar-modified derivatives in mammals, manQ and galQ, which were readily detected in HeLa RNA but absent in *S. pombe* RNA. However, there might be additional, hitherto unknown derivatives of Q present, which were not covered by the analysis. As both Q and derivatives thereof show the same fragmentation pattern at the aminomethyl linker structure and hereby produce the same product ion, a precursor ion scan, which detects the precursor ion of a defined product ion, might be useful to uncover the existence of further Q derivatives in future. Another imaginable approach to investigate subsets of modified nucleosides with untypical fragmentation behavior such as Q might be the adaption of the NLS method. In principle, the loss of any moiety besides the ribose could be investigated using the NLS method, provided that the respective product ion resulting from the cleavage of the moiety is detectable. Although that prerequisite was not fulfilled in the case of Q and its derivatives, adapted NLS methods might be useful for investigation of other hypermodified nucleosides, especially of those carrying larger side groups attached *via* rather labile linker structures. The possibility of performing pseudo-MS<sup>3</sup> scans with the normally for MS<sup>2</sup>-experiments designed triple quadrupole by using in-source fragmentation was exploited in collaboration with Prof. Dr. H. Schwalbe and J. Schmidt. Here, in RNA of *E. coli* (tricarboxylic acid cycle deficient strain) fed with <sup>13</sup>C-2-Glycerol as only carbon

---

source, the positions of the introduced  $^{13}\text{C}$  atoms within the nucleobases were examined. The fragmentation pattern of uracil and guanosine obtained from the respective  $\text{MS}^3$  mass spectra strongly indicated a labeling of the positions 6 in pyrimidines and 5 in purines, which is in good accordance with literature [261]. Altogether, the various types of nucleoside analysis performed using LC-MS/MS in different scan modi demonstrated the broad applicability of the triple quadrupole MS-system. Those applications included not only the highly sensitive detection and quantification of modified nucleosides (DMRM mode), but also the analysis of all nucleosides, including unexpected or unknown ones, present in a sample (NLS), the examination of fragmentation pattern and positions of nucleosides (product ion scan) and even the detailed structural investigation of (modified) nucleobases.



## 5 Materials and Methods

### 5.1 Materials

#### 5.1.1 Chemicals, Reagents and Ready-to-use Buffers and Solutions

Acetic acid, glacial, HPLC grade	Sigma-Aldrich (Steinheim, Germany)
Acetonitrile, LC-MS grade	Sigma-Aldrich
Adenosine	Sigma-Aldrich
Adenosine triphosphate (ATP)	Thermo Fisher Scientific (Waltham, MA, USA)
Ammonium acetate	Sigma-Aldrich
Ammonium peroxydisulfate (APS)	Carl Roth (Karlsruhe, Germany)
Bovine Serum Albumine (BSA, 20 mg/mL)	Thermo Fisher Scientific
Bromphenol Blue	Sigma-Aldrich
Chloroform, HPLC grade	Sigma-Aldrich
Cytidine	Sigma-Aldrich
Cytidine triphosphate (CTP)	Sigma-Aldrich
Dichlorodimethylsilane	Sigma-Aldrich
Disodium hydrogenphosphate (Na <sub>2</sub> HPO <sub>4</sub> )	Carl Roth
Dithiotreitol (DTT)	Thermo Fisher Scientific
D-MEM #61965	Thermo Fisher Scientific
DNase1 buffer with MgCl <sub>2</sub> , 10x	Thermo Fisher Scientific
dNTP mix, 10 mM	Thermo Fisher Scientific
D-PBS #14190	Thermo Fisher Scientific
Dynabeads <sup>®</sup> Streptavidin (M-280, M-270, MyOne <sup>™</sup> T1, MyOne <sup>™</sup> C1) #65801D	Thermo Fisher Scientific
EDTA	Carl Roth
Ethanol, 99.5 %	Carl Roth
FastAP buffer, 10x	Thermo Fisher Scientific
Fetal bovine serum (FBS) #10500	Thermo Fisher Scientific
Formamide	Carl Roth
GelRed #41001	Biotium (Hayward, USA)
Glycerol	Sigma-Aldrich
Glycogen, RNA grade	Thermo Fisher Scientific
Guanosine	Sigma-Aldrich

Guanosine triphosphate (GTP)	Sigma-Aldrich
Isopropanol, LC-MS grade	Sigma-Aldrich
Magnesium chloride (MgCl <sub>2</sub> )	Carl Roth
1-Methyladenosine (m <sup>1</sup> A)	Sigma-Aldrich
N,N,N',N'-Tetramethylethylenediamine (TEMED)	Carl Roth
PCR reaction buffer, 10x	Rapidozym (Berlin, Germany)
Penicillin/Streptomycin 10000 U, #15140	Thermo Fisher Scientific
Potassium chloride (KCl)	Carl Roth
Potassium dihydrogen phosphate (KH <sub>2</sub> PO <sub>4</sub> )	Carl Roth
RNA Binding buffer #R1013-2-25	Zymo Research (Freiburg, Germany)
RNA Prep buffer #R1060-2-25	Zymo Research
RNA Wash buffer concentrate #R1003-3-12	Zymo Research
Rotiphorese sequencing gel buffer concentrate	Carl Roth
Rotiphorese sequencing gel concentrate (denaturing, 25 %)	Carl Roth
Rotiphorese sequencing gel diluent	Carl Roth
Rotiphorese Gel 40 19:1, 40 % non-denaturing	Carl Roth
Sodium chloride (NaCl)	Carl Roth
SYBR <sup>®</sup> Gold nucleic acid gel stain	Thermo Fisher Scientific
TBE buffer, 10x	Carl Roth
2-Thiouridine (s <sup>2</sup> U)	Berry and Associates (Dexter, USA)
Total tRNA, <i>E. coli</i>	Roche Diagnostics (Basel, Switzerland)
Total tRNA, <i>Saccharomyces cerevisiae</i>	Roche Diagnostics
TriReagent #T9424	Sigma-Aldrich
Tris(hydroxymethyl)aminomethane (Tris)	Carl Roth
Tris-HCl	Carl Roth
Triton-X 100	Sigma-Aldrich
Trypsin-EDTA, 0.05 % #25300	Thermo Fisher Scientific
Uridine	Sigma-Aldrich
Uridine triphosphate (UTP)	Sigma-Aldrich
Xylene Cyanol	Sigma-Aldrich

The nucleoside standards of mcm<sup>5</sup>U and mcm<sup>5</sup>s<sup>2</sup>U were kind gifts of Prof. Dr. Andrzej Malkiewicz (Lodz University of Technology, Faculty of Chemistry, Poland). All other chemicals and reagents not listed here were obtained from the Institute of Pharmacy's (University of Mainz, Germany) in-house chemical store.

### 5.1.2 Buffers, Solutions and Media

**Ammonium acetate solutions** 0.5 (for gel elution) and 5 M (for RNA precipitation) ammonium acetate in Milli-Q water.

**APS solution** 10 % APS (m/v) in Milli-Q water.

**1x Binding and Washing buffer** 5 mM Tris-HCl (pH 7.5), 0.5 mM EDTA, 1 M NaCl in Milli-Q water.

**Cell culture medium** 89 % (v/v) D-MEM, 10 % (v/v) FBS, 1 % (v/v) Pen/Strep.

**KL-buffer** 50 mM Tris-HCl (pH 7.4), 10 mM MgCl<sub>2</sub> in Milli-Q water.

**LC-MS/MS solvent A** 5 mM ammonium acetate in Milli-Q water, adjusted to pH 5.3 using glacial acetic acid. Addition of 1 % acetonitrile to prevent rapid spoilage.

**Loading buffer, denat.** 90 % (v/v) formamide, 10 % (v/v) 10x TBE buffer.

**Loading buffer, non-denat.** 50 % (v/v) glycerol, 10 % (v/v) 10x TBE buffer in Milli-Q water.

**NP1 buffer** 90 % (v/v) RNA hydrolysis buffer, 10 % (v/v) 2 mM zinc chloride (ZnCl<sub>2</sub>) solution.

**PAGE pre-mix, 10 % denat.** 40 % (v/v) denaturing gel concentrate (25 %), 50 % (v/v) gel diluent, 10 % (v/v) gel buffer concentrate.

**PAGE pre-mix, 15 % denat.** 60 % (v/v) denaturing gel concentrate (25 %), 30 % (v/v) gel diluent, 10 % (v/v) gel buffer concentrate.

**PAGE pre-mix, 8 % non-denat.** 20 % (v/v) non-denaturing gel concentrate (40 %), 10 % 10x TBE in Milli-Q water.

**PAGE pre-mix, 10 % non-denat.** 25 % (v/v) non-denaturing gel concentrate (40 %), 10 % 10x TBE in Milli-Q water.

**PAGE pre-mix, 15 % non-denat.** 37.5 % (v/v) non-denaturing gel concentrate (40 %), 10 % 10x TBE in Milli-Q water.

**1x PBS** 1:10 dilution of 10x PBS in Milli-Q water, pH 7.4. Final salt concentrations are 137 mM NaCl, 2.7 mM KCl, 1.7 mM KH<sub>2</sub>PO<sub>4</sub>, 10 mM Na<sub>2</sub>HPO<sub>4</sub>.

**10x PBS** 1.37 M NaCl, 27 mM KCl, 17 mM KH<sub>2</sub>PO<sub>4</sub>, 100 mM Na<sub>2</sub>HPO<sub>4</sub> in Milli-Q water (pH 6.8).

**10x RNA hydrolysis buffer** 250 mM ammonium acetate in Milli-Q water, pH adjusted to 5.0 using acetic acid.

**0.1x SSC buffer** 1:10 dilution of 1x SSC buffer (15 mM NaCl, 1.5 mM trisodium citrate).

**1x SSC buffer** 1:20 dilution of 20x SSC buffer (0.15 M NaCl, 15 mM trisodium citrate).

**5x SSC buffer** 1:4 dilution of 20x SSC buffer (0.75 M NaCl, 75 mM trisodium citrate).

**20x SSC buffer** 3 M NaCl, 300 mM trisodium citrate in Milli-Q water, pH 7.0.

**1x TBE buffer** 1:10 dilution of 10x TBE buffer in water.

**5x transcription buffer (Strasbourg buffer)** 40 mM Tris-HCl (pH 8.1), 1 mM Spermidine, 5 mM DTT, 0.01 % Triton-X 100 in Milli-Q water.

### 5.1.3 Enzymes

DNase 1, 50 U/ $\mu$ L	Thermo Fisher Scientific
FastAP thermosensitive Alkaline Phosphatase, 1 U/ $\mu$ L	Thermo Fisher Scientific
Nuclease P1 (NP1) from <i>Penicillium citrinum</i> , lyophilized	Sigma-Aldrich
Snake Venom Phosphodiesterase (SPD) from <i>Crotalus adamanteus</i> venom, lyophilized	Worthington (Lakewood, USA)
Taq DNA Polymerase, 5 U/ $\mu$ L	Rapidozym (Berlin, Germany)
T4 DNA Ligase, 30 U/ $\mu$ L	Thermo Fisher Scientific
T4 Polynucleotide Kinase, 10 U/ $\mu$ L	Thermo Fisher Scientific
T4 RNA Ligase 2	in-lab preparation
T7 RNA Polymerase	in-lab preparation

### 5.1.4 DNA and RNA Oligonucleotides

All DNA probes complementary to tRNAs were designed using the tRNA sequences listed in the tRNADB 2009 ([80], <http://trnadb.bioinf.uni-leipzig.de/>) as templates, except for tRNA<sup>Gln</sup><sub>3UG</sub>, for which the sequence was obtained from the MODOMICS database [79]. For tRNA isoacceptor/isodecoder sequences that differed in less than 9 nucleotides, only one probe was designed, which was expected to hybridize to both isoacceptors. This was the case for the isodecoder pairs of tRNA<sup>Arg</sup><sub>1CU</sub>, tRNA<sup>His</sup><sub>GUG</sub>, tRNA<sup>Pro</sup><sub>NGG</sub>, tRNA<sup>Thr</sup><sub>IGU</sub> and tRNA<sup>Ser</sup><sub>IGA</sub> [80], which all displayed sequence differences of 5 nt or less. DNA probes carrying a fluorescent dye were labeled with fluoresceine except for the probes MH630, MH710, MH765 and MH768, for which Atto488 was used. All oligonucleotides were synthesized by IBA, Göttingen, Germany. DNA probes labeled with AXXX were kindly provided by Prof. Dr. Yuri Motorin (also synthesized by IBA, Germany). In table 5.1, all DNA probes used for quantification and isolation of *Saccharomyces cerevisiae* tRNAs are displayed. In table 5.2 all other DNA or RNA probes applied in MST experiments are listed, and table 5.3 includes all oligonucleotides used for *in vitro* transcription and splint ligation.



**Table 5.1: Sequences of DNA probes used for quantification and isolation of *Saccharomyces cerevisiae* tRNAs** DNA probe ID, target tRNA, tRNAdb ID and sequence are listed for each probe. All DNA probes are labeled with a 5'-biotin moiety (attached to an AAA-overhang) and a 3'-fluoresceine or -Atto488.

DNA probe	tRNA	tRNAdb ID	Sequence
MH772	tRNA <sup>Ala</sup> (IGC)	tdbR00000012	AAATGGTGCACGAGTCCGGAATCGAACCCGGAGACCTTCCCATGCTAAGGGAGCGCGGTACCGACTACGCCACACGCC
MH778	tRNA <sup>Arg</sup> (ICU)	tdbR000000370	AAATGGCACTACGATGGGGTCGAACCCATAATCTTCTGATTAAGAAAGTCAGACGCGGTGCCATTACGCCACGCGGAGC
MH784	tRNA <sup>Arg</sup> (ICG)	tdbR000000369	AAATGGCTTCCCGCCAGGACTTGAAACCTGGAATCTTCTGGTTCTAGCCAGACGCGCGTGACCAATTGGGCCACGAGGAA
MH781	tRNA <sup>Asn</sup> (GUU)	tdbR000000300	AAATGGCGACCCCAAGTGAAGGTTGAACCTACGATCTTGGGATTAACAGTGCACGCGCTTAAACCAACTTGGCCATGGAGTC
MH780	tRNA <sup>Asp</sup> (GUC)	tdbR000000035	AAATGGCTCGCGGACGGGAATTGAACCCCGATCTGGCAGCGGACGACAAGCGCCCATTTGACCAITTAACACTATCACGGA
A682	tRNA <sup>Cys</sup> (GUC)	tdbR000000021	AAATGGAGCTCGCACTCAGGATCGAACTAAGCACCAACAGATTTGCAATCTGCTGGCTACCACTGCGCCATACGAGC
MH779	tRNA <sup>Gln</sup> (3UG)	MODOMICS	AAATGGAGGTCTACCCGGATTGCAACCGGGTTGTCCGCAITCAAACCGAAAGTGATAACCACTACACTATAGGACC
A683	tRNA <sup>Glu</sup> (3UC)	tdbR000000054	AAATGGCTCCGATACGGGGAGTCGAACCCCGTCTCCACGGTGAAGCGTGAATGATAGCCGTTACACTATATATCGGA
MH773	tRNA <sup>Gly</sup> (CC)	tdbR000000130	AAATGGTGACGGGTACGAGAAATCGAAACCCGTGTCCACCTTGGAAAGGTGGGATGATAACCACTACACTAACCCGCC
MH785	tRNA <sup>Gly</sup> (GCC)	tdbR000000129	AAATGGTGGCAAGCCCGGAATCGAACCGGGGCCAACGATGGCAACGTTGGATTTTACCATAAAACCACTTTGGC
MH774	tRNA <sup>His</sup> (GUG)	tdbR000000144	AAATGGTGCCACCTCCTAGAAATCGAACAGGGTTTCAACAGCCACAAATTTGTGTACTAAACCACTATACTAAAGATGGCC
MH710	tRNA <sup>Ile</sup> (IAU)	tdbR000000170	AAATGGTGGTCTTAGCGGGATCGAACCGTGTATCCCGGCTTATCAGCACGGTGCCTTAACCAACTGGGCCAAGAGACC
MH783	tRNA <sup>Ini</sup> (CAU)	tdbR000000526	AAATGGTAGCCCGCTCGGTTTCGATCCGAGGACATCAGGGTTATGAGCCCTGGCGGCTTCCACTGCGCCACGGGGCT
A681	tRNA <sup>Leu</sup> (UAA)	tdbR000000251	AAATGGTGGTTGCTAAGAGATTGGAACCTTGTGCACTTACGATACCTGAGCTTGAATCAGCGGCTTAGACCCGCTGGGCCAAACAAC
MH788	tRNA <sup>Leu</sup> (UAG)	tdbR000000250	AAATGGTGAGACTAAGGATTGCAACCCCTTGATCCGAAAGATATCAGAGCCCTAAATCTGACGCTTAAACCACTGGGCCAAACTCCC
A676	tRNA <sup>Lys</sup> (3UU)	tdbR000000193	AAATGGCTCTCATAGGGGGCTCGAACCCCTGACATTTCCGGTTAAAGCCGAAACCGCTACCAACTGAGCTAACAAAGGA
A677	tRNA <sup>Lys</sup> (CUU)	tdbR000000192	AAATGGAGCCCTGTAGGGGGCTCGAACCCCTAACCTTATGATTAAGAGTATACCGCGCTACCGATTGGCGCCAAACAAGG
MH782	tRNA <sup>Met</sup> (CAU)	tdbR000000284	AAATGGTGTCTCCAGGAGAGGTTCCGAACCTTCAGATTATGAGACTGACGCTCTTCTACTGAGCTACTGAAGC
MH775	tRNA <sup>Pro</sup> (NGG)	tdbR000000323	AAATGGGGGGGAGCTGGGAATTGAAACCCAGGGCTCTCCACCCAAAGCAGAAATCATACCACTAGACCAACGACCGCC
A678	tRNA <sup>Ser</sup> (TGA)	tdbR000000408	AAATGGCGAACATCGAGGACTCGAACCTGGCGGGCAAGCCCAAAGATTCTAATCTTTCGGCTTAACCACTCGGCCAAGTTGCC
A679	tRNA <sup>Ser</sup> (NCA)	tdbR000000406	AAATGGCGAACACGACGATTTGAACCCAGCGGGGAGAGGCCAACAGATTTCAAAGTCTGCGCCTTAACCACTCGGCCATAGTGCC
MH776	tRNA <sup>Thr</sup> (IGU)	tdbR000000443	AAATGGTGTCTTCCAATCGGATTTGAACCGATGATCTCCACATTAAGTGTGGCGCCCTTACCAACTTGGCCATAGAAGC
A675	tRNA <sup>Thr</sup> (BCA)	tdbR000000494	AAATGGTGAACCGACAGGAATGAACTGCAACCCCTCGATTGGAGTGAAGAGCTCTACCATTGAGCCACCGCTTC
A674	tRNA <sup>Tyr</sup> (GPA)	tdbR000000555	AAATGGTCTCCCGGGGGGAGTCCGACGCCGATCTCAAGATTACAGTCTTGGCCCTTAACCAACTTGGCTACCGGAG
MH777	tRNA <sup>Val</sup> (IAC)	tdbR000000464	AAATGGTGTATTTCCGCCAGGATCGAACTGGGACGTTCTCGGTGTTAAGCAGATGCCATAACCGACTAGACCAGAAACC
MH786	tRNA <sup>Val</sup> (&AC)	tdbR000000466	AAATGGTGTATCCAAACCGAGGTTTCGAACTCGGGATCTTCGGCGTGTAAAGGCGAGCTTTGAACCACTGGACCAITGGACC
MH787	tRNA <sup>Val</sup> (CAC)	tdbR000000465	AAATGGTGTTCCAAACCGAGGATCGAACTCGGGACCTTTCGGGTGTGAAGGCCAACGTGATAGCCCGCTACACTAITTGGAAC



**Table 5.3: Oligonucleotides used for IVT and splint ligation** PCR-templates and primers applied in IVT and RNA oligonucleotides used for splint ligation are tabled.

Oligo-nucleotide	Target RNA	Function	Sequence
MH53		T7-universal primer	CGCGCGAAGCTTAATACGACTCACTATA
MH373	tRNA <sup>Met</sup> (MAU) ( <i>E. coli</i> )	T7-template	TGGTGGCTACGACGGGATTTCGAACCTGTGACCCCATCATT-ATGAGTGATGTGCTCTAACCAACTGAGCTACGTAGCCGACGGTACCGGGTACCGTTTCGTCTCACGGACTCATCAGGGC-TACGTATCTCCCTATAGTGAGTCGTATT
MH374	tRNA <sup>Met</sup> (MAU) ( <i>E. coli</i> )	reverse primer	TGGTGGCTACGAC
MH766	mascRNA	T7-template	TGGAGACGCCGCAGGGATTTGAACCCCGTCCTGGAAA-CCAGGAGTGCCAACCACCAGCATCTATAGTGAGTCGTATT
MH767	mascRNA	reverse primer	TGGAGACGCCGCA
MH806	tRNA <sup>Arg</sup> (1CU)	5'-fragment	GCUCGCGUGGCGUAAUGGCAACGCGUCUGACUUCUAA
MH807	tRNA <sup>Arg</sup> (1CU)	3'-fragment	UCAGAAGAUUAUGGGUUCGACCCCAUCGUGAGUGCCA

### 5.1.5 RNA Samples Obtained from Collaborators

#### 5.1.5.1 RNA for MST measurements

**Total tRNA from *S. cerevisiae*, strain S288C, grown at 30 and 39 °C** obtained from Dr. Sebastian Leidel (RNA biology laboratory, Max-Planck-Institut für Molekulare Biomedizin, Münster).

**Total RNA from *S. cerevisiae*, strain BY4741, grown at 30 °C/under heat shock** Wildtype and double mutant ( $\Delta elp3\Delta deg1$ ,  $\Delta elp3\Delta urm1$ ,  $\Delta urm1\Delta deg1$ ,  $\Delta tcd1\Delta elp3$  and  $\Delta tcd1\Delta urm1$ , described in [102, 225]) total RNA samples, prepared by Akif Ciftci, laboratory of Prof. Dr. Raffael Schaffrath (Institut für Biologie, Fachgebiet Mikrobiologie, Universität Kassel).

**Total RNA from *S. cerevisiae*, strain BY4741, empty or inducible PaT vector** (described in [229, 233]) prepared by Akif Ciftci, laboratory of Prof. Dr. Raffael Schaffrath (Institut für Biologie, Fachgebiet Mikrobiologie, Universität Kassel).

***In vitro*-transcribed MelanA/GFP mRNA, 64 nt polyA tail** prepared by Isabell Hellmuth (AK Helm, Institut für Pharmazie und Biochemie, Johannes Gutenberg-Universität, Mainz).

***In vitro*-transcribed mRNAs, 51 and 101 nt polyA tails** obtained from Prof. Dr. Katalin Karikó (BioNTech RNA Pharmaceuticals GmbH, BioNTech AG, Mainz).

#### 5.1.5.2 RNA for LC-MS/MS measurements

**Total tRNA from *S. cerevisiae*, strain S288C, wildtype and  $\Delta elp3$ ,  $\Delta uba4$ ,  $\Delta elp3\Delta uba4$  mutants [102]** obtained from Dr. Roland Klassen, laboratory of Prof. Dr. Raffael Schaffrath (Institut für Biologie, Fachgebiet Mikrobiologie, Universität Kassel).

**Total tRNA from *S. cerevisiae*, strain BY4741, wildtype and  $\Delta urm1$  /  $\Delta uba4$  mutants +/- expression vectors for *S. cerevisiae* or human Urm1/Uba4 [246]** obtained from André Jüdes, laboratory of Prof. Dr. Raffael Schaffrath (Institut für Biologie, Fachgebiet Mikrobiologie, Universität Kassel).

**Total tRNA samples from *S. cerevisiae*, strain BY4741, wildtype and various  $\Delta elp1$  mutants [247]** obtained from Wael Abdel-Fattah, collaboration of the laboratories of Prof. Dr. Raffael Schaffrath (Institut für Biologie, Fachgebiet Mikrobiologie, Universität Kassel) and Prof. Dr. Mike Stark (Centre for Gene Expression and Regulation, College of Life Sciences, University of Dundee, UK).

**Total RNA from *Schizosaccharomyces pombe*, wildtype and  $\Delta pmt1$ , +/- queuine supply in growth medium [255]** obtained from Dr. Martin Müller, laboratory of Prof. Dr. Ann Ehrenhofer-Murray (Institut für Biologie, AG Molekulare Zellbiologie, Humboldt Universität zu Berlin, Berlin).

**Total RNA from *E. coli*, mutant strain DL323, grown under  $^{13}\text{C}$ -2-glycerol supply as only carbon source** (described in [261]), obtained from Jochen Schmidt, laboratory of Prof. Dr. Harald Schwalbe (Institut für Organische Chemie und Chemische Biologie, Zentrum für Biomolekulare Magnetische Resonanz, Johann Wolfgang Goethe-Universität, Frankfurt).

#### 5.1.6 Cell Lines

**HeLa cells** A human cervix carcinoma cell line (DSMZ #ACC 57) obtained from a cancer tissue sample of Henrietta Lacks in 1951. The cells were a kind gift from Prof. Dr. B. Epe (Abteilung Pharmakologie, Institut für Pharmazie und Biochemie, Johannes Gutenberg-Universität, Mainz).

**HEK cells** An immortalized human embryonic kidney cell line (DSMZ #ACC 305). The cells were a kind gift from Prof. Dr. A. Dalpke (Department of Infectious Diseases, Medical Microbiology and Hygiene, University Hospital, Heidelberg).

### 5.1.7 Disposables and Glassware

Cell culture flasks, 75 and 175 cm <sup>2</sup> , tc treated with ventilated cap	Sarstedt (Nümbrecht, Germany)
Cell scraper	Sarstedt
Centrifugation tubes, 15 and 50 mL	Sarstedt
Filter top vacuum bottles, PES, 0.2 µm pore, 500 mL	Sarstedt
Illustra MicroSpin G-25 columns	GE Healthcare Life Sciences (Buckinghamshire, UK)
MEGAclear Transcription Clean-Up kit #AM1908	Thermo Fisher Scientific
Micro inserts #7-0632, conical, 250 µL	NeoLab (Heidelberg, Germany)
NanoTemper standard treated capillaries #MO-K002	Nanotemper Technologies (Munich, Germany)
Pall Nanosep MF centrifugal device 0.45 µm	Pall Life Sciences (Crailsheim, Germany)
PCR vials, 200 µL	Kisker Biotech (Steinfurt, Germany)
Pipet tips with filter, RNase/DNase free, sterile	Greiner (Frickenhausen, Germany)
Reaction tube, 1.5 mL	Carl Roth
RNA Clean & Concentrator Kit™-5	Zymo Research
Serological pipets, sterile, disposable	Sarstedt
Screw cap ND9 with puncture #7-0693	NeoLab
Short crimp-top vials ND9 #7-0675, 1.5 mL	NeoLab

### 5.1.8 Instruments

#### 5.1.8.1 Basic Laboratory Equipment

**Analytical balances** Mettler Toledo PM460 and Mettler Toledo Excellence Plus (Gießen, Germany)

**Electrophoresis** CBS LSG-400-20 NA vertical electrophoresis chamber (CBS Scientific, San Diego, USA), Consort EV232 power supply (Consort, Turnhout, Belgium)

**Incubation and shaking** BIOER heatblock (Biozym, Oldendorf, Germany), Thermomixer Comfort (Eppendorf, Hamburg, Germany), Digital Heatblock (VWR, Darmstadt, Germany)

**Centrifuges** Eppendorf Centrifuge 5810R (Hamburg, Germany), 1-15 PK Sigma (Osterode am Harz, Germany), Beckman Coulter Centrifuge Avanti J20 (Krefeld, Germany)

**Pipetting** Discovery Comfort micropipettes, variable (Abimed, Langen, Germany)

**pH measurements** FiveEasy™ FE20 pH meter (Mettler Toledo)

**Ultrapure water purification system** Milli-Q, Millipore (Darmstadt, Germany)

**UV detection** UV lamp 254 nm (Herolab Molekulare Trenntechnik, Wiesloch, Germany)

**UV spectrophotometry** Nanodrop ND 2000 Spectrophotometer (Peqlab, Erlangen, Germany)

### 5.1.8.2 Instrumentation and Equipment for Special Techniques

**Gel detection** Typhoon 9400 variable mode imager with an external blue laser unit (GE Healthcare, Buckinghamshire, UK)

**HPLC system (part of the LC-MS/MS device)** Synergi Fusion-RP18 column with 4  $\mu\text{m}$  particle size, 80  $\text{\AA}$  pore size and 250  $\times$  2.0 mm dimension (Phenomenex, Aschaffenburg, Germany) connected to an Agilent 1200 series LC-system equipped with a binary pump, a temperature-controllable column compartment, a diode array detector for UV absorption monitoring, a fluorescence detector and a temperature-controllable autosampler (Agilent Technologies, Santa Clara, USA)

**Mass spectrometry (part of the LC-MS/MS device)** Agilent 6460 Triple Quadrupole mass spectrometer equipped with an Agilent ESI Jetstream ion source with orthogonal spray (Agilent Technologies), connected to a Claind Brezza NiGen LCMS 40-1 nitrogen generator (Claind srl, Tremezzina, Italy)

**Microscale Thermophoresis** NanoTemper Monolith<sup>TM</sup> NT.115 (NanoTemper Technologies, Munich, Germany)

**PCR** peqSTAR Thermocycler (Peqlab, Erlangen, Germany)

**Separation of magnetic beads** 6-Tube magnetic separation rack (New England BioLabs NEB, Ipswich, USA)

## 5.2 Methods

### 5.2.1 RNA Preparation and Microscale Thermophoresis

#### 5.2.1.1 RNA Precipitation

For purification and concentration purposes, ammonium acetate was added to aqueous RNA solutions to a final concentration of 0.5 M. The 2.5-fold volume of ice-cold (-80 °C), pure ethanol was subsequently added, followed by RNA precipitation at -20 °C overnight after mixing thoroughly. Pelleting of the RNA was performed by centrifuging at 15493g at -5 °C for at least 30 minutes. Pellets were washed once using 100 µL 70 % ethanol (-20 °C) and centrifuged again for 15-30 min. After removal of the supernatant, RNA pellets were dried at room temperature (open tube lid, loosely covered with foil) for 10 min and dissolved in an appropriate volume of Milli-Q water. RNA concentration was accessed by UV absorbance measurement using the Nanodrop ND 2000 Spectrophotometer, and if necessary, samples were further diluted.

#### 5.2.1.2 Denaturing Polyacrylamide Gel Electrophoresis (PAGE)

For analysis and purification of RNA samples, 10 or 15 % denaturing polyacrylamide gels containing 8 M urea were prepared as follows: 75 mL of the respective 10 or 15 % PAGE pre-mixes were thoroughly mixed with 300 µL 10 % APS and 55 µL TEMED solution and casted between 20x20 or 20x30cm glass plates separated by 1 mm spacers. The size of the gel wells was chosen depending on the application. After polymerization, gels were pre-run in 1x TBE buffer for 20 min before RNA samples (mixed 1:1 with denaturing loading dye) were loaded. Visualization of the RNA bands was either performed by UV shadowing or gel staining using GelRed or SYBR<sup>®</sup>Gold nucleic acid gel staining solutions. Stained gels were scanned on the Typhoon 9400 device with the following scanning filters: GelRed (excitation: 532 nm, emission filter: 610 BP30), SYBR<sup>®</sup>Gold (excitation: 532 nm, emission filter: 526 SP). In case of fluoresceine- or Atto488-labeled oligonucleotides, an additional gel scan was performed prior to the staining, using the settings stated for the SYBR<sup>®</sup>Gold stained gels.

#### 5.2.1.3 Non-Denaturing Polyacrylamide Gel Electrophoresis (PAGE)

For evaluation of hybridization events, non-denaturing polyacrylamide gels were prepared as follows: for 20x20 cm gels, 75 mL 8, 10 or 15 % non-denaturing PAGE pre-mix were mixed thoroughly with 750 µL 10 % APS and 45 µL TEMED solution and casted between glass plates as described for denaturing gels. After polymerization and a 20 min pre-run in 1x TBE buffer, samples were loaded (1:1 mixed with non-denaturing loading dye). To prevent bleaching of the fluorescently labeled oligonucleotides, gels were protected from light during electrophoresis by covering with aluminium foil. After electrophoresis, gels were scanned (Typhoon 9400 device) once to detect the fluorescently labeled oligonucleotides (excitation: 532 nm, emission filter: 526 SP), stained using SYBR<sup>®</sup>Gold nucleic acid gel stain and subsequently scanned again using the same settings to visualize the unlabeled binding partners.

### 5.2.1.4 PAGE Gel Elution

For size separation of tRNA from total RNA and purification of both *in vitro* transcribed and isolated native (t)RNAs, RNA samples were mixed with one volume denaturing loading dye and loaded onto 10 % denaturing PAGE gels. After visualization by UV shadowing or staining (if necessary), gel bands corresponding to the target RNA were excised, mashed thoroughly and eluted in 0.5 M ammonium acetate overnight under shaking at room temperature. Samples were filtered through a Pall Nanosep centrifugal device and ethanol precipitated for clean-up.

### 5.2.1.5 RNA Preparation by *in vitro* Transcription

*In vitro* transcribed tRNA<sub>MAU</sub><sup>Met</sup> (*E. coli*) was prepared as follows: 500 fmol DNA-template MH373 (containing both a T7 RNA-polymerase promoter and a hammerhead ribozyme sequence) was amplified by PCR in presence of 1x reaction buffer, 3 mM MgCl<sub>2</sub>, 400 μM dNTP mix, each 2 μM of forward and reverse primer (MH53, MH374) and 0.05 U/μL Taq-polymerase (35 PCR cycles: denaturation: 2 min (cycle 1) or 30 s (cycle 2-35) at 90 °C, annealing: 30 s at 54 °C, elongation: 45 s (cycle 1-34) or 3 min (cycle 35) at 72 °C, final cooling to 4 °C). The obtained PCR product was then *in vitro* transcribed by in-house prepared T7 RNA-polymerase in 1x transcription buffer in presence of 5 mM NTPs, 5 mM DTT and 2.5 μg/mL BSA at 37 °C for 4 h. Successful *in vitro* transcription was indicated by the precipitation of pyrophosphate. *In vitro* transcripts were purified by 10 % denaturing PAGE and ethanol precipitation prior to downstream applications. The IVT of mascRNA was prepared accordingly, using MH766 as T7 template and MH767 as reverse primer for PCR.

### 5.2.1.6 RNA Preparation by Splint Ligation

The unmodified form of tRNA<sub>ICU</sub><sup>Arg</sup> was prepared by splinted ligation of the RNA oligonucleotides MH806 and MH807 (resembling the 5'- and 3'-fragments of the tRNA) using the complementary probe MH778 as DNA splint. The required 5'-phosphate of the 3'-fragment (2 nmol) was added by T4 Polynucleotide Kinase-mediated phosphorylation (0.75 U/μL) in presence of 5 mM ATP, 5 mM DTT and 1x KL buffer for 1 h at 37 °C. Subsequently, the phosphorylated oligonucleotide was pooled in 1x KL buffer with each 2 nmol the 5'-fragment and the DNA splint and supplemented with 5 mM ATP and 5 mM DTT. The solution was incubated at 75 °C for 4 min followed by a 15 min cool-down to room temperature before T4 DNA ligase (1.5 U/μL) and T4 RNA ligase 2 (82 ng/μL) were added. Adjacent ligation was performed at 16 °C overnight. To remove the DNA splint, the ligation mixture was supplemented with 1x DNase 1 buffer and incubated in presence of 3.33 U/μL DNase 1 for 2 h. The ligation product was purified from the crude reaction mixture by 10 % denaturing PAGE using UV shadowing for detection of the tRNA band. The respective band was eluted from gel (see 5.2.1.4) and further purified by ethanol precipitation.



### 5.2.1.7 Total RNA Extraction from HeLa and HEK Cells

For total RNA isolation, HeLa or HEK cells were cultured in D-MEM medium supplied with 10 % (v/v) FBS and 1 % (v/v) Pen/Strep in 175 cm<sup>2</sup> cell culture flasks and splitted every 48-72 h before harvesting. To harvest the cells, the medium was completely removed and cells were lysed in 17.5 mL TriReagent per flask by incubation for 5 min and detached from the flask surface using a cell scraper. Further steps were performed according to the manufacturer's manual [268]: The solution including the lysed cells was transferred to a 50 mL tube and 3.5 mL chloroform were added. After shaking the tube vigorously followed by 5 min incubation at room temperature, phase separation was achieved by centrifugation at 12,000g (4 °C, 15 min). The upper, aqueous phase containing the RNA was carefully transferred to a new tube, mixed with 8.75 mL isopropanol and incubated at room temperature for 10 min to precipitate the RNA. After centrifugation at 12,000 g (4° C, 10 min), the RNA pellet was washed in 17.5 mL 75 % ethanol and centrifuged again (7500g, 4 °C, 10 min). After drying the RNA pellet carefully at room temperature, it was dissolved in Milli-Q water and submitted to a second ethanol precipitation step to ensure high RNA purity.

### 5.2.1.8 Size Fractionation of HeLa and HEK total RNA

To separate total RNA into a small (<200 nt) and a large (>200 nt) fraction, two commercially available RNA purification kits were combined: The manufacturer's protocol for RNA size separation as well as the required buffers and solutions were taken from the RNA Clean & Concentrator kit (Zymo Research) while columns (due to the higher capacity for RNA) were used from the MEGAclean Transcription Clean-Up kit (Thermo-Fisher Scientific). For the size separation, sample batches of 200 µL total volume containing a maximum of 500 µg total RNA were prepared and mixed with 400 µL adjusted RNA binding buffer (RNA binding buffer diluted 1:1 with pure ethanol, Zymo Research). The mixture was passed through one of the columns (Thermo-Fisher Scientific) by centrifugation (12,000g, 30 s), saving the flow-through (containing the small RNA fraction). The flow-through was mixed with one volume pure ethanol (600 µL) and passed through a new column in two batches, discarding the flow-through. Subsequently, each of the two columns (first one containing the large fraction, second one the small RNA fraction) was rinsed consecutively with 400 µL RNA preparation buffer, 700 µL and 500 µL RNA wash buffer (Zymo Research). To ensure complete removal of the RNA wash buffer, the last centrifugation step (12,000g) was elongated from 30 s to 2 min. The flow-throughs were discarded and columns were transferred to fresh collection tubes. For elution, 50 µL MilliQ water were added to each column and subsequently heated up to 70 °C for 5 min, followed by centrifugation for 1 min (12,000g). The elution was repeated once to increase the yields. Sample purity and size fractionation were verified by denaturing PAGE and samples containing the same RNA size fractions were pooled and concentrated by ethanol precipitation.

### 5.2.1.9 Isolation of Specific RNA Molecules

Specific target RNA molecules were isolated from either total tRNA mixtures or total RNA by hybridization to complementary, 5'-biotin labeled DNA oligonucleotides and immobilization on streptavidin-coated magnetic beads for subsequent separation. For small batch isolations, 100 pmol of the respective complementary DNA oligonucleotide were hybridized to the appropriate amount of total (t)RNA (determined by MST measurements in case of tRNAs) in 5x SSC buffer (100  $\mu$ L total volume) by denaturing the sample at 90 °C for 3 min, followed by a 10 min incubation at 65 °C. Hybridized samples were cooled down to room temperature prior to the immobilization step. Streptavidin-coated, magnetic beads (Dynabeads® MyOne™ T1 or C1, 25  $\mu$ L of the stock solution per sample) were washed 3 times in 1x Binding and Washing buffer and once in 5x SSC buffer (volume equal to initial bead volume, 25  $\mu$ L) before the hybridized samples were added. Each washing and separation step consisted of adding the buffer, short vortexing at half speed for mixing, a brief spin-down and finally separation of the magnetic beads from the remaining solution by placing the tube onto a magnetic rack for 2 min. Immobilization of the biotinylated hybrid was performed by incubation at 25 °C under slight shaking (650 rpm). Subsequently, tubes were put onto the magnetic rack for separation of the supernatant containing non-target RNA. After removal of the supernatant, beads were washed once in 1x SSC buffer and additional 3 times in 0.1x SSC buffer (first step: 50  $\mu$ L, subsequent steps: 25  $\mu$ L) and subsequently resuspended in Milli-Q water (25  $\mu$ L). Elution of the target RNA was achieved by heating to 75 °C for 3 min and immediate removal of the RNA-containing supernatant. To remove any residual DNA oligonucleotide, 3  $\mu$ L of DNase I buffer (1x final concentration) and 2  $\mu$ L (1000 U) DNase I were added followed by incubation at 37 °C for 2 hours. Final clean-up of the sample was carried out by 10 % denaturing PAGE, elution of the target RNA gel band and ethanol precipitation. For larger batch isolations, the described protocol was scaled up as required. As the appropriate amount of the small RNA fraction of HeLa and HEK cells for the isolation of mascRNA could not be determined by MST due to its very low abundance, approximately 400  $\mu$ g HeLa respectively 240  $\mu$ g HEK small RNA were used for the hybridization to 100 pmol MH765 each. Additional changes to the standard protocol were omitting the PAGE purification step (due to the high probability that a band corresponding to mascRNA would not be visible due to its low amount) and instead directly performing an ethanol precipitation step in presence of 2  $\mu$ L RNA-grade glycogen.

### 5.2.1.10 RNA Hybridization

**RNA Titration Series for Non-Denaturing PAGE Analysis** To analyze the hybridization of target RNA and respective DNA probe, a constant amount of fluorescently labeled DNA probe (10 pmol) was hybridized in 1x PBS buffer to increasing amounts of target *in vitro* transcript (2-18 pmol, depending on the target RNA). Hybridization was achieved by heating the samples to 90 °C for 3 min followed by the actual hybridization at 65 °C for 10 min. Samples were cooled down to room temperature under light protection before mixing with an equal amount of non-denaturing loading dye and analysis by non-denaturing PAGE. The samples described

in figure 3.9 were prepared accordingly, using 10 pmol of the indicated DNA probe and 10 pmol of either native or unmodified tRNA<sub>1<sup>Arg</sup>ICU</sub>.

**RNA Titration Series for MST Measurements** Titration series for MST measurements, each consisting of 16 samples, were prepared by titration of a constant concentration of fluorophore-labeled DNA oligonucleotide (standard concentration for tRNA quantification 100 nM (20  $\mu$ L final volume), for polyA measurements 25-50 nM (10  $\mu$ L total volume)) against increasing amounts of either *in vitro* transcribed RNA (concentration range 0-0.2  $\mu$ M for tRNAs, 0-0.28  $\mu$ M for mRNAs), total tRNA (0-15  $\mu$ M) or total RNA (0-2  $\mu$ g/ $\mu$ L). Molar concentrations of total tRNA samples were calculated using UV absorbance measurements and the approximation of 1  $\mu$ g = 40 pmol tRNA. The exact concentration range for each titration series was determined individually for each sample. Hybridizations were performed in 1x PBS buffer (pH 7.4) by denaturing the samples at 90 °C for 3 min and subsequent incubation at 65 °C for 10 min. Before MST measurement, samples were cooled down to room temperature and stored at -20 °C if necessary. The hybridizations of MH784 (tRNA<sub>1<sup>Arg</sup>ICG</sub>) and MH819 (IVT MelanA/GFP mRNA) were carried out at pH 6.5 in 2x and 1x PBS, respectively. In case of the 10, 20 and 30 nt polyT DNA probes (MH824, MH820, MH825), hybridization temperature was decreased to 37 °C.

**Sample Preparation: Section 3.1.2.6 - Application 1** Total tRNA samples of *S. cerevisiae* (strain S288C) were received from the laboratory of Dr. S. Leidel in biological triplicates. Titration series using all 23 functional DNA oligonucleotides complementary to *S. cerevisiae* tRNA isoacceptors were prepared for each total tRNA sample using a constant DNA oligonucleotide concentration of 100 nM as described above. For MH784, hybridizations were carried out in 2x PBS (pH 6.5). RNA concentration ranges were optimized for each DNA oligonucleotide-target tRNA pair individually in order to receive well-shaped, sigmoidal binding curves with enough data points covering all areas of the curve. Titration series were analyzed using the standard settings described below, except for changing the MST power to 60 % for titration series of MH779, MH780, A676 and A682.

**Sample Preparation: Section 3.1.2.6 - Application 2 and 3** Total RNA samples of *S. cerevisiae* (WT strain BY4741) were received from the laboratory of Prof. Dr. R. Schaffrath, prepared by A. Ciftci. The obtained total RNA samples were run on 10 % polyacrylamide gels to extract the total tRNA pools. Titration series were prepared for the target tRNAs employing the extracted tRNA mixtures as described above and using the respective DNA probes. MST measurements were conducted as described below, using an elevated MST power of 60 % for MH779 and A676 titrations. All measurements were performed in technical triplicates by measuring the same titration series three times in a row. Accordingly, total RNA samples of *S. cerevisiae* BY4741 containing either an empty or an inducible PaT-vector (obtained from Akif Ciftci) were prepared for the analysis of tRNA<sub>3<sup>Gln</sup>UG</sub> and tRNA<sub>6<sup>His</sup>GUG</sub>.

**Sample Preparation: PolyA-Measurements** Titration series of 4 polyT DNA oligonucleotides (MH820, MH821, MH822, MH825) were prepared for three different mRNA *in vitro* transcripts (kindly provided by I. Hellmuth and Prof. Dr. K. Karikó) of variable polyA tail length (51, 64 and 101 nt, respectively) according to the standard conditions with the exception of the DNA probe concentration, which was decreased to 25-50 nM to decrease sample consumption. For the 64A mRNA (MelanA-GFP mRNA, kindly provided by I. Hellmuth), titration series were prepared in triplicates. Additionally, titration series of the 64A-*in vitro* transcript with MH824 (10 nt polyT probe) and MH819 (40 nt RNA oligonucleotide complementary to the 3'-UTR) were made using 1x PBS at pH 6.5 for MH819. Concentration ranges of the IVTs were optimized for each DNA probe-IVT pair individually. For polyA measurements in total RNA, titration series of total RNA (HeLa or *S. cerevisiae*) and MH820 or MH825 (20 or 30 nt polyT probes) were pipetted (0.4 ng/ $\mu$ L-4  $\mu$ g/ $\mu$ L). *S. cerevisiae* total RNA (wildtype,  $\Delta$ elp3 $\Delta$ deg1 and PaT-induced, received from Akif Ciftci) was purified using Illustra MicroSpin G-25 columns according to the manual prior to sample preparation. MST experiments were performed under the standard conditions using the following MST power settings: MST power 40 % (MH820, MH822), MST power 60 % (MH825), MST power 70 % (MH821) and MST power 80 % (MH819).

### 5.2.1.11 Microscale Thermophoresis-based RNA Quantification

**MST Measurements** All microscale thermophoresis measurements were performed on a Monolith<sup>TM</sup> NT.115 instrument (NanoTemper Technologies) using the Standard Treated Capillaries of the supplier. Each of the 16 solutions of one titration series was filled into a capillary, which were measured successively to create the respective 16 data points in the experiment. Following general settings were applied for all MST experiments accomplished: manual temperature control: 25 °C, LED laser: blue, fluorescence measurement before MST: 5 s, MST (IR laser) on: 45 s, fluorescence after MST: 15 s, delay: 25 s. LED and MST power settings were chosen individually for each sample by adjusting the LED power to yield fluorescence signals of at least 200 units (typically 40-80 %) and the MST power to achieve an appropriate thermophoretic response (standard setting 40 % MST power, for a few experiments 60-80 %).

**MST Data Analysis** MST measurements were analyzed using the NT analysis software (version 1.5.41) in the "thermophoresis" setting, excluding the T-jump. To keep the parameters equal for all experiments, cold and hot areas were defined as follow: cold (start: 5.8 s, length: 1.1 s) and cold (start: 48.03 s, length: 1.91 s). Normalized fluorescence ratios (hot/cold x1000,  $F_{Norm}$ ) were exported and plotted versus the  $\log_{10}$  of the respective concentration using the GraphPad Prism 7.00 software (for Windows, GraphPad software, La Jolla, California, USA, www.graphpad.com) for each titration experiment. Binding curves were obtained from the data points using a dose-response fit with variable slope (sigmoidal, 4-parameter logistic curve, X is  $\log(\text{concentration})$ ) available in the software employing following model ( $Y = \text{response}$ , Top, Bottom = plateaus of the curve (unit of Y),  $X = \log(\text{concentration})$ , Hillslope = steepness of the

curve,  $EC_{50}$  = concentration at half response between bottom and top(unit of X):

$$Y = \text{Bottom} + \frac{\text{Top-Bottom}}{1 + 10^{\text{Log}(EC_{50}-X) \times \text{Hillslope}}}$$

As fitting model, the “least squares (ordinary) fit” option was applied under default settings without constraint of parameters. The confidence level was set to 95 % and asymmetrical (likelihood) confidence intervals were calculated. The resulting  $EC_{50}$  values, indicating the RNA concentration at which 50 % of the DNA oligonucleotide is bound by hybridization was employed for the following calculations: (i) hybridization ratios in case of *in vitro* transcripts by comparing the RNA amount at 100 % binding to the total DNA oligonucleotide amount in the samples (equation 5.1), (ii) single tRNA abundance in % of total tRNA by dividing the total DNA probe amount (resembling the amount of the target RNA assuming 100 % binding) by the tRNA amount required for full hybridization (equation 5.2) and (iii) the number of polyT probes bound by 1  $\mu\text{g}$  of total RNA (polyT/ $\mu\text{g}$ , equation 5.3).  $c_{\text{probe}}$  probe concentration,  $vol$  sample volume,  $n_{\text{probe}/\text{RNA}}$  mol probe/RNA in sample [pmol],  $m_{\text{total RNA}}$  amount total RNA in sample [ $\mu\text{g}$ ],  $N_{\text{polyT probe}}$  number of probe molecules,  $N_A$  Avogadro constant ( $6.022 \times 10^{23} \text{ mol}^{-1}$ ).

$$\text{Probe:RNA} = \frac{c_{\text{probe}} \times vol}{EC_{50} \times 2 \times vol} = \frac{n_{\text{probe}}}{n_{\text{RNA}}} \quad (5.1)$$

$$\% \text{ target tRNA} = \frac{c_{\text{probe}} \times vol}{EC_{50} \times 2 \times vol} \times 100 = \frac{n_{\text{probe}}}{n_{\text{total tRNA}}} \times 100 = \frac{n_{\text{target}}}{n_{\text{total tRNA}}} \times 100 \quad (5.2)$$

$$\frac{\text{polyT}}{\mu\text{g}} = \frac{c_{\text{polyT probe}} \times vol \times N_A}{EC_{50} \times 2 \times vol} = \frac{n_{\text{polyT probe}} \times N_A}{m_{\text{total RNA}}} = \frac{N_{\text{polyT probe}}}{m_{\text{total RNA}}} \quad (5.3)$$

## 5.2.2 Liquid Chromatography-Tandem Mass Spectrometry (LC-MS/MS)

Procedures and methods required for LC-MS/MS analysis were mainly adapted from [223] and are described in detail in [172].

### 5.2.2.1 RNA Sample Preparation

If required, RNA samples were purified by ethanol precipitation and dissolved in Milli-Q water. To digest up to 10  $\mu\text{g}$  of RNA to the nucleoside level, the following protocol was used [223] (adapted from [171]): The sample was mixed with  $\frac{1}{10}$  volume of 10x nuclease P1 buffer (pH 5.0) and subsequently 0.3 U nuclease P1 (NP1) as well as 0.1 U snake venom phosphodiesterase (SPD) were added followed by a 2 h incubation at 37 °C. Thereafter,  $\frac{1}{10}$  volume 10x FastAP buffer and

1 U FastAP thermosensitive alkaline phosphatase were mixed in and incubated for 1 h at 37 °C. Digested samples were diluted as required and stored at -20 °C if not directly submitted to LC-MS/MS analysis. The calibration series of  $mcm^5U$  and  $mcm^5s^2U$  were prepared by diluting 10 mM stocks of the nucleoside standards to concentrations of 1 nM, 10 nM, 100 nM and 1  $\mu$ M. Injection volumes were 10  $\mu$ L for the 1 nM solution, 2, 5 and 10  $\mu$ L for the 10 and 100 nM solutions and 2  $\mu$ L for the 1  $\mu$ M solution.

### 5.2.2.2 High Performance-Liquid Chromatography

Chromatographic separation of the nucleosides was performed using a polar-embedded reverse phase (RP18) HPLC column (Synergi Fusion RP, 4  $\mu$ m, 80 Å, 250 x 0.2 mm) at 35 °C column temperature on an Agilent 1260 HPLC system additionally equipped with a diode array detector (DAD) for UV detection. The solvents used for the separation consisted of a 5 mM ammonium acetate buffer (pH 5.3, solvent A) and pure acetonitrile (solvent B). The following gradients were used for either DMRM mode, product and pseudo-MS<sup>3</sup> scans (gradient 1, table 5.4) or NLS (gradient 2, table 5.5):

**Table 5.4: Gradient 1 for LC-MS/MS analysis** Gradient 1 used for RNA modification analysis in the DMRM mode as well as for product ion and pseudo-MS<sup>3</sup> scans. Solvent A represented a 5 mM ammonium acetate buffer (pH 5.3) and solvent B pure acetonitrile.

Time [min]	Solvent A [%]	Solvent B [%]
0	100	0
10	92	8
20	60	40
23	100	0
30	100	0

**Table 5.5: Gradient 2 for LC-MS/MS analysis** Gradient 2 used for RNA modification analysis in the NLS mode. Solvent A consisted of a 5 mM ammonium acetate buffer (pH 5.3) and solvent B of pure acetonitrile.

Time [min]	Solvent A [%]	Solvent B [%]
0	100	0
20	90	10
30	75	25
40	20	80
43	100	0
54	100	0

Before entering the mass spectrometer for mass analysis, the UV absorbance of the column eluate at 254 nm was determined using the diode array detector and recorded in a UV chromatogram. UV detection was applied for the high abundant main nucleosides to avoid saturation effects and to preserve the electromultiplier.

### 5.2.2.3 Mass Spectrometry

MS/MS analysis was performed on an Agilent 6460 triple quadrupole mass spectrometer (QQQ) equipped with an Agilent Jetstream ion source which enables efficient electrospray ionization of the nucleosides. As nebulizing and collision gas, high-purity nitrogen generated by a separate nitrogen generator was used. The mass spectrometer was run in the positive ionization mode for all described scan modes and instrument controlling was performed by using the Agilent MassHunter Data Acquisition Software.

**General instrument settings** Following general settings of the mass spectrometer were applied for all scan types described (table 5.6):

**Table 5.6: General settings of the mass spectrometer** Instrument parameter settings applied for all types of LC-MS/MS analysis. Pure nitrogen was used as nebulizing/ sheath gas.

Instrument parameter	Setting
gas temperature	350 °C
gas flow	8 L/min
nebulizer pressure	50 psi
sheath gas temperature	350 °C
sheath gas flow	12 L/min
capillary voltage	3000 V

**DMRM method: Wobble U Modifications and Queuosine** Settings of the parameters fragmentor voltage and collision energy as well as precursor and product ion  $m/z$  values and retention times were adjusted individually for each nucleoside of interest. Retention time windows allowed in the DMRM mode were set to 2-3 minutes depending on close eluting non-target nucleosides. The cell accelerator voltage was 2 V for all of the investigated nucleosides. If applicable, retention times were checked prior to each analysis using synthetic standards or digested total tRNA mixtures, as retention times might shift over time due to column aging. The following instrument settings (table 5.7) were applied for the analysis of the wobble U34 modifications (section 3.3.1) and queuosine (section 3.3.3):

**NLS** For the neutral loss scan of the isolated tRNAs (section 3.3.2), the method described in detail in [173] was applied. The scan included the neutral losses of 132 (ribose), 146 (2'-O-methyl-ribose) and 36 (loss of two water molecules for pseudouridine detection) and was divided into several time segments in order to exclude the main nucleosides from analysis (due to their high abundance the resulting peaks would prevent the detection of the much smaller peaks of coeluting modifications). The  $m/z$  range scanned in quadrupole 1 was 230-600, in segments in which a main nucleoside eluted the respective precursor  $m/z$  (and the  $m/z + 1$ ) was excluded. The eluates of the first 2 and last 9 min of the chromatographic run were sent to the waste compartment and thus not included in the mass analysis. Fragmentor voltage was

**Table 5.7: MS/MS parameters: modified uridines and queuosine** Applied MS/MS parameters for the detection of the modified U34 nucleosides and queuosine in the DMRM mode. Retention times varied slightly depending on column age.

nucleoside	precursor m/z	product m/z	fragmentor voltage [V]	collision energy [eV]	retention time [min]
ncm <sup>5</sup> U	302	170	66	5	6.0
s <sup>2</sup> U	261	129	66	5	11.3
mcm <sup>5</sup> U	317	185	66	5	12.7
mcm <sup>5</sup> s <sup>2</sup> U	333	201	66	5	16.3
Q	410	295	80	10	10.4

80 V for all transitions scanned, and the collision energy employed was either 15 eV (standard fragmentation) or 10 eV (pseudouridine), respectively. Cell accelerator voltage was set to the standard value of 2 V.

**Product Ion Scan of Queuosine** The determination of the fragmentation pattern of queuosine was achieved by performing a product ion scan, in which a defined precursor m/z (protonated nucleoside) passed quadrupole 1, and all fragments generated in the collision cell were detected in quadrupole 2. Below the parameters used for the analysis of queuosine are listed (table 5.8), for the cell accelerator voltage the standard setting of 2 V was applied.

**Table 5.8: MS/MS parameters: Product ion scan of queuosine** MS/MS instrument parameters applied for the product ion scan of queuosine.

nucleoside	precursor m/z	MS2 range [m/z]	scanning time [ms]	fragmentor voltage [V]	collision energy [eV]
Q	410	100-1000	500	80	10

**Pseudo-MS<sup>3</sup> Scan of (Labeled) Nucleobases** To investigate the fragmentation pattern of the nucleobases (instead of the nucleosides), pseudo-MS<sup>3</sup> scans were performed, which basically represent product ion scans of the nucleobases, which were generated during in-source fragmentation. In-source fragmentation was achieved by increasing the fragmentor voltage (to 150-200 V), fragmentation of the nucleobase in the collision cell required the increase of the collision energy (to 25-20 eV). Table 5.9 summarizes the MS/MS parameters applied for the fragmentation of the four main nucleobases (labeled with <sup>13</sup>C and <sup>15</sup>N as described in section 3.3.4) in the product ion scan mode using a cell accelerator voltage of 2 V.

#### 5.2.2.4 Data analysis

Acquired LC-MS/MS data was analyzed employing the Agilent MassHunter Qualitative Analysis Software (version B.05.00). A detailed description of the individual steps required for



**Table 5.9: MS/MS parameters: pseudo-MS<sup>3</sup> scan of labeled nucleobases** MS/MS instrument parameters applied for the pseudo-MS<sup>3</sup> scan of the labeled nucleobases in the product ion scan mode.

nucleoside	precursor m/z	MS2 range [m/z]	scanning time [ms]	fragmentor voltage [V]	collision energy [eV]
G	158	20-158	500	200	30
A	142	20-142	500	200	30
C	116	20-116	500	200	30
U	116	20-116	500	150	25

qualitative and especially quantitative analysis of the data is found in [172]. Analysis of the recorded UV data was performed by extracting the UV chromatogram, assigning the peaks of the four main nucleosides (elution order: cytidine, uridine, guanosine and adenosine, valid for both gradients applied), and, if required, integrating the peaks to receive the respective peak areas. Analysis of the MS/MS data was performed as follows for the different scan types applied:

- 1. DMRM mode** Chromatograms of the single compounds analyzed were extracted using the “find compounds” function in the software and peaks were inspected for errors in the automatically performed peak recognition. Obtained peak areas were normalized to the UV peak area of one main nucleoside to counterbalance differences in the injected RNA amount when comparing different samples. In case of the wobble U34 modifications, U was chosen for normalization, and for queuosine the UV peak of G was used. For relative quantification of modification contents in sample sets, the fold-change of the normalized peak areas compared to the control sample (*e.g.* the wildtype) was calculated (compare figure 3.34 e). Alternatively, the normalized peak areas were directly compared to each other (see figure 3.38 b).
- 2. NLS mode** Each peak in the total ion current (TIC) was inspected individually by extracting the mass spectrum displaying the precursor ion losing either a ribose or a 2'-O-methyl-ribose moiety. For very small, hardly detectable peaks, the precursor ion was verified by extracting the “extracted ion chromatogram” (EIC) for the respective m/z value, which enables an inspection of peaks corresponding to the specific m/z values by excluding all other m/z values from the chromatogram. By the so accomplished exclusion of high abundant peaks smaller peaks could be examined more thoroughly (compare figure 3.36). For all peaks detected, m/z values of the precursor ion were extracted and aligned to possible modified nucleosides using the MODOMICs database [79] as well as the tRNAdb 2009 [80].
- 3. Product ion scan** The total ion current chromatograms received from the product ion scans contained all peaks corresponding to one or more predefined precursor ions, which were manually examined. For each peak detected, the respective mass spectrum displaying the generated product ions was extracted and evaluated regarding the fragmentation pattern.

A typical fragmentation at the glycosidic bond showed a fragment ion with a by 132 or 146 decreased  $m/z$  value (resembling a ribose or 2'-O-methylribose moiety) compared to the precursor ion. The untypical fragmentation positions of queuosine were assigned with the help of information kindly provided by Prof. Dr. Patrick Limbach (Biological Mass Spectrometry, Department of Chemistry, University of Cincinnati, USA).

- 4. Pseudo-MS<sup>3</sup> scan** In principle, pseudo-MS<sup>3</sup> scans were analyzed as described for the product ion scans, with the precursor ion being the nucleobase and the mass spectrum extracted illustrating all fragments generated by fragmentation of the nucleobase. As the resulting mass spectra were considerably more complex than for the fragmentation of the nucleosides, peak assignments to the respective fragment structures were performed by comparing to cleavage pathways described in literature [262–266]. For the labeled nucleosides described in section 3.3.4, peaks were allocated under consideration of the number of labeled atoms in the nucleobase.

## List of Publications

Kellner, S., Ochel, A., Thüring, K., Spenkuch, F., Neumann, J., Sharma, S., Entian, K.-D., Schneider, D. & Helm, M. Absolute and relative quantification of RNA modifications via biosynthetic isotopomers. *Nucleic acids research* 42, e142 (2014).

Abdel-Fattah, W., Jablonowski, D., Di Santo, R., Thüring, K. L., Scheidt, V., Hammermeister, A., Ten Have, S., Helm, M., Schaffrath, R. & Stark, M. J. Phosphorylation of Elp1 by Hrr25 is required for elongator-dependent tRNA modification in yeast. *PLoS Genet* 11, e1004931 (2015).

Klassen, R., Grunewald, P., Thüring, K. L., Eichler, C., Helm, M. & Schaffrath, R. Loss of anticodon wobble uridine modifications affects tRNA Lys function and protein levels in *Saccharomyces cerevisiae*. *PloS one* 10, e0119261 (2015).

Jüdes, A., Ebert, F., Bär, C., Thüring, K. L., Harrer, A., Klassen, R., Helm, M., Stark, M. J. & Schaffrath, R. Urmylation and tRNA thiolation functions of ubiquitin-like Uba4-Urm1 systems are conserved from yeast to man. *FEBS letters* 589, 904–909 (2015).

Schmid, K., Thüring, K., Keller, P., Ochel, A., Kellner, S. & Helm, M. Variable presence of 5-methylcytosine in commercial RNA and DNA. *RNA Biology* 12, 1152-8 (2015).

Hauenschild, R., Tserovski, L., Schmid, K., Thüring, K., Winz, M.-L., Sharma, S., Entian, K.-D., Wacheul, L., Lafontaine, D. L., Anderson, J., Alfonzo, J., Hildebrandt, A., Jäschke, A., Motorin, Y. & Helm, M. The reverse transcription signature of N-1-methyladenosine in RNA-Seq is sequence dependent. *Nucleic acids research* 43, 9950–9964 (2015).

Müller, M., Hartmann, M., Schuster, I., Bender, S., Thüring, K. L., Helm, M., Katze, J. R., Nellen, W., Lyko, F. & Ehrenhofer-Murray, A. E. Dynamic modulation of Dnmt2-dependent tRNA methylation by the micronutrient queuine. *Nucleic acids research* 43, 10952–10962 (2015).

Thüring, K., Schmid, K., Keller, P. & Helm, M. Analysis of RNA modifications by liquid chromatography–tandem mass spectrometry. *Methods* 107, 48-56 (2016).



## Bibliography

1. Hoagland, M. B., Stephenson, M. L., Scott, J. F., Hecht, L. I. & Zamecnik, P. C. A soluble ribonucleic acid intermediate in protein synthesis. *J Biol Chem* **231**, 241–257 (1958).
2. RajBhandary, U. L. & Köhrer, C. Early days of tRNA research: discovery, function, purification and sequence analysis. *Journal of biosciences* **31**, 439–451 (2006).
3. Phizicky, E. M. & Hopper, A. K. tRNA biology charges to the front. *Genes & development* **24**, 1832–1860 (2010).
4. Hopper, A. K. Transfer RNA post-transcriptional processing, turnover, and subcellular dynamics in the yeast *Saccharomyces cerevisiae*. *Genetics* **194**, 43–67 (2013).
5. Shi, H. & Moore, P. B. The crystal structure of yeast phenylalanine tRNA at 1.93 Å resolution: classic structure revisited. *RNA* **6**, 1091–1105 (2000).
6. El Yacoubi, B., Bailly, M. & de Crécy-Lagard, V. Biosynthesis and function of posttranscriptional modifications of transfer RNAs. *Annual review of genetics* **46**, 69–95 (2012).
7. Jackman, J. E. & Alfonzo, J. D. Transfer RNA modifications: nature's combinatorial chemistry playground. *Wiley Interdisciplinary Reviews: RNA* **4**, 35–48 (2013).
8. Helm, M. & Alfonzo, J. D. Posttranscriptional RNA modifications: playing metabolic games in a cell's chemical Legoland. *Chemistry & biology* **21**, 174–185 (2014).
9. Ibba, M. & Söll, D. Aminoacyl-tRNA synthesis. *Annual review of biochemistry* **69**, 617–650 (2000).
10. Jakubowski, H. Quality control in tRNA charging. *Wiley Interdisciplinary Reviews: RNA* **3**, 295–310 (2012).
11. Crick, F. H. Codon—anticodon pairing: the wobble hypothesis. *Journal of molecular biology* **19**, 548–555 (1966).
12. Geslain, R. & Pan, T. Functional analysis of human tRNA isodecoders. *Journal of molecular biology* **396**, 821–831 (2010).
13. Kirchner, S. & Ignatova, Z. Emerging roles of tRNA in adaptive translation, signalling dynamics and disease. *Nature Reviews Genetics* **16**, 98–112 (2015).
14. Ikemura, T. Correlation between the abundance of yeast transfer RNAs and the occurrence of the respective codons in protein genes: differences in synonymous codon choice patterns of yeast and *Escherichia coli* with reference to the abundance of isoaccepting transfer RNAs. *Journal of molecular biology* **158**, 573–597 (1982).
15. Dong, H., Nilsson, L. & Kurland, C. G. Co-variation of tRNA abundance and codon usage in *Escherichia coli* at different growth rates. *Journal of molecular biology* **260**, 649–663 (1996).

16. Puri, P., Wetzel, C., Saffert, P., Gaston, K. W., Russell, S. P., Cordero Varela, J. A., Vlies, P., Zhang, G., Limbach, P. A., Ignatova, Z., *et al.* Systematic identification of tRNAome and its dynamics in *Lactococcus lactis*. *Molecular microbiology* **93**, 944–956 (2014).
17. Dittmar, K. A., Goodenbour, J. M. & Pan, T. Tissue-specific differences in human transfer RNA expression. *PLoS Genet* **2**, e221 (2006).
18. Gingold, H., Tehler, D., Christoffersen, N. R., Nielsen, M. M., Asmar, F., Kooistra, S. M., Christophersen, N. S., Christensen, L. L., Borre, M., Sørensen, K. D., *et al.* A dual program for translation regulation in cellular proliferation and differentiation. *Cell* **158**, 1281–1292 (2014).
19. Plotkin, J. B., Robins, H. & Levine, A. J. Tissue-specific codon usage and the expression of human genes. *Proceedings of the National Academy of Sciences of the United States of America* **101**, 12588–12591 (2004).
20. Gingold, H., Dahan, O. & Pilpel, Y. Dynamic changes in translational efficiency are deduced from codon usage of the transcriptome. *Nucleic acids research*, gks772 (2012).
21. Deng, W., Babu, I. R., Su, D., Yin, S., Begley, T. J. & Dedon, P. C. Trm9-catalyzed tRNA modifications regulate global protein expression by codon-biased translation. *PLoS Genet* **11**, e1005706 (2015).
22. Dedon, P. C. & Begley, T. J. A system of RNA modifications and biased codon use controls cellular stress response at the level of translation. *Chemical research in toxicology* **27**, 330–337 (2014).
23. Chan, C. T., Pang, Y. L. J., Deng, W., Babu, I. R., Dyavaiah, M., Begley, T. J. & Dedon, P. C. Reprogramming of tRNA modifications controls the oxidative stress response by codon-biased translation of proteins. *Nature communications* **3**, 937 (2012).
24. Gu, C., Begley, T. J. & Dedon, P. C. tRNA modifications regulate translation during cellular stress. *FEBS letters* **588**, 4287–4296 (2014).
25. Endres, L., Dedon, P. C. & Begley, T. J. Codon-biased translation can be regulated by wobble-base tRNA modification systems during cellular stress responses. *RNA biology* **12**, 603–614 (2015).
26. Varenne, S., Buc, J., Lloubes, R. & Lazdunski, C. Translation is a non-uniform process: effect of tRNA availability on the rate of elongation of nascent polypeptide chains. *Journal of molecular biology* **180**, 549–576 (1984).
27. Qian, W., Yang, J.-R., Pearson, N. M., Maclean, C. & Zhang, J. Balanced codon usage optimizes eukaryotic translational efficiency. *PLoS Genet* **8**, e1002603 (2012).
28. Nedialkova, D. D. & Leidel, S. A. Optimization of codon translation rates via tRNA modifications maintains proteome integrity. *Cell* **161**, 1606–1618 (2015).
29. Elf, J., Nilsson, D., Tenson, T. & Ehrenberg, M. Selective charging of tRNA isoacceptors explains patterns of codon usage. *Science* **300**, 1718–1722 (2003).

30. Novoa, E. M. & de Poupiana, L. R. Speeding with control: codon usage, tRNAs, and ribosomes. *Trends in Genetics* **28**, 574–581 (2012).
31. Wilusz, J. E. Controlling translation via modulation of tRNA levels. *Wiley Interdisciplinary Reviews: RNA* **6**, 453–470 (2015).
32. Zhang, G., Hubalewska, M. & Ignatova, Z. Transient ribosomal attenuation coordinates protein synthesis and co-translational folding. *Nature structural & molecular biology* **16**, 274–280 (2009).
33. Fedyunin, I., Lehnhardt, L., Böhmer, N., Kaufmann, P., Zhang, G. & Ignatova, Z. tRNA concentration fine tunes protein solubility. *FEBS letters* **586**, 3336–3340 (2012).
34. Ikemura, T. Codon usage and tRNA content in unicellular and multicellular organisms. *Molecular biology and evolution* **2**, 13–34 (1985).
35. Novoa, E. M., Pavon-Eternod, M., Pan, T. & de Poupiana, L. R. A role for tRNA modifications in genome structure and codon usage. *Cell* **149**, 202–213 (2012).
36. Schmitt, B. M., Rudolph, K. L., Karagianni, P., Fonseca, N. A., White, R. J., Talianidis, I., Odom, D. T., Marioni, J. C. & Kutter, C. High-resolution mapping of transcriptional dynamics across tissue development reveals a stable mRNA–tRNA interface. *Genome research* **24**, 1797–1807 (2014).
37. Huang, H.-Y. & Hopper, A. K. Multiple Layers of Stress-Induced Regulation in tRNA Biology. *Life* **6**, 16 (2016).
38. De Nadal, E., Ammerer, G. & Posas, F. Controlling gene expression in response to stress. *Nature Reviews Genetics* **12**, 833–845 (2011).
39. Roberts, D. N., Stewart, A. J., Huff, J. T. & Cairns, B. R. The RNA polymerase III transcriptome revealed by genome-wide localization and activity–occupancy relationships. *Proceedings of the National Academy of Sciences* **100**, 14695–14700 (2003).
40. Kutter, C., Brown, G. D., Gonçalves, Â., Wilson, M. D., Watt, S., Brazma, A., White, R. J. & Odom, D. T. Pol III binding in six mammals shows conservation among amino acid isotypes despite divergence among tRNA genes. *Nature genetics* **43**, 948–955 (2011).
41. Moir, R. D. & Willis, I. M. Regulation of pol III transcription by nutrient and stress signaling pathways. *Biochimica et Biophysica Acta (BBA)-Gene Regulatory Mechanisms* **1829**, 361–375 (2013).
42. Upadhyaya, R., Lee, J. & Willis, I. M. Maf1 is an essential mediator of diverse signals that repress RNA polymerase III transcription. *Molecular cell* **10**, 1489–1494 (2002).
43. Shaheen, H. H. & Hopper, A. K. Retrograde movement of tRNAs from the cytoplasm to the nucleus in *Saccharomyces cerevisiae*. *Proceedings of the National Academy of Sciences of the United States of America* **102**, 11290–11295 (2005).
44. Whitney, M. L., Hurto, R. L., Shaheen, H. H. & Hopper, A. K. Rapid and reversible nuclear accumulation of cytoplasmic tRNA in response to nutrient availability. *Molecular biology of the cell* **18**, 2678–2686 (2007).

45. Czech, A., Wende, S., Mörl, M., Pan, T. & Ignatova, Z. Reversible and rapid transfer-RNA deactivation as a mechanism of translational repression in stress. *PLoS Genet* **9**, e1003767 (2013).
46. Yamasaki, S., Ivanov, P., Hu, G.-f. & Anderson, P. Angiogenin cleaves tRNA and promotes stress-induced translational repression. *The Journal of cell biology* **185**, 35–42 (2009).
47. Netzer, N., Goodenbour, J. M., David, A., Dittmar, K. A., Jones, R. B., Schneider, J. R., Boone, D., Eves, E. M., Rosner, M. R., Gibbs, J. S., *et al.* Innate immune and chemically triggered oxidative stress modifies translational fidelity. *Nature* **462**, 522–526 (2009).
48. Alexandrov, A., Chernyakov, I., Gu, W., Hiley, S. L., Hughes, T. R., Grayhack, E. J. & Phizicky, E. M. Rapid tRNA decay can result from lack of nonessential modifications. *Molecular cell* **21**, 87–96 (2006).
49. Kotelawala, L., Grayhack, E. J. & Phizicky, E. M. Identification of yeast tRNA<sup>Um44</sup> 2'-O-methyltransferase (Trm44) and demonstration of a Trm44 role in sustaining levels of specific tRNA<sup>Ser</sup> species. *RNA* **14**, 158–169 (2008).
50. Whipple, J. M., Lane, E. A., Chernyakov, I., D'Silva, S. & Phizicky, E. M. The yeast rapid tRNA decay pathway primarily monitors the structural integrity of the acceptor and T-stems of mature tRNA. *Genes & Development* **25**, 1173–1184 (2011).
51. Guy, M. P., Young, D. L., Payea, M. J., Zhang, X., Kon, Y., Dean, K. M., Grayhack, E. J., Mathews, D. H., Fields, S. & Phizicky, E. M. Identification of the determinants of tRNA function and susceptibility to rapid tRNA decay by high-throughput in vivo analysis. *Genes & development* **28**, 1721–1732 (2014).
52. Kadaba, S., Krueger, A., Trice, T., Krecic, A. M., Hinnebusch, A. G. & Anderson, J. Nuclear surveillance and degradation of hypomodified initiator tRNA<sup>Met</sup> in *S. cerevisiae*. *Genes & development* **18**, 1227–1240 (2004).
53. Kadaba, S., Wang, X. & Anderson, J. T. Nuclear RNA surveillance in *Saccharomyces cerevisiae*: Trf4p-dependent polyadenylation of nascent hypomethylated tRNA and an aberrant form of 5S rRNA. *Rna* **12**, 508–521 (2006).
54. Wilusz, J. E., Whipple, J. M., Phizicky, E. M. & Sharp, P. A. tRNAs marked with CCACCA are targeted for degradation. *Science* **334**, 817–821 (2011).
55. Phizicky, E. M. & Alfonzo, J. D. Do all modifications benefit all tRNAs? *FEBS letters* **584**, 265–271 (2010).
56. Chan, C. T., Dyavaiah, M., DeMott, M. S., Taghizadeh, K., Dedon, P. C. & Begley, T. J. A quantitative systems approach reveals dynamic control of tRNA modifications during cellular stress. *PLoS Genet* **6**, e1001247 (2010).
57. Alings, F., Sarin, L. P., Fufezan, C., Drexler, H. C. & Leidel, S. A. An evolutionary approach uncovers a diverse response of tRNA 2-thiolation to elevated temperatures in yeast. *RNA* **21**, 202–212 (2015).



58. Damon, J. R., Pincus, D. & Ploegh, H. L. tRNA thiolation links translation to stress responses in *Saccharomyces cerevisiae*. *Molecular biology of the cell* **26**, 270–282 (2015).
59. Kuhn, C.-D., Wilusz, J. E., Zheng, Y., Beal, P. A. & Joshua-Tor, L. On-enzyme refolding permits small RNA and tRNA surveillance by the CCA-adding enzyme. *Cell* **160**, 644–658 (2015).
60. Goodarzi, H., Nguyen, H. C., Zhang, S., Dill, B. D., Molina, H. & Tavazoie, S. F. Modulated Expression of Specific tRNAs Drives Gene Expression and Cancer Progression. *Cell* **165**, 1416–1427 (2016).
61. Winter, A. G., Sourvinos, G., Allison, S. J., Tosh, K., Scott, P. H., Spandidos, D. A. & White, R. J. RNA polymerase III transcription factor TFIIC2 is overexpressed in ovarian tumors. *Proceedings of the National Academy of Sciences* **97**, 12619–12624 (2000).
62. Gomez-Roman, N., Grandori, C., Eisenman, R. N. & White, R. J. Direct activation of RNA polymerase III transcription by c-Myc. *Nature* **421**, 290–294 (2003).
63. Chen, W., Heierhorst, J., Brosius, J. & Tiedge, H. Expression of neural BC1 RNA: induction in murine tumours. *European Journal of Cancer* **33**, 288–292 (1997).
64. Marshall, L. & White, R. J. Non-coding RNA production by RNA polymerase III is implicated in cancer. *Nature Reviews Cancer* **8**, 911–914 (2008).
65. Pavon-Eternod, M., Gomes, S., Geslain, R., Dai, Q., Rosner, M. R. & Pan, T. tRNA overexpression in breast cancer and functional consequences. *Nucleic acids research* **37**, 7268–7280 (2009).
66. Pavon-Eternod, M., Gomes, S., Rosner, M. R. & Pan, T. Overexpression of initiator methionine tRNA leads to global reprogramming of tRNA expression and increased proliferation in human epithelial cells. *RNA* **19**, 461–466 (2013).
67. Clarke, C. J., Berg, T. J., Birch, J., Ennis, D., Mitchell, L., Cloix, C., Campbell, A., Sumpton, D., Nixon, C., Campbell, K., *et al.* The initiator methionine tRNA drives secretion of type II collagen from stromal fibroblasts to promote tumor growth and angiogenesis. *Current Biology* **26**, 755–765 (2016).
68. Birch, J., Clarke, C. J., Campbell, A. D., Campbell, K., Mitchell, L., Liko, D., Kalna, G., Strathdee, D., Sansom, O. J., Neilson, M., *et al.* The initiator methionine tRNA drives cell migration and invasion leading to increased metastatic potential in melanoma. *Biology Open*, bio-019075 (2016).
69. Zhou, Y., Goodenbour, J. M., Godley, L. A., Wickrema, A. & Pan, T. High levels of tRNA abundance and alteration of tRNA charging by bortezomib in multiple myeloma. *Biochemical and biophysical research communications* **385**, 160–164 (2009).
70. Florentz, C., Sohm, B., Tryoen-Tóth, P., P<sup>´</sup>utz, J. & Sissler, M. Human mitochondrial tRNAs in health and disease. *Cellular and Molecular Life Sciences* **60**, 1356–1375 (2003).
71. Wittenhagen, L. M. & Kelley, S. O. Impact of disease-related mitochondrial mutations on tRNA structure and function. *Trends in biochemical sciences* **28**, 605–611 (2003).

72. Levinger, L., Mörl, M. & Florentz, C. Mitochondrial tRNA 3' end metabolism and human disease. *Nucleic acids research* **32**, 5430–5441 (2004).
73. Abbott, J. A., Francklyn, C. S. & Robey-Bond, S. M. Transfer RNA and human disease. *Front. Genet.* **5** (2014).
74. Smits, P., Mattijssen, S., Morava, E., van den Brand, M., van den Brandt, F., Wijburg, F., Pruijn, G., Smeitink, J., Nijtmans, L., Rodenburg, R., *et al.* Functional consequences of mitochondrial tRNA<sup>Trp</sup> and tRNA<sup>Arg</sup> mutations causing combined OXPHOS defects. *European Journal of Human Genetics* **18**, 324–329 (2010).
75. Giordano, C., Perli, E., Orlandi, M., Pisano, A., Tuppen, H. A., He, L., Ierinò, R., Petruzzello, L., Terzi, A., Autore, C., *et al.* Cardiomyopathies due to homoplasmic mitochondrial tRNA mutations: morphologic and molecular features. *Human pathology* **44**, 1262–1270 (2013).
76. Wang, S., Li, R., Fettermann, A., Li, Z., Qian, Y., Liu, Y., Wang, X., Zhou, A., Mo, J. Q., Yang, L., *et al.* Maternally inherited essential hypertension is associated with the novel 4263A>G mutation in the mitochondrial tRNA<sup>Ile</sup> gene in a large Han Chinese family. *Circulation research* **108**, 862–870 (2011).
77. Liu, Y., Li, R., Li, Z., Wang, X.-J., Yang, L., Wang, S. & Guan, M.-X. Mitochondrial transfer RNAMet 4435A>G mutation is associated with maternally inherited hypertension in a Chinese pedigree. *Hypertension* **53**, 1083–1090 (2009).
78. McFarland, R., Clark, K. M., Morris, A. A., Taylor, R. W., Macphail, S., Lightowlers, R. N. & Turnbull, D. M. Multiple neonatal deaths due to a homoplasmic mitochondrial DNA mutation. *Nature genetics* **30**, 145–146 (2002).
79. Machnicka, M. A., Milanowska, K., Oglou, O. O., Purta, E., Kurkowska, M., Olchowik, A., Januszewski, W., Kalinowski, S., Dunin-Horkawicz, S., Rother, K. M., Helm, M., Bujnicki, J. M. & Grosjean, H. MODOMICS: a database of RNA modification pathways—2012 update. *Nucleic acids research*, gks1007 (2012).
80. Jühling, F., Mörl, M., Hartmann, R. K., Sprinzl, M., Stadler, P. F. & Pütz, J. tRNAdb 2009: compilation of tRNA sequences and tRNA genes. *Nucleic acids research* **37**, D159–D162 (2009).
81. Carell, T., Brandmayr, C., Hienzsch, A., M'uller, M., Pearson, D., Reiter, V., Thoma, I., Thumbs, P. & Wagner, M. Structure and Function of Noncanonical Nucleobases. *Angewandte Chemie International Edition* **51**, 7110–7131 (2012).
82. Motorin, Y. & Helm, M. tRNA stabilization by modified nucleotides. *Biochemistry* **49**, 4934–4944 (2010).
83. Helm, M., Giegé, R. & Florentz, C. A Watson-Crick base-pair-disrupting methyl group (m1A9) is sufficient for cloverleaf folding of human mitochondrial tRNA<sup>Lys</sup>. *Biochemistry* **38**, 13338–13346 (1999).

84. Muramatsu, T., Nishikawa, K., Nemoto, F., Kuchino, Y., Nishimura, S., Miyazawa, T. & Yokoyama, S. Codon and amino-acid specificities of a transfer RNA are both converted by a single post-transcriptional modification. *Nature* (1988).
85. Senger, B., Auxilien, S., Englisch, U., Cramer, F. & Fasiolo, F. The modified wobble base inosine in yeast tRNA<sup>Ala</sup> is a positive determinant for aminoacylation by isoleucyl-tRNA synthetase. *Biochemistry* **36**, 8269–8275 (1997).
86. Gustilo, E. M., Vendeix, F. A. & Agris, P. F. tRNA's modifications bring order to gene expression. *Current opinion in microbiology* **11**, 134–140 (2008).
87. Agris, P. F., Vendeix, F. A. & Graham, W. D. tRNA's wobble decoding of the genome: 40 years of modification. *Journal of molecular biology* **366**, 1–13 (2007).
88. Björk, G. R., Jacobsson, K., Nilsson, K., Johansson, M. J., Byström, A. S. & Persson, O. P. A primordial tRNA modification required for the evolution of life? *The EMBO journal* **20**, 231–239 (2001).
89. Lamichhane, T. N., Blewett, N. H., Crawford, A. K., Cherkasova, V. A., Iben, J. R., Begley, T. J., Farabaugh, P. J. & Maraia, R. J. Lack of tRNA modification isopentenyl-A37 alters mRNA decoding and causes metabolic deficiencies in fission yeast. *Molecular and cellular biology* **33**, 2918–2929 (2013).
90. Vendeix, F. A., Murphy, F. V., Cantara, W. A., Leszczynska, G., Gustilo, E. M., Sproat, B., Malkiewicz, A. & Agris, P. F. Human tRNA Lys3 UUU is pre-structured by natural modifications for cognate and wobble codon binding through keto–enol tautomerism. *Journal of molecular biology* **416**, 467–485 (2012).
91. Björk, G. R., Huang, B., Persson, O. P. & Byström, A. S. A conserved modified wobble nucleoside (mcm5s2U) in lysyl-tRNA is required for viability in yeast. *Rna* **13**, 1245–1255 (2007).
92. Johansson, M. J., Esberg, A., Huang, B., Björk, G. R. & Byström, A. S. Eukaryotic wobble uridine modifications promote a functionally redundant decoding system. *Molecular and cellular biology* **28**, 3301–3312 (2008).
93. Huang, B., Johansson, M. J. & Byström, A. S. An early step in wobble uridine tRNA modification requires the Elongator complex. *Rna* **11**, 424–436 (2005).
94. Huang, B., Lu, J. & Byström, A. S. A genome-wide screen identifies genes required for formation of the wobble nucleoside in *Saccharomyces cerevisiae*. *RNA* **14**, 2183–2194 (2008).
95. Karlsborn, T., Tükenmez, H., Mahmud, A. K. M. F., Xu, F., Xu, H. & Byström, A. S. Elongator, a conserved complex required for wobble uridine modifications in Eukaryotes. *RNA Biology* **11**, 1519–1528 (2014).
96. Kalhor, H. R. & Clarke, S. Novel methyltransferase for modified uridine residues at the wobble position of tRNA. *Molecular and cellular biology* **23**, 9283–9292 (2003).

97. Mazauric, M.-H., Dirick, L., Purushothaman, S. K., Björk, G. R. & Lapeyre, B. Trm112p is a 15-kDa zinc finger protein essential for the activity of two tRNA and one protein methyltransferases in yeast. *Journal of Biological Chemistry* **285**, 18505–18515 (2010).
98. Chen, C., Huang, B., Anderson, J. T. & Byström, A. S. Unexpected accumulation of ncm 5 U and ncm 5 S 2 U in a trm9 mutant suggests an additional step in the synthesis of mcm 5 U and mcm 5 S 2 U. *PloS one* **6**, e20783 (2011).
99. Leidel, S., Pedrioli, P. G., Bucher, T., Brost, R., Costanzo, M., Schmidt, A., Aebersold, R., Boone, C., Hofmann, K. & Peter, M. Ubiquitin-related modifier Urm1 acts as a sulphur carrier in thiolation of eukaryotic transfer RNA. *Nature* **458**, 228–232 (2009).
100. Noma, A., Sakaguchi, Y. & Suzuki, T. Mechanistic characterization of the sulfur-relay system for eukaryotic 2-thiouridine biogenesis at tRNA wobble positions. *Nucleic Acids Research* **37**, 1335–1352 (2008).
101. Esberg, A., Huang, B., Johansson, M. J. & Byström, A. S. Elevated levels of two tRNA species bypass the requirement for elongator complex in transcription and exocytosis. *Molecular cell* **24**, 139–148 (2006).
102. Klassen, R., Grunewald, P., Thüring, K. L., Eichler, C., Helm, M. & Schaffrath, R. Loss of anticodon wobble uridine modifications affects tRNA Lys function and protein levels in *Saccharomyces cerevisiae*. *PloS one* **10**, e0119261 (2015).
103. Bauer, F., Matsuyama, A., Candiracci, J., Dieu, M., Scheliga, J., Wolf, D., Yoshida, M. & Hermand, D. Translational Control of Cell Division by Elongator. *Cell Reports* **1**, 424–433 (2012).
104. Yarian, C., Townsend, H., Czestkowski, W., Sochacka, E., Malkiewicz, A. J., Guenther, R., Miskiewicz, A. & Agris, P. F. Accurate Translation of the Genetic Code Depends on tRNA Modified Nucleosides. *The Journal of Biological Chemistry* **277**, 16391–16395 (2002).
105. Ashraf, S. S., Sochacka, E., Cain, R., Guenther, R., Malkiewicz, A. & Agris, P. F. Single atom modification (O→S) of tRNA confers ribosome binding. *RNA* **5**, 188–194 (1999).
106. Durant, P. C., Bajji, A. C., Sundaram, M., Kumar, R. K. & Davis, D. R. Structural Effects of Hypermodified Nucleosides in the *Escherichia coli* and Human tRNA Lys Anticodon Loop: The Effect of Nucleosides s2U, mcm U, mcm5s2U, mnm5s2 U, t 6A, and ms2t6A. *Biochemistry* **44**, 8078–8089 (2005).
107. Rezgui, V. A. N., Tyagi, K., Ranjan, N., Konevega, A. L., Mittelstaet, J., Rodnina, M. V., Peter, M. & Pedrioli, P. G. A. tRNA tKUUU, tQUUG, and tEUUC wobble position modifications fine-tune protein translation by promoting ribosome A-site binding. *Proceedings of the National Academy of Sciences* **110**, 12289–12294 (2013).
108. Patil, A., Chan, C., Dyavaiah, M., Rooney, J. P. & Dedon, P. Translational infidelity-induced protein stress results from a deficiency in Trm9-catalyzed tRNA modifications. *RNA biology* **9**, 990–1001 (2012).

109. Frohloff, F., Fichtner, L., Jablonowski, D., Breunig, K. & Schaffrath, R. Saccharomyces cerevisiae Elongator mutations confer resistance to the Kluyveromyces lactis zymocin. *The EMBO Journal* **20**, 1993–2003 (2001).
110. Jablonowski, D., Frohloff, F., Fichtner, L., Stark, M. J. R. & Schaffrath, R. Kluyveromyces lactis zymocin mode of action is linked to RNA polymerase II function via Elongator. *Molecular Microbiology* **42**, 1095–1105 (2001).
111. Begley, U., Dyavaiah, M., Patil, A., Rooney, J. P., DiRenzo, D., Young, C. M., Conklin, D. S., Zitomer, R. S. & Begley, T. J. Trm9-catalyzed tRNA modifications link translation to the DNA damage response. *Molecular cell* **28**, 860–870 (2007).
112. Patil, A., Dyavaiah, M., Joseph, F., Rooney, J. P., Chan, C. T., Dedon, P. C. & Begley, T. J. Increased tRNA modification and gene-specific codon usage regulate cell cycle progression during the DNA damage response. *Cell Cycle* **11**, 3656–3665 (2012).
113. Fernández-Vázquez, J., Vargas-Pérez, I., Sansó, M., Buhne, K., Carmona, M., Paulo, E., Hermand, D., Rodríguez-Gabriel, M., Ayté, J., Leidel, S. & Hidalgo, E. Modification of tRNA Lys UUU by elongator is essential for efficient translation of stress mRNAs. *PLoS Genet* **9**, e1003647 (2013).
114. Chan, C. T., Deng, W., Li, F., DeMott, M. S., Babu, I. R., Begley, T. J. & Dedon, P. C. Highly predictive reprogramming of tRNA modifications is linked to selective expression of codon-biased genes. *Chemical research in toxicology* **28**, 978–988 (2015).
115. Torres, A. G., Batlle, E. & de Pouplana, L. R. Role of tRNA modifications in human diseases. *Trends in molecular medicine* **20**, 306–314 (2014).
116. Yasukawa, T., Suzuki, T., Suzuki, T., Ueda, T., Ohta, S. & Watanabe, K. Modification defect at anticodon wobble nucleotide of mitochondrial tRNAs<sup>Leu</sup> (UUR) with pathogenic mutations of mitochondrial myopathy, encephalopathy, lactic acidosis, and stroke-like episodes. *Journal of Biological Chemistry* **275**, 4251–4257 (2000).
117. Yasukawa, T., Suzuki, T., Ishii, N., Ueda, T., Ohta, S. & Watanabe, K. Defect in modification at the anticodon wobble nucleotide of mitochondrial tRNA<sup>Lys</sup> with the MERRF encephalomyopathy pathogenic mutation. *FEBS letters* **467**, 175–178 (2000).
118. Kirino, Y., Goto, Y.-i., Campos, Y., Arenas, J. & Suzuki, T. Specific correlation between the wobble modification deficiency in mutant tRNAs and the clinical features of a human mitochondrial disease. *Proceedings of the National Academy of Sciences of the United States of America* **102**, 7127–7132 (2005).
119. Kirino, Y., Yasukawa, T., Ohta, S., Akira, S., Ishihara, K., Watanabe, K. & Suzuki, T. Codon-specific translational defect caused by a wobble modification deficiency in mutant tRNA from a human mitochondrial disease. *Proceedings of the National Academy of Sciences of the United States of America* **101**, 15070–15075 (2004).

120. Yasukawa, T., Suzuki, T., Ishii, N., Ohta, S. & Watanabe, K. Wobble modification defect in tRNA disturbs codon–anticodon interaction in a mitochondrial disease. *The EMBO Journal* **20**, 4794–4802 (2001).
121. Haute, L. V., Dietmann, S., Kremer, L., Hussain, S., Pearce, S. F., Powell, C. A., Rorbach, J., Lantaff, R., Blanco, S., Sauer, S., Kotzaeridou, U., Hoffmann, G. F., Memari, Y., Kolb-Kokocinski, A., Durbin, R., Mayr, J. A., Frye, M., Prokisch, H. & Minczuk, M. Deficient methylation and formylation of mt-tRNA<sup>Met</sup> wobble cytosine in a patient carrying mutations in NSUN3. *Nature Communications* **7**, 12039 (2016).
122. Nakano, S., Suzuki, T., Kawarada, L., Iwata, H., Asano, K. & Suzuki, T. NSUN3 methylase initiates 5-formylcytidine biogenesis in human mitochondrial tRNA<sup>Met</sup>. *Nature Chemical Biology* **12**, 546–551 (2016).
123. Blanco, S., Dietmann, S., Flores, J. V., Hussain, S., Kutter, C., Humphreys, P., Lukk, M., Lombard, P., Treps, L., Popis, M., *et al.* Aberrant methylation of tRNAs links cellular stress to neuro-developmental disorders. *The EMBO journal* **33**, 2020–2039 (2014).
124. Martinez, F. J., Lee, J. H., Lee, J. E., Blanco, S., Nickerson, E., Gabriel, S., Frye, M., Al-Gazali, L. & Gleeson, J. G. Whole exome sequencing identifies a splicing mutation in NSUN2 as a cause of a Dubowitz-like syndrome. *Journal of medical genetics*, jmedgenet–2011 (2012).
125. Frye, M. & Watt, F. M. The RNA methyltransferase Misu (NSun2) mediates Myc-induced proliferation and is upregulated in tumors. *Current biology* **16**, 971–981 (2006).
126. Frye, M., Dragoni, I., Chin, S.-F., Spiteri, I., Kurowski, A., Provenzano, E., Green, A., Ellis, I. O., Grimmer, D., Teschendorff, A., *et al.* Genomic gain of 5p15 leads to over-expression of Misu (NSUN2) in breast cancer. *Cancer letters* **289**, 71–80 (2010).
127. Popis, M. C., Blanco, S. & Frye, M. Posttranscriptional methylation of transfer and ribosomal RNA in stress response pathways, cell differentiation, and cancer. *Current opinion in oncology* **28**, 65–71 (2016).
128. Songe-Møller, L., van den Born, E., Leihne, V., Vågbø, C. B., Kristoffersen, T., Krokan, H. E., Kirpekar, F., Falnes, P. Ø. & Klungland, A. Mammalian ALKBH8 possesses tRNA methyltransferase activity required for the biogenesis of multiple wobble uridine modifications implicated in translational decoding. *Molecular and cellular biology* **30**, 1814–1827 (2010).
129. Shimada, K., Nakamura, M., Anai, S., De Velasco, M., Tanaka, M., Tsujikawa, K., Ouji, Y. & Konishi, N. A novel human AlkB homologue, ALKBH8, contributes to human bladder cancer progression. *Cancer research* **69**, 3157–3164 (2009).
130. Begley, U., Sosa, M. S., Avivar-Valderas, A., Patil, A., Endres, L., Estrada, Y., Chan, C. T., Su, D., Dedon, P. C., Aguirre-Ghiso, J. A., *et al.* A human tRNA methyltransferase 9-like protein prevents tumour growth by regulating LIN9 and HIF1- $\alpha$ . *EMBO molecular medicine* **5**, 366–383 (2013).

131. Czech, A., Fedyunin, I., Zhang, G. & Ignatova, Z. Silent mutations in sight: co-variations in tRNA abundance as a key to unravel consequences of silent mutations. *Molecular Biosystems* **6**, 1767–1772 (2010).
132. Ferro, I. & Ignatova, Z. Quantifying the ‘escapers’ among RNA species. *Biochemical Society Transactions* **43**, 1215–1220 (2015).
133. Hauenschild, R., Tserovski, L., Schmid, K., Thüring, K., Winz, M.-L., Sharma, S., Entian, K.-D., Wacheul, L., Lafontaine, D. L., Anderson, J., Alfonzo, J., Hildebrandt, A., Jäschke, A., Motorin, Y. & Helm, M. The reverse transcription signature of N-1-methyladenosine in RNA-Seq is sequence dependent. *Nucleic acids research* **43**, 9950–9964 (2015).
134. Ryvkin, P., Leung, Y. Y., Silverman, I. M., Childress, M., Valladares, O., Dragomir, I., Gregory, B. D. & Wang, L.-S. HAMR: high-throughput annotation of modified ribonucleotides. *RNA* **19**, 1684–1692 (2013).
135. Hiley, S. L., Jackman, J., Babak, T., Trochesset, M., Morris, Q. D., Phizicky, E. & Hughes, T. R. Detection and discovery of RNA modifications using microarrays. *Nucleic acids research* **33**, e2–e2 (2005).
136. Paris, Z., Horáková, E., Rubio, M. A. T., Sample, P., Fleming, I. M., Armocida, S., Lukes, J. & Alfonzo, J. D. The *T. brucei* TRM5 methyltransferase plays an essential role in mitochondrial protein synthesis and function. *RNA* **19**, 649–658 (2013).
137. Alwine, J. C., Kemp, D. J. & Stark, G. R. Method for detection of specific RNAs in agarose gels by transfer to diazobenzyloxymethyl-paper and hybridization with DNA probes. *Proceedings of the National Academy of Sciences* **74**, 5350–5354 (1977).
138. Varshney, U., Lee, C.-P. & RajBhandary, U. L. Direct analysis of aminoacylation levels of tRNAs in vivo. Application to studying recognition of *Escherichia coli* initiator tRNA mutants by glutamyl-tRNA synthetase. *Journal of Biological Chemistry* **266**, 24712–24718 (1991).
139. Krüger, M. K. & Sørensen, M. A. Aminoacylation of hypomodified tRNA Glu in vivo. *Journal of molecular biology* **284**, 609–620 (1998).
140. Pavon-Eternod, M., Wei, M., Pan, T. & Kleiman, L. Profiling non-lysyl tRNAs in HIV-1. *Rna* **16**, 267–273 (2010).
141. Dittmar, K. A., Mobley, E. M., Radek, A. J. & Pan, T. Exploring the regulation of tRNA distribution on the genomic scale. *Journal of molecular biology* **337**, 31–47 (2004).
142. Jiang, M., Mak, J., Ladha, A., Cohen, E., Klein, M., Rovinski, B. & Kleiman, L. Identification of tRNAs incorporated into wild-type and mutant human immunodeficiency virus type 1. *Journal of virology* **67**, 3246–3253 (1993).
143. Dittmar, K. A., Sørensen, M. A., Elf, J., Ehrenberg, M. & Pan, T. Selective charging of tRNA isoacceptors induced by amino-acid starvation. *EMBO reports* **6**, 151–157 (2005).

144. Honda, S., Shigematsu, M., Morichika, K., Telonis, A. G. & Kirino, Y. Four-leaf clover qRT-PCR: A convenient method for selective quantification of mature tRNA. *RNA biology* **12**, 501–508 (2015).
145. Pang, Y. L. J., Abo, R., Levine, S. S. & Dedon, P. C. Diverse cell stresses induce unique patterns of tRNA up-and down-regulation: tRNA-seq for quantifying changes in tRNA copy number. *Nucleic acids research*, gku945 (2014).
146. Mohr, S., Ghanem, E., Smith, W., Sheeter, D., Qin, Y., King, O., Polioudakis, D., Iyer, V. R., Hunicke-Smith, S., Swamy, S., *et al.* Thermostable group II intron reverse transcriptase fusion proteins and their use in cDNA synthesis and next-generation RNA sequencing. *Rna* **19**, 958–970 (2013).
147. Zheng, G., Qin, Y., Clark, W. C., Dai, Q., Yi, C., He, C., Lambowitz, A. M. & Pan, T. Efficient and quantitative high-throughput tRNA sequencing. *Nature methods* **12**, 835–837 (2015).
148. Clark, W. C., Evans, M. E., Dominissini, D., Zheng, G. & Pan, T. tRNA base methylation identification and quantification via high-throughput sequencing. *RNA* **22**, 1771–1784 (2016).
149. Cozen, A. E., Quartley, E., Holmes, A. D., Hrabeta-Robinson, E., Phizicky, E. M. & Lowe, T. M. ARM-seq: AlkB-facilitated RNA methylation sequencing reveals a complex landscape of modified tRNA fragments. *Nature Methods* **12**, 879–884 (2015).
150. Kellner, S., Burhenne, J. & Helm, M. Detection of RNA modifications. *RNA biology* **7**, 237–247 (2010).
151. Limbach, P. A. & Paulines, M. J. Going global: the new era of mapping modifications in RNA. *Wiley Interdisciplinary Reviews: RNA* (2016).
152. Grippo, P., Iaccarino, M., Rossi, M. & Scarano, E. Thin-layer chromatography of nucleotides, nucleosides and nucleic acid bases. *Biochimica et Biophysica Acta-Nucleic Acids and Protein Synthesis* **95**, 1–7 (1965).
153. Grosjean, H., Keith, G. & Droogmans, L. in *RNA Interference, Editing, and Modification: Methods and Protocols* (ed Gott, J. M.) 357–391 (Humana Press, Totowa, NJ, 2004). ISBN: 978-1-59259-775-8.
154. Pomerantz, S. C. & McCloskey, J. A. Analysis of RNA hydrolyzates by liquid chromatography-mass spectrometry. *Methods in enzymology* **193**, 796–824 (1990).
155. Kowalak, J. A., Pomerantz, S. C., Crain, P. F. & McCloskey, J. A. A novel method for the determination of posttranscriptional modification in RNA by mass spectrometry. *Nucl Acids Res* **21**, 4577–4585 (1993).
156. Li, Y., Wang, Y., Zhang, Z., Zamudio, A. V. & Zhao, J. C. Genome-wide detection of high abundance N6-methyladenosine sites by microarray. *rna* **21**, 1511–1518 (2015).
157. Schaefer, M., Pollex, T., Hanna, K. & Lyko, F. RNA cytosine methylation analysis by bisulfite sequencing. *Nucleic Acids Research* **37**, e12–e12 (2008).



158. Edelheit, S., Schwartz, S., Mumbach, M. R., Wurtzel, O. & Sorek, R. Transcriptome-Wide Mapping of 5-methylcytidine RNA Modifications in Bacteria, Archaea, and Yeast Reveals m<sup>5</sup>C within Archaeal mRNAs. *PLoS Genetics* **9** (ed de Crécy-Lagard, V.) e1003602 (2013).
159. Hussain, S., Sajini, A., Blanco, S., Dietmann, S., Lombard, P., Sugimoto, Y., Paramor, M., Gleeson, J., Odom, D., Ule, J. & Frye, M. NSun2-Mediated Cytosine-5 Methylation of Vault Noncoding RNA Determines Its Processing into Regulatory Small RNAs. *Cell Reports* **4**, 255–261 (2013).
160. Khoddami, V. & Cairns, B. R. Identification of direct targets and modified bases of RNA cytosine methyltransferases. *Nat Biotechnol* **31**, 458–464 (2013).
161. Hussain, S., Aleksic, J., Blanco, S., Dietmann, S. & Frye, M. Characterizing 5-methylcytosine in the mammalian epitranscriptome. *Genome Biol* **14**, 215 (2013).
162. Dominissini, D., Moshitch-Moshkovitz, S., Schwartz, S., Salmon-Divon, M., Ungar, L., Osenberg, S., Cesarkas, K., Jacob-Hirsch, J., Amariglio, N., Kupiec, M., Sorek, R. & Rechavi, G. Topology of the human and mouse m<sup>6</sup>A RNA methylomes revealed by m<sup>6</sup>A-seq. *Nature* **485**, 201–206 (2012).
163. Meyer, K., Saletore, Y., Zumbo, P., Elemento, O., Mason, C. & Jaffrey, S. Comprehensive Analysis of mRNA Methylation Reveals Enrichment in 3' UTRs and near Stop Codons. *Cell* **149**, 1635–1646 (2012).
164. Chen, K., Lu, Z., Wang, X., Fu, Y., Luo, G.-Z., Liu, N., Han, D., Dominissini, D., Dai, Q., Pan, T. & He, C. High-Resolution N<sup>6</sup>-Methyladenosine (m<sup>6</sup>A) Map Using Photo-Crosslinking-Assisted m<sup>6</sup>A Sequencing. *Angewandte Chemie International Edition* **54**, 1587–1590 (2014).
165. Su, D., Chan, C. T., Gu, C., Lim, K. S., Chionh, Y. H., McBee, M. E., Russell, B. S., Babu, I. R., Begley, T. J. & Dedon, P. C. Quantitative analysis of tRNA modifications by HPLC-coupled mass spectrometry. *Nature protocols* **9**, 828 (2014).
166. Cai, W. M., Chionh, Y. H., Hia, F., Gu, C., Kellner, S., McBee, M. E., Ng, C. S., Pang, Y. L. J., Prestwich, E. G., Lim, K. S., *et al.* Chapter Three-A Platform for Discovery and Quantification of Modified Ribonucleosides in RNA: Application to Stress-Induced Reprogramming of tRNA Modifications. *Methods in enzymology* **560**, 29–71 (2015).
167. Kellner, S., Ochel, A., Thüring, K., Spenkuch, F., Neumann, J., Sharma, S., Entian, K.-D., Schneider, D. & Helm, M. Absolute and relative quantification of RNA modifications via biosynthetic isotopomers. *Nucleic acids research* **42**, e142–e142 (2014).
168. Wetzelschaefer, C. & Limbach, P. A. Mass spectrometry of modified RNAs: recent developments. *Analyst* **141**, 16–23 (2016).
169. Gaston, K. W. & Limbach, P. A. The identification and characterization of non-coding and coding RNAs and their modified nucleosides by mass spectrometry. *RNA Biology* **11**, 1568–1585 (2014).

170. Giessing, A. M. & Kirpekar, F. Mass spectrometry in the biology of RNA and its modifications. *Journal of Proteomics* **75**, 3434–3449 (2012).
171. Crain, P. F. Preparation and enzymatic hydrolysis of DNA and RNA for mass spectrometry. *Methods in enzymology* **193**, 782–790 (1990).
172. Thüring, K., Schmid, K., Keller, P. & Helm, M. Analysis of RNA modifications by liquid chromatography–tandem mass spectrometry. *Methods* **107**, 48–56 (2016).
173. Kellner, S., Neumann, J., Rosenkranz, D., Lebedeva, S., Ketting, R. F., Zischler, H., Schneider, D. & Helm, M. Profiling of RNA modifications by multiplexed stable isotope labelling. *Chemical Communications* **50**, 3516–3518 (2014).
174. Brückl, T., Globisch, D., Wagner, M., Müller, M. & Carell, T. Parallel Isotope-Based Quantification of Modified tRNA Nucleosides. *Angewandte Chemie International Edition* **48**, 7932–7934 (2009).
175. Globisch, D., Pearson, D., Hienzsch, A., Brückl, T., Wagner, M., Thoma, I., Thumbs, P., Reiter, V., Kneuttinger, A. C., Müller, M., Sieber, S. A. & Carell, T. Systems-Based Analysis of Modified tRNA Bases. *Angewandte Chemie International Edition* **50**, 9739–9742 (2011).
176. Brandmayr, C., Wagner, M., Brückl, T., Globisch, D., Pearson, D., Kneuttinger, A. C., Reiter, V., Hienzsch, A., Koch, S., Thoma, I., Thumbs, P., Michalakis, S., Müller, M., Biel, M. & Carell, T. Isotope-Based Analysis of Modified tRNA Nucleosides Correlates Modification Density with Translational Efficiency. *Angewandte Chemie International Edition* **51**, 11162–11165 (2012).
177. Abdelhameed, A. S., Attwa, M. W., Abdel-Aziz, H. A. & Kadi, A. A. Induced in-source fragmentation pattern of certain novel (1Z, 2E)-N-(aryl) propanehydrazonoyl chlorides by electrospray mass spectrometry (ESI-MS/MS). *Chemistry Central Journal* **7**, 1–8 (2013).
178. Wilusz, J. E., Freier, S. M. & Spector, D. L. 3' end processing of a long nuclear-retained noncoding RNA yields a tRNA-like cytoplasmic RNA. *Cell* **135**, 919–932 (2008).
179. Sunwoo, H., Dinger, M. E., Wilusz, J. E., Amaral, P. P., Mattick, J. S. & Spector, D. L. MEN $\beta$  nuclear-retained non-coding RNAs are up-regulated upon muscle differentiation and are essential components of paraspeckles. *Genome Research* **19**, 347–359 (2008).
180. Zong, X., Nakagawa, S., Freier, S. M., Fei, J., Ha, T., Prasanth, S. G. & Prasanth, K. V. Natural antisense RNA promotes 3' end processing and maturation of MALAT1 lncRNA. *Nucleic Acids Res* **44**, 2898–2908 (2016).
181. Wilusz, J. E., JnBaptiste, C. K., Lu, L. Y., Kuhn, C.-D., Joshua-Tor, L. & Sharp, P. A. A triple helix stabilizes the 3' ends of long noncoding RNAs that lack poly(A) tails. *Genes & Development* **26**, 2392–2407 (2012).
182. Brown, J. A., Valenstein, M. L., Yario, T. A., Tycowski, K. T. & Steitz, J. A. Formation of triple-helical structures by the 3' -end sequences of MALAT1 and MEN $\beta$  noncoding RNAs. *Proceedings of the National Academy of Sciences* **109**, 19202–19207 (2012).

183. Brown, J. A., Bulkley, D., Wang, J., Valenstein, M. L., Yario, T. A., Steitz, T. A. & Steitz, J. A. Structural insights into the stabilization of MALAT1 noncoding RNA by a bipartite triple helix. *Nat Struct Mol Biol* **21**, 633–640 (2014).
184. Eißmann, M., Gutschner, T., Hämmerle, M., Günther, S., Caudron-Herger, M., Groß, M., Schirmacher, P., Rippe, K., Braun, T., Zörnig, M. & Diederichs, S. Loss of the abundant nuclear non-coding RNA MALAT1 is compatible with life and development. *RNA Biology* **9**, 1076–1087 (2012).
185. Hutchinson, J. N., Ensminger, A. W., Clemson, C. M., Lynch, C. R., Lawrence, J. B. & Chess, A. A screen for nuclear transcripts identifies two linked noncoding RNAs associated with SC35 splicing domains. *BMC Genomics* **8**, 39 (2007).
186. Ji, P., Diederichs, S., Wang, W., Böing, S., Metzger, R., Schneider, P. M., Tidow, N., Brandt, B., Buerger, H., Bulk, E., *et al.* MALAT-1, a novel noncoding RNA, and thymosin  $\beta$ 4 predict metastasis and survival in early-stage non-small cell lung cancer. *Oncogene* **22**, 8031–8041 (2003).
187. Zhang, B., Arun, G., Mao, Y., Lazar, Z., Hung, G., Bhattacharjee, G., Xiao, X., Booth, C., Wu, J., Zhang, C. & Spector, D. The lncRNA Malat1 Is Dispensable for Mouse Development but Its Transcription Plays a cis-Regulatory Role in the Adult. *Cell Reports* **2**, 111–123 (2012).
188. Gutschner, T., Hämmerle, M. & Diederichs, S. MALAT1 - a paradigm for long noncoding RNA function in cancer. *Journal of Molecular Medicine* **91**, 791–801 (2013).
189. Yoshimoto, R., Mayeda, A., Yoshida, M. & Nakagawa, S. MALAT1 long non-coding RNA in cancer. *Biochimica et Biophysica Acta (BBA) - Gene Regulatory Mechanisms* **1859**, 192–199 (2016).
190. Yang, L., Lin, C., Liu, W., Zhang, J., Ohgi, K., Grinstein, J., Dorrestein, P. & Rosenfeld, M. ncRNA- and Pc2 Methylation-Dependent Gene Relocation between Nuclear Structures Mediates Gene Activation Programs. *Cell* **147**, 773–788 (2011).
191. Gutschner, T., Hammerle, M., Eissmann, M., Hsu, J., Kim, Y., Hung, G., Revenko, A., Arun, G., Stentrup, M., Gross, M., Zornig, M., MacLeod, A. R., Spector, D. L. & Diederichs, S. The Noncoding RNA MALAT1 Is a Critical Regulator of the Metastasis Phenotype of Lung Cancer Cells. *Cancer Research* **73**, 1180–1189 (2012).
192. Michalik, K. M., You, X., Manavski, Y., Doddaballapur, A., Zornig, M., Braun, T., John, D., Ponomareva, Y., Chen, W., Uchida, S., Boon, R. A. & Dimmeler, S. Long Noncoding RNA MALAT1 Regulates Endothelial Cell Function and Vessel Growth. *Circulation Research* **114**, 1389–1397 (2014).
193. Tee, A. E., Liu, B., Song, R., Li, J., Pasquier, E., Cheung, B. B., Jiang, C., Marshall, G. M., Haber, M., Norris, M. D., Fletcher, J. I., Dinger, M. E. & Liu, T. The long noncoding RNA MALAT1 promotes tumor-driven angiogenesis by up-regulating pro-angiogenic gene expression. *Oncotarget* **7**, 8663–8675 (2016).

194. Cesana, M., Cacchiarelli, D., Legnini, I., Santini, T., Sthandier, O., Chinappi, M., Tramontano, A. & Bozzoni, I. A Long Noncoding RNA Controls Muscle Differentiation by Functioning as a Competing Endogenous RNA. *Cell* **147**, 358–369 (2011).
195. Salmena, L., Poliseno, L., Tay, Y., Kats, L. & Pandolfi, P. A ceRNA Hypothesis: The Rosetta Stone of a Hidden RNA Language? *Cell* **146**, 353–358 (2011).
196. Luan, W., Li, L., Shi, Y., Bu, X., Xia, Y., Wang, J., Djangmah, H. S., Liu, X., You, Y. & Xu, B. Long non-coding RNA MALAT1 acts as a competing endogenous RNA to promote malignant melanoma growth and metastasis by sponging miR-22. *Oncotarget*. DOI: 10.18632/oncotarget.11564 (2016).
197. Feng, T., Shao, F., Wu, Q., Zhang, X., Xu, D., Qian, K., Xie, Y., Wang, S., Xu, N., Wang, Y. & Qi, C. miR-124 downregulation leads to breast cancer progression via LncRNA-MALAT1 regulation and CDK4/E2F1 signal activation. *Oncotarget* **7**, 16205–16216 (2016).
198. Gast, M., Schroen, B., Voigt, A., Haas, J., Kuehl, U., Lassner, D., Skurk, C., Escher, F., Wang, X., Kratzer, A., Michalik, K., Papageorgiou, A., Peters, T., Loebel, M., Wilk, S., Althof, N., Prasanth, K. V., Katus, H., Meder, B., Nakagawa, S., Scheibenbogen, C., Schultheiss, H.-P., Landmesser, U., Dimmeler, S., Heymans, S. & Poller, W. Long noncoding RNA MALAT1-derived mascRNA is involved in cardiovascular innate immunity. *Journal of Molecular Cell Biology* **8**, 178–181 (2016).
199. Xu, C., Yang, M., Tian, J., Wang, X. & Li, Z. MALAT-1: A long non-coding RNA and its important 3' end functional motif in colorectal cancer metastasis. *Int J Oncol* **39**, 169–175 (2011).
200. Jerabek-Willemsen, M., Wienken, C. J., Braun, D., Baaske, P. & Duhr, S. Molecular interaction studies using microscale thermophoresis. *Assay and drug development technologies* **9**, 342–353 (2011).
201. Seidel, S. A., Dijkman, P. M., Lea, W. A., van den Bogaart, G., Jerabek-Willemsen, M., Lazic, A., Joseph, J. S., Srinivasan, P., Baaske, P., Simeonov, A., Katritch, I., Melo, F. A., Ladbury, J. E., Schreiber, G., Watts, A., Braun, D. & Duhr, S. Microscale thermophoresis quantifies biomolecular interactions under previously challenging conditions. *Methods* **59**, 301–315 (2013).
202. Jerabek-Willemsen, M., André, T., Wanner, R., Roth, H. M., Duhr, S., Baaske, P. & Breitsprecher, D. MicroScale Thermophoresis: Interaction analysis and beyond. *Journal of Molecular Structure* **1077**, 101–113 (2014).
203. Ludwig, C. *Diffusion zwischen ungleich erwärmten Orten gleich zusammengesetzter Lösung* (Aus der KK Hof- und Staatsdruckerei, in Commission bei W. Braumüller, Buchhändler des KK Hofes und der K. Akademie der Wissenschaften, 1856).
204. Braun, D. & Libchaber, A. Trapping of DNA by thermophoretic depletion and convection. *Physical review letters* **89**, 188103 (2002).

205. Duhr, S. & Braun, D. Why molecules move along a temperature gradient. *Proceedings of the National Academy of Sciences* **103**, 19678–19682 (2006).
206. Baaske, P., Wienken, C. J., Reineck, P., Duhr, S. & Braun, D. Optical thermophoresis for quantifying the buffer dependence of aptamer binding. *Angewandte Chemie International Edition* **49**, 2238–2241 (2010).
207. Wienken, C. J., Baaske, P., Rothbauer, U., Braun, D. & Duhr, S. Protein-binding assays in biological liquids using microscale thermophoresis. *Nature communications* **1**, 100 (2010).
208. Wienken, C. J., Baaske, P., Duhr, S. & Braun, D. Thermophoretic melting curves quantify the conformation and stability of RNA and DNA. *Nucleic acids research* **39**, e52–e52 (2011).
209. Reineck, P., Wienken, C. J. & Braun, D. Thermophoresis of single stranded DNA. *Electrophoresis* **31**, 279–286 (2010).
210. Reichl, M., Herzog, M., Götz, A. & Braun, D. Why charged molecules move across a temperature gradient: the role of electric fields. *Physical review letters* **112**, 198101 (2014).
211. Duhr, S., Arduini, S. & Braun, D. Thermophoresis of DNA determined by microfluidic fluorescence. *The European Physical Journal E* **15**, 277–286 (2004).
212. Reichl, M. R. & Braun, D. Thermophoretic manipulation of molecules inside living cells. *Journal of the American Chemical Society* **136**, 15955–15960 (2014).
213. Maeda, Y. T., Buguin, A. & Libchaber, A. Thermal separation: interplay between the Soret effect and entropic force gradient. *Physical review letters* **107**, 038301 (2011).
214. Maeda, Y. T., Tlustý, T. & Libchaber, A. Effects of long DNA folding and small RNA stem-loop in thermophoresis. *Proceedings of the National Academy of Sciences* **109**, 17972–17977 (2012).
215. Reichl, M., Herzog, M., Greiss, F., Wolff, M. & Braun, D. Understanding the similarity in thermophoresis between single- and double-stranded DNA or RNA. *Physical Review E* **91**, 062709 (2015).
216. Zhan, Y., Yan, Y., Deng, Z., Chen, M., Lu, W., Lu, C., Shang, L., Yang, Z., Zhang, W., Wang, W., *et al.* The novel regulatory ncRNA, NfiS, optimizes nitrogen fixation via base pairing with the nitrogenase gene nifK mRNA in *Pseudomonas stutzeri* A1501. *Proceedings of the National Academy of Sciences*, 201604514 (2016).
217. Yu, L.-H. & Chen, Y.-F. Concentration-dependent thermophoretic accumulation for the detection of DNA using DNA-functionalized nanoparticles. *Analytical chemistry* **87**, 2845–2851 (2015).
218. Entzian, C. & Schubert, T. Studying small molecule–aptamer interactions using MicroScale Thermophoresis (MST). *Methods* **97**, 27–34 (2016).
219. Zillner, K., Jerabek-Willemsen, M., Duhr, S., Braun, D., Längst, G. & Baaske, P. Microscale thermophoresis as a sensitive method to quantify protein: nucleic acid interactions in solution. *Functional Genomics: Methods and Protocols*, 241–252 (2012).

220. Spenkuch, F., Hinze, G., Kellner, S., Kreutz, C., Micura, R., Basché, T. & Helm, M. Dye label interference with RNA modification reveals 5-fluorouridine as non-covalent inhibitor. *Nucleic acids research* **42**, 12735–12745 (2014).
221. Filarsky, M., Zillner, K., Araya, I., Villar-Garea, A., Merkl, R., Längst, G. & Németh, A. The extended AT-hook is a novel RNA binding motif. *RNA biology* **12**, 864–876 (2015).
222. Spenkuch, F. *Enzyme tRNA interaction and (t)RNA conformation probed via environmentally sensitive cyanine dyes* PhD thesis (Johannes Gutenberg-Universität Mainz, Germany, 2014).
223. Kellner, S. *Functionalization and Detection of RNA and its Modifications* PhD thesis (Johannes Gutenberg-Universität Mainz, Germany, 2012).
224. Zallot, R., Brochier-Armanet, C., Gaston, K. W., Forouhar, F., Limbach, P. A., Hunt, J. F. & de Crécy-Lagard, V. Plant, animal, and fungal micronutrient queuosine is salvaged by members of the DUF2419 protein family. *ACS chemical biology* **9**, 1812–1825 (2014).
225. Klassen, R., Ciftci, A., Funk, J., Bruch, A., Butter, F. & Schaffrath, R. tRNA anticodon loop modifications ensure protein homeostasis and cell morphogenesis in yeast. *Nucleic Acids Research*, gkw705 (2016).
226. Lecointe, F., Simos, G., Sauer, A., Hurt, E. C., Motorin, Y. & Grosjean, H. Characterization of yeast protein Deg1 as pseudouridine synthase (Pus3) catalyzing the formation of  $\Psi$ 38 and  $\Psi$ 39 in tRNA anticodon loop. *Journal of Biological Chemistry* **273**, 1316–1323 (1998).
227. Miyauchi, K., Kimura, S. & Suzuki, T. A cyclic form of N6-threonylcarbamoyladenine as a widely distributed tRNA hypermodification. *Nature chemical biology* **9**, 105–111 (2013).
228. Han, L., Kon, Y. & Phizicky, E. M. Functional importance of  $\Psi$ 38 and  $\Psi$ 39 in distinct tRNAs, amplified for tRNAGln (UUG) by unexpected temperature sensitivity of the s2U modification in yeast. *RNA* **21**, 188–201 (2015).
229. Klassen, R., Paluszynski, J. P., Wemhoff, S., Pfeiffer, A., Fricke, J. & Meinhardt, F. The primary target of the killer toxin from *Pichia acaciae* is tRNAGln. *Molecular microbiology* **69**, 681–697 (2008).
230. Chang, H., Lim, J., Ha, M. & Kim, V. N. TAIL-seq: genome-wide determination of poly (A) tail length and 3' end modifications. *Molecular cell* **53**, 1044–1052 (2014).
231. Subtelny, A. O., Eichhorn, S. W., Chen, G. R., Sive, H. & Bartel, D. P. Poly (A)-tail profiling reveals an embryonic switch in translational control. *Nature* **508**, 66 (2014).
232. Klassen, R. & Meinhardt, F. Induction of DNA damage and apoptosis in *Saccharomyces cerevisiae* by a yeast killer toxin. *Cell Microbiol* **7**, 393–401 (2005).
233. Klassen, R., Teichert, S. & Meinhardt, F. Novel yeast killer toxins provoke S-phase arrest and DNA damage checkpoint activation. *Molecular Microbiology* **53**, 263–273 (2004).
234. Hilgers, V. Translation-independent inhibition of mRNA deadenylation during stress in *Saccharomyces cerevisiae*. *RNA* **12**, 1835–1845 (2006).

235. Mortazavi, A., Williams, B. A., McCue, K., Schaeffer, L. & Wold, B. Mapping and quantifying mammalian transcriptomes by RNA-Seq. *Nature Methods* **5**, 621–628 (2008).
236. Wang, Z., Gerstein, M. & Snyder, M. RNA-Seq: a revolutionary tool for transcriptomics. *Nature Reviews Genetics* **10**, 57–63 (2009).
237. Nolan, T., Hands, R. E. & Bustin, S. A. Quantification of mRNA using real-time RT-PCR. *Nature Protocols* **1**, 1559–1582 (2006).
238. Kumazawa, Y., Yokogawa, T., Tsurui, H., Miura, K.-i. & Watanabe, K. Effect of the higher-order structure of tRNAs on the stability of hybrids with oligodeoxyribonucleotides: separation of tRNA by an efficient solution hybridization. *Nucleic acids research* **20**, 2223–2232 (1992).
239. Tsurui, H., Kumazawa, Y., Sanokawa, R., Watanabe, Y., Kuroda, T., Wada, A., Watanabe, K. & Shirai, T. Batchwise purification of specific tRNAs by a solid-phase DNA probe. *Analytical biochemistry* **221**, 166–172 (1994).
240. Miyauchi, K., Ohara, T. & Suzuki, T. Automated parallel isolation of multiple species of non-coding RNAs by the reciprocal circulating chromatography method. *Nucleic acids research* **35**, e24 (2007).
241. Suzuki, T. & Suzuki, T. Chaplet column chromatography: isolation of a large set of individual RNAs in a single step. *Methods in enzymology* **425**, 231–239 (2007).
242. Yokogawa, T., Kitamura, Y., Nakamura, D., Ohno, S. & Nishikawa, K. Optimization of the hybridization-based method for purification of thermostable tRNAs in the presence of tetraalkylammonium salts. *Nucleic acids research* **38**, e89–e89 (2010).
243. Roovers, M., Wouters, J., Bujnicki, J. M., Tricot, C., Stalon, V., Grosjean, H. & Droogmans, L. A primordial RNA modification enzyme: the case of tRNA (m1A) methyltransferase. *Nucleic acids research* **32**, 465–476 (2004).
244. Tserovski, L., Marchand, V., Hauenschild, R., Blanloeil-Oillo, F., Helm, M. & Motorin, Y. High-throughput sequencing for 1-methyladenosine (m<sup>1</sup>A) mapping in RNA. *Methods* (2016).
245. Anderson, J., Phan, L., Cuesta, R., Carlson, B. A., Pak, M., Asano, K., Björk, G. R., Tamame, M. & Hinnebusch, A. G. The essential Gcd10p–Gcd14p nuclear complex is required for 1-methyladenosine modification and maturation of initiator methionyl-tRNA. *Genes & development* **12**, 3650–3662 (1998).
246. Jüdes, A., Ebert, F., Bär, C., Thüring, K. L., Harrer, A., Klassen, R., Helm, M., Stark, M. J. & Schaffrath, R. Urmylation and tRNA thiolation functions of ubiquitin-like Uba4–Urm1 systems are conserved from yeast to man. *FEBS letters* **589**, 904–909 (2015).
247. Abdel-Fattah, W., Jablonowski, D., Di Santo, R., Thüring, K. L., Scheidt, V., Hammermeister, A., ten Have, S., Helm, M., Schaffrath, R. & Stark, M. J. Phosphorylation of Elp1 by Hrr25 is required for elongator-dependent tRNA modification in yeast. *PLoS Genet* **11**, e1004931 (2015).

248. Dominissini, D., Nachtergaele, S., Moshitch-Moshkovitz, S., Peer, E., Kol, N., Ben-Haim, M. S., Dai, Q., Di Segni, A., Salmon-Divon, M., Clark, W. C., *et al.* The dynamic N1-methyladenosine methylome in eukaryotic messenger RNA. *Nature* **530**, 441–446 (2016).
249. Macon, J. B. & Wolfenden, R. 1-Methyladenosine. Dimroth rearrangement and reversible reduction. *Biochemistry* **7**, 3453–3458 (1968).
250. Kasai, H., Ohashi, Z., Harada, F., Nishimura, S., Oppenheimer, N., Crain, P., Liehr, J., Von Minden, D. & McCloskey, J. Structure of the modified nucleoside Q isolated from *Escherichia coli* transfer ribonucleic acid. 7-(4, 5-cis-Dihydroxy-1-cyclopenten-3-ylaminomethyl)-7-deazaguanosine. *Biochemistry* **14**, 4198–4208 (1975).
251. Fergus, C., Barnes, D., Alqasem, M. A. & Kelly, V. P. The queuine micronutrient: charting a course from microbe to man. *Nutrients* **7**, 2897–2929 (2015).
252. Harada, F. & Nishimura, S. Possible anticodon sequences of tRNA<sup>His</sup>, tRNA<sup>Asn</sup>, and tRNA<sup>Asp</sup> from *Escherichia coli*. Universal presence of nucleoside O in the first position of the anticodons of these transfer ribonucleic acid. *Biochemistry* **11**, 301–308 (1972).
253. Stengl, B., Reuter, K. & Klebe, G. Mechanism and Substrate Specificity of tRNA–Guanine Transglycosylases (TGTs): tRNA-Modifying Enzymes from the Three Different Kingdoms of Life Share a Common Catalytic Mechanism. *ChemBioChem* **6**, 1926–1939 (2005).
254. Phillipson, D., Edmonds, C., Crain, P., Smith, D. L., Davis, D. & McCloskey, J. Isolation and structure elucidation of an epoxide derivative of the hypermodified nucleoside queuosine from *Escherichia coli* transfer RNA. *Journal of Biological Chemistry* **262**, 3462–3471 (1987).
255. Müller, M., Hartmann, M., Schuster, I., Bender, S., Thüring, K. L., Helm, M., Katze, J. R., Nellen, W., Lyko, F. & Ehrenhofer-Murray, A. E. Dynamic modulation of Dnmt2-dependent tRNA methylation by the micronutrient queuine. *Nucleic acids research* **43**, 10952–10962 (2015).
256. Kasai, H., Nakanishi, K., Macfarlane, R., Torgerson, D., Ohashi, Z., McCloskey, J., Gross, H. & Nishimura, S. The structure of Q\* nucleoside isolated from rabbit liver transfer ribonucleic acid. *Journal of the American Chemical Society* **98**, 5044–5046 (1976).
257. Okada, N., Shindo-Okada, N. & Nishimura, S. Isolation of mammalian tRNA<sup>Asp</sup> and tRNA<sup>Tyr</sup> by lectin-Sepharose affinity column chromatography. *Nucleic acids research* **4**, 415–423 (1977).
258. Thumbs, P. C. *Synthese der natürlichen tRNA-Modifikation Galaktosylqueuosin und Untersuchungen zur Struktur der natürlichen tRNA-Modifikation Mannosylqueuosin* PhD thesis (Fakultät für Chemie und Pharmazie, Ludwig-Maximilians-Universität München, 2013).
259. Salazar, J. C., Ambrogelly, A., Crain, P. F., McCloskey, J. A. & Söll, D. A truncated aminoacyl-tRNA synthetase modifies RNA. *Proceedings of the National Academy of Sciences of the United States of America* **101** (2004).



260. Yamauchi, Y., Nobe, Y., Izumikawa, K., Higo, D., Yamagishi, Y., Takahashi, N., Nakayama, H., Isobe, T. & Taoka, M. A mass spectrometry-based method for direct determination of pseudouridine in RNA. *Nucleic acids research* **44**, e59–e59 (2016).
261. Thakur, C. S., Sama, J. N., Jackson, M. E., Chen, B. & Dayie, T. K. Selective <sup>13</sup>C labeling of nucleotides for large RNA NMR spectroscopy using an E. coli strain disabled in the TCA cycle. *Journal of biomolecular NMR* **48**, 179–192 (2010).
262. Nelson, C. C. & McCloskey, J. A. Collision-induced dissociation of uracil and its derivatives. *Journal of the American Society for Mass Spectrometry* **5**, 339–349 (1994).
263. Gregson, J. M. & McCloskey, J. A. Collision-induced dissociation of protonated guanine. *International journal of mass spectrometry and ion processes* **165**, 475–485 (1997).
264. Nelson, C. C. & McCloskey, J. A. Collision-induced dissociation of adenine. *Journal of the American Chemical Society* **114**, 3661–3668 (1992).
265. Jensen, S. S., Ariza, X., Nielsen, P., Vilarrasa, J. & Kirpekar, F. Collision-induced dissociation of cytidine and its derivatives. *Journal of mass spectrometry* **42**, 49–57 (2007).
266. Beach, D. G. & Gabryelski, W. Revisiting the reactivity of uracil during collision induced dissociation: tautomerism and charge-directed processes. *Journal of The American Society for Mass Spectrometry* **23**, 858–868 (2012).
267. Park, J.-E., Yi, H., Kim, Y., Chang, H. & Kim, V. N. Regulation of Poly(A) Tail and Translation during the Somatic Cell Cycle. *Molecular Cell* **62**, 462–471 (2016).
268. Chomczynski, P. & Sacchi, N. Single-step method of RNA isolation by acid guanidinium thiocyanate-phenol-chloroform extraction. *Analytical biochemistry* **162**, 156–159 (1987).



# A Appendix

## Appendix to Chapter 3.1

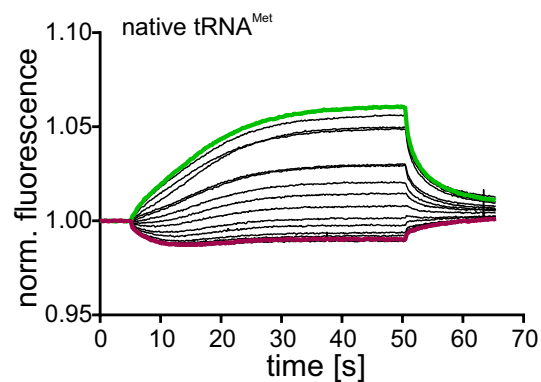


**Figure A.1: Fluorescence time traces of native tRNA<sup>Met</sup>(MAU) (*E. coli*)** Fluorescence time traces corresponding to the binding curve shown in section 3.1.2.3, figure 3.6. Native tRNA<sup>Met</sup>(MAU) was isolated from *E. coli* total tRNA (section 3.2.2) and submitted to MST measurements using probe MH630 (100 nM). Changes of the fluorescence time traces upon increasing tRNA concentration demonstrated the binding of the probe to the native tRNA<sup>Met</sup>(MAU). Time traces of labeled and completely bound probe are indicated (green or magenta, respectively).

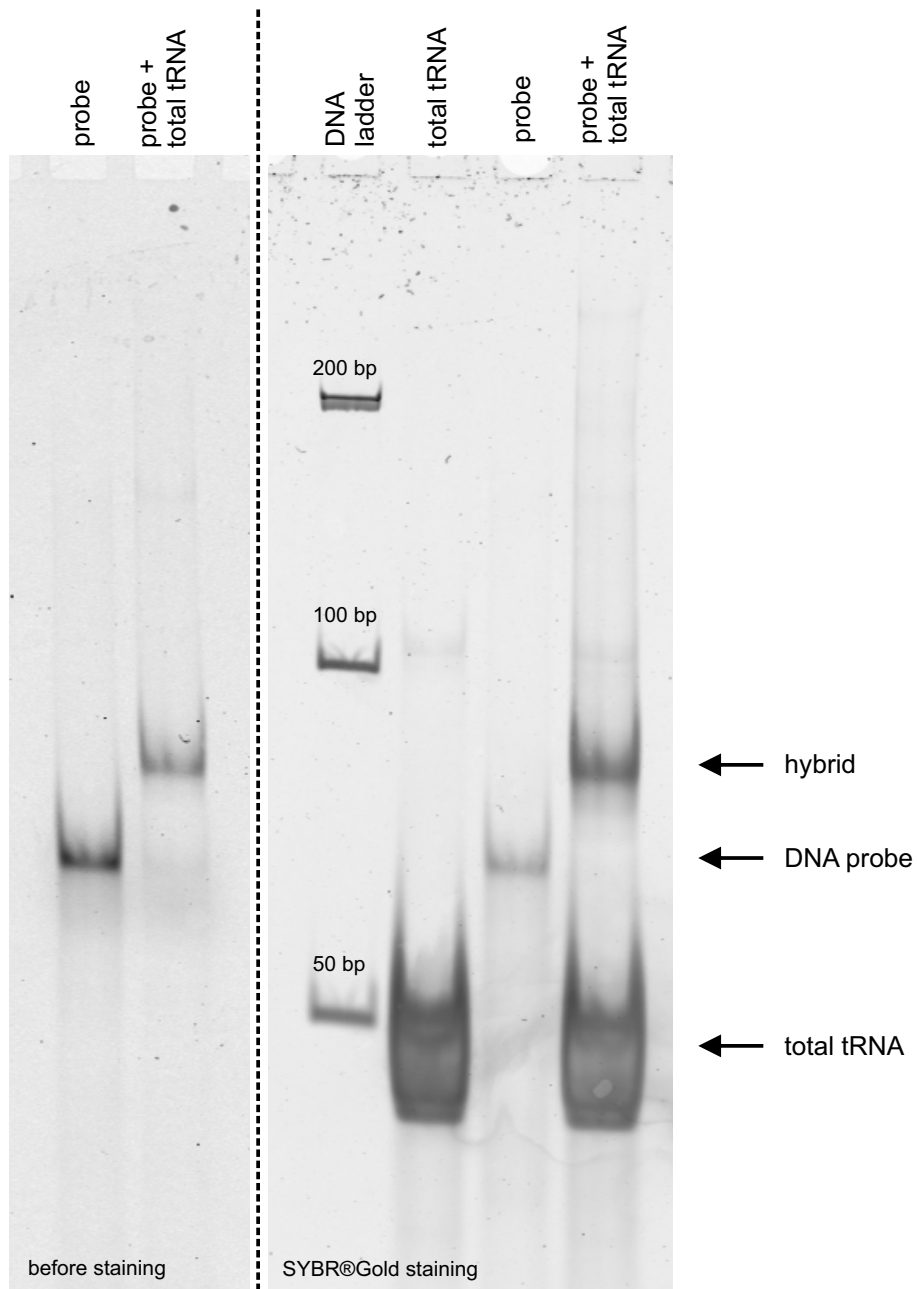


**Figure A.2: Detection of tRNA<sup>Met</sup>(MAU) in total tRNA by PAGE** A non-denaturing PAGE (8 %) gel was run to confirm the hybridization of the DNA probe MH630 to native tRNA<sup>Met</sup>(MAU) in a total tRNA mixture (corresponding section: 3.1.2.2). 5 pmol of the DNA probe were hybridized to 2.5 µg total tRNA (*E. coli*). The shift of the labeled DNA probe detectable in the sample compared to the control lane (probe only) indicated the successful hybridization of the probe to tRNA<sup>Met</sup>(MAU). Scans of both unstained (left) and SYBR®Gold stained (right) gel are displayed, respective bands of hybrid, probe and tRNA are indicated by arrows.

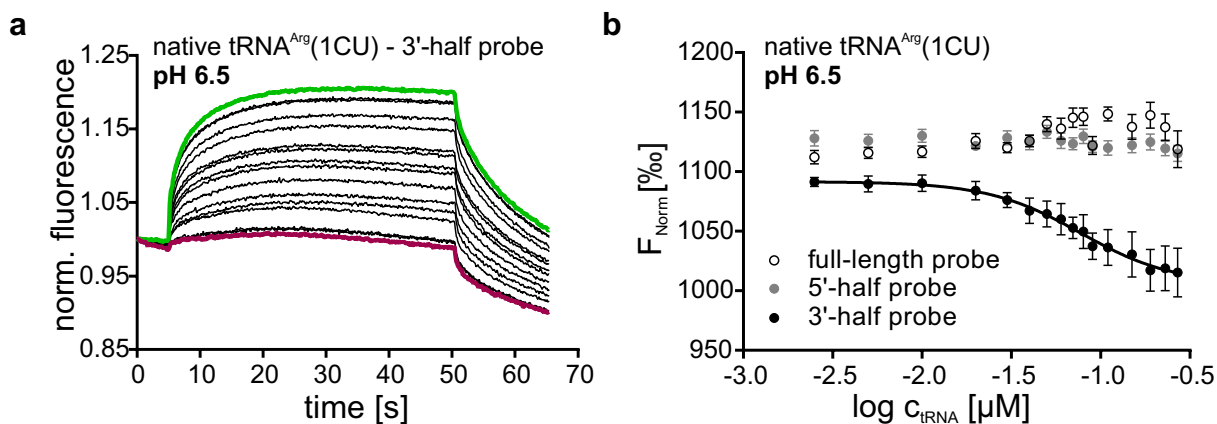


**Figure A.3: MST measurement of native tRNA<sup>Arg</sup>(1CU) at pH 6.5** Hybridization of the full-length as well as the 5'- and 3'-half probes to native tRNA<sup>Arg</sup>(1CU) at pH 6.5 was tested in MST measurements. (a) displays the fluorescence time traces of the 3'-half probe, the only probe that showed a change in thermophoresis upon hybridization. Time traces of the lowest and highest tRNA concentration are marked in green and magenta, respectively. In (b), respective  $F_{\text{Norm}}$  vs.  $\log(\text{concentration})$  plots are shown for each probe, demonstrating that only for the 3'-half probe (black) a binding curve was received. Probe concentration was 0.1  $\mu\text{M}$ .

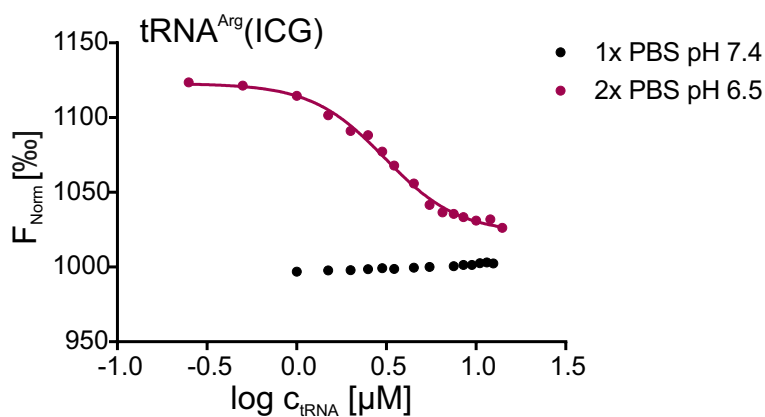


**Figure A.4: Hybridization conditions for MST measurement of tRNA<sup>Arg</sup>(ICG)** Using a commercial total tRNA mixture (*S. cerevisiae*), hybridization conditions for tRNA<sup>Arg</sup>(ICG) were optimized. The binding curves received from MST measurements displayed a clear thermophoretic response when using 2x PBS at pH 6.5 instead of the standard hybridization conditions indicated (magenta). Under the standard conditions, a thermophoretic response was completely absent (black). Thus, for quantification of tRNA<sup>Arg</sup>(ICG), the adapted annealing conditions were applied. Probe concentration was 0.1  $\mu\text{M}$ .

**Table A.1: EC<sub>50</sub> values of *S. cerevisiae* tRNA species, application 1** EC<sub>50</sub> values determined for the 23 *S. cerevisiae* tRNAs, correlating to the binding curves presented in figures A.5, A.6 and A.7, are displayed. Presented data corresponds to application 1 (section 3.1.2.6) and figure 3.14. Total tRNA samples of *S. cerevisiae*, strain S288C, grown at 30 and 39 °C were obtained from Dr. S. Leidel, DNA probe concentration was 0.1 μM . Mean values of biological triplicates are tabled and 95 % confidence intervalls (CI) are indicated.

tRNA	EC <sub>50</sub> 30 °C [μM]	95 % CI	EC <sub>50</sub> 39 °C [μM]	95 % CI
tRNA <sup>Ala</sup> (IGC)	1.363	1.261-1.474	1.264	1.165-1.373
tRNA <sup>Arg</sup> (1CU)	1.504	1.363-1.680	1.522	1.371-1.700
tRNA <sup>Arg</sup> (ICG)	3.623	3.357-3.955	3.399	3.197-3.631
tRNA <sup>Asn</sup> (GUU)	1.946	1.824-2.065	2.087	1.943-2.228
tRNA <sup>Asp</sup> (GUC)	1.652	1.460-1.877	1.747	1.544-2.011
tRNA <sup>Cys</sup> (GUC)	5.409	5.114-5.739	6.328	5.782-7.152
tRNA <sup>Gln</sup> (3UG)	3.275	2.889-3.957	2.841	2.538-3.298
tRNA <sup>Glu</sup> (3UC)	2.203	2.036-2.374	2.143	1.947-2.333
tRNA <sup>Gly</sup> (.CC)	4.807	4.437-5.181	4.733	4.536-4.927
tRNA <sup>Gly</sup> (GCC)	1.742	1.583-1.910	1.825	1.703-1.951
tRNA <sup>His</sup> (GUG)	3.724	3.386-4.130	3.972	3.698-4.321
tRNA <sup>Ile</sup> (IAU)	1.313	1.219-1.416	1.270	1.205-1.338
tRNA <sup>Leu</sup> (UAA)	2.999	2.851-3.153	3.348	3.253-3.448
tRNA <sup>Lys</sup> (3UU)	1.683	1.468-1.955	1.692	1.404-2.116
tRNA <sup>Lys</sup> (CUU)	3.070	2.893-3.278	2.862	2.705-3.044
tRNA <sup>Met</sup> (CAU)	4.394	4.167-4.643	4.660	4.368-4.990
tRNA <sup>Met</sup> (CAU), Ini	4.188	3.840-4.638	3.970	3.219-5.908
tRNA <sup>Pro</sup> (NGG)	1.696	1.576-1.827	1.593	1.473-1.720
tRNA <sup>Ser</sup> (IGA)	1.571	1.379-1.822	1.610	1.309-2.095
tRNA <sup>Thr</sup> (IGU)	1.093	0.995-1.195	1.146	1.007-1.316
tRNA <sup>Trp</sup> (BCA)	6.257	5.971-6.583	7.251	6.842-7.861
tRNA <sup>Tyr</sup> (GPA)	2.692	2.581-2.817	3.148	2.915-3.484
tRNA <sup>Val</sup> (IAC)	0.873	0.803-0.942	1.015	0.949-1.085

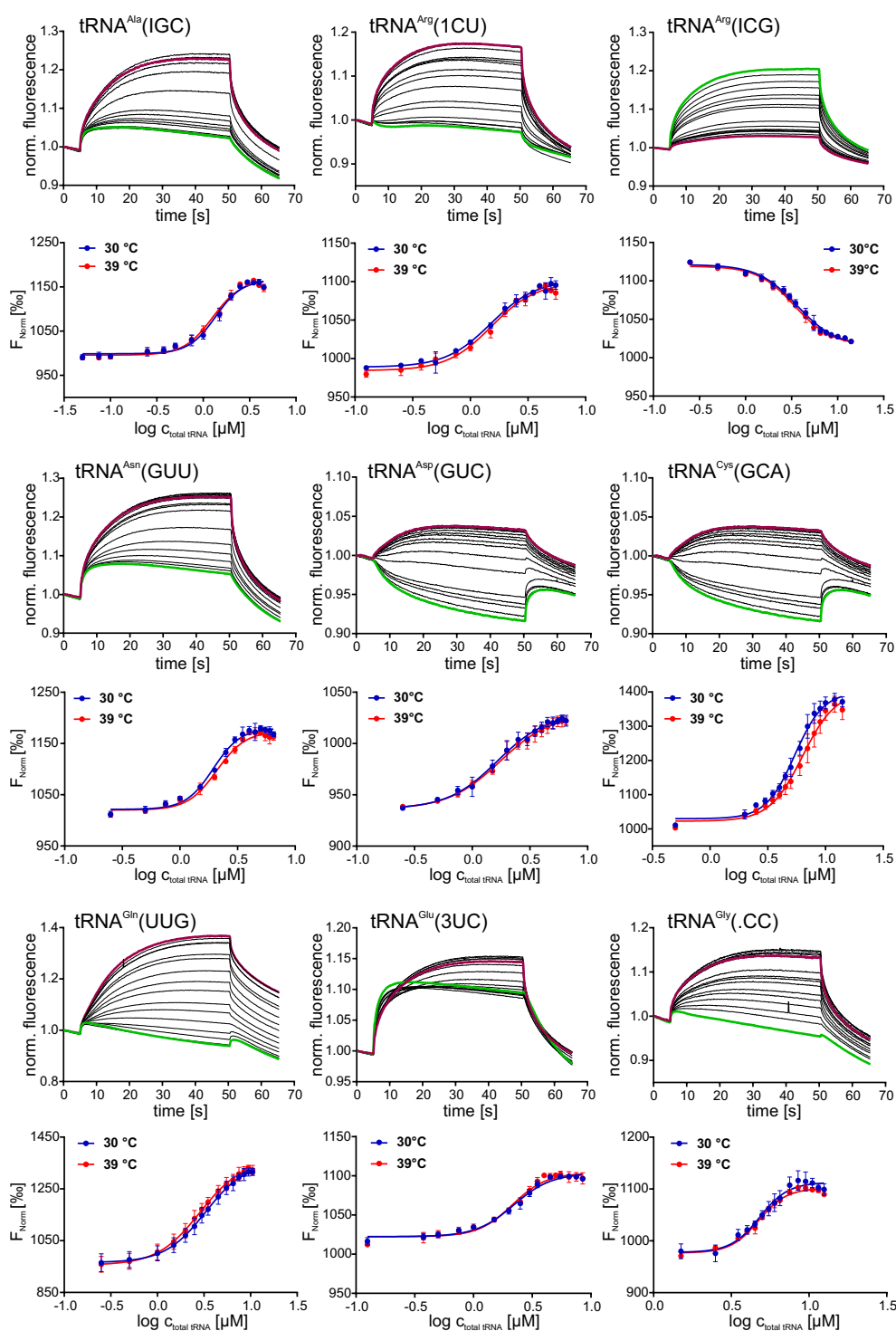


**Figure A.5: Fluorescence time traces and binding curves of *S.cerevisiae* tRNAs - 1** For the first set of the 23 analyzed *S. cerevisiae* tRNA species, example fluorescence time traces as well as the binding curves from which the abundances in section 3.1.2.6 (Application 1, compare figure 3.14) were extracted are displayed. Time traces of the lowest (green) and highest (magenta) concentration in each titration series are labeled, respectively, corresponding to free and bound DNA probe. Total tRNA samples of *S. cerevisiae*, strain S288C, grown at 30 and 39 °C were obtained from Dr. S. Leidel. Error bars represent the standard deviation of biological triplicates,  $n=3$ .

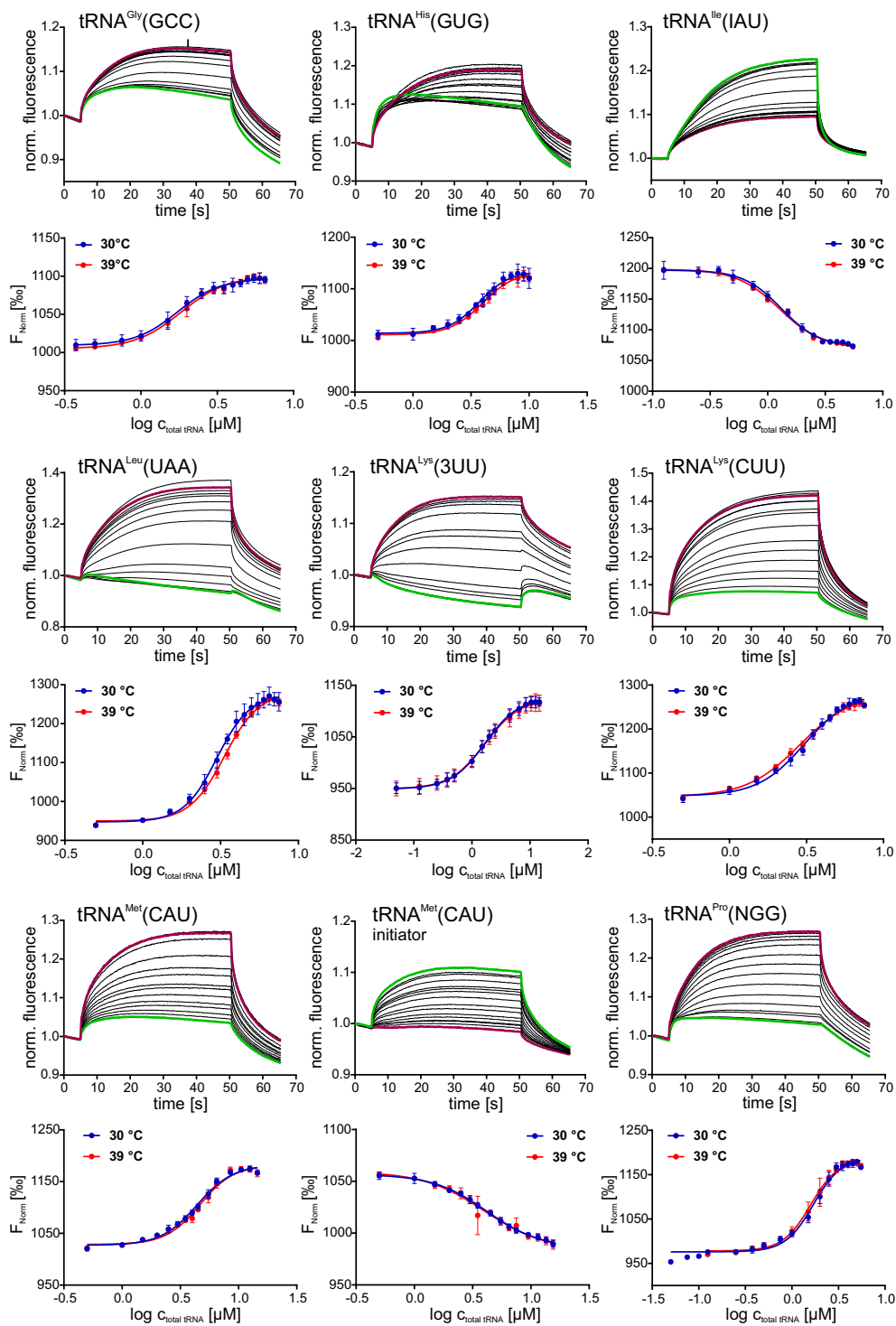


**Figure A.6: Fluorescence time traces and binding curves of *S.cerevisiae* tRNAs - 2** For the second set of the 23 analyzed *S. cerevisiae* tRNA species, example fluorescence time traces as well as the binding curves from which the abundances in section 3.1.2.6 (Application 1, compare figure 3.14) were extracted are displayed. Time traces of the lowest (green) and highest (magenta) concentration in each titration series are labeled, respectively, corresponding to free and bound DNA probe. Total tRNA samples of *S. cerevisiae*, strain S288C, grown at 30 and 39 °C were obtained from Dr. S. Leidel. Error bars represent the standard deviation of biological triplicates, n=3.



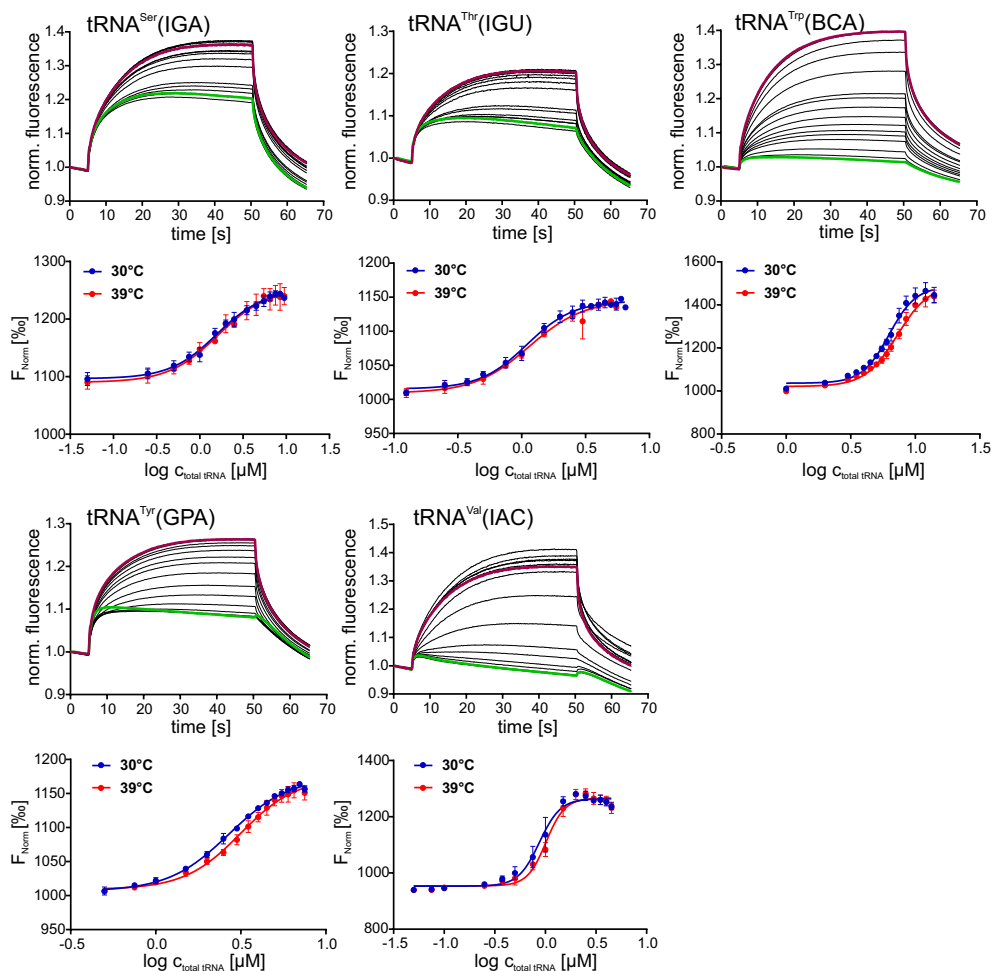


**Figure A.7: Fluorescence time traces and binding curves of *S.cerevisiae* tRNAs - 3** For the third set of the 23 analyzed *S. cerevisiae* tRNA species, example fluorescence time traces as well as the binding curves from which the abundances in section 3.1.2.6 (Application 1, compare figure 3.14) were extracted are displayed. Time traces of the lowest (green) and highest (magenta) concentration in each titration series are labeled, respectively, corresponding to free and bound DNA probe. Total tRNA samples of *S. cerevisiae*, strain S288C, grown at 30 and 39 °C were obtained from Dr. S. Leidel. Error bars represent the standard deviation of biological triplicates,  $n=3$ .

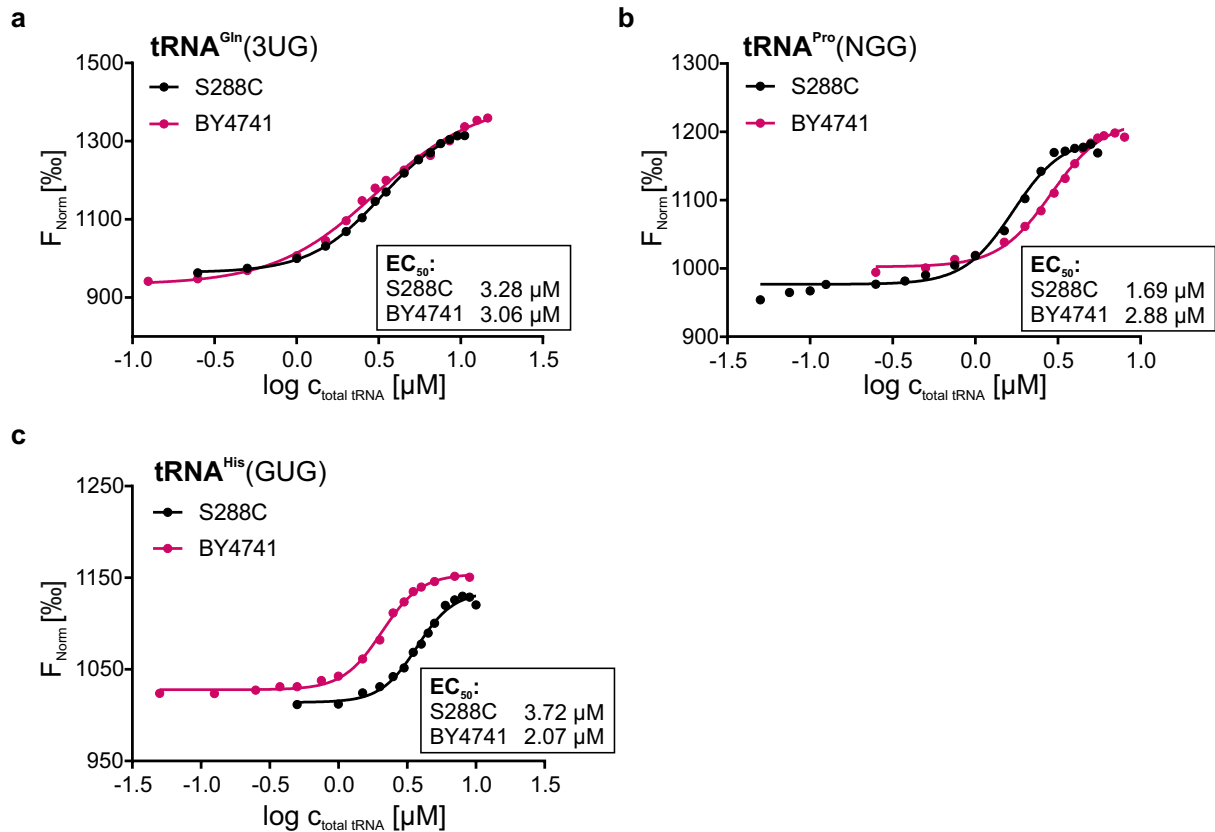


**Figure A.8: Consistency of tRNA abundances in *S. cerevisiae* strains** Binding curves of tRNA<sup>Gln</sup>(3UG), tRNA<sup>Pro</sup>(NGG) and tRNA<sup>His</sup>(GUG) measured in *S. cerevisiae* total tRNA of S288C (black) and BY4741 (magenta), related to section 3.1.2.5 and figure 3.12 b. While tRNA<sup>Gln</sup>(3UG) levels were well comparable in the two strains (< 10% deviation), abundances of tRNA<sup>Pro</sup>(NGG) and tRNA<sup>His</sup>(GUG) showed more pronounced differences (approximately 45 % lower EC<sub>50</sub> values corresponding to elevated tRNA levels in BY4742). Total tRNA samples of *S. cerevisiae*, strain S288C, grown at 30, were obtained from Dr. S. Leidel. Total RNA samples of strain BY4741 were prepared by Akif Ciftci. EC<sub>50</sub> values are indicated, probe concentration was 0.1 μM.

**Table A.2: EC<sub>50</sub> values determined for *S. cerevisiae* tRNA<sup>Lys</sup>(3UU), application 2** Quantification of tRNA<sup>Lys</sup>(3UU) in total tRNA from wildtype and double mutant *S. cerevisiae* (background strain BY4741), data given corresponds to section 3.1.2.6, application 2. EC<sub>50</sub> values obtained from MST measurements as well as 95 % confidence intervalls are listed. Total RNA samples were prepared by Akif Ciftci. DNA probe concentration was 0.1 μM.

strain	EC <sub>50</sub> [μM] 30 °C	95 % CI	EC <sub>50</sub> [μM] heat shock	95 % CI
WT (BY4741)	1.815	1.714-1.930	1.661	1.565-1.768
Δelp3Δdeg1	2.221	2.117-2.340	2.087	1.929-2.282
Δurm1Δdeg1	1.584	1.460-1.727	1.522	1.438-1.612
Δelp3Δurm1	1.698	1.566-1.857	1.77	1.649-1.912
Δtcd1Δelp3	1.745	1.615-1.900	1.808	1.648-2.006
Δtcd1Δurm1	1.641	1.499-1.812	1.420	1.301-1.557

**Table A.3: EC<sub>50</sub> values determined for *S. cerevisiae* tRNA<sup>Pro</sup>(NGG), application 2** Quantification of tRNA<sup>Pro</sup>(NGG) in total tRNA from wildtype and double mutant *S. cerevisiae* (background strain BY4741), data given corresponds to section 3.1.2.6, application 2. EC<sub>50</sub> values obtained from MST measurements as well as 95 % confidence intervalls are listed. Total RNA samples were prepared by Akif Ciftci. DNA probe concentration was 0.1 μM.

strain	EC <sub>50</sub> [μM] 30 °C	95 % CI	EC <sub>50</sub> [μM] heat shock	95 % CI
WT (BY4741)	2.88	2.700-3.096	3.311	3.041-3.723
Δelp3Δdeg1	3.008	2.823-3.231	2.063	1.969-2.157
Δurm1Δdeg1	3.045	2.884-3.260	2.890	2.677-3.140
Δelp3Δurm1	2.253	2.125-2.383	3.166	2.948-3.456
Δtcd1Δelp3	2.719	2.553-2.909	2.823	2.593-3.118
Δtcd1Δurm1	3.221	2.979-3.579	3.535	3.168-4.234

**Table A.4: EC<sub>50</sub> values determined for *S. cerevisiae* tRNA<sup>Gln</sup>(3UG), application 2** Quantification of tRNA<sup>Gln</sup>(3UG) in total tRNA from wildtype and double mutant *S. cerevisiae* (background strain BY4741), data given corresponds to section 3.1.2.6, application 2. EC<sub>50</sub> values (means of technical triplicates) obtained from MST measurements as well as 95 % confidence intervalls are listed. Total RNA samples were prepared by Akif Ciftci. DNA probe concentration was 0.1 μM.

strain	EC <sub>50</sub> [μM] 30 °C	95 % CI	EC <sub>50</sub> [μM] heat shock	95 % CI
WT (BY4741)	3.059	2.769-3.477	2.28	2.006-2.686
Δelp3Δdeg1	2.790	2.554-3.103	1.999	1.812-2.221
Δurm1Δdeg1	2.762	2.499-3.125	1.881	1.681-2.103
Δelp3Δurm1	2.884	2.510-3.508	2.247	1.997-2.590
Δtcd1Δelp3	3.186	2.786-3.860	2.847	2.475-3.477
Δtcd1Δurm1	3.343	2.850-4.300	2.155	1.879-2.558

**Table A.5: EC<sub>50</sub> values determined for *S. cerevisiae* tRNA<sup>His</sup>(GUG), application 2** Quantification of tRNA<sup>His</sup>(GUG) in total tRNA from wildtype and double mutant *S. cerevisiae* (background strain BY4741), data given corresponds to section 3.1.2.6, application 2. EC<sub>50</sub> values (means of technical triplicates) obtained from MST measurements as well as 95 % confidence intervalls are listed. Total RNA samples were prepared by Akif Ciftci. DNA probe concentration was 0.1 μM.

strain	EC <sub>50</sub> [μM] 30 °C	95 % CI	EC <sub>50</sub> [μM] heat shock	95 % CI
WT (BY4741)	2.074	1.887-2.274	2.216	2.038-2.405
Δelp3Δdeg1	2.110	1.924-2.297	2.013	1.868-2.171
Δurm1Δdeg1	2.251	2.059-2.469	1.995	1.870-2.125
Δelp3Δurm1	1.980	1.775-2.186	1.935	1.842-2.028
Δtcd1Δelp3	2.076	1.921-2.241	2.426	2.207-2.683
Δtcd1Δurm1	2.242	2.040-2.478	2.210	2.035-2.394

**Table A.6: EC<sub>50</sub> values and hybridization ratios determined for the polyT-DNA probes to the *in vitro*-transcribed mRNAs** EC<sub>50</sub> values (given in [μM]) and binding ratios (DNA probe:mRNA, in brackets) obtained for each combination of the four polyT-DNA probes and the *in vitro*-transcribed mRNAs (51, 64 and 101 nt polyA tail length). The data displayed corresponds to section 3.1.3.1 and figure 3.24. The concentration of the probes was set to 50 nM in each experiment. IVTs were kindly provided by Prof. Dr. Katalin Karikó and Isabell Hellmuth.

	51 nt polyA mRNA	64 nt polyA mRNA	101 nt polyA mRNA
specific RNA probe		0.023 (1.09:1)	
20 nt polyT probe	0.015 (1.6:1)	0.013 (1.9:1)	0.010 (2.5:1)
30 nt polyT probe	0.025 (1:1)	0.017 (1.5:1)	0.014 (1.8:1)
50 nt polyT probe	0.034 (0.7:1)	0.034 (0.7:1)	0.020 (1.2:1)
80 nt polyT probe	0.061 (0.4:1)	0.052 (0.5:1)	0.040 (0.6:1)

## MST-based quantification of 5S rRNA in *E. coli* total tRNA

To show the transferability of the MST-based quantification methods to single small RNA species other than tRNAs, *E. coli* 5S rRNA was chosen and quantified in commercially available total tRNA. The presence of 5S rRNA in the total tRNA mixture was obvious from PAGE analysis (compare figure A.10) and thus the degree of contamination was intended to be quantified by MST. The observed MST fluorescence time traces and the corresponding binding curve of a titration series of total tRNA and the respective DNA probe (MH768) are displayed in figure A.9. Results indicate a contamination of the total tRNA mixture with approximately 6.6 % (m/m) 5S rRNA.

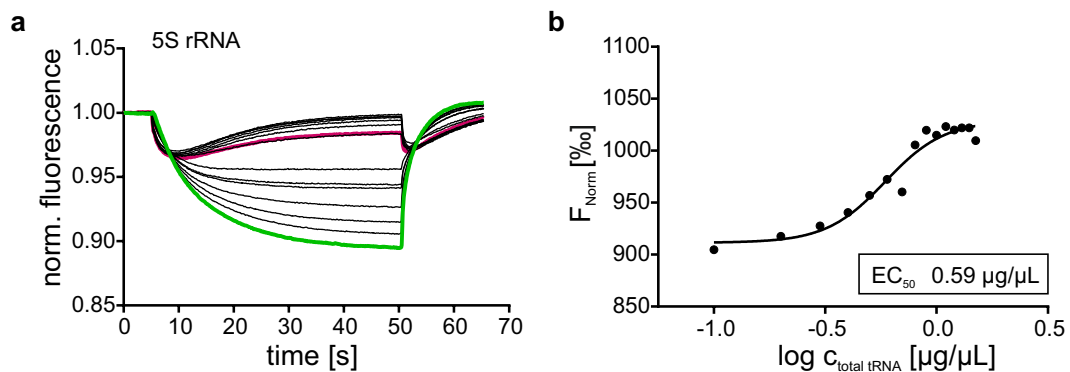


**Figure A.9: Quantification of 5S rRNA in *E. coli* total tRNA** Fluorescence time traces (a) and corresponding binding curve (b) obtained from MST-measurement of 5S rRNA in *E. coli* total tRNA. Time traces of free and bound probe are marked in green and magenta, respectively. The results indicate a contamination of the total tRNA mixture with approximately 6.6 % 5S rRNA (m/m). Probe concentration was 0.1 µM, measurements were performed at 60 % MST power.

Appendix to Chapter 3.2.4

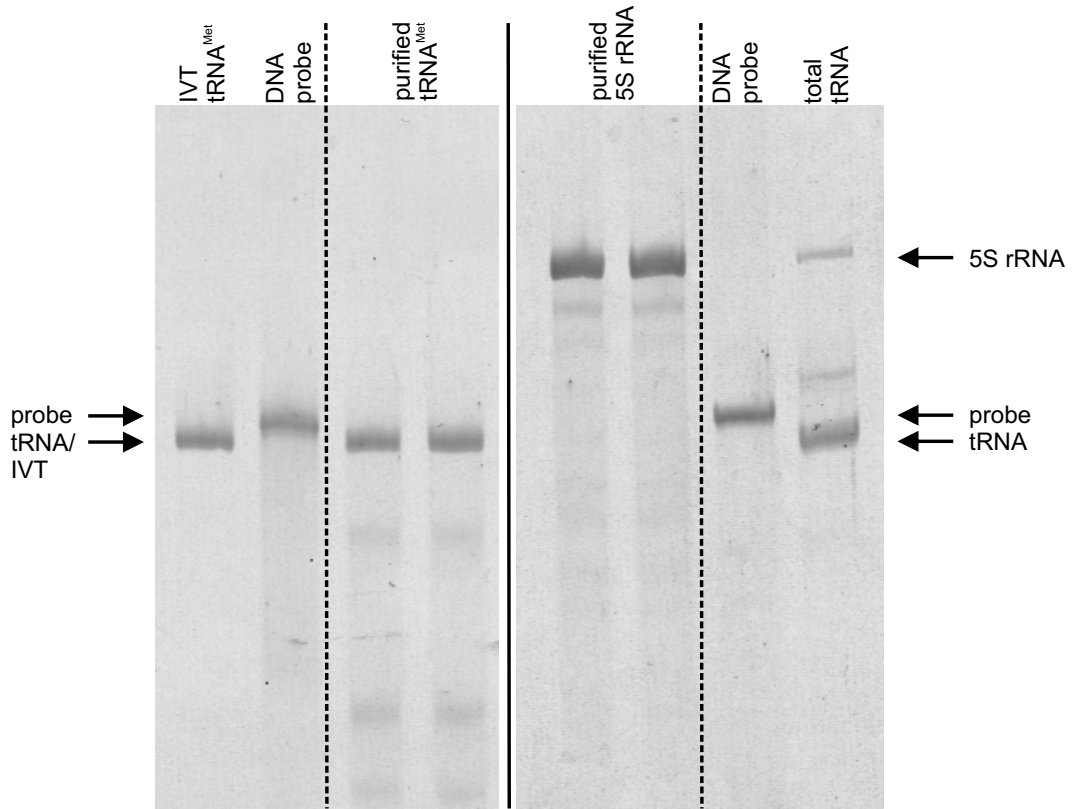


**Figure A.10: Isolation of *E. coli* tRNA<sup>Met</sup>(MAU) and 5S rRNA** 10 % denaturing PAGE gel indicating the successful isolation of *E. coli* tRNA<sup>Met</sup>(MAU) and 5S rRNA employing the protocol described in section 3.2.1. Input RNA was in both cases a commercially available total tRNA mixture, which contained substantial amounts of 5S rRNA as visible in the total tRNA band. Biotinylated DNA probes were MH630 for tRNA<sup>Met</sup> and MH768 for 5S rRNA. As size control for tRNA<sup>Met</sup>(MAU), the respective IVT was used as indicated. Bands corresponding to tRNA, probes and 5S rRNA are labeled with arrows. The gel was stained using GelRed.

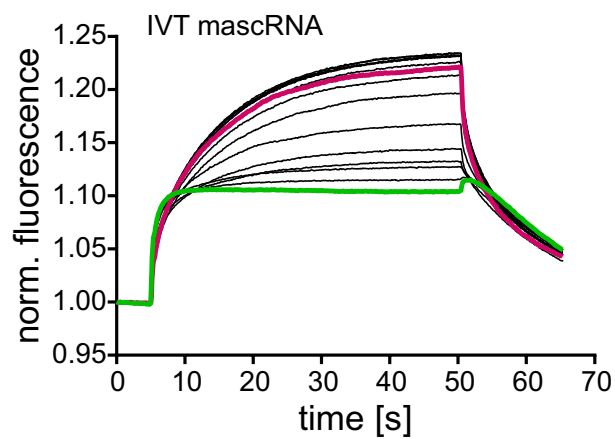


**Figure A.11: MST measurement of *in vitro* transcribed mascRNA** A titration series of mascRNA IVT and its complementary DNA probe MH765 was analyzed *via* MST. Fluorescence time traces corresponding to the binding curve depicted in figure 3.30 c are illustrated, showing a clear difference in the thermophoretic response of free and bound probe, labeled in green and magenta, respectively. Measurements were performed at 60 % MST power using a probe concentration of 0.1  $\mu$ M.

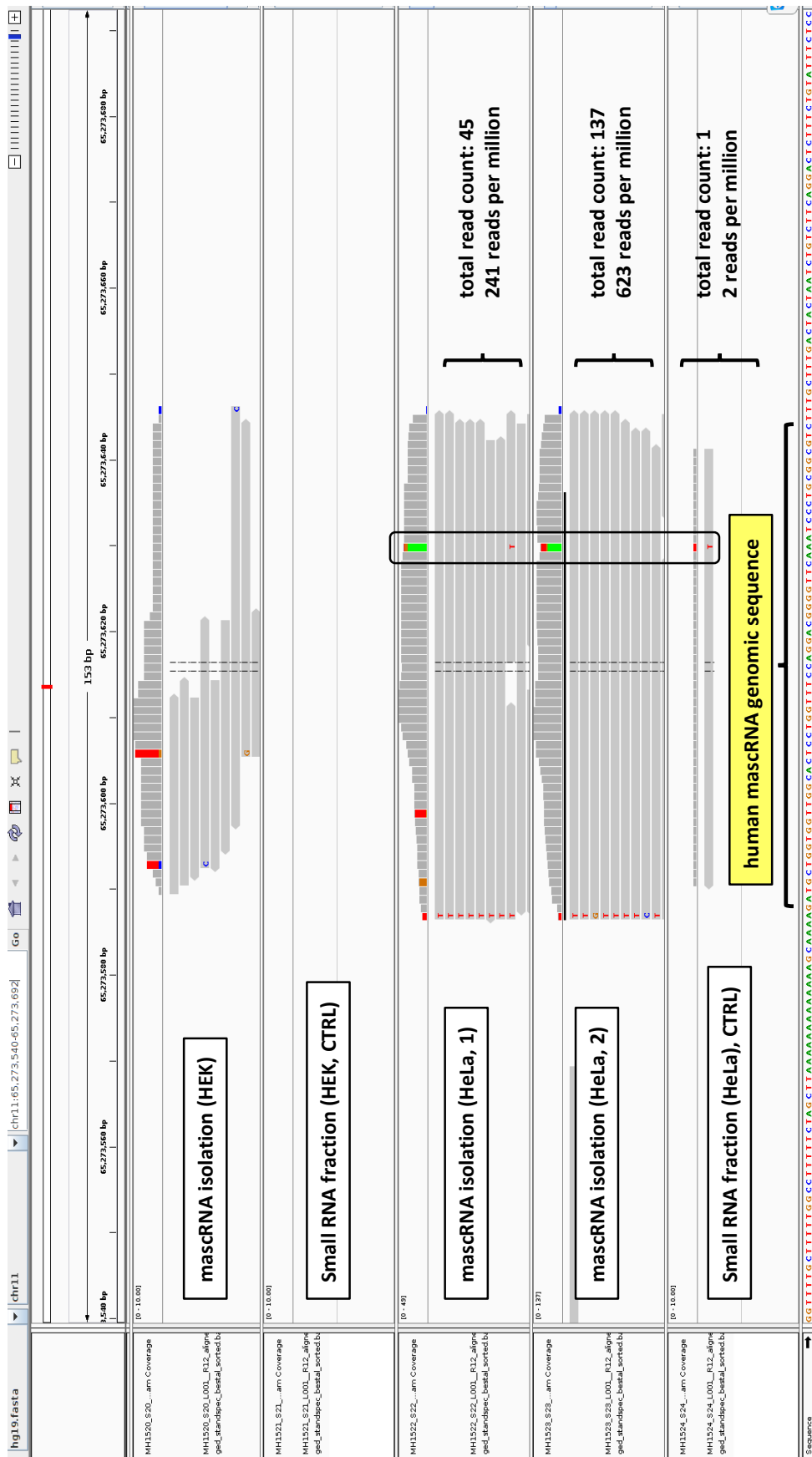


**Figure A.12: Enrichment of mascRNA confirmed by RNA-Seq** Illumina MiSeq results of the mascRNA samples isolated from small RNA fractions of HEK and HeLa cells as described in section 3.2.3.3. Reads mapping to human mascRNA are displayed for each sample indicated, the position of the putatively modified adenosine, for which a mismatch pattern was observed, is marked by the black box. In case of the HeLa small RNA fraction, mascRNA was isolated in two batches, respective sample 1 corresponds to a test isolation using the small RNA fractions collected during optimization of the size-separation process and sample 2 represents the main sample described in section 3.2.3.3. Relative read numbers obtained for mascRNA in the HeLa samples are indicated. Library preparation was kindly performed by L. Tserovski, S. Werner and D. Jacob, Illumina Sequencing by Prof. Dr. Y. Motorin, and data analysis by L. Tserovski.



## Appendix to Chapter 3.3.5

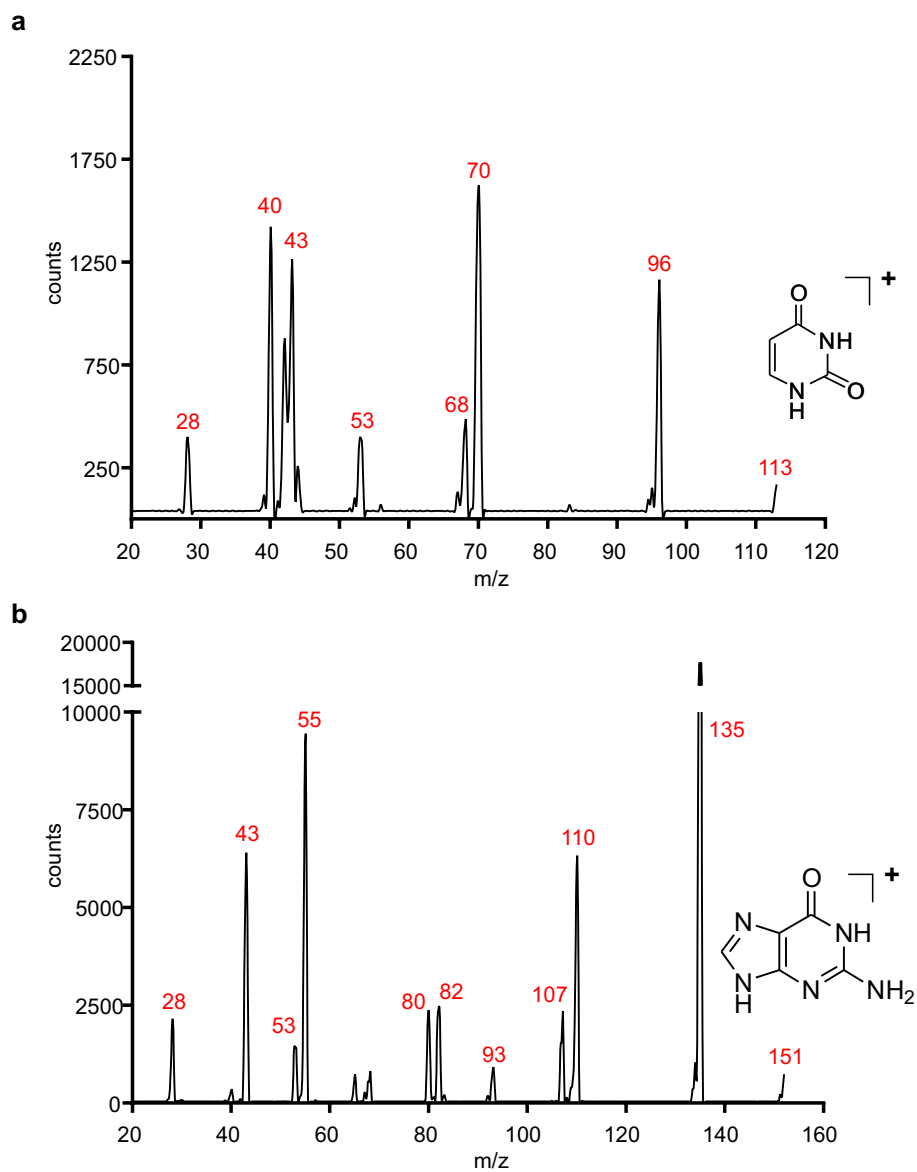


**Figure A.13: Pseudo-MS<sup>3</sup> spectra of unlabeled uracil and guanine** Mass spectra displaying the fragmentation of unlabeled uracil (a) and guanine (b) detected using an pseudo-MS<sup>3</sup> scan. Total tRNA of *E. coli* was used as RNA sample, m/z values of the main peaks are indicated in red.

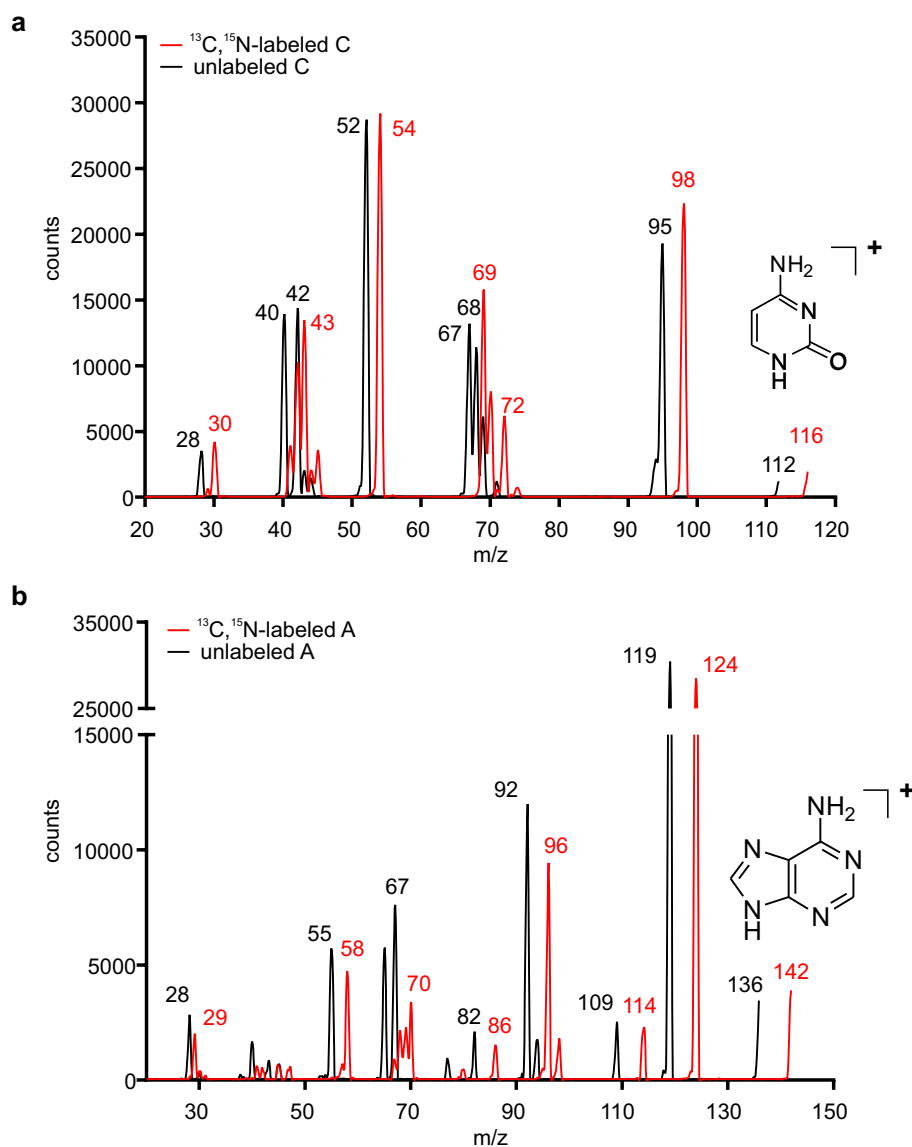


**Figure A.14: Pseudo-MS<sup>3</sup> spectra of unlabeled and labeled cytosine and adenine** Mass spectra displaying the fragmentation of unlabeled (black) and  $^{13}\text{C}, ^{15}\text{N}$ -labeled (red) cytosine (a) and adenine (b) detected using an pseudo-MS<sup>3</sup> scan. Total tRNA of *E. coli* was used as RNA sample for measuring the spectra of the unlabeled nucleosides, RNA samples for the measurements of the labeled nucleosides originated from *E. coli* cells grown under  $^{13}\text{C}$ -2-glycerol supply (samples provided by J. Schmidt). The m/z values of the main peaks are indicated in black (unlabeled) or red (labeled), respectively.

# Curriculum Vitae